UNIVERSITY OF CALIFORNIA, SAN DIEGO

Self–Consistent Treatment of Neutrino Physics in Cosmology

A dissertation submitted in partial satisfaction of the
requirements for the degree
Doctor of Philosophy

in

Physics

by

Evan Grohs

Committee in charge:

Professor George Fuller, Chair
Professor Brian Keating
Professor Kurt Marti
Professor David Tytler
Professor Nolan Wallach

2015

The dissertation of Evan Grohs is approved, and it is acceptable in quality and form for publication on microfilm and electronically:

_____

_____

_____

_____

_____

Chair

University of California, San Diego

2015

TABLE OF CONTENTS

LIST OF ABBREVIATIONS

Abbreviation	Definition
Eq.	Equation
Ch.	Chapter
Sec.	Section, subsection, etc.
Tb.	Table
Fig.	Figure
CMB	Cosmic Microwave Background
CMBR	CMB Radiation
BSM	Beyond Standard Model
CνB	Cosmic Neutrino Background
BBN	Big Bang Nucleosynthesis
SBBN	Standard BBN
CSM	Cosmological Standard Model
SC	Standard Cosmology
D/H	Relative abundance of deuterium with respect to hydrogen
QCD	Quantum Chromo(color)–Dynamics
QED	Quantum ElectroDynamics
LSS	Large Scale Sturcture
QKE	Quantum Kinetic Equation
ΛCDM	Lambda Cold Dark Matter
BURST	BBN Unitary Self–consistent Transport
FLRW	Friedmann-Lemaître-Robertson-Walker
BE	Bose–Einstein
FD	Fermi–Dirac
MB	Maxwell–Boltzmann
const.	Constant
lhs	Left–Hand–Side
rhs	Right–Hand–Side
νMR	Neutrino–Mass/Recombination
NSE	Nuclear Statistical Equilibrium
ODE	Ordinary Differential Equation
RK#	Runge–Kutta method of order #
frs	Forward–Reverse–Summed
wrt	With Respect To
#K	# times one thousand
Rxn.	Reaction

LIST OF SYMBOLS

Symbol	Explanation
T, T_γ	Plasma, photon temperature
H	Hubble expansion rate
H_0	Hubble expansion rate at current epoch
h	Hubble parameter ($H_0 = 100h$ km/s/Mpc)
Ω_i	Fractional contribution to closure density of component i
ω_i	Density of component i ($\omega_i = \Omega_i h^2$)
$N_{\rm eff}$	Effective number of relativistic degrees of freedom
Y_P	Primordial helium mass fraction
$\sum m_\nu$	Sum of the light neutrino masses statistic
ν_i	Neutrino in weak eigenstate i or mass eigenstate i
$\overline{\nu}_i$	Anti–neutrino in weak eigenstate i or mass eigenstate i
r_s	Sound horizon
r_d	Photon diffusion length
t	Time coordinate
$a(t)$	Scale factor as a function of time
$\dot{a}$	Derivative of scale factor wrt time
G	Newton's gravitational constant
$\mu, \nu, \lambda, \rho, \sigma, \alpha, \beta$	Indicies ranging over all four coordinates
i, j, k	Indicies ranging over three spatial coordinates
$g_{\mu\nu}$	Metric components μ, ν
$m_{\rm pl}$	Planck mass
ρ, p	Energy density, pressure
$\Gamma^\lambda_{\mu\nu}$	Christoffel symbol
g	Internal degrees of freedom or spin degrees of freedom or internal partition function
$f(v_1, v_2, ...)$	Phase–space occupation probability in terms of variables $v_1, v_2, ...$
ε	Ratio of energy to temperature
$g_{\star S}$	Effective–entropic–spin statistic
$g_\star$	Effective–energy degrees–of–freedom
$T_{\rm cm}$	Comoving temperature

m, p, E	Mass, three–momentum magnitude, energy
z	Ratio of mass to temperature
n	Proper number density
η	Ratio of non-relativistic to ultra-relativistic particle number densities
$N_{\rm eff}^{\rm (th)}$	$N_{\rm eff}$ deduced at BBN
$\tilde{N}_{\rm eff}$	$N_{\rm eff}$ deduced at photon decoupling
ΔQ	Absolute change in quantity Q
δQ	Relative change in quantity Q
P, Q	Four–momenta for massless, massive particles
$e^{\pm}, \gamma$	Positron, Electron, Photon
Y_i	Abundance of species i
A_i, z_i	Atomic mass number, Atomic number of species i
$\langle \sigma v \rangle$	Thermal average of product of cross section and relative velocity
z	Ratio of electron mass to plasma temperature
i, j, k, l, m	Indicies for nuclides
μ	Chemical potential
G_F	Fermi coupling constant
Γ	Rate
$E_{\rm therm}$	Thermalization energy value
θ_s	Angle subtended by the sound horizon
θ_d	Angle subtended by the photon diffusion length
R	Ratio involving the baryon and photon energy densities
σ_T	Thomson cross section
k_d	Damping diffusion wave number
X_e	Free–electron fraction
I, J	Integrals
z	Redshift
$\hat{C}[f]$	Collision integral for occupation probability f
$\langle \lvert \mathcal{M} \rvert^2 \rangle$	Summed–squared amplitude
$N_{\rm bins}$	Number of bins in neutrino spectrum

LIST OF FIGURES

LIST OF TABLES

ACKNOWLEDGEMENTS

The dissertation author would like to acknowledge the Institutional Computing Program at Los Alamos National Laboratory for use of their HPC cluster resources. The author acknowledges the San Diego Supercomputer Center for their use of HPC resources and helpful technical support. This work was supported in part by NSF grant PHY-1307372 at UC San Diego, and by the Los Alamos National Laboratory Institute for Geophysics, Space Sciences and Signatures subcontracts.

The author thanks the following people for useful conversations: George Fuller; Mark Paris; Chad Kishimoto; Alexey Vlasenko; JJ Cherry; Amol Patwardhan; Eric Michelsen; Vincenzo Cirigliano; Daniel Plaschke; Christel Sutterley; LLoyd Knox; Lauren Gilbert; and Jeremy Ariche.

Section 1.1, section 2.1, section 2.5, section 4.3, in part, section 4.4.1, section 4.4.6, section 4.5, chapter 6, in full, and section 8.2 are reprints of some of the material as it appears in: Grohs, E.; Fuller, G. M.; Kishimoto, C. K.; Paris, M. W. "Probing neutrino physics with a self-consistent treatment of the weak decoupling, nucleosynthesis, and photon decoupling epochs", J. Cosmology Astropart., 5 (May 2015) 17. The dissertation author was the primary investigator and author of this paper.

Chapter 5, in full, is a reprint of the material as submitted for publication: Grohs, E.; Fuller, G. M.; Kishimoto, C. K.; Paris, M. W. "Effects of neutrino rest mass on $N_{\rm eff}$ and ionization equilibrium freeze-out". The dissertation author was the primary investigator and author of this paper.

Chapter 7, in full, is a reprint of the material being prepared for submission of publication: Fuller, G. M.; Grohs, E.; Kishimoto, C. K.; Paris, M. W.; Vlasenko, A. "Energy transport in neutrino decoupling and big bang nucleosynthesis". The dissertation author is the primary investigator and author of this paper.

VITA

2005	B. A. in Physics, University of Chicago
2005	B. S. in Mathematics, University of Chicago
2008-2012	Graduate Teaching Assistant, University of California, San Diego
2009	M. A. in Physics, University of California, San Diego
2015	Ph. D. in Physics, University of California, San Diego

PUBLICATIONS

Grohs, E.; Fuller, G. M.; Kishimoto, C. K.; Paris, M. W. “Probing neutrino physics with a self-consistent treatment of the weak decoupling, nucleosynthesis, and photon decoupling epochs”, J. Cosmology Astropart., 5 (May 2015) 17.

ABSTRACT OF THE DISSERTATION

Self–Consistent Treatment of Neutrino Physics in Cosmology

by

Evan Grohs

Doctor of Philosophy in Physics

University of California, San Diego, 2015

Professor George Fuller, Chair

We are developing a code to self–consistently treat beyond–standard–model physics in the early universe. This work details the calculations done with regards to the epochs of weak decoupling, weak freeze–out, big bang nucleosynthesis, recombination, and includes exploratory work on dilution and electron–positron annihilation. We assess the predictions made by the standard model, and investigate how new physics in the neutrino sector may alter or preserve those predictions. Throughout this work, we use natural units: $\hbar = c = k_b = 1$.

Chapter 1

Introduction

1.1 Motivation

In this work we demonstrate how a self-consistent treatment of the physics of the early universe (from temperature $T \sim 10$ MeV down to $T \sim 0.1$ eV) enables cosmic microwave background (CMB) observations, in concert with light-element abundances, to be used as new probes of beyond-standard-model (BSM) physics in the neutrino sector. In a sense, these probes are tantamount to probes of the CνB (relic Cosmic Neutrino Background). Recent observations [4, 5, 6, 7] of the CMB and observationally-inferred primordial abundances of deuterium and helium [8, 9, 1, 3] formed in big bang nucleosynthesis (BBN) already place tight constraints on both the cosmological standard model (CSM) and BSM physics. However, future observations will usher in a higher level of precision with even better prospects for BSM probes, see for example Ref. [10].

We anticipate that observations will bring about an overdetermined situation where BSM physics may manifest itself if it is present. The existing or anticipated observations and measurements of greatest utility for the present purposes are: (1) high-precision measurements of the baryon-to-photon ratio, or the equivalent baryon density

($\omega_b \equiv \Omega_b h^2$); (2) high-precision measurements of the "effective number of relativistic degrees of freedom" ($N_{\rm eff}$); (3) high-precision measurements of the primordial deuterium abundance (D/H) from quasar absorption lines; (4) measurements of the primordial helium abundance (Y_P) directly from CMB polarization data; and (5) measurements of the sum of the light neutrino masses ($\sum m_\nu$), i.e. the collisionless damping scale associated with neutrinos.

The physics that determines the relic neutrino energy spectra in weak decoupling and that of primordial nucleosynthesis affects observables of the CMB. These distinct, disparate epochs, however, depend not only on the values of parameters describing the cosmology (such as ω_b, $N_{\rm eff}$, relevant cosmic constituents, etc.) but also on the parameters derived from these base, input parameters (such as primordial abundances, recombination history, etc.). This is the basis for what we will term "self-consistency." The requirement for self-consistency between the BBN and CMB epochs, for example, in current data analyses depends on the parametrization of the energy density in terms of $N_{\rm eff}$ and upon the baryon-to-photon ratio. These two parameters, as measured at photon decoupling, are the sole determinants of the primordial helium abundance at the epoch of alpha particle formation ($T \sim 0.1$ MeV) in "standard" (*i.e.* zero lepton numbers, no BSM physics) BBN calculations. Though this procedure is adequate for the CSM and standard model physics, here we argue that it can be insufficient to probe varieties of BSM physics when confronting model cosmologies with next-generation, high-precision CMB and light element abundance data. In the case of the helium and $N_{\rm eff}$ self-consistency mentioned above, the relationship between the helium yield in BBN and $N_{\rm eff}$ is a non-trivial function of the interplay of expansion rate and neutron-to-proton ratio, as is well known [11]. The latter ratio is, in turn, a sensitive function of the ν_e and $\bar{\nu}_e$ energy distribution functions, and these can be affected by BSM issues like lepton numbers, flavor mixing, sterile neutrino states, heavy particle decay, etc.

Handling and analyzing the observed data while imposing self-consistency over multiple epochs in the early universe can require new procedures. The approach developed in Ref. [11] and employed in Planck XVI [2] has been highly successful. There, self-consistency is imposed approximately by the addition of a term in the log-likelihood function. A very small theoretical uncertainty ensures the posterior distributions are close to the corresponding theoretical values. However, when we impose self-consistency among the different epochs the need may arise to solve for the various derived parameters iteratively. Returning to the helium/$N_{\rm eff}$ example discussed above, Y_P and the recombination history of the universe both depend on the radiation energy density, usually parametrized by $N_{\rm eff}$. Subsequently, the recombination history is affected by the the primordial abundance of helium. The values of these two derived parameters, in turn, affect CMB observables, which recommends an iterative and therefore self-consistent approach.

Ideally, we would want a procedure to self-consistently treat neutrino and BSM physics from the post-QCD epoch to the onset of non-linearities in large scale structure (LSS). Recently, the quantum-kinetic equations (QKEs) governing neutrino flavor evolution in dense environments have been derived from first principles [12, 13, 14]. Such a program to treat neutrino physics in the early universe would incorporate a QKE treatment through weak decoupling at the very least. Weak freeze-out and BBN necessitate a neutrino-energy Boltzmann-equation or QKE treatment fully coupled to a nuclear reaction network. The recombination, photon decoupling, and advent of LSS epochs require a Boltzmann-equation treatment of neutrino clustering. Verification of any models related to neutrinos and BSM physics would then rely on agreement with direct cosmological observables, including but not limited to: primordial abundances; CMB power spectra; and the total matter power spectrum.

As outlined, this is a challenging undertaking. We therefore employ a limited

approach to show why self-consistency is required and how such a treatment can be efficacious in probing some issues in neutrino sector physics. To that end, we calculate the ratio of sound horizon to photon diffusion length, r_s/r_d, as a simple parametrization of the CMB, as described in detail in Sec. 4.5. It would, of course, be preferable to compute the full CMB power spectra in the self-consistent manner described above. There are two limiting factors that temper this ambitious proposal, however. The first is that the observable r_s/r_d is largely insensitive to the poorly constrained equation of state of the dark, vacuum energy component while the CMB power spectra are not. Additionally, current computations of the CMB power spectra [15] would need to be generalized to the BSM scenarios we contemplate here.

Our procedure for calculating derived cosmological quantities utilizes the neutrino occupation probabilities. Since we are developing the capacity to compute the effects of BSM physics that couples to the active neutrino sector, we do not restrict the form of the neutrino distribution functions to that of equilibrium Fermi-Dirac distributions. General forms are permitted and may be handled analytically or numerically. Neutrino occupation probabilities are taken in the present work in the flavor eigenbasis during weak decoupling, weak freeze-out and BBN.[1] During recombination and last scattering, we transform the occupation probabilities to the mass eigenbasis. When we consider the case of massive neutrinos, the statistic for the sum of the light neutrino masses, $\sum m_\nu$, is simply the sum of the three lightest mass eigenstates.

We might further clarify the fact that this limited approach does not rely on the assumption that the radiation energy density can be described in terms of the single parameter $N_{\rm eff}$. Indeed, an original motivation for using r_s/r_d as a proxy for $N_{\rm eff}$ (see Sec. 4.5) is the fact that the usual definition for $N_{\rm eff}$ does not apply to non-equilibrium neutrino distributions. A corollary of this observation is the possibility that $N_{\rm eff}$ may depend on the

[1] This is a matter that is properly resolved by utilizing a QKE approach [12], the subject of a future study.

scale factor $a(t)$; that is, we do not assume that $N_{\rm eff}$ is independent of scale factor. When extended, our approach is able to handle BSM scenarios such as the decay of massive sterile neutrinos and other weakly interacting massive particles, which result in neutrino distributions that may differ substantially from a Fermi-Dirac distribution [16].

Our approach aims to be general; it does not rely on particular cosmological models but is appropriate to the class of Λ cold-dark matter (ΛCDM) models. It extends and explicates recent work [11, 10, 17, 18] on the consistent incorporation of precision observations of the CMB [2] and observations of the light element abundances of helium and deuterium (mass fraction Y_P and relative abundance D/H). The deuterium abundance [9, 3] is now more precisely measured by a significant factor (4 or 5) in relative precision than Y_P. Our results indicate that deuterium is sufficiently well determined to be incorporated into CSM analyses as a fixed prior.

The present work is the first result in an ongoing campaign to incorporate neutrino energy transport into a self-consistent treatment of BBN and recombination. Our approach is being implemented in FORTRAN90/95 as a suite of codes under the working title of "BBN Unitary Recombination Self-consistent Transport" (BURST), which will be made publicly available for use on parallel computing platforms using OPENMPI. The current work is a prerequisite in an ongoing collaboration to develop codes that consistently handle BBN and neutrino energy transport from weak decoupling to the advent of LSS.

The chapter is outlined as follows. We briefly review the pertinent equations from general relativity needed to describe the physics of the comoving frame in Sec.1.2. For all of the physics in this work, entropy plays a dominant role, as detailed in Sec.1.3. We will use entropy and energy conservation to investigate how the plasma temperature changes in Sec.1.4. Our differential equations are derived in conditions close to equilibrium, and so we give a derivation of the covariant form of the Boltzmann equation in Sec.1.5. We end this chapter in Sec.1.6 by transitioning to topics we can study with the techniques

developed in this chapter.

1.2 General Relativity Summary

1.2.1 FLRW

We need general relativity to properly describe the kinematics of the universe. To begin, we make the assumption that the universe is homogeneous and isotropic. This is strictly not true, but the CMBR provides ample evidence that the universe is close (smaller than one part in 10^4) to this geometry[19]. The metric for homogeneous and isotropic conditions, which we write in spherical coordinates for the square of the differential line element ds, is the Friedmann-Lemaître-Robertson-Walker (FLRW) metric:

$$ds^2 = dt^2 - a(t)^2 \left(\frac{dr^2}{1-kr^2} + r^2 d\theta^2 + r^2 \sin^2\theta \, d\phi^2 \right), \tag{1.1}$$

where t, r, θ, ϕ are spacetime coordinates, k is the curvature parameter, and $a(t)$ is the scale factor. Homogeneity and isotropy imply that a is only a function of time t. We will only consider "flat" cosmologies in this work, i.e. when $k = 0$:

$$ds^2 = dt^2 - a(t)^2 \left(dr^2 + r^2 d\theta^2 + r^2 \sin^2\theta \, d\phi^2 \right). \tag{1.2}$$

It will prove useful at this point to switch to rectangular coordinates:

$$ds^2 = dt^2 - a(t)^2 \left(dx^2 + dy^2 + dz^2 \right), \tag{1.3}$$

and write the metric in matrix-form as:

$$g_{\mu\nu} = \begin{pmatrix} 1 & 0 & 0 & 0 \\ 0 & -a^2 & 0 & 0 \\ 0 & 0 & -a^2 & 0 \\ 0 & 0 & 0 & -a^2 \end{pmatrix}. \tag{1.4}$$

We would like to determine the evolution of the scale factor. We need the Einstein field equations to accomplish this task[19]:

$$G_{\mu\nu} = \frac{8\pi}{m_{\rm pl}^2} T_{\mu\nu} + \Lambda g_{\mu\nu}, \tag{1.5}$$

where $G_{\mu\nu}$ is the Einstein tensor, $T_{\mu\nu}$ is the stress–energy tensor, and Λ is the cosmological constant. The Planck mass, $m_{\rm pl}$, is related to Newton's gravitational constant by $G = 1/m_{\rm pl}^2$. The stress–energy tensor is diagonal in homogeneous and isotropic conditions. Therefore, we can write the stress-energy tensor in matrix form as[19]:

$$T^{\mu}_{\nu} = \begin{pmatrix} \rho & 0 & 0 & 0 \\ 0 & -p & 0 & 0 \\ 0 & 0 & -p & 0 \\ 0 & 0 & 0 & -p \end{pmatrix}, \tag{1.6}$$

where ρ is the total energy density and p is the total pressure. Both the energy density and pressure are functions of time. The Einstein tensor is defined by[20]

$$G_{\mu\nu} = R_{\mu\nu} - \frac{1}{2} R g_{\mu\nu}, \tag{1.7}$$

where $R_{\mu\nu}$ and R are the Ricci tensor and Ricci scalar, respectively:

$$R_{\mu\nu} = R^{\lambda}{}_{\mu\lambda\nu}, \tag{1.8}$$

$$R = g^{\mu\nu} R_{\mu\nu}. \tag{1.9}$$

The Ricci tensor uses the Riemann curvature tensor, which in turn we write using the Christoffel symbols:

$$\Gamma^{\lambda}_{\mu\nu} = \frac{1}{2} g^{\lambda\rho} \left(g_{\rho\mu,\nu} + g_{\rho\nu,\mu} - g_{\mu\nu,\rho} \right) \tag{1.10}$$

$$R^{\rho}{}_{\mu\sigma\nu} = \Gamma^{\rho}_{\mu\nu,\sigma} - \Gamma^{\rho}_{\mu\sigma,\nu} + \Gamma^{\rho}_{\sigma\lambda}\Gamma^{\lambda}_{\mu\nu} - \Gamma^{\rho}_{\nu\lambda}\Gamma^{\lambda}_{\mu\sigma}, \tag{1.11}$$

where we have used the notation of the ordinary partial derivative:

$$Q_{,\mu} \equiv \frac{\partial Q}{\partial x^{\mu}}, \tag{1.12}$$

for quantity Q as a function of coordinate x^{μ}. The Christoffel symbols are symmetric in the two lower indicies. In addition, the metric is diagonal and each spatial component of the metric is identical (in cartesian coordinates). Therefore, there are only six unique Christoffel symbols. Of those six, four of the symbols vanish:

$$\Gamma^{0}_{00} = \frac{1}{2} g^{0\rho} \left(g_{\rho 0,0} + g_{\rho 0,0} - g_{00,\rho} \right) = 0, \tag{1.13}$$

$$\Gamma^{i}_{00} = \frac{1}{2} g^{i\rho} \left(g_{\rho 0,0} + g_{\rho 0,0} - g_{00,\rho} \right) = 0, \tag{1.14}$$

$$\Gamma^{0}_{0i} = \frac{1}{2} g^{0\rho} \left(g_{\rho 0,i} + g_{\rho i,0} - g_{i0,\rho} \right) = 0, \tag{1.15}$$

$$\Gamma^{k}_{ij} = \frac{1}{2} g^{k\rho} \left(g_{\rho i,j} + g_{\rho j,i} - g_{ij,\rho} \right) = 0. \tag{1.16}$$

The only non–zero symbols are the one with one time component, and two spatial

components:

$$\Gamma^0_{ij} = \frac{1}{2} g^{0\rho} \left(g_{\rho i,j} + g_{\rho j,i} - g_{ij,\rho} \right) = \frac{1}{2} g^{00} (-g_{ij,0}) = -\frac{1}{2} \frac{2\dot{a}}{a} g_{ij} = -\frac{\dot{a}}{a} g_{ij} = a\dot{a}\,\delta_{ij}, \tag{1.17}$$

$$\Gamma^i_{0j} = \frac{1}{2} g^{i\rho} \left(g_{\rho 0,j} + g_{\rho j,0} - g_{ij,\rho} \right) = \frac{1}{2} g^{ii} g_{ij,0} = \frac{1}{2} g^{ii} \delta^j_i \frac{2\dot{a}}{a} g_{jj} = \frac{\dot{a}}{a} \delta^i_j. \tag{1.18}$$

The notation $\dot{Q}$ indicates differentiation with respect to time.

$T_{\mu\nu}$ is diagonal, so we only need to compute the diagonal components of $G_{\mu\nu}$. First, the time–time component:

$$R_{00} = R^{\rho}{}_{0\rho 0} = \Gamma^{\rho}_{00,\rho} - \Gamma^{\rho}_{0\rho,0} + \Gamma^{\rho}_{\rho\lambda}\Gamma^{\lambda}_{00} - \Gamma^{\rho}_{0\lambda}\Gamma^{\lambda}_{0\rho} \tag{1.19}$$

$$= 0 - 3\,\partial_t \left(\frac{\dot{a}}{a} \right) + 3\frac{\dot{a}}{a} 0 - 3 \left(\frac{\dot{a}}{a} \right)^2 \tag{1.20}$$

$$= -3\frac{\ddot{a}}{a}. \tag{1.21}$$

Next, the spatial components:

$$R_{ii} = R^{\rho}{}_{i\rho i} = \Gamma^{\rho}_{ii,\rho} - \Gamma^{\rho}_{i\rho,i} + \Gamma^{\rho}_{\rho\lambda}\Gamma^{\lambda}_{ii} - \Gamma^{\rho}_{i\lambda}\Gamma^{\lambda}_{i\rho} \tag{1.22}$$

$$= \partial_t (a\dot{a}) - 0 + 3 \left(\frac{\dot{a}}{a} \right) (a\dot{a}) - 2 \left(\frac{\dot{a}}{a} \right) (a\dot{a}) \tag{1.23}$$

$$= \dot{a}^2 + a\ddot{a} + \dot{a}^2 \tag{1.24}$$

$$= 2\dot{a}^2 + a\ddot{a}. \tag{1.25}$$

The Ricci Scalar is:

$$R = g^{\mu\nu}R_{\mu\nu} \tag{1.26}$$
$$= -3\frac{\ddot{a}}{a} - \frac{3}{a^2}(2\dot{a}^2 + a\,\ddot{a}) \tag{1.27}$$
$$= -6\left[\frac{\ddot{a}}{a} + \left(\frac{\dot{a}}{a}\right)^2\right], \tag{1.28}$$

and the Einstein tensor components are:

$$G_{00} = R_{00} - \frac{1}{2}g_{00}R \tag{1.29}$$
$$= -3\frac{\ddot{a}}{a} + 3\left[\frac{\ddot{a}}{a} + \left(\frac{\dot{a}}{a}\right)^2\right] \tag{1.30}$$
$$= 3\left(\frac{\dot{a}}{a}\right)^2, \tag{1.31}$$
$$G_{ii} = R_{ii} - \frac{1}{2}g_{ii}R \tag{1.32}$$
$$= 2\dot{a}^2 + a\,\ddot{a} - 3a^2\left[\frac{\ddot{a}}{a} + \left(\frac{\dot{a}}{a}\right)^2\right] \tag{1.33}$$
$$= -\dot{a}^2 - 2a\,\ddot{a}. \tag{1.34}$$

We will take the cosmological constant to be zero. For cosmologies with a non-zero constant, we will simply add an energy density term to model the presence of dark energy

(see Sec.1.4.4). For the time–time component, Eq.(1.5) yields:

$$G_{00} = \frac{8\pi}{m_{\rm pl}^2} T_{00} \tag{1.35}$$

$$\implies 3\left(\frac{\dot{a}}{a}\right)^2 = \frac{8\pi}{m_{\rm pl}^2} g_{0\mu} T_0^{\mu} \tag{1.36}$$

$$\implies \left(\frac{\dot{a}}{a}\right)^2 = \frac{8\pi}{3m_{\rm pl}^2}\rho \tag{1.37}$$

$$\implies H \equiv \frac{\dot{a}}{a} = \sqrt{\frac{8\pi}{3m_{\rm pl}^2}\rho}. \tag{1.38}$$

Eq.(1.38) is the Friedmann equation and serves to define the Hubble expansion rate H. To simplify, Eq.(1.38) states that the expansion of the universe is proportional to the contents of the universe.

The spatial components of the Einstein field equations give:

$$G_{ii} = \frac{8\pi}{m_{\rm pl}^2} T_{ii}, \tag{1.39}$$

$$\implies -\dot{a}^2 - 2a\ddot{a} = \frac{8\pi}{m_{\rm pl}^2} g_{i\mu} T_i^{\mu} \tag{1.40}$$

$$= \frac{8\pi}{m_{\rm pl}^2}(-a^2)(-p), \tag{1.41}$$

$$\implies \frac{\ddot{a}}{a} = -\frac{1}{2}\left[\left(\frac{\dot{a}}{a}\right)^2 + \frac{8\pi}{m_{\rm pl}^2} p\right] \tag{1.42}$$

$$= -\frac{1}{2}\left[\frac{8\pi}{3m_{\rm pl}^2}\rho + \frac{8\pi}{m_{\rm pl}^2} p\right] \tag{1.43}$$

$$= -\frac{4\pi}{3m_{\rm pl}^2}(\rho + 3p). \tag{1.44}$$

1.2.2 Redshift

We consider a reference frame with an observer at rest at the origin ($r = \theta = \phi = 0$, or equivalently $x = y = z = 0$) at some early time in an FLRW geometry. At a later time,

after the medium has expanded (or contracted), the observer remains at rest (i.e. no change in spatial coordinates)[19]. Now consider another observer which has a four–velocity, u^μ, with non–zero spatial components:

$$u^\mu \equiv \frac{dx^\mu}{ds}, \tag{1.45}$$

where ds is the differential line element used in Eq.(1.3). To describe u^μ, we use the geodesic equation for a freely–streaming observer[19]:

$$\frac{du^\mu}{d\lambda} + \Gamma^\mu_{\alpha\beta} u^\alpha \frac{dx^\beta}{d\lambda} = 0, \tag{1.46}$$

where λ is an affine parameter characterizing the evolution of u^μ on the world line of the second observer. The equivalence principle[20] guarantees there exists a local inertial reference frame where the four–velocity of the second observer satisfies:

$$g_{\mu\nu} u^\mu u^\nu = 1. \tag{1.47}$$

In the reference frame of the first observer:

$$g_{\mu\nu} u^\mu u^\nu = (u^0)^2 - a^2 |\vec{u}|^2 = 1 \tag{1.48}$$

$$\implies du^0 = a^2 \frac{|\vec{u}|}{u^0} d|\vec{u}|, \tag{1.49}$$

where u^0 is the time component of the four–velocity, and $\vec{u}$ is the magnitude of the spatial components. If we set $d\lambda = ds$, then the time component of Eq.1.46 becomes:

$$0 = \frac{du^0}{ds} + \Gamma^0_{\alpha\beta} u^\alpha \frac{dx^\beta}{ds} \tag{1.50}$$

$$= \frac{du^0}{ds} + a\dot{a}\delta_{ij} u^i \frac{dx^j}{ds} \tag{1.51}$$

$$= \frac{du^0}{ds} + a\dot{a}\delta_{ij} u^i u^j \tag{1.52}$$

$$= \frac{du^0}{ds} + a\dot{a}|\vec{u}|^2. \tag{1.53}$$

If we substitute Eq.(1.49) into Eq.(1.53), we have:

$$0 = \frac{du^0}{ds} + a\dot{a}|\vec{u}|^2 \tag{1.54}$$

$$= a^2 \frac{|\vec{u}|}{u^0} \frac{d|\vec{u}|}{ds} + a\dot{a}|\vec{u}|^2 \tag{1.55}$$

$$\implies 0 = \frac{1}{u^0} \frac{d|\vec{u}|}{ds} + \frac{\dot{a}}{a}|\vec{u}|. \tag{1.56}$$

Recall that $u^0 \equiv dt/ds$, implying:

$$0 = \frac{d|\vec{u}|}{dt} + \frac{\dot{a}}{a}|\vec{u}|, \tag{1.57}$$

$$\implies d|\vec{u}| = -\frac{|\vec{u}|}{a} da, \tag{1.58}$$

$$\implies |\vec{u}| \propto \frac{1}{a}. \tag{1.59}$$

Eq.(1.59) is the redshift (or alternatively the blueshift) in an expanding (contracting) universe. The four–momentum is proportional to the four–velocity: $p^\mu \sim u^\mu$, implying the three-momentum redshifts with increasing a, regardless of whether the particle is massive or not. If the second observer is a particle on a timelike trajectory (e.g. a massive particle), then the particle will asymptotically come to rest in the reference frame of the

first observer in a continuously expanding universe[19]. We call the reference frame of the first observer the *comoving* frame. This choice of reference frame allows us to define thermodynamic quantities like temperature, pressure, chemical potential, and energy distributions, which we already implicitly assumed when writing Eq.(1.6).

In that vein, we take the covariant derivative (notated as $Q^{\nu}_{;\mu} = Q^{\nu}_{,\mu} + \Gamma^{\nu}_{\mu\sigma} Q^{\sigma}$) of the zero-component of the stress-energy tensor to find[19]:

$$T^{0\mu}{}_{;\mu} \equiv T^{0\mu}{}_{,\mu} + \Gamma^{0}_{\mu\nu} T^{\mu\nu} + \Gamma^{\mu}_{\mu\nu} T^{0\nu} = 0 \tag{1.60}$$

$$= \partial_t \rho + \Gamma^{0}_{\mu\nu} g^{\lambda\nu} T^{\mu}_{\lambda} + \Gamma^{\mu}_{\mu\nu} g^{\lambda\nu} T^{0}_{\lambda} \tag{1.61}$$

$$= \partial_t \rho + 3a\dot{a} \left(-\frac{1}{a^2} \right) (-p) + 3\frac{\dot{a}}{a}\rho \tag{1.62}$$

$$= \frac{1}{a^3} \left(a^3 \partial_t \rho + 3a^2 \dot{a} \rho + 3pa^2 \dot{a} \right), \tag{1.63}$$

where $\partial_\mu Q = \partial Q / \partial x^\mu$. A comoving volume V element scales as $\sim a^3$, implying:

$$a^3 \partial_t \rho + 3a^2 \dot{a} \rho = -3pa^2 \dot{a} \tag{1.64}$$

$$\implies V \partial_t \rho + \rho \, \partial_t V = -p \, \partial_t V \tag{1.65}$$

$$\implies d(\rho V) = -p \, dV, \tag{1.66}$$

recovering the first law of thermodynamics at constant entropy. For a simple equation of state, $p = w\rho$, for constant w [19]:

$$d(\rho V) = -p \, dV \tag{1.67}$$

$$\implies V \, d\rho + \rho \, dV = -w\rho \, dV \tag{1.68}$$

$$\implies V \, d\rho = -(1+w)\rho \, dV \tag{1.69}$$

$$\implies \rho \propto V^{-(1+w)} \propto a^{-3(1+w)} \tag{1.70}$$

In radiation-dominated conditions, $w = 1/3 \implies \rho \propto a^{-4}$. In equilibrium, the energy density of an ultra-relativistic boson species is:

$$\rho = g\frac{\pi^2}{30}T^4 \propto a^{-4} \implies T \propto \frac{1}{a}, \tag{1.71}$$

where g is the single–particle internal degrees of freedom. Eqs.(1.59) and (1.71) show the three-momentum and the temperature redshift with increasing scale factor, in equilibrium. Therefore, the quantity:

$$\varepsilon \equiv \frac{p}{T} \sim \text{const.} \tag{1.72}$$

is a comoving invariant, where we have called the magnitude of the three–momentum p. We will use ε when we discretize energy spectra. For example, in homogeneous and isotropic conditions, the phase-space occupation probability for an ultra–relativistic $(E = p)$ fermion in equilibrium is:

$$f(\vec{x},\vec{p}) = f(p) = \frac{1}{e^{p/T}+1} \tag{1.73}$$

$$\implies f(\varepsilon) = \frac{1}{e^{\varepsilon}+1}. \tag{1.74}$$

We have placed many conditions on $f(\varepsilon)$ when writing Eq.(1.74), chief among them being the condition of thermal equilibrium. We will discuss the choice of T in Sec.1.5.

1.3 Entropy considerations

The entropy will play an important role in the description of the early universe. We can describe the entropy, S, of an ideal gas using its extensive property[21]:

$$S = \frac{E + pV - \sum \mu_i N_i}{T}. \tag{1.75}$$

For the purposes of this work, we will assume the chemical potentials, μ_i, are small for the plasma constituents which carry the bulk of the entropy. If we write the total internal energy in terms of the energy density, $E = \rho V$, we can rearrange terms to find the entropic density:

$$s_V \equiv \frac{S}{V} = \frac{\rho + p}{T}, \tag{1.76}$$

in terms of the energy density, pressure, and temperature.

We are interested in epochs of the early universe where the energy density (and by extension entropic density) is dominated by radiation. The equation of state for radiation is $p = \rho/3$, and the energy density is:

$$\rho = \begin{cases} g\dfrac{\pi^2}{30}T^4 & \text{BE} \\ g\dfrac{7}{8}\dfrac{\pi^2}{30}T^4 & \text{FD} \end{cases}, \tag{1.77}$$

for Bose-Einstein (BE) and Fermi-Dirac (FD) statistics. The quantity g is the spin degrees of freedom, and we have assumed zero chemical potentials in both cases for the energy density. Our expression for the entropic density is:

$$\begin{aligned} s_V &= \frac{\rho + p}{T} && (1.78)\\ &= \frac{4}{3T}\left[\sum_i g_i^{(b)}\frac{\pi^2}{30}T_i^4 + \sum_j g_j^{(f)}\frac{7}{8}\frac{\pi^2}{30}T_j^4\right] && (1.79)\\ &= \frac{4}{3T}\frac{\pi^2}{30}T^4\left[\sum_i g_i^{(b)}\left(\frac{T_i}{T}\right)^4 + \frac{7}{8}\sum_j g_j^{(f)}\left(\frac{T_j}{T}\right)^4\right] && (1.80)\\ &\equiv \frac{2\pi^2}{45}g_{\star S}T^3, && (1.81) \end{aligned}$$

where $g_{\star S}$ is an effective–entropic–spin statistic[19]. In the definition of $g_{\star S}$, we allow for the plasma constituents to have different temperatures, although in practice this is unnecessary.

Assuming no heat flow into or out of the plasma, the total entropy remains constant. This fact allows us to determine how the temperature changes between an initial epoch (i) and a final epoch (f):

$$S_i = S_f \implies \frac{2\pi^2}{45} g_{\star S,i} T_i^3 V_i = \frac{2\pi^2}{45} g_{\star S,f} T_f^3 V_f \tag{1.82}$$

$$\implies \frac{T_i}{T_f} = \left(\frac{g_{\star S,f} V_f}{g_{\star S,i} V_i}\right)^{1/3} = \frac{a_f}{a_i}\left(\frac{g_{\star S,f}}{g_{\star S,i}}\right)^{1/3}. \tag{1.83}$$

We define the comoving temperature $T_{\rm cm}$ as:

$$T_{{\rm cm},f} \equiv T_{{\rm cm},i}\frac{a_i}{a_f} = T\frac{a_i}{a_f}, \tag{1.84}$$

where we have taken the initial comoving temperature equal to the plasma temperature. Therefore:

$$\frac{T_i}{T_f}\frac{a_i}{a_f} = \frac{T_{{\rm cm},f}}{T_f} = \left(\frac{g_{\star S,f}}{g_{\star S,i}}\right)^{1/3}. \tag{1.85}$$

An important example is the epoch of electron–positron annihilation. At a temperature of ~ 1 MeV, the plasma contains photons, electrons, and positrons all in thermal and chemical equilibrium with one another. If we make the following assumptions:

1. the neutrinos are completely decoupled at this temperature,
2. the positrons and electrons have a negligible chemical potential,
3. the mass of the electron m_e is also negligible;

then we find the entropic degrees of freedom to be:

$$g_{\star S,i} = 2 + \frac{7}{8}(2+2) = \frac{11}{2}. \tag{1.86}$$

The positrons and electrons annihilate with one another at a temperature of $T \sim 100$ keV,

and the positrons are effectively gone at $T \sim 10$ keV, implying $g_{\star S,f} = 2$. Therefore:

$$\frac{T_{\rm cm}}{T} = \left(\frac{2}{11/2}\right)^{1/3} = \left(\frac{4}{11}\right)^{1/3}, \tag{1.87}$$

where we have dropped the f subscripts for convenience.

At this point, we diverge and discuss particles which have relativistic dispersion relations but non-negligible mass terms. In the case of a non-degenerate ($\mu = 0$) fermionic species, the energy density is:

$$\rho = \frac{g}{(2\pi)^3}\int d^3p \frac{E}{e^{E/T}+1} \tag{1.88}$$

$$= \frac{g}{2\pi^2}\int_0^\infty dp\, p^2 E e^{-E/T}\frac{1}{1+e^{-E/T}} \tag{1.89}$$

$$= \frac{g}{2\pi^2}\int_0^\infty dp\, p^2 E e^{-E/T}\sum_{n=0}^{\infty}(-1)^n e^{-nE/T} \tag{1.90}$$

$$= \frac{g}{2\pi^2}\sum_{n=0}^{\infty}(-1)^n \int_0^\infty dp\, p^2 E e^{-(n+1)E/T} \tag{1.91}$$

$$= \frac{g}{2\pi^2}\sum_{n=1}^{\infty}(-1)^{n+1} \int_0^\infty dp\, p^2 E e^{-nE/T}. \tag{1.92}$$

The dispersion relation for relativistic particles with small masses is:

$$E = \sqrt{p^2+m^2} \tag{1.93}$$

$$\simeq p + \frac{m^2}{2p}, \tag{1.94}$$

to second order in m. Substituting Eq.(1.94) into Eq.(1.92), we find:

$$\rho = \frac{g}{2\pi^2}\sum_{n=1}^{\infty}(-1)^{n+1}\int_0^{\infty} dp\, p^2 E e^{-nE/T} \tag{1.95}$$

$$\simeq \frac{g}{2\pi^2}\sum_{n=1}^{\infty}(-1)^{n+1}\int_0^{\infty} dp\, p^2\left(p+\frac{m^2}{2p}\right)\exp\left[-\frac{n}{T}\left(p+\frac{m^2}{2p}\right)\right] \tag{1.96}$$

$$= \frac{g}{2\pi^2}\sum_{n=1}^{\infty}(-1)^{n+1}\int_0^{\infty} dp\, p^3\left(1+\frac{m^2}{2p^2}\right)\exp\left(-\frac{np}{T}\right)\exp\left(-\frac{nm^2}{2pT}\right) \tag{1.97}$$

$$\simeq \frac{g}{2\pi^2}\sum_{n=1}^{\infty}(-1)^{n+1}\int_0^{\infty} dp\, p^3 e^{-np/T}\left(1+\frac{m^2}{2p^2}\right)\left(1-\frac{nm^2}{2pT}\right) \tag{1.98}$$

$$\equiv \frac{gT^4}{2\pi^2}\sum_{n=1}^{\infty}(-1)^{n+1}\int_0^{\infty} d\varepsilon\,\varepsilon^3 e^{-n\varepsilon}\left(1+\frac{z^2}{2\varepsilon^2}\right)\left(1-\frac{nz^2}{2\varepsilon}\right). \tag{1.99}$$

Eq.(1.99) serves to define the dimensionless mass $z \equiv m/T$. We are only keeping terms to order z^2. Therefore, Eq.(1.99) reduces to:

$$\rho = \frac{gT^4}{2\pi^2}\sum_{n=1}^{\infty}(-1)^{n+1}\int_0^{\infty} d\varepsilon\,\varepsilon^3 e^{-n\varepsilon}\left(1+\frac{z^2}{2\varepsilon^2}-\frac{nz^2}{2\varepsilon}\right) \tag{1.100}$$

$$= \frac{gT^4}{2\pi^2}\sum_{n=1}^{\infty}(-1)^{n+1}\left(\int_0^{\infty} d\varepsilon\,\varepsilon^3 e^{-n\varepsilon}+\frac{z^2}{2}\int_0^{\infty} d\varepsilon\,\varepsilon e^{-n\varepsilon}-\frac{nz^2}{2}\int_0^{\infty} d\varepsilon\,\varepsilon^2 e^{-n\varepsilon}\right) \tag{1.101}$$

$$= \frac{gT^4}{2\pi^2}\sum_{n=1}^{\infty}(-1)^{n+1}\left(\frac{3!}{n^3}+\frac{z^2}{2}\frac{1!}{n^2}-\frac{nz^2}{2}\frac{2!}{n^3}\right) \tag{1.102}$$

$$= \frac{gT^4}{2\pi^2}\left(6\frac{7}{8}\frac{\pi^4}{90}-\frac{z^2}{2}\frac{1}{2}\frac{\pi^2}{6}\right) \tag{1.103}$$

$$= \frac{7}{8}\frac{g\pi^2 T^4}{30}\left(1-\frac{5}{7\pi^2}z^2\right) \tag{1.104}$$

$$= \rho^{(m=0)}\left(1-\frac{5}{7\pi^2}z^2\right) \tag{1.105}$$

Similarily, for the pressure:

$$p = g\int \frac{d^3p}{(2\pi)^3}\frac{p^2}{3E}\frac{1}{e^{E/T}+1} \tag{1.106}$$

$$= p^{(m=0)}\left(1-\frac{15}{7\pi^2}z^2\right), \tag{1.107}$$

and the entropy:

$$s_V = \frac{7}{8}\frac{g\pi^2T^3}{30}\left[1-\frac{5}{7\pi^2}z^2+\frac{1}{3}\left(1-\frac{15}{7\pi^2}z^2\right)\right] \tag{1.108}$$

$$= \frac{7}{8}\frac{g\pi^2T^3}{30}\frac{4}{3}\left(1-\frac{15}{14\pi^2}z^2\right) \tag{1.109}$$

$$= s_V^{(m=0)}\left(1-\frac{15}{14\pi^2}z^2\right) \tag{1.110}$$

If we re-examine the example of electron–positron annihilation, but drop the assumption that $m_e = 0$:

$$S_i = S_f \implies \frac{2\pi^2}{45}T_i^3a_i^3\left[2+\frac{7}{8}(2+2)\left(1-\frac{15}{14\pi^2}z^2\right)\right] = \frac{2\pi^2}{45}T_f^3a_f^3[2], \tag{1.111}$$

where $z = m_e/T_i$. Solving for the ratio of temperatures:

$$\left(\frac{T_{\rm cm}}{T}\right)^3 = \frac{2}{\frac{11}{2}-\frac{15}{4\pi^2}z^2} \tag{1.112}$$

$$\implies \frac{T_{\rm cm}}{T} = \left(\frac{4}{11}\right)^{1/3}\left(1-\frac{15}{22\pi^2}z^2\right)^{-1/3} \tag{1.113}$$

$$= \left(\frac{4}{11}\right)^{1/3}\left(1+\frac{5}{22\pi^2}z^2\right) \tag{1.114}$$

$$\equiv \left(\frac{4}{11}\right)^{1/3}(1+\delta_{\rm est.}), \tag{1.115}$$

yields the second–order correction to the factor $(4/11)^{1/3}$, where we have defined the

Table 1.1: Table of T_i, $\delta_{\text{est.}}$, and $\delta_{\text{calc.}}$. The differences between $\delta_{\text{est.}}$ and $\delta_{\text{calc.}}$ are due to the inclusion of nucleosynthesis terms in the actual calculations.

T_i (MeV)	δ_{est}	δ_{calc}
1.0	6.013×10^{-3}	5.911×10^{-3}
2.0	1.503×10^{-3}	1.404×10^{-3}
3.0	6.681×10^{-4}	5.593×10^{-4}
5.0	2.405×10^{-4}	1.250×10^{-4}
6.0	1.670×10^{-4}	5.013×10^{-5}
7.0	1.227×10^{-4}	5.012×10^{-6}
8.0	9.395×10^{-5}	-2.427×10^{-5}
9.0	7.423×10^{-5}	-4.438×10^{-5}
10.0	6.013×10^{-5}	-5.874×10^{-5}
20.0	1.503×10^{-5}	-1.047×10^{-4}
30.0	6.681×10^{-6}	-1.132×10^{-4}

relative change from $(4/11)^{1/3}$ as $\delta_{\text{est.}}$.

Table 1.1 gives various values of the initial temperature (same as the initial comoving temperature), estimated relative changes using $\delta_{\text{est.}}$, and calculated relative changes using BURST, encoded in the value $\delta_{\text{calc.}}$. The calculated values include changes from nucleosynthesis. The predictions get worse as the initial temperature increases as the nucleosynthesis corrections dominate the change by increasing the plasma temperature, yet are not included in the $\delta_{\text{est.}}$ correction.

Figure 1.1 shows the evolution of the temperature ratio T_{cm}/T as a function of the comoving temperature for a calculation where $T_i = 3$ MeV. The epoch of electron–positron annihilation occurs mostly in the temperature range of 100's keV to 10's keV. The quantity $g_{\star S}$ is dynamic and not analytically calculable. In a universe with no asymmetry between electrons and positrons, the curve of Fig.1.1 would require an evolution of only the plasma temperature, the subject of the next section, with respect to either time or scale factor. In the case of non-zero baryon content as in Fig.1.1, the plasma temperature, electron chemical potential, and nuclear abundances all need to be evolved. This is the

subject of chapter 2.

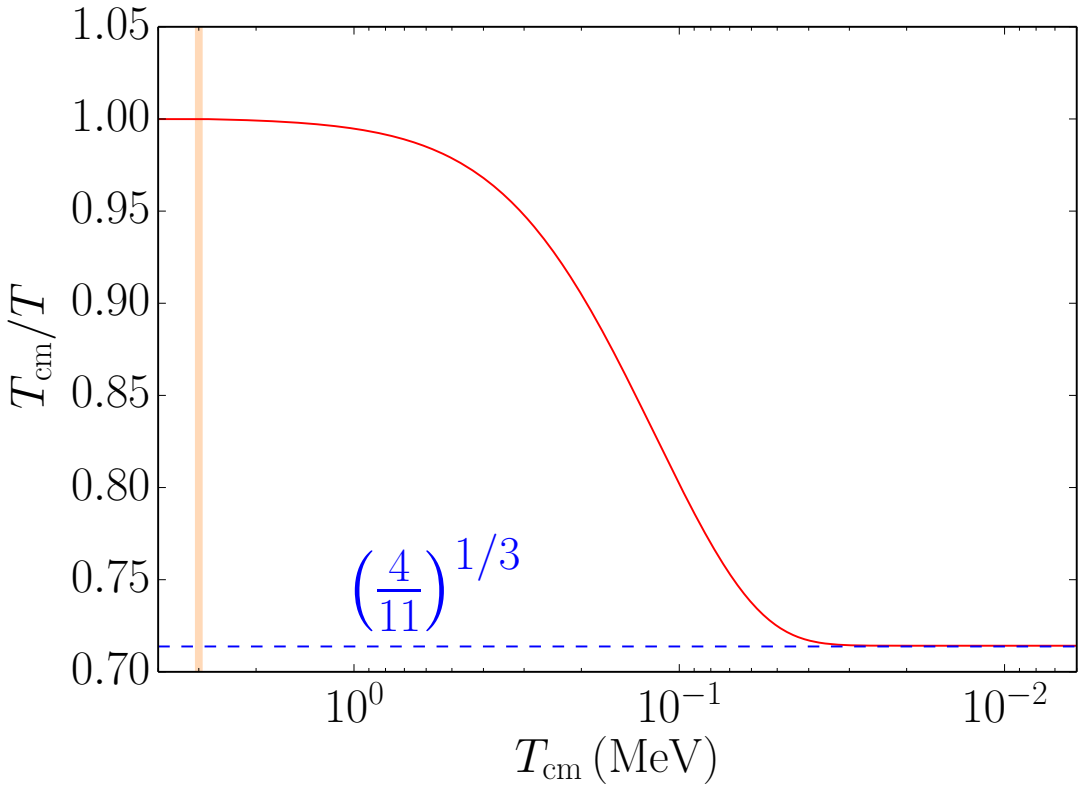

Figure 1.1: The evolution of $T_{\rm cm}/T$ as a function of $T_{\rm cm}$. The vertical shaded bar is located at $T_i = 3$ MeV.

1.4 Plasma temperature derivative

The constituents of the plasma are in thermal equilibrium and may or may not be in chemical equilibrium. The temperature follows a non-trivial evolution. The first law of thermodynamics in comoving coordinates states[22]:

$$d(\rho V) + p\,dV - dQ|_{(a,T)} = 0 \tag{1.116}$$

$$\Longrightarrow V\,d\rho + (\rho + p)dV - dQ|_{(a,T)} = 0, \tag{1.117}$$

where the heat added dQ is at fixed scale factor and temperature. Eq.(1.116) is Eq.(1.66) with a non-zero heat term. Dividing Eq.(1.116) by dt:

$$V\frac{d\rho}{dt}+(\rho+p)\frac{dV}{dt}-\left(\frac{\partial Q}{\partial t}\right)_{a,T}=0. \tag{1.118}$$

If we use the chain rule on $d\rho/dt$, we find:

$$V\frac{d\rho}{dT}\frac{dT}{dt}+(\rho+p)\frac{dV}{dt}-\left(\frac{\partial Q}{\partial t}\right)_{a,T}=0 \tag{1.119}$$

$$\Longrightarrow \frac{dT}{dt}=-\frac{(\rho+p)\frac{dV}{dt}-\left(\frac{\partial Q}{\partial t}\right)_{a,T}}{V\frac{d\rho}{dT}}. \tag{1.120}$$

$V\sim a^3 \implies dV/dt=(3V/a)(da/dt)=3VH$ where H is the Hubble rate. Thus:

$$\frac{dT}{dt}=-3H\frac{\rho+p-\frac{1}{3H}\left(\frac{\partial\rho}{\partial t}\right)_{a,T}}{\frac{d\rho}{dT}}, \tag{1.121}$$

is our conditional expression for the temperature derivative. We will evaluate this expression in certain limits to fully understand each term. The inclusion of the heat density term:

$$\left(\frac{\partial\rho}{\partial t}\right)_{a,T}, \tag{1.122}$$

allows for out-of-equilibrium processes. Examples of microphysical processes which produce non-zero heat density include: binding energy release from nucleosynthesis; cooling from partial heating of decoupled species; and entropy injection by heavy-particle decay. We will ignore the heat density and consider some limiting situations in the following subsections.

1.4.1 Radiation energy density

The equation of state for radiation is $p = \rho/3 \sim T^4$. The derivative of the energy density with respect to temperature is $d\rho/dT = 4\rho/T$, giving the temperature derivative as:

$$\frac{dT}{dt} = -3H\frac{\rho + p}{\frac{d\rho}{dT}} = -3H\frac{\frac{4}{3}\rho}{\frac{4\rho}{T}} = -HT. \tag{1.123}$$

1.4.2 Matter energy density

The equation of state is normally written as $p = 0$. However, we will use the ideal gas law from kinetic theory for point particles to write the pressure as $p = nT$ and the energy density as $\rho = mn + 3nT/2$ since interacting matter has a well-defined temperature. The quantity n is the number density, and m is the mass of the matter particles. Observe:

$$\frac{d\rho}{dT} = \frac{3}{2}n + \left(m + \frac{3}{2}T\right)\frac{dn}{dT} \tag{1.124}$$

$$= \frac{3}{2}n + \left(m + \frac{3}{2}T\right)\frac{dn}{da}\frac{da}{dt}\frac{dt}{dT}. \tag{1.125}$$

$n \sim a^{-3} \implies dn/da = -3n/a$. Thus:

$$\frac{d\rho}{dT} = \frac{3}{2}n - \left(m + \frac{3}{2}T\right)3nH\frac{dt}{dT} = \frac{3}{2}n - 3H\rho\frac{dt}{dT}. \tag{1.126}$$

Multiplying Eq.(1.121) by $d\rho/dT$ gives:

$$\frac{dT}{dt}\left[\frac{3}{2}n - 3H\rho\frac{dt}{dT}\right] = -3H(\rho + p) \tag{1.127}$$

$$\implies \frac{dT}{dt} = -3H\frac{p}{\frac{3}{2}n} \tag{1.128}$$

$$\implies \frac{dT}{dt} = -2HT. \tag{1.129}$$

1.4.3 Mixed radiation and matter densities

We will define η to be the ratio of matter and radiation number densities: $\eta \equiv n_m/n_r$. When both radiation and matter are present, and in thermal equilibrium with one another, we arrive at the following expression for the temperature derivative:

$$\frac{dT}{dt} = -3H\frac{\frac{4}{3}\rho_r + n_m T}{\frac{4\rho_r}{T} + \frac{3}{2}n_m} \tag{1.130}$$

$$= -HT\frac{\rho_r + \frac{3}{4}n_m T}{\rho_r + \frac{3}{8}n_m T}, \tag{1.131}$$

where Eq.(1.130) used Eq.(1.128) for the matter terms in the numerator and denominator. For radiation, the energy density and product of number density and temperature are related by a constant: $\rho_r = C_1 n_r T$, leaving us with:

$$\frac{dT}{dt} = -HT\frac{1+3C_2\eta}{1+\frac{3}{2}C_2\eta} \rightarrow \begin{cases} -HT & \text{as } \eta \rightarrow 0 \\ -2HT & \text{as } \eta \rightarrow \infty \end{cases}, \tag{1.132}$$

where $C_2 = 1/4C_1$. We recover the expressions for dT/dt in pure radiation or pure matter conditions when we take the appropriate limit. Note that even in a matter–energy–dominated environment, a high entropy condition (correspondingly small η) gives a temperature derivative typical to a radiation–dominated environment – assuming the matter and radiation are still thermally coupled.

1.4.4 Dark energy density

To calculate the time derivative of the temperature in a dark–energy–dominated universe, we refer back to Eq.(1.5) with a non-zero Λ:

$$G_{\mu\nu} = \frac{8\pi}{m_{\rm pl}^2} T_{\mu\nu} + \Lambda g_{\mu\nu} \tag{1.133}$$

$$\equiv \frac{8\pi}{m_{\rm pl}^2} T_{\mu\nu} + \frac{8\pi}{m_{\rm pl}^2} \rho_\Lambda g_{\mu\nu}, \tag{1.134}$$

where we have defined the cosmological constant Λ in terms of an energy–density–like quantity ρ_Λ. The rhs of Eq.(1.134) is:

$$\frac{8\pi}{m_{\rm pl}^2}(T_{\mu\nu} + \rho_\Lambda g_{\mu\nu}) = \frac{8\pi}{m_{\rm pl}^2}(g_{\mu\sigma} T^\sigma_\nu + \rho_\Lambda g_{\mu\nu}) \tag{1.135}$$

$$= \frac{8\pi}{m_{\rm pl}^2} \begin{pmatrix} \rho_T + \rho_\Lambda & 0 & 0 & 0 \\ 0 & a^2 p_T - a^2 \rho_\Lambda & 0 & 0 \\ 0 & 0 & a^2 p_T - a^2 \rho_\Lambda & 0 \\ 0 & 0 & 0 & a^2 p_T - a^2 \rho_\Lambda \end{pmatrix}, \tag{1.136}$$

where we have adorned a subscript T to the quantities in the stress–energy tensor that do not involve the dark energy (i.e. the radiation and matter components). We take the matrix in Eq.(1.136) (call it $\widetilde{T}$) and write it like the stress–energy tensor:

$$\widetilde{T}^\mu_\nu = g^{\mu\sigma}\widetilde{T}_{\sigma\nu} = \begin{pmatrix} \rho_T + \rho_\Lambda & 0 & 0 & 0 \\ 0 & -(p_T - \rho_\Lambda) & 0 & 0 \\ 0 & 0 & -(p_T - \rho_\Lambda) & 0 \\ 0 & 0 & 0 & -(p_T - \rho_\Lambda) \end{pmatrix}. \tag{1.137}$$

We define the time–time component to be $\rho_{\rm tot}$, and the space–space components to be $p_{\rm tot}$:

$$\begin{cases} \rho_{\rm tot} = \rho_T + \rho_\Lambda \\ p_{\rm tot} = p_T - \rho_\Lambda \end{cases} . \tag{1.138}$$

In the dark–energy–dominated limit, $\rho_T, p_T \to 0$. $\rho_{\rm tot}$ is simply ρ_Λ and $p_{\rm tot} = -\rho_\Lambda$. Therefore, the equation of state for dark energy is $p = -\rho = \text{const}$. In this case, $d\rho/dT = 0$ and $p + \rho = 0$, thereby affecting no change in the denominator and numerator of Eq.(1.121). If there are small amounts of coupled radiation and matter in the dark–energy–dominated universe, the presence of dark energy does not explicitly affect the temperature derivative.

1.4.5 Final expression for the temperature derivative

In the case where the universe is dominated by a paticle species which is neither ultra-relativistic nor ultra-massive, the temperature derivative is the same as Eq.(1.121). We cannot obtain a simple expression in this case, and would have to integrate the differential equation to determine the temperature evolution. To summarize, the expression for the temperature derivative is:

$$\frac{dT}{dt} = -3H \frac{\tilde{\rho} + p - \frac{1}{3H}\left(\frac{\partial \rho}{\partial t}\right)_{a,T}}{\overline{\frac{d\rho}{dT}}}, \tag{1.139}$$

where $\tilde{\rho}$ is the total energy density less the energy density of an ultra-massive species, and $\overline{\frac{d\rho}{dT}}$ is the total derivative of the energy density with respect to temperature, where scale factor is held constant for the case of an ultra-massive particle species. Sec.2.2.3 explains the integration of Eq.(1.139).

1.5 Boltzmann equation

Neutrino energy transport requires the examination of the occupation probabilities, denoted f. To study this evolution, we use the Boltzmann equation[23]:

$$\frac{df}{d\lambda} = \hat{C}'[f], \tag{1.140}$$

where $\hat{C}'$ is a collision operator, and λ is an affine parameter implicitly defined using the four–momentum as [23]:

$$p^\mu = \frac{dx^\mu}{d\lambda}. \tag{1.141}$$

Using the chain rule, we can write the lhs of the Boltzmann equation as:

$$\frac{df}{d\lambda} = \frac{df}{dx^\mu}\frac{dx^\mu}{d\lambda} = p^\mu \frac{df}{dx^\mu}. \tag{1.142}$$

We will assume that the occupation probabilities are functions of time $t = x^0$, position x^i, energy $E = p^0$, and momentum direction p^i. We write the spatial components of the four-momentum such that:

$$g_{\mu\nu} p^\mu p^\nu = E^2 - a^2 p^2 = m^2. \tag{1.143}$$

It will elucidate the present task if we define a "local momentum" $\overline{p}$ such that[24]:

$$E^2 - \overline{p}^2 = m^2 \implies \overline{p}^i = a p^i. \tag{1.144}$$

Returning to Eq.(1.142), we write the full derivative of f in terms of its components:

$$\frac{df}{dx^\mu} = \frac{\partial f}{\partial x^\mu} + \frac{\partial f}{\partial p^\nu}\frac{dp^\nu}{dx^\mu} \tag{1.145}$$

$$= \frac{\partial f}{\partial x^\mu} + \frac{\partial f}{\partial p^\nu}\frac{dp^\nu}{d\lambda}\frac{d\lambda}{dx^\mu}. \tag{1.146}$$

The only term in Eq.(1.146) which we need to deduce is $dp^\nu/d\lambda$. To decipher this term, we use the geodesic equation with our choice of affine parameter:

$$\frac{dp^\mu}{d\lambda} + \Gamma^\nu_{\alpha\beta} p^\alpha p^\beta = 0 \tag{1.147}$$

$$\implies \frac{dp^\mu}{d\lambda} = -\Gamma^\nu_{\alpha\beta} p^\alpha p^\beta \tag{1.148}$$

$$\implies \hat{L}'[f] \equiv \frac{df}{d\lambda} = p^\mu \frac{\partial f}{\partial x^\mu} - \Gamma^\nu_{\alpha\beta} p^\alpha p^\beta \frac{\partial f}{\partial p^\nu}, \tag{1.149}$$

where Eq.(1.149) serves to define a form of the Liouville operator, $\hat{L}'$. We can apply the FLRW symmetries to simplify Eq.(1.149):

$$\text{Homogeneity}: \quad p^\mu \frac{\partial f}{\partial x^\mu} = E\frac{\partial f}{\partial t}, \tag{1.150}$$

$$\text{Isotropy}: \quad \Gamma^\nu_{\alpha\beta} p^\alpha p^\beta \frac{\partial f}{\partial p^\nu} = \Gamma^0_{\alpha\beta} p^\alpha p^\beta \frac{\partial f}{\partial E}. \tag{1.151}$$

The only non-zero Chistoffel symbols in the isotropy condition are $\Gamma^0_{ij} = a\dot{a}\delta_{ij}$, leaving the Boltzmann equation as:

$$\hat{L}^{'}[f] = E\frac{\partial f}{\partial t} - \Gamma^0_{\alpha\beta}p^{\alpha}p^{\beta}\frac{\partial f}{\partial E} \tag{1.152}$$

$$= E\frac{\partial f}{\partial t} - a\dot{a}\delta_{ij}p^i p^j\frac{\partial f}{\partial E} \tag{1.153}$$

$$= E\frac{\partial f}{\partial t} - a\dot{a}p^2\frac{\partial f}{\partial E} \tag{1.154}$$

$$= E\frac{\partial f}{\partial t} - \frac{\dot{a}}{a}\overline{p}^2\frac{\partial f}{\partial E} \tag{1.155}$$

$$= E\frac{\partial f}{\partial t} - H\overline{p}^2\frac{\partial f}{\partial E} = \hat{C}^{'}[f]. \tag{1.156}$$

At this point, for convenience, we will drop the bar notation on the local momentum and simply set $\overline{p}^i \to p^i$. For particles with ultra-relativistic kinematics, the Liouville operator and Boltzmann equation can be written as:

$$\hat{L}[f] = \frac{\partial f}{\partial t} - Hp\frac{\partial f}{\partial p}, \tag{1.157}$$

$$\hat{L}[f] = \hat{C}[f], \tag{1.158}$$

where $\hat{C}[f]$ is a different form of the collision operator than the one defined in Eq.(1.140). If we assume ultra-relativistic kinematics, Eq.(1.156) becomes:

$$\hat{L}^{'}[f] = p\left(\frac{\partial f}{\partial t} - Hp\frac{\partial f}{\partial p}\right) = \hat{C}^{'}[f] \tag{1.159}$$

$$\implies \hat{L}[f] = \left(\frac{\partial f}{\partial t} - Hp\frac{\partial f}{\partial p}\right) = \frac{1}{p}\hat{C}^{'}[f] = \hat{C}[f], \tag{1.160}$$

relating the two forms of the collision operators. Per Sec.1.2.2, we choose to use ε over p as the independent variable in our occupation probabilities. With this choice:

$$\frac{\partial f}{\partial p} = \frac{\partial f}{\partial \varepsilon}\frac{d\varepsilon}{dp} \tag{1.161}$$

$$= \frac{\partial f}{\partial \varepsilon}\left(\frac{1}{T} - \frac{p}{T^2}\frac{dT}{dt}\frac{dt}{dp}\right). \tag{1.162}$$

Using the geodesic equation:

$$\frac{dp}{dt} = \frac{dp}{d\lambda}\frac{d\lambda}{dt} \tag{1.163}$$

$$= \frac{1}{p}\frac{dp^0}{dt} \tag{1.164}$$

$$= \frac{1}{p}\left(-\Gamma^0_{\alpha\beta}p^\alpha p^\beta\right) \tag{1.165}$$

$$= \frac{1}{p}\left(-a\dot{a}\delta_{ij}\frac{p^i p^j}{a^2}\right) \tag{1.166}$$

$$= \frac{1}{p}\left(-\frac{\dot{a}}{a}p^2\right) \tag{1.167}$$

$$= -pH \tag{1.168}$$

If we choose a "comoving temperature parameter" $T = T_{\rm cm}$ such that:

$$\frac{dT_{\rm cm}}{dt} \equiv -HT, \tag{1.169}$$

then Eq.(1.162) vanishes, and the lhs of the Boltzmann equation simplifies such that:

$$\frac{df(t,\varepsilon)}{dt} = \hat{C}[f]. \tag{1.170}$$

The comoving temperature need not be a temperature describing an equilibrium distribution. It is simply an energy scale we use to convert ε values into momentum values. We

have defined $T_{\rm cm}$ in Eq.(1.169) such that it is consistent with the comoving temperature in Eq.(1.84) used for entropy calculations.

1.6 Topics of study

Figure 1.2 shows the epochs relevant to this work. We will assume that at a high temperature $T \sim 30$ MeV, the neutrinos are in thermal and chemical equilibrium with the photon–electron–positron plasma. At temperatures of $T \sim 3$ MeV, the neutrinos decouple from the plasma and free–stream. This is the weak decoupling epoch (WD). Although the neutrinos decouple from the plasma constiuents, the sparse number of baryons still experience comparatively large fluxes of electron–flavor neutrinos and anti-neutrinos. The neutrinos are able to maintain weak equilibrium with the neutrons and protons until temperatures of $T \sim 1$ MeV, at the onset of weak–freeze–out (WFO). The positrons and electrons remain in thermal and chemical equilibrium at temperatures below the rest mass of the electron. The deficit of electron–positron pairs at low temperatures $T \sim 10$ keV arises from the epoch of positron–electron–annihilation ($e^{\pm}$A). Before the electrons and positrons have completely vanished, the temperature cools low enough to assemble nuclei from the free neutrons and protons at temperatures $T \sim 100$ keV. Big bang nucleosynthesis forms helium-4, and trace amounts of deuterium and lithium. The four epochs of WD, WFO, $e^{\pm}$A, and BBN have neither distinct starting nor ending times. Rather, all four epochs require self-consistently solving the coupled set of Boltzmann integral–differential equations through a wide dynamic scale. In the course of studying the first four epochs, we deemed it necessary to gain an understanding of ionization freeze–out (IFO, or simply stated as recombination). This epoch is not coupled to the previous four epochs in time, but is certainly related to the neutrino and BBN epochs. We opine that a self-consistent treatment of neutrino dynamics in the early universe

requires the calculation of recombination, again using Boltzmann equations for atomic recombination and ionization processes.

We conclude this chapter by briefly outlining the remainder of this work. In Ch.2, we discuss BBN and how to calculate the primordial abundances. We proceed to give an example of a non-standard cosmology containing a diluton particle and the ramifications of heavy–particle decay within BBN in Ch.3. In the context of the sound horizon and the photon diffusion length, we discuss the physics and numerical techniques of the recombination epoch in Ch.4. With these techniques from Ch.4, Chs.5 and 6 consider the examples of the νMR effect and BSM physics. Finally, we present preliminary neutrino energy–transport calculations in Ch.7. We conclude in Ch.8 with an outlook of future topics of study.

Appendix A describes the linearization procedure for the BBN network. App.B gives preliminary work on electron–positron annihilation. App.C describes the decay spectra of dilutons in regards to pions. Aps.D, E, F, G, and H explain the mathematics necessary for coding the neutrino–energy–transport integrals.

Section 1.1 is a reprint of some of the material as it appears in "Probing neutrino physics with a self-consistent treatment of the weak decoupling, nucleosynthesis, and photon decoupling epochs." Grohs, E.; Fuller, G. M.; Kishimoto, C. K.; Paris, M. W., J. Cosmology Astropart., 5 (May 2015) 17. The dissertation author was the primary investigator and author of this paper.

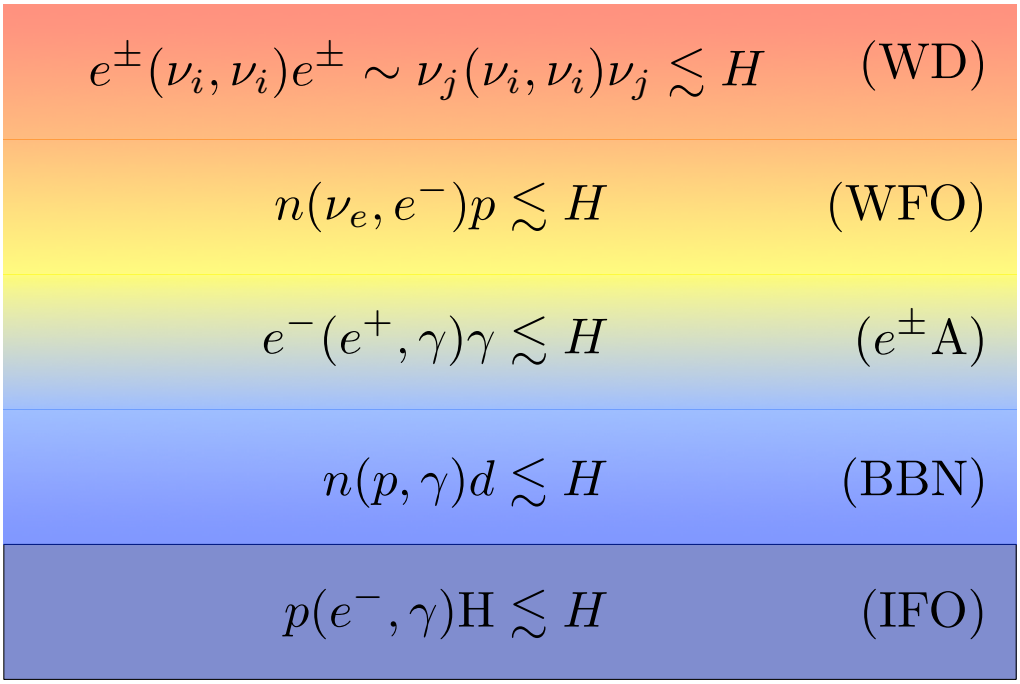

Figure 1.2: Diagram of the evolution of the universe through weak decoupling (WD), weak freeze-out (WFO)), electron-positron annihilation ($e^{\pm}$A), big bang nucleosynthesis (BBN), and ionization freeze-out (IFO). The reactions indicate processes typical to that specific epoch. H is the Hubble expansion rate.

Chapter 2

Big bang nucleosynthesis

2.1 Introduction

Recently there has been a dramatic increase in precision in the determination of D/H [3]. This improvement in observational precision drives the need to improve the standard tools used to calculate observables during the BBN and CMB epochs. This development allows us to consider improved descriptions of nuclear physics and non-standard particle and cosmological models.

We have developed a generalized BBN subroutine, part of the larger BURST code. The current BBN routine handles general distribution functions for particles out of equilibrium. It numerically integrates the binned neutrino occupation probabilities to obtain thermodynamic variables and number and energy densities for $\nu_e, \bar{\nu}_e, \nu_\mu, \bar{\nu}_\mu, \nu_\tau, \bar{\nu}_\tau$. It is worthwhile, therefore, to summarize our approach to BBN even though it is substantially similar in some respects to that given in Refs. [25, 26, 27].

We assume that the cosmic fluid is homogeneous and isotropic and that the comoving number density of baryons is covariantly conserved. Neutrinos can experience, in addition to gravity, essentially arbitrary interactions within the Boltzmann transport

approximation.[1] We allow for the possibility that neutrinos may decouple from the plasma with non-equilibrium distributions. This assumption implies that there may be deviations from the Fermi-Dirac momentum distribution [28, 29, 30]. In fact, it was this observation that provided initial motivation for developing the current approach.

BBN codes evolve light nuclide abundances $Y_i(t)$, defined as

$$Y_i(t) = \frac{n_i(t)}{n_b(t)}, \tag{2.1}$$

as a function of comoving time t in the background of the Friedmann-Lemaître-Robertson-Walker (FLRW) geometry. Here $n_i(t)$ is the proper number density of nuclide $i = n$, p, ^{2}H, ^{3}He, ^{4}He,... and $n_b(t)$ is the proper baryon number density. We will focus on two specific nuclides in this paper: the ^{4}He mass fraction ($Y_P \equiv 4Y_{^4He}$), and the ^{2}H relative abundance (D/H $\equiv Y_D/Y_H$). The evolution starts from a time when the plasma temperature T is near 30 MeV. Weak equilibrium obtains at this temperature. The time dependence of the metric is determined by the energy density $\rho(a)$ as

$$H(a) = \frac{\dot{a}}{a} = \sqrt{\frac{8\pi}{3m_{\rm pl}^2}\rho(a)}, \tag{2.2}$$

where $H(a)$ is the Hubble parameter, $m_{\rm pl}$ is the Planck mass, and the 'dot' indicates differentiation with respect to the FLRW-coordinate time t. The energy density is computed as the integral of the single-particle energy over the momentum distribution:

$$\rho(a) = \sum_j \int \frac{d^3p}{(2\pi)^3} f_j(p;a)\sqrt{p^2+m_j^2} \tag{2.3}$$

where the sum over j reflects all species contributing to the energy density, including but not limited to: photons, baryons, dark matter, $e^{\pm}$, and neutrinos. Consistent with the

[1] However, the code can handle limited generalizations of the Boltzmann approximation to incorporate effects associated with neutrino quantum kinetics.

above discussion, we do not need to assume a well defined temperature for any of the cosmic species. The time dependence of the distribution function $f_i(p;a)$ is indicated by the presence of the scale factor $a(t)$ in its argument. Evolution in time of the distribution functions is accomplished by solving transport equations, such as the Boltzmann equation, in FLRW geometry.

Given initial conditions for the temperature T and momentum distributions of the cosmological constituents (assumed to be in equilibrium through weak and strong interactions), the BBN code determines the evolution, with respect to the scale factor $a(t)$ (related to time as $dt = da/(aH(a))$), of the temperature of the plasma $T(a)$, the electron chemical potential $\mu_e(a)$, and the nuclide abundances relative to baryon number $Y_i(a)$.

The interactions of the light nuclear species is governed by the nuclear reaction network.[2] The reaction network, which is determined by a chosen set of nuclides and the thermally averaged reactivities $n_{\alpha_1} n_{\alpha_2} \langle \sigma_{\beta\alpha} v_\alpha \rangle$, is proportional to the rate of change of the number density of nuclides participating either in the initial state n_{α_i} or final state n_{β_j} where i, j indexes particles (up to 3) in the initial α or final β channel for the process $\alpha \to \beta$; that is, α and β are two- or three-body reaction channels and α_i is the i^{th} nuclide of the channel α. The nuclear reaction network includes nuclides with mass number $A \leq 9$. Our code allows for the inclusion of additional nuclides with $A > 9$, but we maintain the smaller network as the larger network provides no new insights for this paper. The nuclides are taken to be in thermal equilibrium with the photon–electron plasma. We are currently employing an updated [31] version of the reaction network from Ref. [27]. We also couple in all relevant $e^{\pm}$ and neutrino-induced weak interactions (charged and neutral current) [32].

[2]The nuclear reaction network should be derived from reaction cross sections that are governed by the principles of quantum mechanics, such as unitarity. We are currently developing a unitary reaction network for application in future work.

2.2 Standard big bang nucleosynthesis

We need to describe the universe before the commencement of BBN. We start at a high temperature, but lower than the Quantum-Chrmodynamic (QCD) phase transition, e.g. $T \sim 30$ MeV. There are no quark or gluon relativistic degrees of freedom at this temperature. The remaining quarks and gluons from the QCD epoch are bound into baryons. The only two types of baryons are the nucleons: protons and neutrons, and there are roughly equal numbers of each. The plasma consists of relativistic bosons and fermions. The only bosonic species is the photon. The fermionic species consist of electrons, positrons, three flavors of neutrinos, and three flavors of anti-neutrinos. There is a slight excess of electrons over positrons to maintain overall charge neutrality with the positvely-charged protons. There may exist unequal numbers of neutrinos for a given flavor. All of the plasma constiuents are in thermal equilibrium with one another, and the electrons/positrons have well defined chemical potentials, i.e. $\mu_{e^-} = -\mu_{e^+}$. Dark matter and dark energy have no interactions with the plasma or baryons, except for gravitational interactions. The energy densities in those sectors are negligible during the epochs surrounding BBN.

The only inputs for SBBN are the number of baryons and the neutrino degeneracy parameters. The baryon content is parameterized using:

$$\eta \equiv \frac{n_b}{n_\gamma} \propto \frac{1}{s}, \tag{2.4}$$

for the proper baryon number denisty n_b and proper photon number density n_γ. η is proportional to the inverse of the entropy per baryon, and can also be related to the baryon contribution to closure at the current epoch. The neutrino degeneracy parameter for a

given flavor $\xi_i \equiv \mu_i/T$ is parameterized using the lepton number L_i:

$$L_i \equiv \frac{n_{\nu_i} - n_{\bar{\nu}_i}}{n_\gamma} = \frac{1}{12\zeta(3)}\left(\pi^2\xi_\nu + \xi_\nu^3\right). \tag{2.5}$$

If there exists equal numbers of neutrinos and anti-neutrinos for a given flavor, then $\xi_i = 0$ and the corresponding lepton number is zero. If the preceeding conditional is false, then the lepton number is non-zero. Another common input parameter into SBBN is the radiation energy density ρ_r, parameterized by the quantity $N_{\rm eff}$:

$$\rho_r = \left[2 + \frac{7}{4}\left(\frac{4}{11}\right)^{4/3} N_{\rm eff}\right]\frac{\pi^2}{30}T^4. \tag{2.6}$$

We do not take this quantity as an input parameter of the standard cosmology, but instead take $N_{\rm eff}$ to be a calculable output quantity sensitive to beyond-standard-model physics. The calculation of $N_{\rm eff}$ is non-trivial and the subject of Sec.4.5.

BBN begins roughly after the weak-freeze out epoch, i.e. once the neutrinos no longer efficiently convert neutrons into protons at about $T \sim 1$ MeV. Weak freeze-out sets the initial neutron to proton ratio which allows for the fusion of nucleons into heavier nuclei. Nucleosynthesis terminates once the nuclear reaction rates become slow compared to the expansion rate at about $T \sim 10$ keV. The temperature T is the plasma temperature. The product Ta does not behave like a comoving invariant, due to the epoch of positron-electron annihilation coincident with BBN.

To properly follow SBBN, we evolve three thermodynamic quantities:

$$\begin{cases} T : \text{Photon (plasma) temperature} \\ h_v : \text{Ratio of baryon energy density to } T^3 \\ \phi_e : \text{electron degeneracy parameter} \end{cases},$$

and the nuclear abundances Y_i. Each quantity is evolved with time using an adaptive time step. We use an explicit second–order Runge–Kutta (RK2) algorithm to integrate the ODEs for the three thermodynamic quantities. The abundances require a semi-implicit RK2 method. We discuss the calculation of the time derivative of each quantity, or set of quanities in the case of $\{Y_i\}$ in the following subsections.

2.2.1 h_ν quantity

The quantity h_ν is defined to be:

$$h_\nu = \frac{\rho_b}{T^3}. \tag{2.7}$$

To calculate the derivative of h_ν, we will approximate that the rest mass, (m), contribution to the baryon energy density dominates over the kinetic term:

$$\rho_b \simeq \rho_b^{(\mathrm{m})} \sim \frac{1}{a^3} \implies \frac{d\rho_b}{dt} = -3H\rho_b. \tag{2.8}$$

Therefore:

$$\frac{dh_\nu}{dt} = -3H\frac{\rho_b}{T^3} - 3\frac{\rho_b}{T^4}\frac{dT}{dt} \tag{2.9}$$

$$= -3h_\nu\left(H + \frac{1}{T}\frac{dT}{dt}\right). \tag{2.10}$$

To calculate the derivative of h_ν, we need the temperature derivative.

2.2.2 Electron degeneracy parameter

The electron degeneracy parameter is defined to be $\phi_e = \mu_{e^-}/T$ where μ_{e^-} is the total chemical potential of electrons. We begin by considering the equation for charge

neutrality:

$$n_- - n_+ = n_{\rm p}, \tag{2.11}$$

where n_- is the number density of electrons, n_+ is the number density of positrons, and $n_{\rm p}$ is the total number density of protons. If we assume thermal and chemical equilibrium:

$$\int \frac{d^3p}{(2\pi)^3}\frac{1}{e^{E/T-\phi_e}} - \int \frac{d^3p}{(2\pi)^3}\frac{1}{e^{E/T+\phi_e}} = n_b \sum_i z_i Y_i, \tag{2.12}$$

where the energy is given by the dispersion relation $E = \sqrt{p^2+m_e^2}$ and z_i is the atomic number of nuclide i. The lhs of Eq.(2.12) is a function of ϕ_e and T. The rhs is a function of scale factor and the nuclear abundances. We can write the time derivative of ϕ_e as the following:

$$\frac{d\phi_e}{dt} = \frac{\partial\phi_e}{\partial T}\frac{dT}{dt} + \frac{\partial\phi_e}{\partial a}\frac{da}{dt} + \sum_i \frac{\partial\phi_e}{\partial Y_i}\frac{dY_i}{dt}. \tag{2.13}$$

Eq.(2.13) involves the expression for the time derivatives of the temperature and abundances. We can find the partial derivatives if we use Eq.(2.12). As an example, we investigate the derivative $\frac{\partial\phi_e}{\partial T}$:

$$\frac{d}{dT}\left(\int \frac{d^3p}{(2\pi)^3}\frac{1}{e^{E/T-\phi_e}+1} - \int \frac{d^3p}{(2\pi)^3}\frac{1}{e^{E/T+\phi_e}+1}\right) = \frac{d}{dT}\left(n_b\sum_i z_i Y_i\right) \tag{2.14}$$

$$\begin{aligned}\Longrightarrow \frac{1}{2\pi^2}\Bigg[&\int p^2dp\left(-\frac{e^{E/T-\phi_e}}{(e^{E/T-\phi_e}+1)^2}\right)\left(-\frac{E}{T^2}-\frac{\partial\phi_e}{\partial T}\right)\\ &-\int p^2dp\left(-\frac{e^{E/T+\phi_e}}{(e^{E/T+\phi_e}+1)^2}\right)\left(-\frac{E}{T^2}+\frac{\partial\phi_e}{\partial T}\right)\Bigg] = 0.\end{aligned} \tag{2.15}$$

If we collect terms in $\partial\phi_e/\partial T$, we find:

$$\begin{aligned}&\frac{\partial\phi_e}{\partial T}\int p^2dp\left(\frac{e^{E/T-\phi_e}}{(e^{E/T-\phi_e}+1)^2}+\frac{e^{E/T+\phi_e}}{(e^{E/T+\phi_e}+1)^2}\right)\\ =&\frac{1}{T^2}\int p^2dpE\left(-\frac{e^{E/T-\phi_e}}{(e^{E/T-\phi_e}+1)^2}+\frac{e^{E/T+\phi_e}}{(e^{E/T+\phi_e}+1)^2}\right).\end{aligned} \tag{2.16}$$

The integrals above can be simplified through integration by parts:

$$\frac{\partial\phi_e}{\partial T}\int E\sqrt{E^2-m_e^2}dE\left(-T\frac{\partial f_-}{\partial E}-T\frac{\partial f_+}{\partial E}\right)=\frac{1}{T^2}\int E^2\sqrt{E^2-m_e^2}dE\left(T\frac{\partial f_-}{\partial E}-T\frac{\partial f_+}{\partial E}\right) \tag{2.17}$$

$$\implies \frac{\partial\phi_e}{\partial T}\int dE\frac{2E^2-m_e^2}{\sqrt{E^2-m_e^2}}(f_-+f_+)=-\frac{1}{T^2}\int dE\frac{E(3E^2-2m_e^2)}{\sqrt{E^2-m_e^2}}(f_--f_+), \tag{2.18}$$

where:

$$f_-=\frac{1}{e^{E/T-\phi_e}+1}\text{ and }f_+=\frac{1}{e^{E/T+\phi_e}+1} \tag{2.19}$$

are the Fermi-Dirac expressions for the occupation probabilities of electrons and positrons, respectively. Solving for $\partial\phi_e/\partial T$ yields:

$$\frac{\partial\phi_e}{\partial T}=-\frac{1}{T^2}\frac{\int dE\frac{E(3E^2-2m_e^2)}{\sqrt{E^2-m_e^2}}(f_--f_+)}{\int dE\frac{2E^2-m_e^2}{\sqrt{E^2-m_e^2}}(f_-+f_+)}. \tag{2.20}$$

If we use the expression[33]:

$$K_\alpha(z)=\int_0^\infty dt\,e^{-z\cosh t}\cosh(\alpha t), \tag{2.21}$$

we can write the denominator of Eq.(2.20) as:

$$\int dE \frac{2E^2 - m_e^2}{\sqrt{E^2 - m_e^2}}(f_- + f_+) = 2m_e^2 \sum_{n=1}^{\infty} (-1)^{n+1} \cosh(n\phi_e) \left[\frac{2}{nz} K_1(nz) + K_0(nz)\right], \tag{2.22}$$

where $K_\alpha(z)$ is the modified Bessel function of the second kind and $z = m_e/T$. A similar expression with K_α exists for the numerator of Eq.(2.20). In addition, we can use K_α to approximate the derivatives of ϕ_e with respect to scale factor and abundance. The polynomial expansions of $K_\alpha(x)$ are truncated at seven terms, and the summations over n in Eq.(2.22) are truncated at five terms. Section 2.3 outlines another method to follow the thermodynamics of electrons and positrons.

2.2.3 Temperature

The plasma temperature evolves according to Eq.(1.139):

$$\frac{dT}{dt} = -3H \frac{\tilde{\rho} + p - \frac{1}{3H}\left(\frac{\partial \rho}{\partial t}\right)_{a,T}}{\frac{d\rho}{dT}}. \tag{2.23}$$

p is the pressure and $\tilde{\rho}$ is the energy density less the massive contribution:

$$\tilde{\rho} = \rho_\gamma + \rho_{e^-} + \rho_{e^+} \equiv \rho_\gamma + \rho_e \tag{2.24}$$

$$p = p_\gamma + p_e + p_b, \tag{2.25}$$

where the subscript e refers to the sum of electron and positron, and the subscript b to baryon. The denominator of Eq.(2.23) is:

$$\overline{\frac{d\rho}{dT}} = \frac{d\rho_\gamma}{dT} + \frac{d\rho_e}{dT} + \left(\frac{\partial \rho_b}{\partial T}\right)_a \tag{2.26}$$

$$= \frac{4\rho_\gamma}{T} + \frac{\partial \rho_e}{\partial T} + \frac{\partial \rho_e}{\partial \phi_e}\frac{\partial \phi_e}{\partial T} + \frac{3}{2}\frac{\rho_b}{m_u}, \tag{2.27}$$

where we have made the approximation that the energy density of baryons resides mostly in the rest mass, but the derivative with respect to temperature is non-zero. Using the same methods of the previous subsection, we can write the partial derivatives involving ρ_e as an infinite series of modified Bessel functions of the second kind. The last term in Eq.(2.23) is the heat density:

$$\frac{1}{3H}\left(\frac{\partial \rho}{\partial t}\right)_{a,T} = \frac{1}{3H}\left[\left(\frac{\partial \rho_b}{\partial t}\right)_{a,T} + \left(\frac{\partial \rho_e}{\partial t}\right)_{a,T}\right], \tag{2.28}$$

which describes the heat change introduced by nucleosynthesis. A more complete description of ρ_b is:

$$\rho_b = \sum_i n_i \left(m_i + \frac{3}{2}T\right) \tag{2.29}$$

$$= n_b \sum_i Y_i \left(m_i + \frac{3}{2}T\right) \tag{2.30}$$

where the sum is over all of the nuclide species. Therefore:

$$\left(\frac{\partial \rho_b}{\partial t}\right)_{a,T} = n_b \sum_i \frac{dY_i}{dt}\left(m_i + \frac{3}{2}T\right). \tag{2.31}$$

We can write the derivative of ρ_e in Eq.(2.28) as:

$$\left(\frac{\partial \rho_e}{\partial t}\right)_{a,T} = \frac{\partial \rho_e}{\partial \phi_e}\left(\frac{d\phi_e}{dt} + \sum_i \frac{\partial \phi_e}{\partial Y_i}\frac{dY_i}{dt}\right). \tag{2.32}$$

The derivative $\partial\phi_e/\partial Y_i$ is known as it is needed for the calculation of the total time derivative of ϕ_e. The derivative $d\phi_e/dt$ was the topic of the last subsection and relied on knowledge of the derivative dT/dt, the topic of this subsection. To avoid the mutual dependence, we use the Hubble rate:

$$\left(\frac{\partial \rho_e}{\partial t}\right)_{a,T} = \frac{\partial \rho_e}{\partial \phi_e}\left(\frac{\partial \phi_e}{\partial a}\frac{da}{dt} + \sum_i \frac{\partial \phi_e}{\partial Y_i}\frac{dY_i}{dt}\right) \tag{2.33}$$

$$= \frac{\partial \rho_e}{\partial \phi_e}\left(\frac{\partial \phi_e}{\partial a}aH + \sum_i \frac{\partial \phi_e}{\partial Y_i}\frac{dY_i}{dt}\right). \tag{2.34}$$

The derivative $\partial\phi_e/\partial a$ contains a $1/a$ term which will cancel with the a term multiplying the Hubble rate.

2.2.4 Nuclear Abundances

The last quantities to evolve are the nuclear abundances. We write an expression for the nuclear reactions assuming at most four unique nuclides:

$$N_i({}^{A_i}X_{z_i}) + N_j({}^{A_j}X_{z_j}) \leftrightarrow N_k({}^{A_k}X_{z_k}) + N_l({}^{A_l}X_{z_l}), \tag{2.35}$$

where N_m is the number of nuclide X with atomic number z_m and atomic mass A_m participating in Rxn.2.35. The nuclear reactions conserve baryon number and charge.

For strong and electromagnetic reactions, the implications are:

$$N_i z_i + N_j z_j = N_k z_k + N_l z_l \tag{2.36}$$

$$N_i A_i + N_j A_j = N_k A_k + N_l A_l. \tag{2.37}$$

For weak interactions, baryon number is conserved, and the overall charge is conserved. However, there exists electrons or positrons in the final state, implying that the charge of the nucleons is not conserved. The change in the charges of the nucleons is compensated for with changes in the electron degeneracy parameter and subsequent derivatives. The implications for the nuclear abundance derivative of Y_i for Rxn.(2.35) are summations over the three indicies j,k,l [26]:

$$\frac{dY_i}{dt} = \sum_{j,k,l} N_i \left(-\frac{Y_i^{N_i} Y_j^{N_j}}{N_i! N_j!} [ij]_k + \frac{Y_k^{N_k} Y_l^{N_l}}{N_k! N_l!} [kl]_j \right), \tag{2.38}$$

where $[ij]_k$ is the reaction rate for $i + j \leftarrow k + l$ and $[kl]_j$ is the reverse rate. For reactions with $N_m = 1$ for each nuclide, $[ij]_k = n_b \langle \sigma v \rangle$ where $\langle \sigma v \rangle$ is the thermally–averaged product of cross section and relative velocity.

Eq.(2.38) makes the Boltzmann approximation to employ the thermally–averaged $\langle \sigma v \rangle$. Ref.[26] gives a procedure for linearizing Eq.(2.38) such that:

$$\frac{dY_i}{dt}(t + \Delta t) = \sum_j C_{ij} Y_j (t + \Delta t), \tag{2.39}$$

where C_{ij} is a matrix independent of the abundances at the future time step, $Y_j(t + \Delta t)$, but does use the abundances at the previous time step, $Y_j(t)$. Appendix A describes the linearization procedure in detail. We use the linearization technique to semi-implicitly integrate the ODEs for the evolution of the abundances.

2.3 Epoch of electron–positron annihilation

As mentioned in Sec.2.2, the electron/positron energy densities are assumed to be Fermi-Dirac with the same temperature and opposite sign chemical potentials. The leptons interact weakly with the neutrinos, and interact electromagnetically with the photons. The relevant electromagnetic interactions are:

$$e^{\pm} + \gamma \leftrightarrow e^{\pm} + \gamma, \tag{2.40}$$

$$e^{-} + e^{+} \leftrightarrow 2\gamma. \tag{2.41}$$

For Compton scattering, Rxn.(2.40), the rates are fast at the BBN epoch, so the approximation of equal temperatures between elecron, positron, and photon species is accurate. To maintain chemical equilibrium, the forward and reverse rates of Rxn.(2.41) must be fast compared to the Hubble rate. The forward rate $(e^{-} + e^{+} \rightarrow 2\gamma)$ will be fast due to the Coulomb attraction of the reactants. The reverse rate requires an energy threshold of $2m_e \simeq 1$ MeV and will freeze out. As an estimate, the reverse rate of Rxn.(2.41) goes as the product of the Thomson cross section and the number density of photons with energies larger than the rest mass of the electron. We can approximate the rate as:

$$\Gamma_{2\gamma \rightarrow e^{\pm}} \simeq \sigma_{\mathrm{T}} T^3 e^{-2m_e/T} \tag{2.42}$$

$$= 2.596 \times 10^{18}\,\mathrm{s}^{-1} \left(\frac{T}{\mathrm{MeV}}\right)^3 \exp\left(-1.022\,\frac{\mathrm{MeV}}{T}\right). \tag{2.43}$$

For comparison, we estimate the Hubble expansion rate as:

$$H \simeq 1\,\mathrm{s}^{-1} \left(\frac{\mathrm{MeV}}{T}\right)^2. \tag{2.44}$$

At a temperature of $T \sim 1$ MeV, the annihilation rate $\Gamma_{2\gamma\to e^{\pm}}$ is much larger than the Hubble rate. At a temperature of 10 keV:

$$\Gamma_{2\gamma\to e^{\pm}} \simeq 1.070\times 10^{-32}\,\mathrm{s}^{-1} \text{ and } H \simeq 10^{-6}\,\mathrm{s}^{-1}. \tag{2.45}$$

The above calculations are only estimates. Clearly, the dynamics in the sea of electrons and positrons are highly sensitive to temperature and there is a rapid freeze–out of the electron–positron creation rate. A proper description of that dynamics requires a Boltzmann equation with a Klein–Nishina summed–squared–amplitude[34]:

$$e^-(P_1) + e^+(P_2) \to \gamma(P_3) + \gamma(P_4) \tag{2.46}$$

$$\implies \langle|\mathcal{M}|^2\rangle = -2e^4\left[\frac{P_1\cdot P_4}{P_1\cdot P_3} + \frac{P_1\cdot P_3}{P_1\cdot P_4} + 2m_e^2\left(\frac{1}{P_1\cdot P_3}+\frac{1}{P_1\cdot P_4}\right) - m_e^4\left(\frac{1}{P_1\cdot P_3}+\frac{1}{P_1\cdot P_4}\right)^2\right], \tag{2.47}$$

where P_i is the four-momentum of particle i in the comoving frame. For weak interactions, $\langle|\mathcal{M}|^2\rangle$ can be separated into two distinct functions $P_i\cdot P_j$ and $P_i\cdot P_k$, simplifying the collision integral in the Boltzmann equation. Eq.(2.47) cannot be separated into two functions like the weak interaction. App.B describes a preliminary treatment of the collision integral for a similar matrix element to Eq.(2.47).

2.4 Equilibrium

BBN begins in conditions close to equilibrium. We make the approximation that the constituent particles relevant to BBN all begin in equilibrium with one another, with the important exception of the baryons being out of chemical equilibrium.

We have already made the implicit assumption of thermal equilibrium among

the plasma particles when we defined a plasma temperature. We will study chemical equilibrium within the reaction:

$$R_1 + R_2 \leftrightarrow P_3 + P_4, \tag{2.48}$$

for reactants R_i and products P_j. If the rates of the forward and reverse reactions in Eq.(2.48) are fast, then chemical equilibrium is obtained:

$$\mu_1 + \mu_2 = \mu_3 + \mu_4, \tag{2.49}$$

where μ_i is the chemical potential of species i. To determine the chemical potential, we use the free energy F:

$$\mu = \left(\frac{\partial F}{\partial N}\right)_{T,V}, \tag{2.50}$$

where N, T, V are the number, temperature, and volume of the system. We can use the multi-particle partition function, Z, to find the free energy:

$$F = -T \ln Z. \tag{2.51}$$

For the single-particle partition function of a non-relativistic gas particle:

$$Z_1 = g\int \frac{d^3x\,d^3p}{(2\pi)^3} e^{-E/T} \tag{2.52}$$

$$= g\int \frac{d^3x\,d^3p}{(2\pi)^3} e^{-m/T - p^2/2mT} \tag{2.53}$$

$$= \frac{g}{2\pi^2} V\, e^{-m/T} \int dp\, p^2\, e^{-p^2/2mT} \tag{2.54}$$

$$= \frac{g}{2\pi^2} V\, e^{-m/T} (2mT)^{3/2} \int dx x^2\, e^{-x^2} \tag{2.55}$$

$$= \frac{g}{2\pi^2} V\, e^{-m/T} (2mT)^{3/2} \frac{1}{4}\sqrt{\pi} \tag{2.56}$$

$$= gVe^{-m/T} \left(\frac{mT}{2\pi}\right)^{3/2}. \tag{2.57}$$

g is the internal partition function and m is the mass of the individual gas particle. We can relate the multi-particle partition function to the single-particle partition function:

$$Z = \frac{1}{N!} Z_1^N \tag{2.58}$$

$$= \frac{1}{N!} g^N V^N e^{-mN/T} \left(\frac{mT}{2\pi}\right)^{3N/2}. \tag{2.59}$$

The expression for the free energy is:

$$F = -T \ln Z \tag{2.60}$$

$$= -T\left[N\ln(gV) - N\frac{m}{T} + \frac{3}{2}N\ln\left(\frac{mT}{2\pi}\right) - \ln N!\right] \tag{2.61}$$

$$\simeq -T\left[N\ln(gV) - N\frac{m}{T} + \frac{3}{2}N\ln\left(\frac{mT}{2\pi}\right) - N\ln N + N\right], \tag{2.62}$$

where we have used Stirling's formula to approximate $\ln N!$. If we substitute Eq.(2.62)

into Eq.(2.50), we find:

$$\mu = \left(\frac{\partial F}{\partial N}\right)_{T,V} \tag{2.63}$$

$$= -T\left[\ln(gV) - \frac{m}{T} + \frac{3}{2}\ln\left(\frac{mT}{2\pi}\right) - \ln N\right] \tag{2.64}$$

$$= -T\ln\left[\frac{gV}{N}\left(\frac{mT}{2\pi}\right)^{3/2}\right] + m \tag{2.65}$$

$$= -T\ln\left[\frac{g}{n}\left(\frac{mT}{2\pi}\right)^{3/2}\right] + m, \tag{2.66}$$

where we have used the number density $n = N/V$. Eq.(2.66) assumes non-relativistic kinematics, but is applicable to any microphysical process which produces chemical equilibrium.

2.4.1 Weak Equilibrium

If the leptons can efficiently change isospin, then Eq.(2.49) states:

$$n + \nu_e \leftrightarrow p + e^- \tag{2.67}$$

$$\Longrightarrow \mu_n + \mu_{\nu_e} = \mu_p + \mu_{e^-}. \tag{2.68}$$

For the standard cosmology, the chemical potential of the electrons is small at the temperatures of weak freeze–out. We assume the chemical potential of the electron neutrino is zero for the purposes of this section. The chemical potentials of neutrons and

protons are equal and:

$$-T\ln\left[\frac{g_n}{n_n}\left(\frac{m_nT}{2\pi}\right)^{3/2}\right]+m_n=-T\ln\left[\frac{g_p}{n_p}\left(\frac{m_pT}{2\pi}\right)^{3/2}\right]+m_p \tag{2.69}$$

$$\Longrightarrow\ \frac{m_n-m_p}{-T}=\ln\left[\frac{n_n}{n_p}\frac{g_p}{g_n}\left(\frac{m_p}{m_n}\right)^{3/2}\right] \tag{2.70}$$

$$\Longrightarrow\ n/p\equiv\frac{n_n}{n_p}=\frac{g_n}{g_p}\left(\frac{m_n}{m_p}\right)^{3/2}\exp\left(-\frac{m_n-m_p}{T}\right)\rightarrow e^{-\delta m_{np}/T}, \tag{2.71}$$

where we have defined the neutron–to–proton ratio n/p. The ratio corresponds to the total number of neutrons and total number of protons – including free hadrons and bound nucleons. We take the neutron mass to be the same as the proton mass for the multiplicative factor, but use the non-zero difference for the exponential factor: $\delta m_{np}\equiv m_n-m_p\simeq 1.3\,\mathrm{MeV}$. The internal partition functions for neutrons and protons are taken to be close to 2.

We define the electron fraction as:

$$Y_e\equiv\frac{n_e}{n_b}=\frac{n_p}{n_p+n_n}=\frac{1}{1+n/p}=\frac{1}{1+e^{-\delta m_{np}/T}}. \tag{2.72}$$

Figure 2.1 shows a plot of how the electron fraction changes with decreasing temperature. The green curve is from a computation with a calculation of the explicit neutron–to–proton rates. It assumes a baryon density of $\omega_b=0.022068$. The blue curve is a plot of Eq.(2.72), and is not particular to the early universe. At a temperature of $T\sim 1\,\mathrm{MeV}$, the rates which convert neutrons to protons are not fast enough to maintain weak equilibrium. This is the so-called weak freeze–out epoch. Nuclear interactions can also change n/p. Fig.2.1 shows the freeze–out of the total electron fraction at $T\sim 100\,\mathrm{keV}$, when helium–4 forms to set $n/p\sim 1/7$. Alpha–particle formation is quick, and depends sensitively on n/p at a temperature $T\sim 1\,\mathrm{MeV}$.

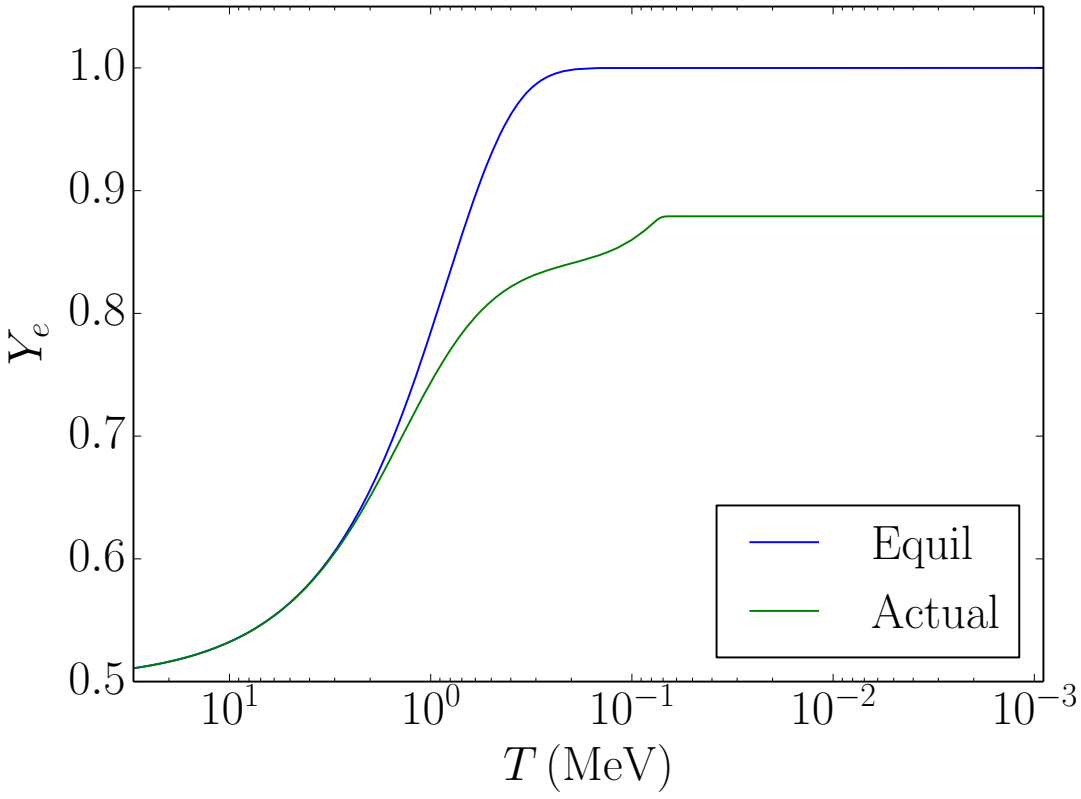

Figure 2.1: The evolution of the electron fraction is given as a function of plasma temperature T. The blue line corresponds to the assumption of weak equilibrium between the neutrino seas, electrons, positrons, and baryons. The green line corresponds to a Boltzmann treatment of the weak interactions.

2.4.2 Nuclear Statistical Equilibrium

BBN occurs close to nuclear statistical equilibrium (NSE). We use Eq.(2.49) to compute the NSE abundances of the heavy nuclides:

$$\mu_A = z\mu_p + (A-z)\mu_n, \tag{2.73}$$

where μ_A is the chemical potential of the nucleus with atomic mass A and atomic number z. We obtain Eq.(2.73) by summing all of the intermediate NSE expressions for the

assembly of lighter nuclei. If we substitute Eq.(2.66) into Eq.(2.73), we find:

$$-T\ln\left[\frac{g_A}{n_A}\left(\frac{m_AT}{2\pi}\right)^{3/2}\right]+m_A=z\left\{-T\ln\left[\frac{g_p}{n_p}\left(\frac{m_pT}{2\pi}\right)^{3/2}\right]+m_p\right\}$$
$$+(A-z)\left\{-T\ln\left[\frac{g_n}{n_n}\left(\frac{m_nT}{2\pi}\right)^{3/2}\right]+m_n\right\}, \quad (2.74)$$

implying:

$$\ln\left[\frac{g_A}{n_A}\left(\frac{m_AT}{2\pi}\right)^{3/2}\right]=z\ln\left[\frac{g_p}{n_p}\left(\frac{m_pT}{2\pi}\right)^{3/2}\right]$$
$$+(A-z)\ln\left[\frac{g_n}{n_n}\left(\frac{m_nT}{2\pi}\right)^{3/2}\right]+\frac{m_A-zm_p-(A-z)m_n}{T}. \quad (2.75)$$

The last term of Eq.(2.75) we relate to the nuclear binding energy of nucleus ${}^AX_z$:

$$B\equiv zm_p+(A-z)m_n-m_A. \quad (2.76)$$

Eq.(2.75) becomes:

$$\frac{g_A}{n_A}\left(\frac{m_AT}{2\pi}\right)^{3/2}=\frac{g_p^z}{n_p^z}\left(\frac{m_pT}{2\pi}\right)^{3z/2}\frac{g_n^{A-z}}{n_n^{A-z}}\left(\frac{m_nT}{2\pi}\right)^{3(A-z)/2}e^{-B/T} \quad (2.77)$$

$$\Longrightarrow\frac{n_A}{g_A}\left(\frac{2\pi}{m_AT}\right)^{3/2}=\frac{n_p^z}{g_p^z}\left(\frac{2\pi}{m_pT}\right)^{3z/2}\frac{n_n^{A-z}}{g_n^{A-z}}\left(\frac{2\pi}{m_nT}\right)^{3(A-z)/2}e^{B/T} \quad (2.78)$$

$$\Longrightarrow n_A=n_p^zn_n^{A-z}\frac{g_A}{g_p^zg_n^{A-z}}\left(\frac{2\pi}{T}\right)^{3(A-1)/2}\left(\frac{m_A}{m_p^zm_n^{A-z}}\right)^{3/2}e^{B/T} \quad (2.79)$$

$$\Longrightarrow\frac{n_A}{n_b}=\left(\frac{n_p}{n_b}\right)^z\left(\frac{n_n}{n_b}\right)^{A-z}n_b^{A-1}\frac{g_A}{g_p^zg_n^{A-z}}\left(\frac{2\pi}{T}\right)^{3(A-1)/2}\left(\frac{m_A}{m_p^zm_n^{A-z}}\right)^{3/2}e^{B/T}. \quad (2.80)$$

The entropy per baryon can be determined from Eq.(1.81):

$$s=\frac{1}{n_b}\frac{2\pi^2}{45}g_{\star S}T^3\implies n_b=\frac{1}{s}\frac{2\pi^2}{45}g_{\star S}T^3. \quad (2.81)$$

Eq.(2.80) becomes:

$$Y_A = Y_p^z Y_n^{A-z} \left(\frac{1}{s}\frac{2\pi^2 g_{\star S} T^3}{45}\right)^{A-1} \frac{g_A}{g_p^z g_n^{A-z}} \left(\frac{2\pi}{T}\right)^{3(A-1)/2} \left(\frac{m_A}{m_p^z m_n^{A-z}}\right)^{3/2} e^{B/T} \tag{2.82}$$

$$\begin{aligned} \Longrightarrow Y_A &= Y_p^z Y_n^{A-z} \left(\frac{g_{\star S}}{s}\right)^{A-1} \frac{2^{5(A-1)/2}\pi^{7(A-1)/2}}{45^{A-1}} \frac{g_A}{g_p^z g_n^{A-z}} \\ &\quad \times T^{3(A-1)/2} \left(\frac{m_A}{m_p^z m_n^{A-z}}\right)^{3/2} e^{B/T}. \end{aligned} \tag{2.83}$$

The quantities Y_p and Y_n are the total proton and neutron abundances, respectively. We will make the approximation that $g_p = g_n = 2$, $m_p = m_n = m_u$, and $m_A = Am_u$, where m_u is the atomic mass unit. We do not make the mass approximations when considering the binding energy term in the exponential – only in the multiplicative factor. This approximation is consistent with what we did for weak equilibrium in the previous section. Eq.(2.83) becomes:

$$Y_A = Y_p^z Y_n^{A-z} \left(\frac{g_{\star S}}{s}\right)^{A-1} \frac{2^{5(A-1)/2}\pi^{7(A-1)/2}}{45^{A-1}} \frac{g_A}{2^A} T^{3(A-1)/2} \left(\frac{A}{m_u^{A-1}}\right)^{3/2} e^{B/T} \tag{2.84}$$

$$= Y_p^z Y_n^{A-z} \left(\frac{g_{\star S}}{s}\right)^{A-1} g_A A^{3/2} \frac{2^{(3A-5)/2}\pi^{7(A-1)/2}}{45^{A-1}} \left(\frac{T}{m_u}\right)^{3(A-1)/2} e^{B/T} \tag{2.85}$$

$$= Y_p^z Y_n^{A-z} \left(\frac{g_{\star S}}{s}\right)^{A-1} g_A A^{3/2} \frac{1}{2} \left(\frac{2^{3/2}\pi^{7/2}}{45}\right)^{A-1} \left(\frac{T}{m_u}\right)^{3(A-1)/2} e^{B/T} \tag{2.86}$$

$$= \frac{3.454^{A-1}}{2} Y_p^z Y_n^{A-z} \left(\frac{g_{\star S}}{s}\right)^{A-1} g_A A^{3/2} \left(\frac{T}{m_u}\right)^{3(A-1)/2} e^{B/T}. \tag{2.87}$$

Figure 2.2 shows a plot of the BBN abundances evolving with decreasing temperature. We plot relative abundance with respect to hydrogen–1. The baryon density is $\omega_b = 0.022068$. The solid curves are for the standard cosmology and depart from the dashed NSE curves of Eq.(2.87) divided by Y_H. Unlike the equilibrium curve for Fig.2.1,

the NSE curves are particular to the early universe. We do not assume weak equilibrium, and so we follow the evolution of the inputs Y_p, Y_n, and $g_{\star S}$ as a function of temperature.

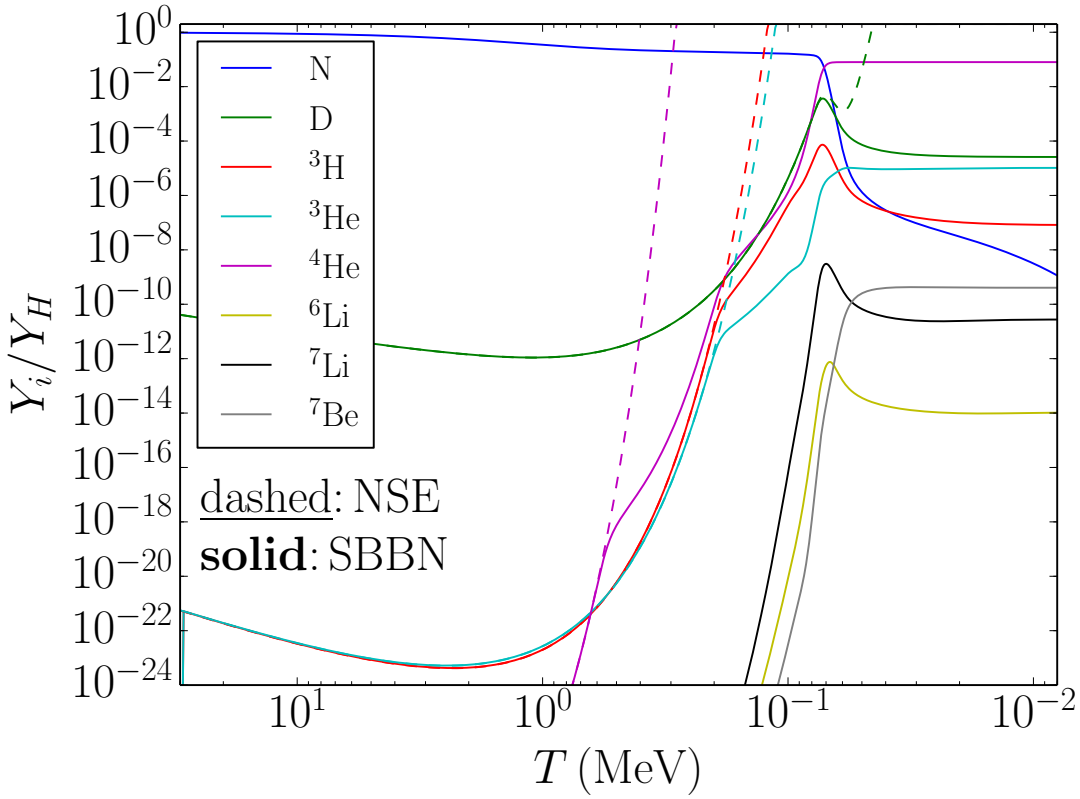

Figure 2.2: The relative abundance evolution is given as a function of plasma temperature T. The dashed lines correspond to the assumption of NSE, while the solid lines correspond to a Boltzmann treatment of nuclear reactions. The abundances are free neutrons (N), deuterium (D), tritium (^{3}H), helium–3 (^{3}He), helium–4 (^{4}He), lithium–6 (^{6}Li), lithium–7 (^{7}Li), and beryllium–7 (^{7}Be). Only the NSE abundances for D, ^{3}H, ^{3}He, and ^{4}He are shown.

We only show the NSE abundances for deuterium, tritium, helium–3, and helium–4. The NSE abundances for lithium–6, lithium–7, and beryllium–7 are much larger than the actual abundances and show no convergence for the temperature and abundance ranges shown in Fig.2.2. Helium–4 departs from equilibrium at a temperature $T \sim 700\,\mathrm{keV}$. Although the binding energy of an alpha particle is $B \sim 30$ MeV, the helium–4 abundance maintains NSE to significantly lower temperatures due to the high-entropy environment.

Tritium and helium–3 maintain equilibrium to even lower temperature than helium–4. Deuterium is the last abundance to depart from NSE. After alpha–particle formation, there are few available free–neutron–reactants to synthesize deuterium. The binding energy of deuterium is small ($B \sim 1\,\mathrm{MeV}$), and so deuterium is easily destroyed and freezes-out at $\mathrm{D/H} \sim 2.5 \times 10^{-5}$.

We modify the standard cosmology by adding physics into the epochs surrounding BBN. To maintain self-consistency, we modify the equations of the previous sections to include any new testable physics.

2.5 Verification of cosmological parameters

We provide an example of how to use BBN to constrain beyond–standard–model physics.

We adopt the point of view advocated in Refs. [35, 36, 11] that the constraint provided by predictions of BBN should be incorporated simultaneously with constraints due to recombination effects in the extraction of cosmological parameters. We also require, as previously discussed, that BBN and recombination be solved iteratively. In this section, we demonstrate the self-consistent extraction of these parameters by employing a simple model for the radiation energy density that avoids solving, for example, the Boltzmann equation, for the set of distribution functions of the cosmic constituents, in particular the neutrinos.

We follow the standard paradigm for the BBN epoch as originally discussed in Ref. [25] and subsequently in Refs. [26, 27]. To that extent, we use BURST to verify our results with those of other theoretical groups [37, 38, 39]. For example, at $\omega_b = 0.022068$

and $\tilde{N}_{\rm eff} = 3.046$, Ref. [2] finds:

$$Y_P = 0.24725 \pm 0.00032 \tag{2.88}$$

$$\text{D/H} = (2.656 \pm 0.067) \times 10^{-5} \tag{2.89}$$

using the code PARTHENOPE [40]. This compares favorably to our values:

$$Y_P = 0.24307 \pm 0.00002, \tag{2.90}$$

$$\text{D/H} = (2.631 \pm 0.006) \times 10^{-5}, \tag{2.91}$$

where the error bar is only from the uncertainty in ω_b. Ref. [2] includes effects of non-thermal neutrino spectral distortions [40], whereas our model only includes dark radiation. The non-thermal spectra alters the neutron to proton ratio which is the source of the disagreement for Y_P. We give a detailed description of the dark-radiation model to distinguish between it and the models of Ch. 6.

The model we explore in this section is identical to ΛCDM except for one additional constituent: dark radiation. The dark radiation energy density is radiation at all epochs and does not interact with the other energy-density constituents through any force except gravitation.

The total energy density as given in terms of radiation, matter, and vacuum energy components is

$$\rho(a) = \rho_r(a) + \rho_m(a) + \rho_v(a), \tag{2.92}$$

which depend on the scale factor a as a^{-4}, a^{-3}, a^0, respectively, as long as there is no energy transfer between the species. We assume for the purposes of this section that the neutrinos are massless, always acting as radiation energy density. The matter energy

density consists of contributions from baryons and cold dark matter. Modeling the matter as a pressureless gas and observing that the comoving matter energy density is conserved, we write the proper energy density as

$$\rho_m = \frac{3H_0^2 m_{\rm pl}^2}{8\pi}(\Omega_b + \Omega_c)\left(\frac{a_0}{a}\right)^3. \tag{2.93}$$

The vacuum energy is the least understood of the energy densities. Assuming the universe to be critically closed, the sum of the three energy densities must be equal to the critical energy density, specified only by the Hubble rate at the current epoch. Hence, $\rho_v = \rho_c - \rho_{r,0} - \rho_{m,0}$. The vacuum energy density is negligible at all epochs of interest in this paper but is included for completeness.

The radiation component is given as:

$$\rho_r = \rho_\gamma + \rho_\nu + \rho_{\rm dr} \tag{2.94}$$

where ρ_γ is the photon energy density, ρ_ν is the neutrino energy density, and $\rho_{\rm dr}$ is the dark-radiation energy density. We parametrize $\rho_{\rm dr}$ as

$$\rho_{\rm dr} = \frac{7}{4}\left(\frac{4}{11}\right)^{4/3}\frac{\pi^2}{30}T^4\,\delta_{\rm dr}, \tag{2.95}$$

where $\delta_{\rm dr}$ is the dark-radiation parameter and is always assumed to be non-negative. In principle, we could entertain negative values of $\delta_{\rm dr}$ since it is an adjustable parameter of ρ_r. Such a change requires a fundamental reworking of the ΛCDM model so that $\sum_i \Omega_i = 1$. These non-standard cosmologies obtain when considering, for example, neutrino oscillations. These models, however, are not continuously connected with our model at $\delta_{\rm dr} = 0$, for any values of the parameters, thus motivating the maintenance of $\delta_{\rm dr} > 0$.

We write $N_{\rm eff}^{\rm (th)} = 3 + \Delta N_{\rm eff}^{\rm (th)}$ and assume that the contribution to $N_{\rm eff}^{\rm (th)}$ from ρ_ν is 3. Then the contribution from $\rho_{\rm dr}$ is given as $\Delta N_{\rm eff}^{\rm (th)}$. We see then that $\Delta N_{\rm eff}^{\rm (th)} = \delta_{\rm dr}$. This is simply a statement of the fact that $\tilde{N}_{\rm eff} = 3 + \Delta N_{\rm eff}^{\rm (th)} = N_{\rm eff}^{\rm (th)}$ for 'standard' cosmologies. It is, therefore, unnecessary for this simple dark-radiation model, to deduce $\tilde{N}_{\rm eff}$ from r_s/r_d since $N_{\rm eff}^{\rm (th)} = \tilde{N}_{\rm eff}$ by construction. This model of dark radiation is the usual model applied, for example in Ref. [2] and we explore, in this section, the predictions of the present BURST code to verify our results against those of prior results within the community. We will use $\tilde{N}_{\rm eff}$, for the remainder of this section, to denote the "effective number of relativistic degrees of freedom[3]."

Figures 2.3–2.6 show the results of computations in which the four parameters ω_b, Y_P, D/H, and $\tilde{N}_{\rm eff}$ are varied. We begin by varying the two model inputs: ω_b and $\tilde{N}_{\rm eff}$. The upper panel in Fig. 2.3 shows the dependence of $\tilde{N}_{\rm eff}$ on ω_b for curves of constant Y_P; the vertical band is the Planck value of $\omega_b = 0.02207 \pm 0.00033$. The figure is generated by first choosing a value for the baryon density in the range $0.004 \leq \omega_b \leq 0.029$. Each selected value of the dark radiation parameter in the range $3 \leq \tilde{N}_{\rm eff} \leq 4.5$ allows for the prediction of Y_P and D/H by parametrizing the radiation energy density as in Eq. (2.6). The values so obtained are plotted as contours in the $\tilde{N}_{\rm eff}$-ω_b plane in the upper and lower panels of Fig. 2.3. The solid curve is the preferred value $Y_P = 0.2465 \pm 0.0097$ of Ref. [1], which is a selection of observations of metal poor extragalactic H II regions. The contours are spaced by roughly $0.0097/3$ showing that $\tilde{N}_{\rm eff}$ is not strongly constrained by values of Y_P alone; this is a manifestation of the degeneracy of $\tilde{N}_{\rm eff}$ and Y_P. For example, at $Y_P = 0.2465 \pm 0.0035$, corresponding to the contours closest to $Y_P = 0.2465$, the range allowed $\tilde{N}_{\rm eff}$ is nearly consistent with both the standard, calculated value $N_{\rm eff} = 3.046$ and the Ref. [2] derived value of $N_{\rm eff} = 3.30 \pm 0.27$.

Predictions of the primordial deuterium abundance are a much more sensitive

[3] We refer to $N_{\rm eff}$ as the effective number of relativistic degrees of freedom although there are factors that complicate this interpretation, among them the temperature parameter, and fermionic nature of neutrinos.

constraint upon allowed values of $\tilde{N}_{\rm eff}$. This can be seen in the lower panel of Fig. 2.3. The solid line contour with $10^5 \times {\rm D/H} = 2.530 \pm 0.04$ corresponds to the recent measurement of Ref. [3]. Contours in this figure are separated by the one standard deviation of Ref. [3]. There are two points of interest regarding the deuterium figure. First, as noted in Ref. [3], observation of the primordial component of deuterium is precise enough to begin to constrain the microscopic physics of the thermally averaged nuclear reaction rates and their cross sections. Additionally, given the precision of the current and forthcoming deuterium measurements and the strong dependence of $\tilde{N}_{\rm eff}$ on its value (at constant ω_b), we advocate using D/H as a prior, over Y_P, for future base model parameter searches as recommended by Refs. [41, 9, 3].

The degeneracy between $\tilde{N}_{\rm eff}$ and Y_P is again evident in Fig. 2.4. Each plot explores the D/H vs. ω_b contour space, where the upper plot contains contours of constant Y_P and the lower plot contains contours of constant $\tilde{N}_{\rm eff}$. The shaded bands in each figure indicate the one-sigma observations of ω_b and D/H from Refs. [2, 3], respectively. Deuterium is not an input parameter into our model. We compute it by choosing a baryon number and iteratively change the dark-radiation parameter, $\delta_{{\rm d}r}$ until matching the chosen deuterium target. The outputs from the process are $\tilde{N}_{\rm eff}$ and Y_P. Values of ω_b, D/H and $\tilde{N}_{\rm eff}$ are in satisfactory agreement with the standard cosmology at the precision of current observations.

The quantities D/H and ω_b are the tightest observationally-constrained parameters we are currently investigating. Figure 2.5 shows two plots in the Y_P-$N_{\rm eff}$ plane with contours of constant ω_b (upper plot), and contours of constant $10^5 \times$ D/H (lower plot). The horizontal band in each figure indicates the one-sigma observation of Y_P from Ref. [1]. Like D/H, Y_P is not an input into our model. Consequently, we adopt the identical iterative method for Y_P in Fig. 2.5 as we do for D/H in Fig. 2.4. For the ω_b (upper) plot of Fig. 2.5, the solid contour line is the best-fit value of Ref. [2] with nine-sigma spacing of

the contours. The contours exist in a subspace of the Y_P-$N_{\rm eff}$ plane which is well within current observations, but nevertheless could span a range of radically different physics. Similarly, the bottom plot shows the $10^5 \times$ D/H value of Ref. [3] as the solid contour with the other contours spaced fifteen-sigma apart. Clearly, Y_P and $\tilde{N}_{\rm eff}$ do not constrain the cosmological model as tightly as ω_b and D/H. This observation indicates the import of using the next generation of 30-meter class telescopes and CMB observation to better determine the light element abundances, particularly, Y_P with high precision.

Figure 2.6 shows how $\tilde{N}_{\rm eff}$ changes in the Y_P-ω_b plane. The shaded bands in each figure indicate the one-sigma observations of ω_b and Y_P from Refs. [2, 1], respectively. We may conclude from this plot that there could exist many different values of $\tilde{N}_{\rm eff}$ consistent with the observations of Y_P and ω_b. However, we caution against such a conclusion without considering the effect on D/H. In fact, we choose not to include a figure of contours of D/H in the Y_P-ω_b plane because the strong sensitivity of D/H to ω_b produces too large a range of values for Y_P to be useful as a constraint of the cosmological model.

All calculations show a consistency between ω_b, $\tilde{N}_{\rm eff}$, D/H, and Y_P to a conservative limit of two-sigma error range in each observation. We expect the uncertainties in each observation to improve in the coming years with large ground-based CMB experiments [42, 43] and 30-meter class telescopes [44, 45, 46]. Future high-precision measurements may result in tensions for the best-fit values of ω_b, $\tilde{N}_{\rm eff}$, and D/H. These tensions could be indications of the need for more precise theoretical and numerical approaches or could signal the presence of physics beyond the standard model. As it stands here, the bottom panels of Figs. 2.3 and 2.4 shows that the tension between ω_b and D/H cannot be resolved with the addition of extra radiation energy density. Uncertainties in nuclear reactions may produce disagreement between ω_b and D/H, allowing D/H to become a probe of nuclear physics. It is also possible that the spectroscopic determination

of D/H may be subject to small systematic errors only recognizable at such precision. An exciting prospect is the need to revise the CSM to resolve tensions with the observations of D/H and ω_b, possibly leading to the conclusion of BSM physics active during BBN.

2.6 Conclusion

The contour plots of Sec.2.5 show consistency between D/H, ω_b, and $\tilde{N}_{\rm eff}$. The prediction of the deuterium abundance from BBN provides support for the standard cosmology. SBBN begins close to equilibrium, and only requires the evolution of the plasma temperature, the scale factor, the electron degeneracy parameter, and the nuclear abundances. Non-standard BBN may require more advanced techniques. We will address implications arising from non-standard cosmologies in future chapters.

We thank Christel Sutterley for originally providing the numerical codes to calculate the BBN abundances.

Sections 2.1 and 2.5 are reprints of some of the material as it appears in "Probing neutrino physics with a self-consistent treatment of the weak decoupling, nucleosynthesis, and photon decoupling epochs." Grohs, E.; Fuller, G. M.; Kishimoto, C. K.; Paris, M. W., J. Cosmology Astropart., 5 (May 2015) 17. The dissertation author was the primary investigator and author of this paper.

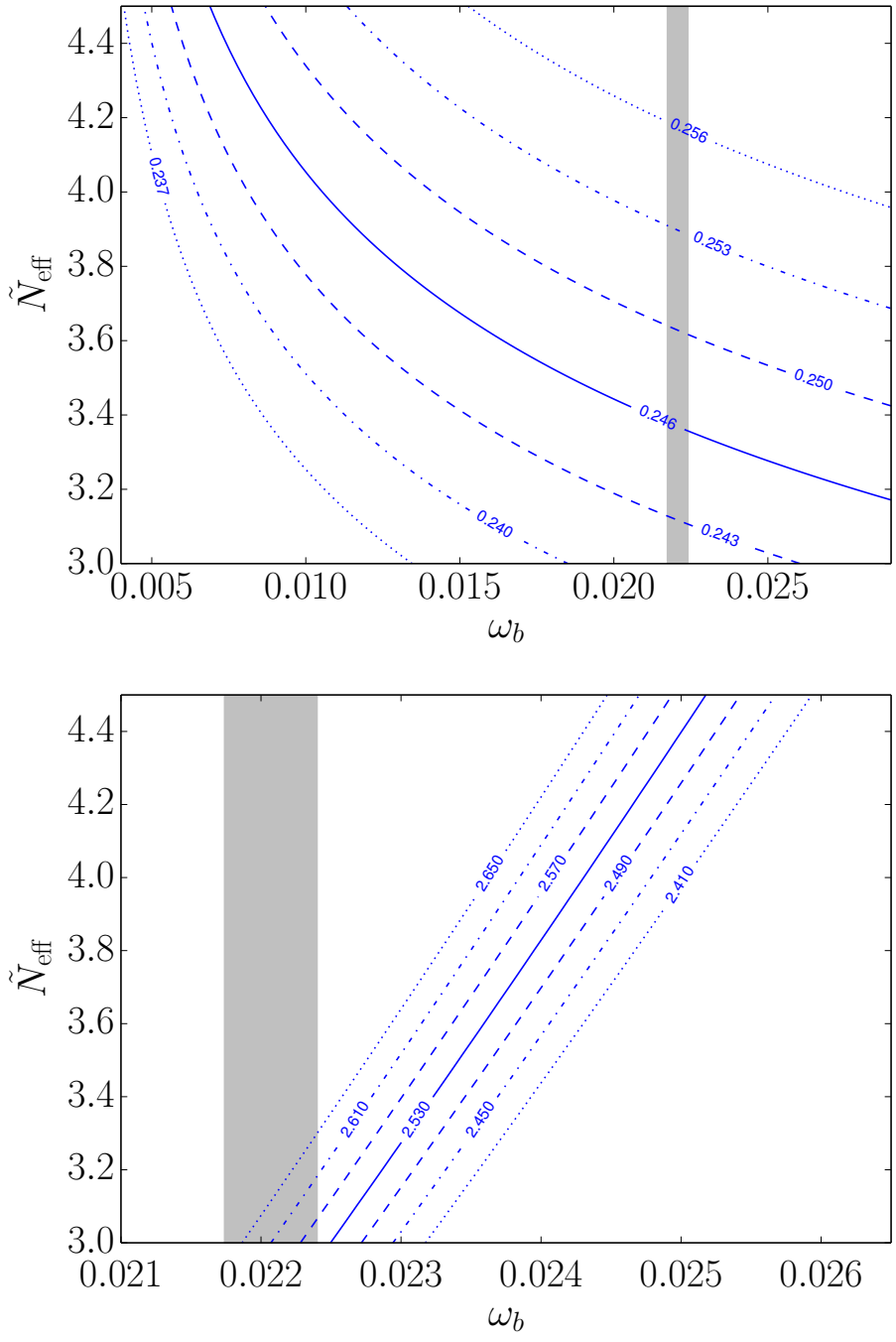

Figure 2.3: (Top) $\tilde{N}_{\rm eff}$ plotted against ω_b for contours of constant values of Y_P (labeled by mass fraction). The solid curve is the preferred value of Ref. [1]. The contours are spaced by $\Delta Y_P \approx 0.003$. (Bottom) $\tilde{N}_{\rm eff}$ versus ω_b for contours of constant values of $10^5 \times$ D/H. The solid curve is the preferred value of Ref. [3]. The contours are spaced by $\Delta(10^5 \times {\rm D/H}) = 0.04$. The vertical shaded band in each figure indicates the one-sigma observation of ω_b from Ref. [2]. In each case, abundances are determined in a self-consistent BBN calculation.

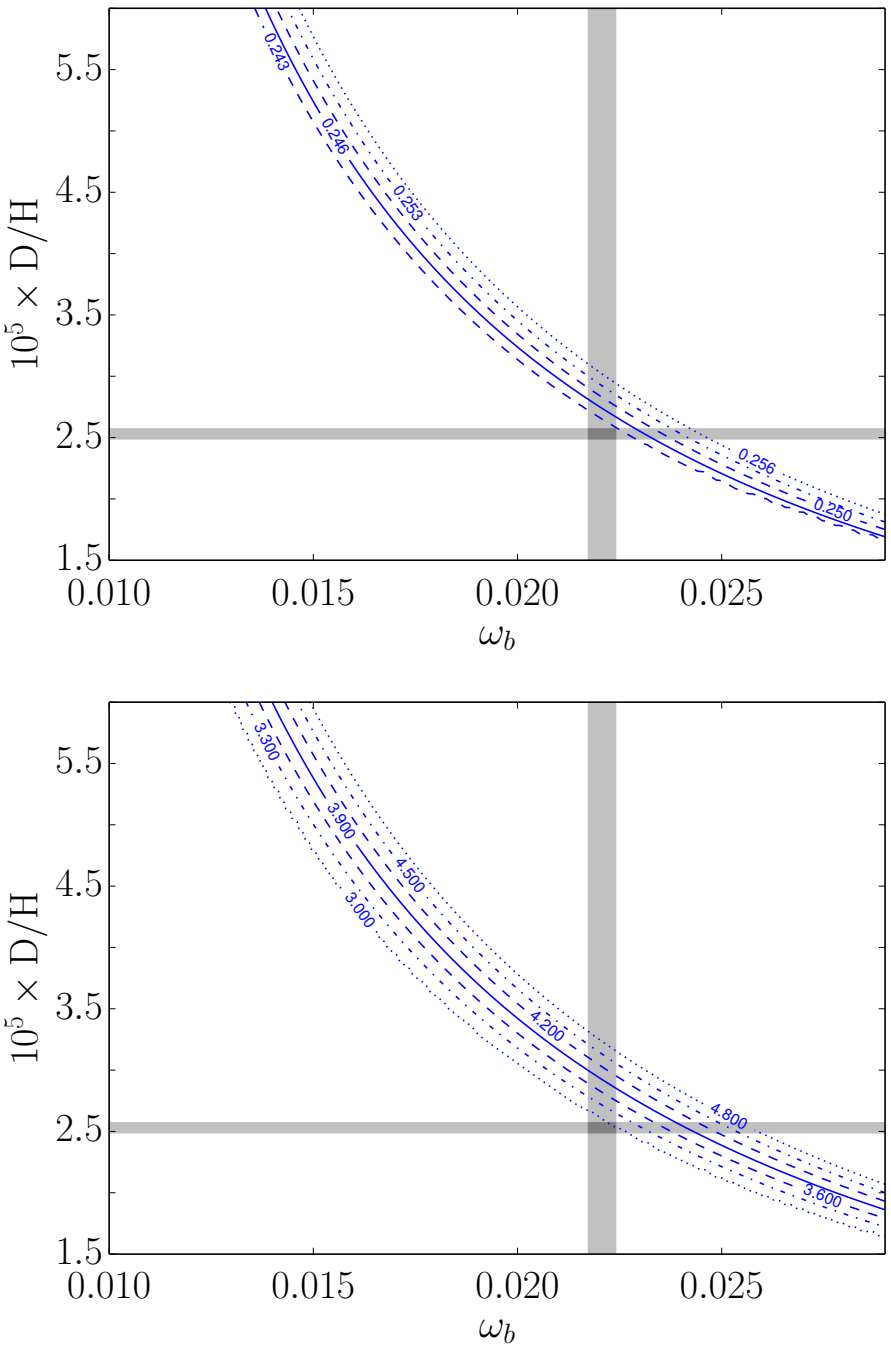

Figure 2.4: (Top) $10^5 \times$ D/H plotted against ω_b for contours of constant Y_P. The solid curve is the preferred value of Ref. [1]. The contours are spaced by $\Delta Y_P \approx 0.003$. (Bottom) $10^5 \times$ D/H versus ω_b for contours of constant $\tilde{N}_{\rm eff}$. The shaded bands in each figure indicate the one-sigma observations of ω_b and D/H from Refs. [2, 3], respectively. The contours are spaced by $\Delta\tilde{N}_{\rm eff} = 0.3$

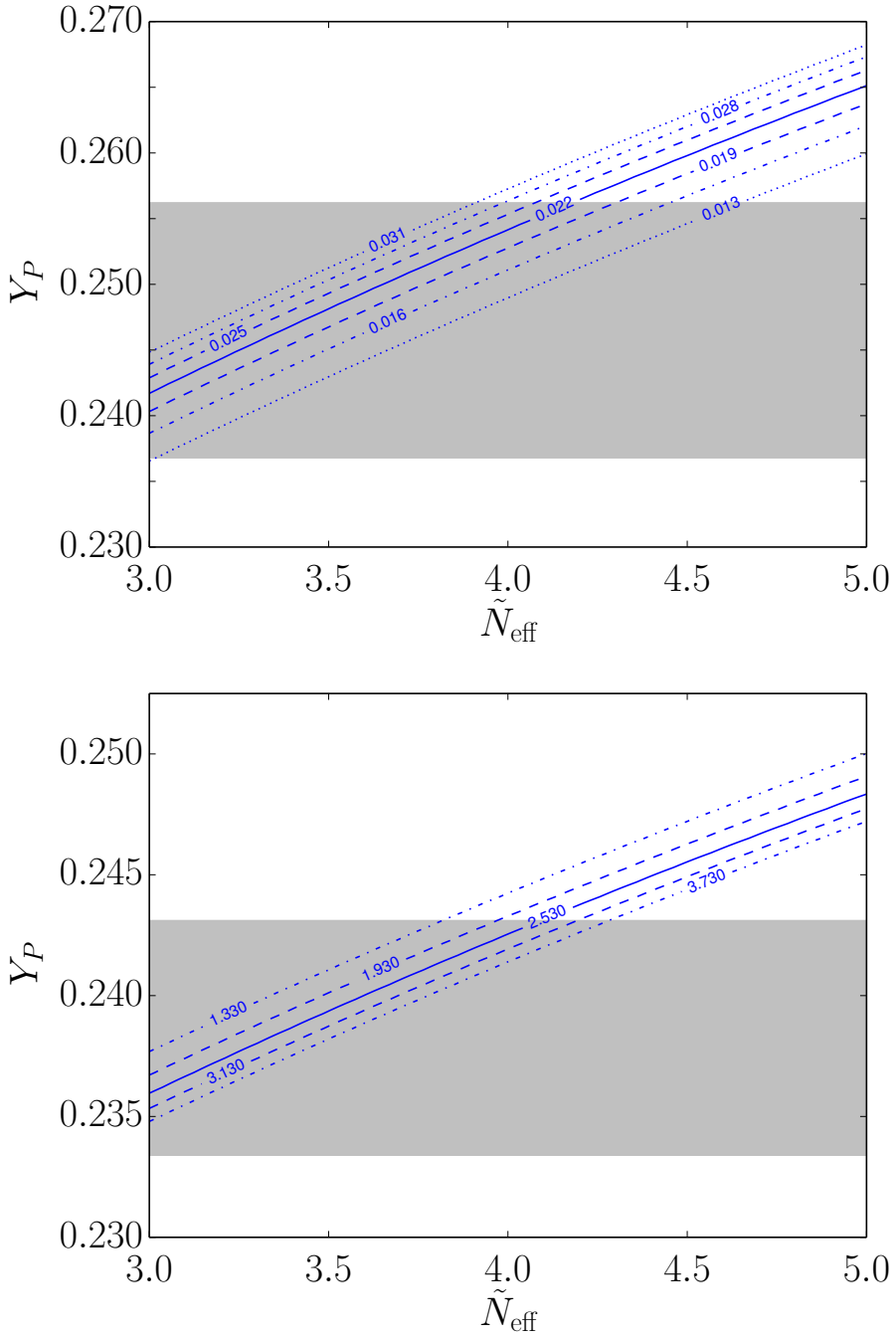

Figure 2.5: (Top) Y_P plotted against $\tilde{N}_{\rm eff}$ for contours of constant ω_b. The solid curve is the best-fit value of Ref. [2]. The contours are spaced by $\Delta\omega_b = 0.003$. (Bottom) Y_P versus $\tilde{N}_{\rm eff}$ for contours of constant $10^5 \times$ D/H. The solid curve is the preferred value of Ref. [3]. The contours are spaced by $\Delta(10^5 \times {\rm D/H}) = 0.6$. The horizontal band in each figure indicates the one-sigma observation of Y_P from Ref. [1].

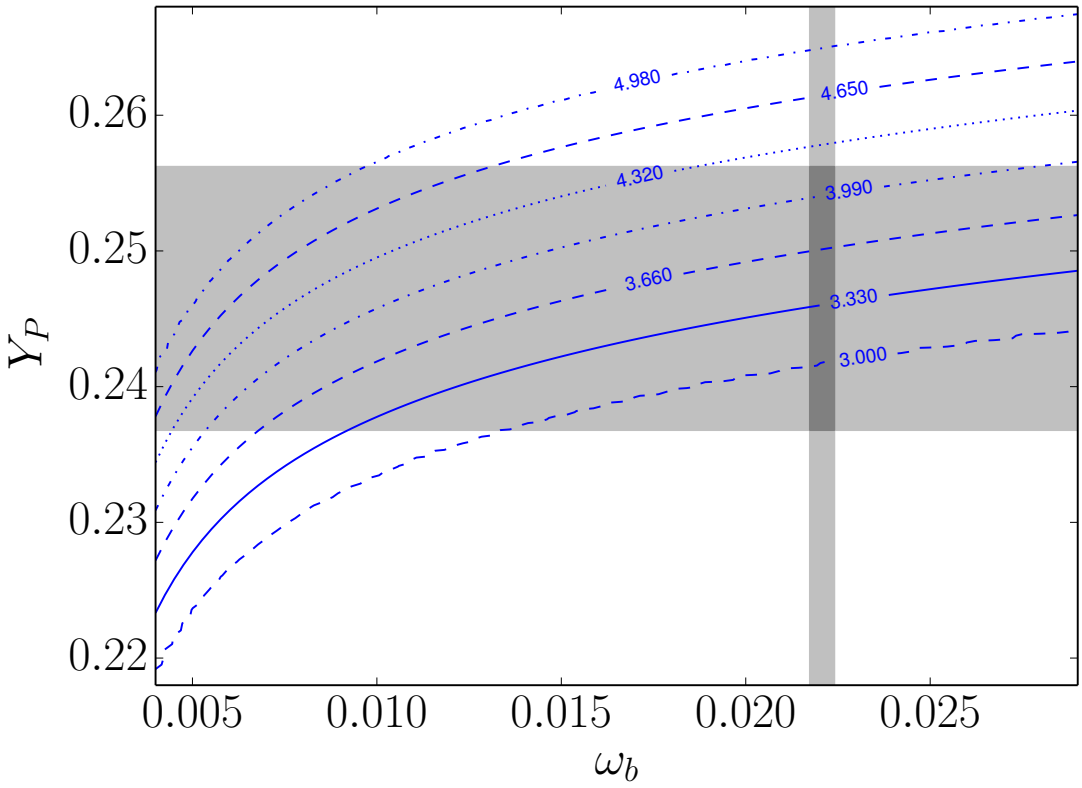

Figure 2.6: Y_P plotted against ω_b for contours of constant $\tilde{N}_{\rm eff}$. The contours are spaced by $\Delta\tilde{N}_{\rm eff} = 0.33$. The shaded bands in each figure indicate the one-sigma observations of ω_b and Y_P from Refs. [2, 1], respectively.

Chapter 3

Dilution

3.1 Introduction

Dark matter makes up roughly 25% of the energy density of the universe. The nature of the dark matter particle is unknown. Primary candidates include the lightest super–symmetric particle, primordial black holes, axions, and sterile neutrinos among others. We focus on sterile neutrinos and investigate a specific mechanism for sterile–neutrino production called dilution. Dilution posits the existence of two sterile neutrinos. One particle is the dark matter candidate with a lifetime longer than the age of the current universe. The other particle is shorter lived and decays in the early universe. We will study the ramifications of the diluton, the second sterile neutrino, during weak decoupling and big bang nucleosynthesis (BBN).

The diluton decays into standard model particles. Photons, electrons, positrons, and all three flavors of neutrinos and anti-neutrinos are the only particles to appear in the final state. The energy in the plasma particles will thermalize with the background plasma. For an ultra-relativistic bosonic species coupled to the plasma (e.g. photons), the

number density of the particle in thermal equilibrium goes as:

$$n_{\text{coup}} = g\frac{\zeta(3)}{\pi^2}T^3, \tag{3.1}$$

where g is the internal partition function, $\zeta(3)$ is the Riemann zeta function of argument 3, T is the plasma temperature, and we have assumed zero degeneracy. For a fermionic species with ultra-relativistic kinematics (e.g. neutrinos), the number density is the same as Eq.(3.1) multiplied by an overall factor of $3/4$. If a particle has decoupled from the plasma, i.e. it no longer partakes in energy transfer between the particles constituing the plasma, then the number density, n_{dec}, of the particle changes with respect to scale factor, a, as the following:

$$n_{\text{dec}} = n_0\left(\frac{a_0}{a}\right)^3, \tag{3.2}$$

where n_0 is the proper number density of the decoupled species at the current epoch, and $a_0 \equiv 1$ Mpc is the scale factor at the current epoch. The kinematics of the particle are irrelevant to the form of the number density, i.e. Eq.(3.2) is applicable at all epochs when the particle is decoupled. Eq.(3.2) also applies to massive particles still thermally coupled to the plasma, but no longer in chemical equilibrium with the plasma particles. An example of this phenomenon would be baryons. If we define the baryon–to–photon, η_b, to be the ratio of the baryon number density to photon number density, then:

$$\frac{\eta_{b,f}}{\eta_{b,i}} = \left(\frac{n_{b,f}}{n_{b,i}}\right)\left(\frac{n_{\gamma,i}}{n_{\gamma,f}}\right) = \left(\frac{a_i}{a_f}\right)^3\left(\frac{T_i}{T_f}\right)^3, \tag{3.3}$$

where the subscripts i and f refer to initial and final values, respectively.

We can relate the temperatures of Eq.(3.3) to numerous quantities. We choose to relate the temperature to the entropy density. For an ultra-relativistic species, the entropy

density is:

$$s_{V,i} \equiv g_i \frac{2\pi^2}{45} T_i^3, \tag{3.4}$$

where g_i is the internal partition function, and T_i is the temperature of species i. For the total entropy density in relativstic particles, we need the quantity $g_{\star S}$, the effective, relativistic, entropic, degrees–of–freedom statistic from Eq.(1.81). In this chapter, we consider a different quantity $g_\star$, the effective relativistic-energy degrees-of-freedom statistic:

$$g_\star \equiv \sum_i g_i^{(b)} \left(\frac{T_i}{T}\right)^4 + \frac{7}{8} \sum_j g_j^{(f)} \left(\frac{T_j}{T}\right)^4, \tag{3.5}$$

where the $\sum_i$ is a sum over the bosonic degrees of freedom, and $\sum_j$ is a sum over the fermionic degrees of freedom. $g_{\star S}$ has the same form as Eq.(3.5), except for a power of three on the ratios $(T_{i,j}/T)$. Eq.(3.5) allows for different temperatures of each particle species, but still assumes each species maintains an ultra-relativistic equilibrium energy density. We will not consider the scenario where the species have different temperatures, implying that $g_{\star S} = g_\star$. Our expression for the total entropy density in relativistic particles is:

$$s_V = g_{\star S} \frac{2\pi^2}{45} T^3 = g_\star \frac{2\pi^2}{45} T^3 \implies T^3 \propto \frac{s_V}{g_\star}, \tag{3.6}$$

giving a new ratio of $\eta_{b,f}$ to $\eta_{b,i}$ of:

$$\frac{\eta_{b,f}}{\eta_{b,i}} = \left(\frac{a_i}{a_f}\right)^3 \left(\frac{T_i}{T_f}\right)^3 = \left(\frac{n_{b,f}}{n_{b,i}}\right) \left(\frac{s_{V,i}}{s_{V,f}}\right) \left(\frac{g_{\star,f}}{g_{\star,i}}\right) \equiv \left(\frac{s_i}{s_f}\right) \left(\frac{g_{\star,f}}{g_{\star,i}}\right) \equiv \frac{1}{F} \left(\frac{g_{\star,f}}{g_{\star,i}}\right), \tag{3.7}$$

where we have defined s as the entropy per baryon, and the dilution factor F as the ratio of the final to initial entropy per baryon. Our reason for using s as an alternative to T is for time–evolution purposes. The classical entropy S evolves as:

$$dS = \frac{dQ}{T} \implies \frac{dS}{dt} = \frac{1}{T} \frac{dQ}{dt}, \tag{3.8}$$

for added heat Q. The total entropy and entropy per baryon are constants as the universe expands, assuming no heat flow.

During the evolution of the early universe, the relativistic–energy degrees–of–freedom decreases due to two separate processes: particle/anti-particle annihilation; and decoupling. In the first process, annihilation of the particle/anti-particle seas convert internal energy to heat. The plasma experiences no net heat flow, and the entropy per baryon is constant. There must be an associated relative increase in temperature with the decrease in $g_\star$. This relative increase in temperature need not be an absolute increase in temperature. The increase is with respect to a comoving quantity, such as the product of the cube–root of baryon density multiplied by scale factor. Therefore:

$$\begin{aligned} \text{If } s_f = s_i &\implies g_{\star,i} a_i^3 T_i^3 = g_{\star,f} a_f^3 T_f^3 \\ &\implies T_f = T_i \frac{a_i}{a_f} \left(\frac{g_{\star,i}}{g_{\star,f}} \right)^{1/3}, \end{aligned} \tag{3.9}$$

gives the final temperature in terms of the initial temperature, scale factors, and $g_\star$ before and after an epoch of annihilation. In the second process, a particle species decouples from the plasma and reduces $g_\star$ and the entropy per baryon. There is no change in the internal energy, so the temperature remains constant. The ratio of baryon–to–photon ratios becomes:

$$\frac{\eta_{b,f}}{\eta_{b,i}} = \left(\frac{s_i}{g_{\star,i}} \right) \left(\frac{g_{\star,f}}{s_f} \right) = \frac{2\pi^2 T_i^3}{45} \frac{45}{2\pi^2 T_f^3} = \left(\frac{T_i}{T_f} \right)^3 = 1, \tag{3.10}$$

, implying no change in the baryon-to-photon ratio.

In the case of a diluton decaying in the early universe, the heat added is non-zero.

If all of the heat goes into the plasma, the entropy per baryon evolves as:

$$\frac{ds}{dt} = -\frac{1}{n_b T}\frac{\partial \rho_s}{\partial t}\bigg|_{a,T}. \tag{3.11}$$

The overall negative sign indicates that the change in entropy per baryon is positive as the diluton energy density, ρ_s, decreases due to particle decay. Eq.(3.11) assumes that all of the energy from decay flows into the plasma and no energy flows into decoupled seas. We will abandon this assumption later in the chapter.

We have considered the baryon to photon ratio, although we are interested in a relic energy density of dark matter. The ratio of final to initial dark–matter–energy densities, $\rho_{\rm DM}$, is the same as the ratio of number densities, $n_{\rm DM}$, (assuming the initial number density refers to an epoch when the dark matter particle is decoupled):

$$\begin{aligned}\frac{\rho_{{\rm DM},f}}{\rho_{{\rm DM},i}} = \frac{m_{\rm DM} n_{{\rm DM},f}}{m_{\rm DM} n_{{\rm DM},i}} = \left(\frac{a_i}{a_f}\right)^3 &= \frac{1}{F}\left(\frac{g_{\star,f}}{g_{\star,i}}\right)\left(\frac{T_f}{T_i}\right)^3 \\ \implies \rho_{{\rm DM},f} &= \frac{1}{F}\left(\frac{g_{\star,f}}{g_{\star,i}}\right)\left(\frac{T_f}{T_i}\right)^3 m_{\rm DM} n_{{\rm DM},i} \\ &= \frac{1}{F}\left(\frac{g_{\star,f}}{g_{\star,i}}\right)\left(\frac{T_f}{T_i}\right)^3 m_{\rm DM}\left(\frac{3}{4} g_{\rm DM}\frac{\zeta(3)}{\pi^2} T_i^3\right), \end{aligned} \tag{3.12}$$

where we have taken the initial number density of the dark–matter candidate to be at an epoch immediately before the particle decouples. We will set the internal partition function of the dark-matter candidate to 2. The dark matter density at the current epoch is defined to be the ratio of the dark matter energy density to the critical energy density, multiplied by the square of the hubble parameter:

$$\omega_{\rm DM} \equiv \Omega_{\rm DM} h^2 = \frac{\rho_{{\rm DM},0}}{\rho c, 0} h^2 = \frac{\rho_{{\rm DM},0}}{3H_0^2 m_{\rm pl}^2/8\pi} h^2, \tag{3.13}$$

where the Hubble rate at the current epoch is defined to be $H_0 \equiv h \times 100$ km/s/Mpc

and $h \sim 0.7$ from measurements. If we: (1) set the initial quantities (subscript i) to the quantities at dark–matter decoupling (subscript dec); (2) set the final quantities (subscript f) to the quantities at the current epoch (subscript 0); and (3) substitute Eq.(3.12) into Eq.(3.13), we find:

$$\omega_{\rm DM} = 0.1203 \times \left(\frac{T_0}{2.726\ {\rm K}}\right)^3 \times \left(\frac{m_{\rm DM}}{7.1\ {\rm keV}}\right) \times \left(\frac{g_{\star,{\rm dec}}/g_{\star,0}}{53.375}\right)^{-1} \times \left(\frac{F}{32.34}\right)^{-1}. \tag{3.14}$$

The calculation of the dilution factor F is non-trivial and is the subject of this chapter. The motivation for the diluton is the dark–matter production mechanism, but we stress that the results are applicable to generic treatments of heavy–particle decay during weak-decoupling and BBN. The structure of this chapter proceeds as follows. Section 3.2 outlines a primitive particle model for sterile neutrinos and applies it to the early universe. Sec.3.3 discusses the the rates and spectra of the different decay channels of the diluton. Sec.3.4 gives the approximate scheme for thermalizing the neutrino and plasma energy from the decays. Sec.3.5 presents first results on the evolution of the entropy, weak–interaction rates, and nuclear abundances. We conclude in Sec.3.6.

3.2 Preliminaries

3.2.1 Sterile Neutrino Basics

Sterile neutrinos mix with active neutrinos on scales below the weak–interaction. If we consider the toy model of one active and one sterile neutrino, we can write the representation of each flavor eigenstate as a superposition of mass eigenstates:

$$|\nu_a\rangle = \cos\theta|\nu_1\rangle + \sin\theta|\nu_2\rangle \tag{3.15}$$

$$|\nu_s\rangle = -\sin\theta|\nu_1\rangle + \cos\theta|\nu_2\rangle, \tag{3.16}$$

where $\nu_{a,s}$ are the active/sterile eigenstates, $\nu_{1,2}$ are the mass eigenstates, and θ is the mixing angle. The set of equations (3.15), (3.16) is incomplete as there are three active neutrinos and possibly more sterile neutrinos. However, because the mixing angle is small ($\sin\theta << 1$) between any active-sterile pair, Eqs.(3.15) and (3.16) serve to show that the heavier mass eigenstate is nearly coincident with the sterile flavor state. Typical integrated cross–sections, $\langle\sigma v\rangle$, as a function of energy E for sterile neutrinos behave like:

$$\langle\sigma v\rangle \sim G_F^2 \sin^2\theta E^2 \tag{3.17}$$

where $G_F = 1.166364 \times 10^{-11}$ MeV^{-2} is the weak coupling constant, also called the Fermi coupling constant.

3.2.2 Diluton Basics

We investigate the sterile neutrino as a diluton using estimation arguments. The diluton is produced thermally in the big bang, and exists in thermal and chemical equilibrium with the primeval plasma if $\Gamma_s \gtrsim H$, where Γ_s is a typical scattering rate of dilutons with active neutrinos, and H is the Hubble rate. We use $\langle\sigma v\rangle$ from Eq.(3.17) to approximate Γ_s as:

$$\Gamma_s \sim \langle\sigma v\rangle n_s, \tag{3.18}$$

where $n_s \sim T^3$ is the number density of the diluton species at temperature T. To determine the temperature where $\Gamma_s \sim H$, we use Eq.(3.5) to express the Hubble rate as:

$$H = \sqrt{\frac{8\pi}{3m_{\rm pl}^2} g_\star \frac{\pi^2}{30} T^4} = 1.66 g_\star^{1/2} \frac{T^2}{m_{\rm pl}}, \tag{3.19}$$

where $m_{\rm pl} = 1.220932 \times 10^{22}$ MeV is the Planck mass. If we take the energy variable in Eq.(3.17) to be $E \sim T$, we find a relation between Γ_s and H in terms of temperature and

$g_\star$:

$$\langle \sigma v \rangle n_s \sim G_F^2 \sin^2\theta T^5 \sim 1.66 g_\star^{1/2} \frac{T^2}{m_{\rm pl}} \tag{3.20}$$

$$\implies T_{\rm dec} \sim g_\star^{1/6} \left(\frac{1}{\sin^2\theta}\right)^{1/3} \left(\frac{1}{G_F^2 m_{\rm pl}}\right)^{1/3} \tag{3.21}$$

$$= g_\star^{1/6} \left(\frac{10^{-9}}{\sin^2\theta}\right)^{1/3} 10^3 \text{ MeV} \tag{3.22}$$

where we have used the approximate relation $G_F^2 m_{\rm pl} \sim 1 \text{ MeV}^{-3}$. We exercise caution in the use of Eq.(3.22), as $g_\star$ is a function of temperature. For the diluton mass and mixing angles germane to our discussion of weak decoupling and BBN, the decoupling temperature is $\sim 10^3$ MeV, implying $g_\star \sim 60$ and maintaining consistency with Eq.(3.22).

Once the diluton decouples from the plasma, the product of the cube of the scale factor and the number density, $a^3 n_s$, would become a comoving invariant if the species were stable to decay. We can use a comoving temperature T_s to describe the evolution in phase-space density of the diluton species and an exponential decay expression to describe the decay of the diluton post decoupling. The energy density is simply equal to the number density multiplied by the average energy of a given particle:

$$\rho_s \sim \overline{E} T_s^3 e^{-t/\tau}, \tag{3.23}$$

where τ is the lifetime of the diluton. In general, $\bar{E}$ would follow from a general dispersion relation relating the momentum, mass, and energy. For the diluton masses and epochs we consider: $\bar{E} \sim m_s$, the mass of the diluton. The energy density is:

$$\rho_s \sim m_s T_s^3 e^{-t/\tau} \to m_s \frac{3}{2\pi^2} \zeta(3) T_s^3 e^{-t/\tau}, \tag{3.24}$$

where we have explicitly written out the expression for the energy density so as to

implement it in a calculation. We assume no asymmetry between particles and anti-particles, implying Eq.(3.24) contains an overall multiplicative factor of 2. For the diluton temperature, we use the entropy in ultra-relativistic particles to relate the diluton temperature to the plasma temperature at weak decoupling. If we assume that the diluton decouples after the termination of tau/anti-tau particle annihilation, but before the quark-hadron phase transition, the relativistic-energy degrees of freedom is:

$$g_\star^{(\mathrm{sd})} = 2+2\times 8+\frac{7}{8}(2\times 2+2\times 2+1\times 2\times 3+2\times 2\times 3\times 3) = 61.75, \tag{3.25}$$

$$\gamma \qquad g \qquad \mu \qquad e \qquad \nu \qquad q \tag{3.26}$$

for photons (γ), gluons (g), muons/anti-muons (μ), electrons/positrons (e), neutrinos/anti-neutrinos (ν), and quarks/anti-quarks (q). At the onset of weak decoupling, only the photons, electrons/positrons, and neutrinos carry the entropy in relativistic particles, implying:

$$g_\star^{(\mathrm{wd})} = 2+\frac{7}{8}(2\times 2+1\times 2\times 3) = 10.75. \tag{3.27}$$

Therefore, the ratio of the diluton to plasma temperature at the onset of weak decoupling is:

$$\frac{T_s}{T} = \left(\frac{g_\star^{(\mathrm{wd})}}{g_\star^{(\mathrm{sd})}}\right) = \frac{1}{1.79}. \tag{3.28}$$

Eq.(3.28) is only applicable at the start of weak decoupling. During the epoch of positron–electron annihilation, the plasma temperature experiences a non-trivial evolution and Eq.(3.28) is no longer applicable. During this epoch, the diluton temperature parameter redshifts with the expansion. It suffices to find the diluton lifetime in order to determine all of the quantities in Eq.(3.24)

3.3 Decay channels

The diluton decays into several channels. We consider the following channels in our analysis:

$$\nu_s \to \nu_i + \nu_j + \bar{\nu}_j \tag{3.29}$$

$$\nu_s \to \nu_i + \gamma \tag{3.30}$$

$$\nu_s \to \nu_i + \pi^0 \tag{3.31}$$

$$\nu_s \to \pi^{\pm} + e^{\mp} \tag{3.32}$$

$$\nu_s \to \pi^{\pm} + \mu^{\mp} \tag{3.33}$$

$$\nu_s \to \nu_i + e^- + e^+ \tag{3.34}$$

$$\nu_s \to \nu_i + \mu^- + \mu^+. \tag{3.35}$$

The corresponding channels for $\bar{\nu}_s$ are symmetric. We will consider diluton masses well in excess of active neutrino masses. Therefore, Rxns.(3.29) and (3.30) are always present. Rxn.(3.31) - (3.35) require a mass threshold for m_s. We do not consider diluton masses heavy enough for τ particles in the final state. In addition, we do not include decays into $K^{\pm,0}$ channels for this analysis.

We make the approximation that Pauli blocking of fermions in the final state is negligible at the epochs of interest. Therefore, the rate of disintegration for a given channel is constant in temperature, and given as a function of m_s, $\sin^2\theta$, and fundamental constants[16].

3.3.1 Decay into three neutrinos

The decay rate for this process is[16]:

$$\Gamma_{3\nu} = \frac{G_F^2}{192\pi^3} m_s^5 \sin^2\theta \tag{3.36}$$

$$\approx 3.47 \times 10^{-5}\,\mathrm{s}^{-1} \left(\frac{m_s}{\mathrm{MeV}}\right)^5 \sin^2\theta. \tag{3.37}$$

For the decay spectrum, we approximate that all three neutrinos equally share the initial energy, implying for a given neutrino species i:

$$\left.\frac{df_i}{dE\,dt}\right|_{3\nu} = \Gamma_{3\nu}\delta\left(E - \frac{m_s}{3}\right)\frac{2}{3}. \tag{3.38}$$

where p is the momentum/energy of the neutrino and $\delta(x-x_0)$ is the Dirac-delta-function. The factor of $2/3$ arises from the assumption that the probability the decay produces each neutrino species (e,μ,τ) is equally likely. For anti-neutrinos, the factor would be $1/3$. The factors are switched when considering the decay of an anti-diluton.

3.3.2 Decay into active neutrino and a photon

The decay rate for this process is[16]:

$$\Gamma_{\nu\gamma} \approx \frac{9G_F^2}{512\pi^4}\alpha m_s^5 \sin^2\theta \tag{3.39}$$

$$\approx 2.72 \times 10^{-7}\,\mathrm{s}^{-1} \left(\frac{m_s}{\mathrm{MeV}}\right)^5 \sin^2\theta, \tag{3.40}$$

where $\alpha \approx 1/137$ is the fine-structure constant. The neutrino and photon are assumed to be ultra-relativistic. Therefore, the energy is shared equally among the two daughter particles:

$$\left.\frac{df_i}{dE\,dt}\right|_{\nu\gamma} = \Gamma_{\nu\gamma}\delta\left(E - \frac{m_s}{2}\right)\frac{1}{3}. \tag{3.41}$$

3.3.3 Decay into active neutrino and neutral pion

Assuming the diluton has a larger mass than the neutral pion ($m_{\pi^0} \sim 135.0$ MeV), the decay rate for this process is[16]:

$$\Gamma_{\nu\pi^0} = \frac{G_F^2 f_\pi^2}{16\pi} m_s (m_s^2 - m_{\pi^0}^2) \sin^2\theta \tag{3.42}$$

$$\approx 70.56\,\mathrm{s}^{-1} \left(\frac{m_s}{\mathrm{MeV}}\right)^3 (1-x^2) \sin^2\theta, \tag{3.43}$$

where $x \equiv m_{\pi^0}/m_s$ and $f_\pi = 131$ MeV. The decay is into two particles, so the decay spectra for each particle is monoenergetic. For the resulting neutrino:

$$\left.\frac{df_i}{dE\,dt}\right|_{\nu\pi^0} = \Gamma_{\nu\pi^0} \delta\left[E - \frac{m_s}{2}(1-x^2)\right] \frac{1}{3}. \tag{3.44}$$

We assume the neutral pion instantaneously decays into two photons.

3.3.4 Decay into charged pion and electron

Assuming the diluton has a larger mass than the sum of the charged pion and electron ($m_\pi + m_e \sim 140$ MeV), the decay rate for this process is[16]:

$$\Gamma_{\pi e} = 2\frac{G_F^2 f_\pi^2}{16\pi} m_s \left\{\left[m_s^2 - (m_\pi + m_e)^2\right]\left[m_s^2 - (m_\pi - m_e)^2\right]\right\}^{1/2} \sin^2\theta \tag{3.45}$$

$$\approx 1.411 \times 10^2\,\mathrm{s}^{-1} \left(\frac{m_s}{\mathrm{MeV}}\right)^3 \left\{\left[1-(x+y)^2\right]\left[1-(x-y)^2\right]\right\}^{1/2} \sin^2\theta, \tag{3.46}$$

where $x \equiv \frac{m_\pi}{m_s}$ and $y \equiv \frac{m_e}{m_s}$. The extra factor of 2 arises from two equally likely decay channels: $\nu_s \to \pi^+ + e^-$ and $\nu_s \to \pi^- + e^+$. We assume that the charged pion instantaneously decays into a muon. Without loss of generality, let us consider the case with $\nu_s \to \pi^+ + e^-$. The resulting decay of the π^+ is $\pi^+ \to \nu_\mu + \mu^+$. We also assume that the muon instantaneously decays via $\mu^+ \to \bar{\nu}_\mu + \nu_e + e^+$. This decay channel produces three

distinct flavor/parity neutrinos: ν_e, ν_μ, and $\bar{\nu}_\mu$. Appendix C explains the derivation for the spectra of each neutrino. For the ν_μ:

$$\left.\frac{df_{\nu_\mu}}{dE\,dt}\right|_{\pi e} = \Gamma_{\pi e}\frac{m_\pi}{2E^{(2)}p^{(1)}}\theta\left[E - E^{(2)}\frac{E^{(1)}-p^{(1)}}{m_\pi}\right]\theta\left[E^{(2)}\frac{E^{(1)}+p^{(1)}}{m_\pi} - E\right], \quad (3.47)$$

where the quantities $E^{(1)}$, $p^{(1)}$, and $E^{(2)}$ are defined in App.C and given in terms of the masses of the diluton, charged pion (m_π), muon, and electron.

For the ν_e resulting from μ^+ decay, the spectrum is:

$$\left.\frac{df_{\nu_e}}{dE\,dt}\right|_{\pi e} = \frac{m_\pi m_\mu}{4E^{(2)}p^{(1)}}\int_{E_\mu^{(\min)}}^{E_\mu^{(\max)}} dE_\mu \frac{1}{p_\mu}\int_{E_{\nu_e}^{(\min)'}}^{E_{\nu_e}^{(\max)'}} dE'_{\nu_e}\frac{df_{\nu_e}}{dE'_{\nu_e}}\frac{1}{E'_{\nu_e}}, \quad (3.48)$$

where the quantities $E_\mu^{(\max)}$, $E_\mu^{(\min)}$, $E_{\nu_e}^{(\min)'}$, and $E_{\nu_e}^{(\max)'}$ are defined in App.C. $E_\mu^{(\max)}$ and $E_\mu^{(\min)}$ are given in terms of masses. $E_{\nu_e}^{(\min)'}$ and $E_{\nu_e}^{(\max)'}$ are given in terms of masses and E_μ, the dummy variable of the outer integral. The quantity df_{ν_e}/dE'_{ν_e} is the probability density for producing a ν_e with energy E'_{ν_e} unique to muon decay.

For $\bar{\nu}_\mu$, we make the approximation that the decay spectrum is similar enough to the ν_e spectrum that we do not execute another computation, i.e.:

$$\left.\frac{df_{\bar{\nu}_\mu}}{dE_{\bar{\nu}_\mu}\,dt}\right|_{\pi e} = \left.\frac{df_{\nu_e}}{dE_{\nu_e}\,dt}\right|_{\pi e}. \quad (3.49)$$

3.3.5 Decay into charged pion and muon

Assuming the diluton has a larger mass than the sum of the charged pion and muon ($m_\pi + m_\mu \sim 245$ MeV), the decay rate for this process is[16]:

$$\Gamma_{\pi\mu} = 2\frac{G_F^2 f_\pi^2}{16\pi} m_s \left\{ \left[m_s^2 - (m_\pi + m_\mu)^2\right] \left[m_s^2 - (m_\pi - m_\mu)^2\right] \right\}^{1/2} \sin^2\theta \tag{3.50}$$

$$\approx 1.411 \times 10^2\,\mathrm{s}^{-1} \left(\frac{m_s}{\mathrm{MeV}}\right)^3 \left\{ \left[1 - (x+y)^2\right] \left[1 - (x-y)^2\right] \right\}^{1/2} \sin^2\theta, \tag{3.51}$$

where, for this channel, $x \equiv m_\pi/m_s$ and $y \equiv m_\mu/m_s$. We assume that the pion and muons (from both ν_s and $\pi^\pm$ decays) decay instantaneously. Therefore, this ν_s–decay channel produces five neutrinos. The spectra of the three neutrinos arising from pion decay have similar spectra to those of section 3.3.4, with a modification of some parameters due to the difference in m_μ compared to m_e. Without loss of generality, we consider the decay $\nu_s \to \pi^+ + \mu^-$. The μ^- decays by $\mu^- \to \nu_\mu + \overline{\nu}_e + e^-$. For the $\overline{\nu}_e$, App.C gives the spectrum as:

$$\left.\frac{df_{\overline{\nu}_e}}{dE\,dt}\right|_{\pi\mu} = \Gamma_{\pi\mu} \frac{m_\mu}{2p^{(3)}} \int_{\tilde{E}^{(\mathrm{min})'}_{\overline{\nu}_e}}^{\tilde{E}^{(\mathrm{max})'}_{\overline{\nu}_e}} dE'_{\overline{\nu}_e} \frac{df_{\overline{\nu}_e}}{dE'_{\overline{\nu}_e}} \frac{1}{E'_{\overline{\nu}_e}}, \tag{3.52}$$

where the quantities $E^{(3)}$, $p^{(3)}$, $\tilde{E}^{(\mathrm{min})'}_{\overline{\nu}_e}$, and $\tilde{E}^{(\mathrm{max})'}_{\overline{\nu}_e}$ are defined in App.C. We assume a similar spectrum for the ν_μ resulting in the muon decay.

3.3.6 Decay into active neutrino and electron–positron pair

Assuming the diluton has a larger mass than twice the electron mass, the decay rate for this process is related to the three neutrino decay rate. There is only one possibility for the particle/anti-particle pair in this channel, as compared to the three–neutrino channel

where there are three possibilities. Thus:

$$\Gamma_{\nu e^{\pm}} = \frac{1}{3}\Gamma_{3\nu}. \tag{3.53}$$

We will approximate the spectrum of the neutrino as monoenergetic. To calculate the energy, we assume that all three particles have the same geometry as three-neutrino decay, implying that they each particle is separated by an angle of 120°. Therefore, the spectrum of the neutrino is:

$$\left.\frac{df_i}{dE\,dt}\right|_{\nu e^{\pm}} = \Gamma_{\nu e^{\pm}}\delta(E - E_{\nu e^{\pm}})\frac{1}{3}, \tag{3.54}$$

where:

$$E_{\nu e^{\pm}} \equiv \frac{m_s}{3}\left(2\sqrt{1-3x^2}-1\right), \tag{3.55}$$

for $x = m_e/m_s$.

3.3.7 Decay into active neutrino and muon/anti-muon pair

Assuming the diluton has a larger mass than twice the muon mass, the decay rate for this process is equal to the $\nu e^{\pm}$ decay rate. We again assume that the decay products from the ν_s decay are monoenergetic and separated by 120°. This channel produces five neutrinos, one from the ν_s decay and two each from the $\mu^{\pm}$ decays. The spectrum for the daughter neutrino resulting from the ν_s decay is similar to that of Eq.(3.54) in Sec. 3.3.6. The monoenergetic muons cause the resulting spectra of the muon-decay neutrinos to be similar to the spectrum of Eq.(3.52) in Sec. 3.3.5, with a substitution of the $E^{(3)}$ quantity to that of the muon energy:

$$E_{\nu e^{\pm}} \equiv \frac{m_s}{3}\left(2\sqrt{1-3x^2}-1\right), \tag{3.56}$$

for $x = m_\mu/m_s$.

3.3.8 Total Decay rate

The total decay rate is given as the sum of the seven rates:

$$\Gamma_s \equiv \Gamma_{3\nu} + \Gamma_{\nu\gamma} + \Gamma_{\nu\pi^0} + \Gamma_{\pi e} + \Gamma_{\pi\mu} + \Gamma_{\nu e^\pm} + \Gamma_{\nu\mu^\pm}. \tag{3.57}$$

The rate for each decay channel contains an identical overall factor of $\sin^2\theta$, implying that we can write the total decay rate as:

$$\Gamma_s = R\sin^2\theta \equiv \frac{1}{\tau}, \tag{3.58}$$

where R is a function of the diluton mass (and other masses, constants, etc.) but independent of the mixing angle, and τ is the mean lifetime of the diluton. We define the branching ratios ,$f_{\rm br}^{(\rm i)}$, as the probability the diluton decays into any one given channel i:

$$f_{\rm br}^{(\rm i)} \equiv \frac{\Gamma_i}{\Gamma_s}, \tag{3.59}$$

which also are independent of mixing angle. Therefore, we can change the lifetime of the diluton by altering the mixing angle, while preserving the branching ratios at a given diluton mass. This allows us to study masses and lifetimes of consequence in weak decoupling and BBN.

3.4 Thermalization Procedure

All of the spectra in Sec. 3.3 have corresponding spectra for a $\bar{\nu}_s$. We assume zero degeneracy between the dilutons and anti-dilutons, implying we can mirror the spectra for the $\bar{\nu}_s$ with the spectra from ν_s decay.

The decay channels of Sec.3.3 produce photons, electrons, and positrons in the

final state. That energy immediately thermalizes with the primeval plasma, thereby changing the temperature of the plasma. The termperature, T, changes as a function of time t according to Eq.(1.139):

$$\frac{dT}{dt} = -3H \frac{\tilde{\rho} + p - \frac{1}{3H}\frac{\partial \rho}{\partial t}|_{a,T}}{\frac{d\rho}{dT}}, \tag{3.60}$$

where ρ is the energy density, p is the pressure, and $(\partial\rho/\partial t)_{a,T}$ is the energy density added through heating at constant T and scale factor a. In the standard cosmology (SC), the heat added has three terms in the weak decoupling/BBN epochs:

$$\left(\frac{\partial \rho}{\partial t}\right)^{(\mathrm{SC})}_{a,T} = -\left[\frac{\partial \rho_e}{\partial t} + \frac{\partial \rho_b}{\partial t} + \frac{\partial \rho_\nu}{\partial t}\right]_{a,T}, \tag{3.61}$$

where the first and second terms are the heat changes in the charged lepton and baryon sectors from nuclear reactions, and the third term is the heat change in the neutrino sector from the non-sharp weak–decoupling transition. The overall minus sign indicates that a reduction in energy density for any one sector raises the plasma temperature. The first two terms of Eq.(3.61) tend to be negative, as nuclear fusion releases binding energy. The neutrino term is positive within the standard cosmology, implying a net flow of heat from the plasma to the neutrinos. Calculating the third term requires a full Boltzmann treatment to accurately describe the kinematics of the neutrinos and positrons/electrons. This is the subject of Chapter 7. The case of a decaying particle requires one more term in Eq.(3.61):

$$\left.\frac{\partial \rho}{\partial t}\right|_{a,T} = -\left[\frac{\partial \rho_e}{\partial t} + \frac{\partial \rho_b}{\partial t} + \frac{\partial \rho_\nu}{\partial t} + f_{\mathrm{pl}}\frac{\partial \rho_s}{\partial t}\right]_{a,T}. \tag{3.62}$$

We use Eq.(3.24) to find:

$$\left.\frac{\partial \rho_s}{\partial t}\right|_{a,T} = -\frac{3\zeta(3)}{2\pi^2}\frac{m_s}{\tau}T_s^3 e^{-t/\tau}. \tag{3.63}$$

The negative sign shows that as the diluton decays, heat flows into the plasma. However, not all the heat from diluton decays flows into the plasma. Therefore, the factor $f_{\rm pl}$ denotes the fraction of heat flowing into the plasma per decay.

3.4.1 Injection of entropy into plasma

The fraction of heat flow is different for each decay channel, and different for each micro-decay for a given channel in the cases of pions or muons in the intermediate state. To calculate $f_{\rm pl}$, we calculate the average energy in neutrinos for a given decay channel:

$$\overline{E}_\nu^{(i)} = \sum_{j=1}^{N_i}\int_0^{m_s} dE\,\frac{df_j^{(i)}}{dE}\,E, \tag{3.64}$$

where the sum over j is for the N_i neutrinos created in decay channel i. The average energy per diluton decay is the weighted average of the average energy in neutrinos for a given decay and the branching ratios of Eq.(3.59):

$$\overline{E}_\nu = \sum_{i=1}^{7} f_{\rm br}^{(\rm i)}\overline{E}_\nu^{(i)}. \tag{3.65}$$

With Eq.(3.65), we can compute $f_{\rm pl}$:

$$f_{\rm pl} \equiv \frac{m_s - \bar{E}_\nu}{m_s}. \tag{3.66}$$

3.4.2 Scattering of decay neutrinos on electrons and positrons

The injection of entropy into the plasma is not the only way for heat to flow out of the diluton sector. High energy neutrinos born from diluton decays scatter on the active neutrinos, thereby increasing the total energy and skewing the spectra in the neutrino seas. The decay neutrinos can also scatter on electrons and positrons, thereby raising the temperature of the plasma (a negative $(\partial\rho_\nu/\partial t)_{a,T}$ in Eq.(3.61).) A proper treatment of the energy transport requires a Boltzmann treatment and will be left to later work. For the purposes of the present work, we will institute the approximation that neutrinos with energies above a certain energy value scatter down to that energy value via electron/positron interactions only (thereby heating the plasma), within one time step. We label this energy value $E_{\rm therm}$. Neutrinos with energies below $E_{\rm therm}$ free–stream.

We can calculate $E_{\rm therm}$ by approximating the rate of scattering with the expansion rate. The scattering rate approximation is $\Gamma \sim \langle\sigma v\rangle n_{\rm tar}$, where $\langle\sigma v\rangle$ is an average product of an integrated cross section with a relative velocity, and $n_{\rm tar}$ is the number density of the target particles. For weak interactions, typical cross sections go as $\sim G_F^2 E^2$. We take the square of the energy to be $\sim E_{\rm therm} T$, a combination of the neutrino energy ($E_{\rm therm}$) and the electron/positron energy $(\sim T)$. The number density of the target electrons/positrons is that of a relativistic species, and is $\sim T^3$. Our expression for the equality of the expansion rate and scattering rate is:

$$H \sim G_F^2 E_{\rm therm} T^4 \implies E_{\rm therm} = A_{\rm dec} \frac{H}{G_F^2 T^4}, \tag{3.67}$$

where $A_{\rm dec} = 4.8419$ is a constant. In radiation–dominated conditions, $H \sim T^2$, implying $E_{\rm therm}$ rises with decreasing temperature: $E_{\rm therm} \sim 1/T^2$.

The functional form of $E_{\rm therm}$ in terms of H, G_F and T is reasonable, given the approximation of Eq.(3.67). Our implementation of $E_{\rm therm}$ is cause for suspicion. One

limitation of the $E_{\rm therm}$ program is the poor description of high temperatures. If neutrinos down scatter to $E_{\rm therm}$, then at high temperatures $E_{\rm therm}$ will be a value much lower than the average energy of a thermal spectrum. Clearly, neutrinos at energies above $E_{\rm therm}$ can down scatter, but they can also up scatter. Our prescription for $E_{\rm therm}$ does not allow such a process. In addition, in the epochs when $E_{\rm therm}$ accurately depicts a barrier for thermalization, the thermalized decay neutrinos are grouped into a delta function at the value of $E_{\rm therm}$. In reality, the thermalized neutrinos would scatter into a spectrum approaching an ultra-relativistic Fermi–Dirac blackbody. Lastly, we approximated that the neutrinos are only down scattering on electrons and positrons. Cross sections for neutrino–neutrino scattering are comparable to those of neutrino–electron. Therefore, more energy density should be added to the neutrino seas, and equivalently less energy density to the plasma. These limitations are further proof that only a Boltzmann treatment between the neutrinos and electrons/positrons can accurately describe the energy transport.

3.5 Evolution of the early universe

The previous sections provide the framework to evolve the diluton energy density and associated quantities throughout weak decoupling and BBN. To see how the diluton affects the abundances, we need to pick a mass and lifetime in accordance with weak decoupling scales. The relict neutrinos begin to go out of chemical equilibrium with the electrons and positrons at $T \sim 3$ MeV which corresponds to a time of ~ 0.1 s. If the dilutons decay away before this time, then the relict neutrinos are still coupled to the plasma and we can use Eqs.(3.61) and (3.62) to study the evolution of the equilibrium distributions. In addition, BBN ends at $T \sim 30$ keV, corresponding to a time of $\sim 10^3$ s. If the dilutons were to decay at this late of a time, they would not interact with the plasma, although they could interact with the ambient protons causing a later epoch of

nucleosynthesis. We do not consider that case, and instead focus on diluton lifetimes with ranges of 0.1-100 seconds.

We investigate the diluton mass ranges such that all seven decay channels of Sec.3.3 are present. This requires masses in excess of 250 MeV. We will not venture too far from this lower bound, as this results in a considerable increase in entropy with manifest implications for BBN. Figure 3.1 shows the evolution of the entropy per baryon, s, in a scenario where the diluton has a mass of 350 MeV and a lifetime of 5.2 s. We define the dilution factor F as the following:

$$F \equiv \frac{s_{\rm final}}{s_{\rm initial}}. \tag{3.68}$$

The initial and final values of the entropy per baryon correspond to epochs before and after the decay of the diluton, respectively. The final value of s must agree with the CMB–inferred value, $s^{(\rm CMB)} \sim 5.90 \times 10^9$. Fig.3.1 has an initial value of $s \sim 6.0 \times 10^8$. An analytical calculation of the predicted $s_{\rm initial}$ is tedious due to the complexity of the decay spectra and the $E_{\rm therm}$ program. Therefore, we iterate on $s_{\rm initial}$ to find a value which produces a final value of s in agreement with the CMB. The change in s occurs primarily during the weak decoupling epoch, necessitating a transport calculation. The end of the dilution epoch occurs before the onset of helium formation.

We note that the predicted value of $N_{\rm eff}$ is much lower than that predicted by the standard model. We stress that one of the limitations of our $E_{\rm therm}$ program is the underestimate of the energy flow into the active neutrino seas. If a proper Boltzmann treatment produced an $N_{\rm eff}$ as low as the scenario in Fig.3.1, then the scenario would be incompatible with observed results.

The diluton acts in two separate ways to affect the active neutrino spectra: (1) it creates high-energy non-thermal neutrinos and (2) it dilutes the background neutrinos by

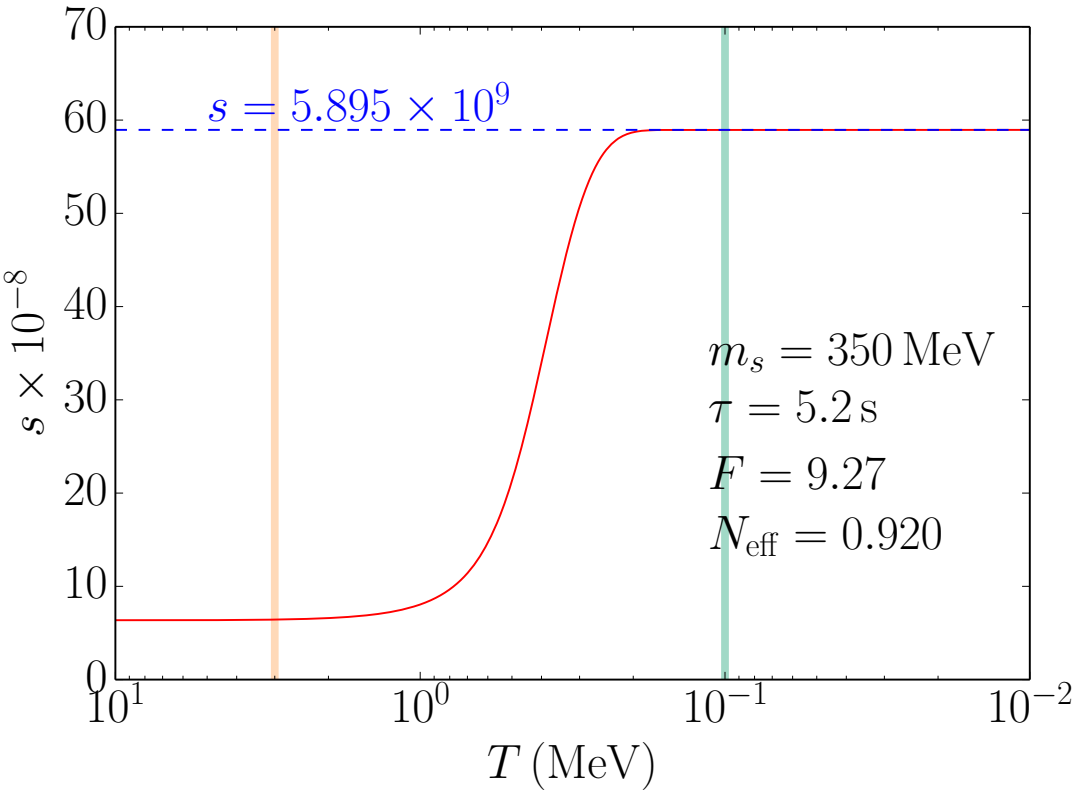

Figure 3.1: The entropy per baryon, s, is given as a function of plasma temperature T. The diluton has a mass $m_s = 350$ MeV and a lifetime of 5.2 s. The shaded vertical bar at $T \sim 3$ MeV indicates the start of weak decoupling. The shaded vertical bar at $T \sim 0.1$ MeV indicates the epoch of helium formation.

injecting entropy into the plasma. These competing effects require a numerical treatment of the weak interaction rates with nucleons, namely:

$$n + \nu_e \leftrightarrow p^+ + e^- \tag{3.69}$$

$$n + e^+ \leftrightarrow p^+ + \overline{\nu}_e \tag{3.70}$$

$$n \leftrightarrow p^+ + e^- + \overline{\nu}_e. \tag{3.71}$$

Fig.3.2 shows the evolution of the combined forward ($n \to p$) and combined reverse ($p \to n$) rates in Rxns.3.69 - 3.71, plotted along with the Hubble rate. The figure compares

the rates between the standard cosmology (SC - dashed curves), and a cosmology with a $m_s = 350$ MeV, $\tau = 5.2$ s diluton (DS - solid curves). At the temperaures plotted, the Hubble rate and forward $n \to p$ rate are similar in the SC and DS simulations. The reverse $p \to n$ rate is highly sensitive to the specific cosmology. The reverse rate requires an energy threshold for the $\bar{\nu}_e$ equal to the sum of the electron mass and the neutron–proton mass difference. No such threshold exists for the forward rate. The diluton is able to create neutrinos with energies in excess of 100 MeV. Therefore, the reverse rate is disproportionately larger in the DS case than the SC case. The implications for a larger $p \to n$ rate are more ambient neutrons at later times.

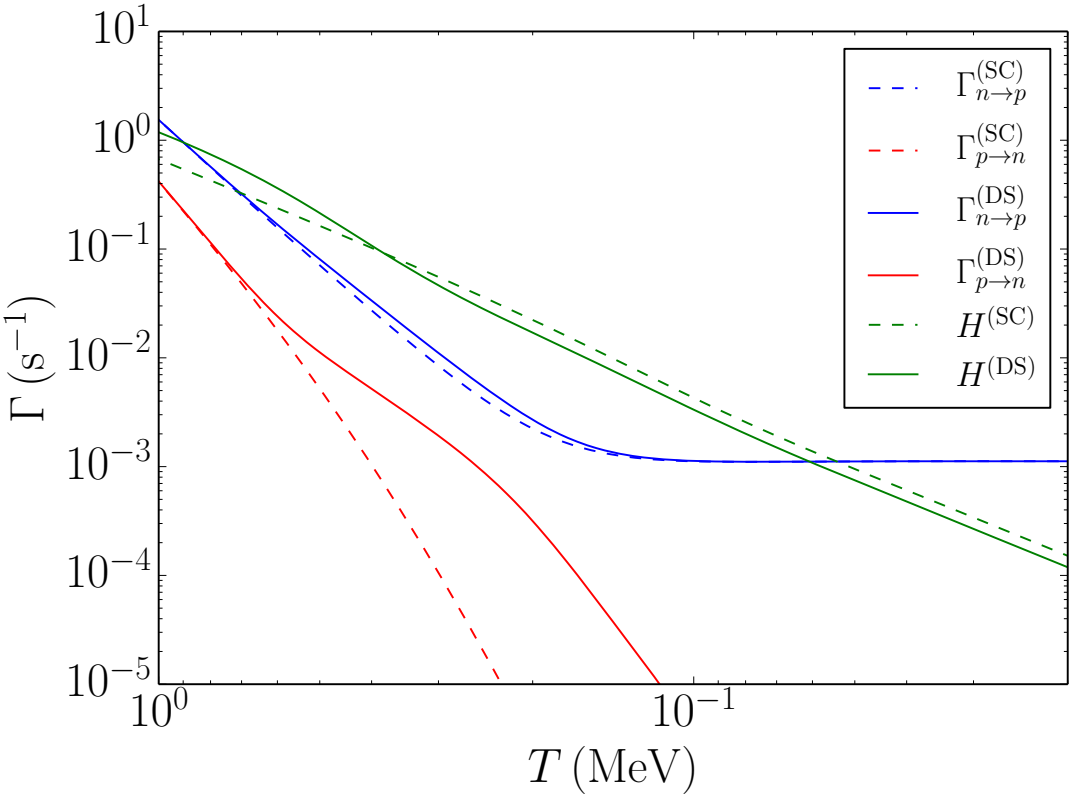

Figure 3.2: The neutron to proton rates and Hubble rate are given as a function of plasma temperature T. The dashed lines correspond to the standard cosmology (SC), while the solid lines correspond to a diluton scenario (DS). The diluton has a mass $m_s = 350$MeV and a lifetime of 5.2 s.

Fig.3.1 shows that the diluton has decayed away before ^{4}He formation. However, the high-energy decay neutrinos can still interact with protons, through the reverse rate of Rxn.(3.70). Fig.3.3 shows the evolution of the relative abundances with respect to the plasma temperature. The abundance, Y_i, is defined through the mass fraction, X_i:

$$Y_i \equiv \frac{X_i}{A_i} = \frac{n_i}{n_b}, \tag{3.72}$$

where A_i is the atomic number of species i, n_i is the proper number density, and n_b is the proper number density of all baryons. We look at relative abundances with respect to single–proton hydrogen, $Y_i/Y_{\rm H}$, in Fig.3.3. We only consider light abundances with $A \leq 7$. The dashed lines correspond to SBBN (within the SC), and the solid lines to the DS of $m_s = 350$ MeV, $\tau = 5.2$ s. Notice that at low temperatures ($T \sim 60$ keV) after ^{4}He formation, there is a larger abundance of free neutrons for DS as compared to SBBN, the result of the enhanced $p \to n$ rate. The extra neutron abundance is too low to affect the deuterium and ^{4}He abundances. However, the additional neutrons imply faster strong interactions for heavier nuclides. Specifically, the reactions:

$$n + {}^7\mathrm{Be} \to 2\,{}^4\mathrm{He} \tag{3.73}$$

$$n + {}^7\mathrm{Be} \to {}^7\mathrm{Li} + p \text{ followed by } {}^7\mathrm{Li} + p \to 2\,{}^4\mathrm{He}, \tag{3.74}$$

are enhanced with more neutrons and will destroy ^{7}Be. For the DS, the relative abundance of ^{7}Be is 2.3×10^{-10}, a factor of ~ 2 smaller than the SBBN prediction. ^{7}Be decays via electron capture to ^{7}Li during the recombination epoch, thereby alleving tension (although not eliminating it in this specific DS) between primordial predictions and observations of lithium, while preserving the deuterium and ^{4}He abundances.

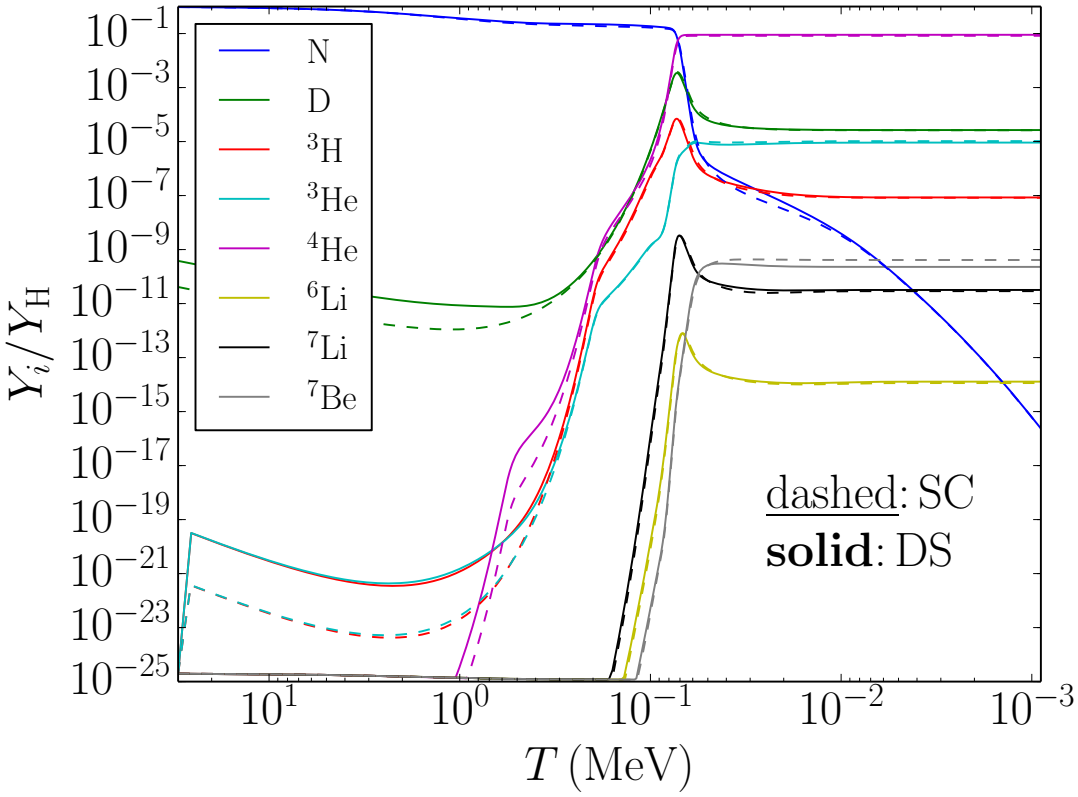

Figure 3.3: The relative abundance evolution is given as a function of plasma temperature T. The dashed lines correspond to the standard cosmology, while the solid lines correspond to a diluton scenario. The diluton has a mass $m_s = 350$ MeV and a lifetime of 5.2 s. The abundances are neutrons (N), deuterium (D), hydrogen-3 (^{3}H), helium-3 (^{3}He), helium-4 (^{4}He), lithium-6 (^{6}Li), lithium-7 (^{7}Li), and beryllium-7 (^{7}Be).

3.6 Conclusion

The inclusion of a diluton in the early universe is a major departure from the standard cosmology. We initially posed the problem as a mechanism to create a relic abundance of dark matter particles congruent with observations. If the lifetime of the diluton is short or long compared to weak decoupling/BBN time scales, then observable quantities from those epochs are largely unaffected, while the dark matter candidate is diluted to the present density. We chose to focus on lifetimes close to weak–decoupling/BBN time scales, causing pronounced effects on primordial abundances and $N_{\rm eff}$. We classify the

analysis done here as a first approximation to a Boltzmann treatment. The diluton problem is inherently non-perturbative and a difficult computational challenge, encompassing many Hubble times and decades of neutrino and plasma energies. We emphasize the necessity to follow the evolution of the active neutrino seas in order to constrain the radiation energy density (through $N_{\rm eff}$) and the dynamically evolving neutron–to–proton ratio (though the ν_e and $\overline{\nu}_e$ spectra). The diluton provides a means to change the primordial lithium abundance through a late epoch of proton transmutation, while preserving the other abundances.

The non-thermal spectra from diluton decays could affect other cosmological observables. Specifically, the sum of the light neutrino masses statistic includes the inherent assumption of the neutrinos decoupling in roughly thermal distributions. A cosmology with a diluton adds energy into the neutrino seas through a non-thermal mechanism, and changes the interpretation of a statistic like the sum of the neutrino masses.

Future work will include the transport of the decay neutrinos. In addition, the high energy neutrinos at later times can interact with nuclei. Therefore, we will need to include nuclear–weak interactions to properly follow the nucleosynthesis. In addition, our spectra are incomplete, as decay channels for three–neutrino, neutrino and electron/positron pair, and neutrino and muon/anti-muon pair are not monoenergetic. These spectra need to be included. Finally, we need a Boltzmann treatment in the case where the decay products have energies on order the temperature of the plasma. This occurs for shorter lifetimes and lighter–mass dilutons then what we considered here.

We thank Chad Kishimoto, Alex Kusenko, Amol Patwardhan and George Fuller for useful conversations with respect to cosmology, sterile neutrino physics, and early-universe computations.

Chapter 4

Recombination

4.1 Introduction

In this chapter, we present a method to determine an alternative to the quantity N_{eff}, usually presented in the following way:

$$\rho_r = 2\left[1+\frac{7}{8}\left(\frac{4}{11}\right)^{4/3} N_{\text{eff}}\right]\frac{\pi^2}{30}T^4, \tag{4.1}$$

where ρ_r is the radiation energy density and T is the photon temperature. Based on the construction of the rhs of Eq.(4.1), N_{eff} serves as the effective number of neutrinos. We note several important qualifiers of Equation (4.1). First, Eq.(4.1) is only valid after the epoch of positron–electron annihilation, when the ratio of comoving temperature to photon temperature attains the value $(4/11)^{1/3}$. Second, the ratio $(4/11)^{1/3}$ assumes a sharp transition in weak decoupling. Chapter 7 discusses in detail the Boltzmann–equation treatment of weak decoupling, and shows the ratio of temperatures does not obtain $(4/11)^{1/3}$ exactly. Third, radiation is by definition composed of massless particles, yet neutrinos have small non-zero masses. Fourth, even if neutrinos were massless, the cosmological radiation–energy–density does not necessarily have to be composed of only

photons and neutrinos. Lastly, the radiation energy density is not directly measurable at either the BBN or CMB epochs. It can only be inferred through the examination of primordial abundances (in the case of BBN) or the examination of angles (in the case of CMB power spectra). These qualifications place strict limits on the utility of $N_{\rm eff}$, and thus result in an inconsistent analysis with regards to beyond–standard–model physics. Therefore, we attempt to describe early–universe physics through a different yet similar quantity than $N_{\rm eff}$ in Eq.(4.1).

We term our new quantity $\tilde{N}_{\rm eff}$, and construct it such that $\tilde{N}_{\rm eff} = N_{\rm eff}$ in the standard cosmology. Initially, our motivation for using $\tilde{N}_{\rm eff}$ was to assign a $N_{\rm eff}$ value at photon-decoupling in a non-standard cosmology containing light sterile neutrinos ($m_s \sim 1$ eV.) For the purposes of discussion, we consider a toy–model where the sterile neutrino (and corresponding anti-neutrino) species has an identical spectrum to the three active neutrinos. The kinematics for particles at the sterile–neutrino mass scale are ultra-relativistic at the BBN epoch. Therefore, $N_{\rm eff} = 4$ during BBN. At photon decoupling, the temperature is ~ 0.2 eV. The sterile–neutrino spectrum would have a similar temperature–like parameter, implying that the sterile–neutrinos are neither ultra-relativistic nor non-relativistic. In this case, $N_{\rm eff}$ is indeterminate. Our parameter, $\tilde{N}_{\rm eff}$, uses the sound horizon and photon diffusion length and is able to characterize the $N_{\rm eff}$ contribution from the sterile neutrino sector. Light sterile neutrinos are only one example of the greater utility of $\tilde{N}_{\rm eff}$. In Ch.6, we present more examples of non-standard cosmologies and the predictions of $\tilde{N}_{\rm eff}$.

Fig.4.1 shows a diagram of the sound horizon (r_s), photon diffusion length (r_d), and related angles imprinted on the surface of the comoving two-sphere in an expanding universe. Calculating the diffusion length requires an extensive computation of recombination, and is the principal subject of this chapter. The rest of the chapter is outlined as follows. In section 4.2,we begin by discussing the physics, mathematics,

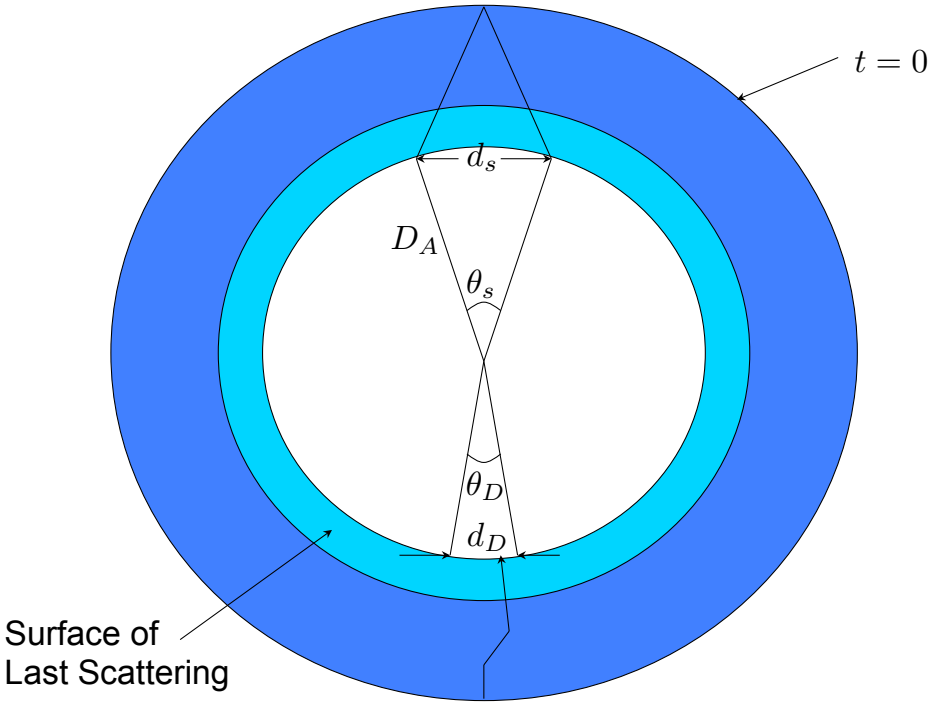

Figure 4.1: Diagram of the sound horizon r_s, photon diffusion length r_d, angular diameter distance of last scattering D_A, and the angles subtended by r_s and r_d.

and models needed to calculate the Hubble radius. We use the techniques of Sec.4.2 to calculate an analytical expression for the sound horizon in 4.3. Sec.4.4 details the non-trivial calculation of the photon diffusion length. Using the results from Secs.4.3 and 4.4, we asseble the sound horizon and photon diffusion length into $\tilde{N}_{\text{eff}}$ in Sec.4.5. We conclude in Sec.4.6.

4.2 Hubble Radius

The Hubble radius is not needed to calculate N_{eff}. However, in calculating the Hubble radius, we will demonstrate and explicitly use the physics, mathematics, and

models necessary for calculating the sound horizon and the diffusion length. Therefore, we proceed as follows.

The Hubble radius is the proper distance a photon could travel in the age of the universe. In a homogeneous and isotropic universe, we write the square of the line element (or metric) as:

$$ds^2 = dt^2 - a^2(t)\left(\frac{dr^2}{1-kr^2} + r^2 d\Omega\right). \tag{4.2}$$

The units of ds and dt are length implying that the unit of $a\,r$ must also be length. In the denominator of the radial-radial coefficient, we have $1-kr^2$. The quantity k describes the curvature of spacetime. We would like to use coordinates where k takes on values $0, \pm 1$. If we ascribe a length unit to r, then k has units 1/length^2 implying that a change in units will change the value of k if $k \neq 0$. Therefore, we will take r to be dimensionless and ascribe a dimension of length on the scale factor a.

For calculating the Hubble radius, take $d\theta = d\phi = 0$. Define the conformal time η such that:

$$\eta = \int_0^t \frac{dt'}{a} \implies d\eta = \frac{dt}{a}. \tag{4.3}$$

Taking $k = 0$, we can rewrite the metric as:

$$ds^2 = a^2 d\eta^2 - a^2 dr^2. \tag{4.4}$$

Photons follow null geodesics, or $ds = 0$. Therefore, the comoving Hubble radius $r_\star$ is given as:

$$r_\star \equiv \int_0^{r_\star} dr = \int_0^{\eta_\star} d\eta. \tag{4.5}$$

The comoving distance reflects the fact that the physical distance between coordinates changes with an expanding universe. To determine the proper Hubble–radius distance,

scale the differential line element dr by the radial–radial component of the metric:

$$d_\star(t_\star) = \int_0^{r_\star} \sqrt{-g_{rr}(t_\star)}\, dr = \int_0^{r_\star} a(t_\star)\, dr. \tag{4.6}$$

Note that we have $a(t_\star)$, not $a(t)$. This is because we concern ourselves with the proper distance at a certain epoch, namely $t_\star$. In other words, to calculate a proper distance at the epoch of interest, we need to know how spacetime is curved at that epoch. How spacetime got into that state is irrelevant for calculating the proper distance. Thus, we pull $a(t_\star)$ outside of the integral. Using our expression for the comoving Hubble radius:

$$d_\star(t_\star) = a(t_\star) \int_0^{r_\star} dr = a(t_\star) \int_0^{\eta_\star} d\eta = a(t_\star) \int_0^{t_\star} \frac{dt}{a}. \tag{4.7}$$

We cannot take the a in the denominator out of the integral in Eq.(4.7) because we are tracing the path followed by a theoretical photon (a real photon would scatter on other particles, thereby decreasing the distance) as it moves through an expanding universe. We will use this prescription when calculating other proper distances from comoving distances, namely $d(t_\star) = a(t_\star)\, r(t_\star)$.

We need to choose a value to use for the scale factor at the epoch of interest $t_\star$. The scale factor is fixed to be zero at the big bang. Since we ascribe a length unit to the scale factor, the scale factor will have a different numerical value depending on the choice of units. We will use the following strategy to mitigate any problems arising from this arbitrary choice. First, whenever we derive an equation, we will attempt to use ratios of scale factors at different epochs instead of an absolute scale factor. Secondly, we will adopt a value of the scale factor at the current epoch so that coordinate distances are exactly equal to proper distances, measured in Mpc. In other words: $a_0 = 1$ Mpc. Many authors combine the above strategy and convention into making a dimensionless scale factor, i.e. $a \to a/a_0$. This eliminates the need for a length unit and simplifies notation.

In an effort to be clear and lucid in this chapter, we will not adopt a dimensionless scale factor.

We need to write the coordinate time in terms of the scale factor. From the Friedmann equation, we obtain the Hubble rate H:

$$H \equiv \frac{1}{a}\frac{da}{dt} \text{ where } H^2 = \frac{8\pi G}{3}\rho, \tag{4.8}$$

where ρ is the energy density of the universe and G is Newton's gravitational constant. Thus the comoving Hubble radius is:

$$r_\star = \int_0^{a_\star} \frac{da}{a^2 H}. \tag{4.9}$$

To determine H as a function of a, we need to resort to a model of the energy density. Ignoring dark energy, the universe is filled with matter and radiation, implying:

$$H = \left[\frac{8\pi G}{3}(\rho_m + \rho_r)\right]^{1/2}. \tag{4.10}$$

We use the following "model–parameter forms" for radiation and matter:

$$\rho_r \equiv \left(1 + \frac{7}{8}\left(\frac{4}{11}\right)^{4/3} N_{\text{eff}}\right)\rho_\gamma \tag{4.11}$$

$$= \left(1 + \frac{7}{8}\left(\frac{4}{11}\right)^{4/3} N_{\text{eff}}\right)\frac{\pi^2}{15}T_\gamma^4 \tag{4.12}$$

$$= \left(1 + \frac{7}{8}\left(\frac{4}{11}\right)^{4/3} N_{\text{eff}}\right)\frac{\pi^2}{15}T_{\gamma,0}^4\left(\frac{a_0}{a}\right)^4, \tag{4.13}$$

$$\rho_m \equiv \rho_{m,0}\left(\frac{a_0}{a}\right)^3 \tag{4.14}$$

$$= \Omega_m \rho_{c,0}\left(\frac{a_0}{a}\right)^3 \tag{4.15}$$

$$= \Omega_m \frac{3H_0^2}{8\pi G}\left(\frac{a_0}{a}\right)^3. \tag{4.16}$$

$\rho_c = 3H^2/8\pi G$ is the critical density and the subscript 0 denotes values at the current epoch. Ω_m is the matter contribution to the critical density at the current epoch (we do not adorn a 0 on Ω_m). The photon temperature goes as $1/a$ due to the expanding universe and the small baryon number density. Hence the a^{-4} scaling in ρ_r. The model–parameter forms are used for ease in computation, even if they do not reflect physical reality properly. To simplify the computations, we will examine the epoch of matter-radiation equality, denoted eq. By definition, $\rho_{r,\mathrm{eq}} = \rho_{m,\mathrm{eq}}$. Using the model–parameter forms of ρ_r and ρ_m, and solving for a_{eq}/a_0:

$$\frac{a_{\mathrm{eq}}}{a_0} = \frac{\left(1 + \frac{7}{8}\left(\frac{4}{11}\right)^{4/3} N_{\mathrm{eff}}\right) 8\pi^3 G T_{\gamma,0}^4}{45 H_0^2 \Omega_m}. \tag{4.17}$$

Putting in factors of $\hbar, c, k_b$ and using the CMB temperature of $T_{\gamma,0} = 2.726$ K and defining $H_0 \equiv h \times 100$ km/s/Mpc, we have:

$$\frac{a_{\mathrm{eq}}}{a_0} = \frac{1 + 0.2271 N_{\mathrm{eff}}}{4.067 \times 10^4\, \Omega_m h^2}. \tag{4.18}$$

We can write the matter density at equality as

$$\rho_{m,\mathrm{eq}} = \rho_{m,0}\left(\frac{a_0}{a_{\mathrm{eq}}}\right)^3 = \frac{3\Omega_m H_0^2}{8\pi G}\left(\frac{a_0}{a_{\mathrm{eq}}}\right)^3. \tag{4.19}$$

We can write the Hubble rate as the following:

$$H = \left[\frac{8\pi G}{3}\left(\rho_m + \rho_r\right)\right]^{1/2} \tag{4.20}$$

$$= \left[\frac{8\pi G}{3}\left(\rho_{m,\mathrm{eq}}\left(\frac{a_{\mathrm{eq}}}{a}\right)^3 + \rho_{r,\mathrm{eq}}\left(\frac{a_{\mathrm{eq}}}{a}\right)^4\right)\right]^{1/2} \tag{4.21}$$

$$= \left[\frac{8\pi G}{3}\rho_{m,\mathrm{eq}}\left(\frac{a_{\mathrm{eq}}}{a}\right)^4\left(1 + \frac{a}{a_{\mathrm{eq}}}\right)\right]^{1/2}. \tag{4.22}$$

Thus, the comvoing Hubble radius can be computed:

$$r_\star = \int_0^{a_\star} \frac{da}{a^2 H} \tag{4.23}$$

$$= \int_0^{a_\star} \frac{da}{a^2} \left(\frac{8\pi G}{3}\rho_{m,\mathrm{eq}}\right)^{-1/2} \left(\frac{a}{a_{\mathrm{eq}}}\right)^2 \left(1+\frac{a}{a_{\mathrm{eq}}}\right)^{-1/2} \tag{4.24}$$

$$= \sqrt{\frac{3}{8\pi G\rho_{m,\mathrm{eq}}}} \frac{1}{a_{\mathrm{eq}}^2} \int_0^{a_\star} \frac{da}{\sqrt{1+\frac{a}{a_{\mathrm{eq}}}}} \tag{4.25}$$

$$= \sqrt{\frac{3}{8\pi G\rho_{m,\mathrm{eq}}}} \frac{2}{a_{\mathrm{eq}}} \left(\sqrt{1+\frac{a_\star}{a_{\mathrm{eq}}}} - 1\right) \tag{4.26}$$

$$= \sqrt{\frac{a_{\mathrm{eq}}^3}{\Omega_m H_0^2 a_0^3}} \frac{2}{a_{\mathrm{eq}}} \left(\sqrt{1+\frac{a_\star}{a_{\mathrm{eq}}}} - 1\right) \tag{4.27}$$

$$= \frac{2}{a_0} \sqrt{\frac{a_{\mathrm{eq}}}{\Omega_m H_0^2 a_0}} \left(\sqrt{1+\frac{a_\star}{a_{\mathrm{eq}}}} - 1\right) \tag{4.28}$$

$$r_H = 5.99 \times 10^3 \sqrt{\frac{a_{\mathrm{eq}}}{a_0}} (\Omega_m h^2)^{-1/2} \left(\sqrt{1+\frac{a}{a_{\mathrm{eq}}}} - 1\right) \frac{\mathrm{Mpc}}{a_0}, \tag{4.29}$$

where we have dropped the $\star$ notation and renamed the comoving Hubble radius r_H for ease. a_{eq} is a function of N_{eff} and uses the quantities $\Omega_m h^2$ and $T_{\gamma,0}$. Fig.4.2 shows a plot of the comoving Hubble radius versus N_{eff}.

4.3 Sound Horizon

The sound horizon is defined as

$$r_s(a_{\gamma d}) = \int_0^{a_{\gamma d}} da \, \frac{1}{a^2 H(a) \sqrt{3(1+R(a))}} \tag{4.30}$$

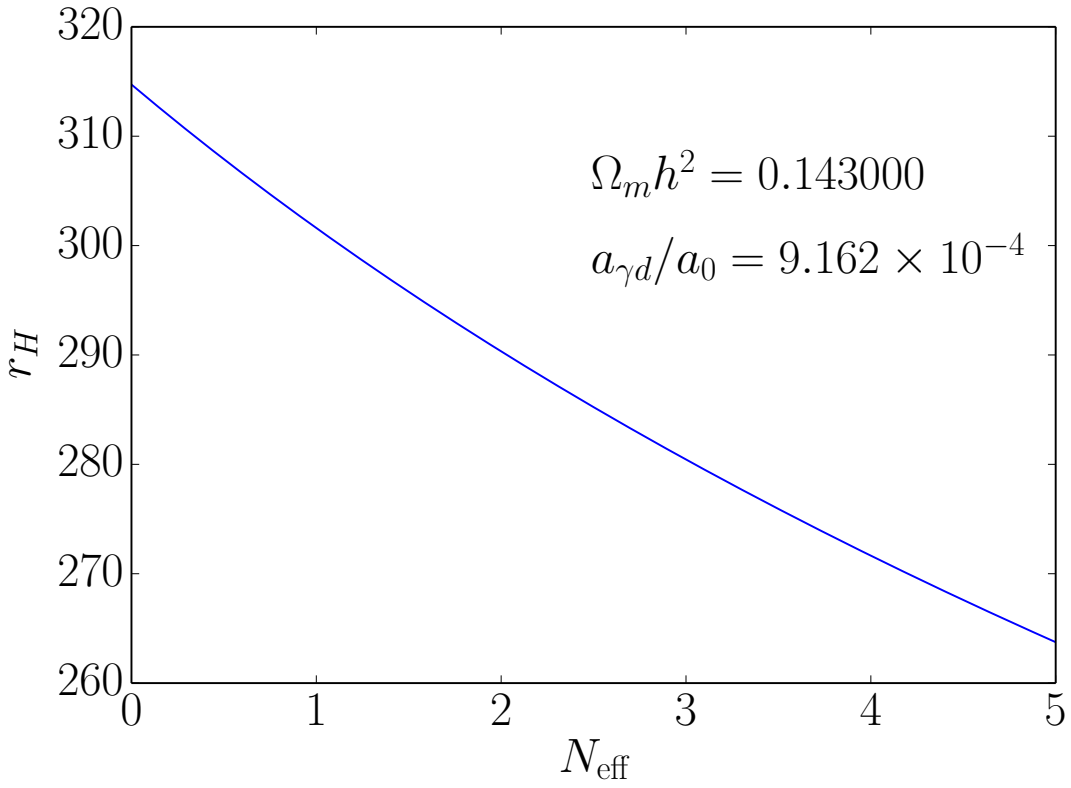

Figure 4.2: Comoving Hubble radius versus $N_{\rm eff}$. The comoving Hubble radius is calculated at the epoch of photon decoupling, defined as $a_{\gamma d}/a_0 \equiv 1/1091.43$.

where $a_{\gamma d}$ is the scale factor at photon decoupling.[1] The ratio $R(a)$ is given as

$$R(a) = \frac{3\rho_b(a)}{4\rho_\gamma(a)}, \tag{4.31}$$

where ρ_b and ρ_γ are the baryon rest mass and photon field energy densities, respectively.

The angular size of the sound horizon θ_s[2], determined from the spacing of the acoustic peaks in the CMB temperature power spectrum, is related to the sound horizon

[1] Reference [2] takes $a_{\gamma d} \to a_\star$ where the optical depth is unity.
[2] Reference [2] takes $\theta_s \to \theta_\star$.

by the angular diameter distance $D_A(a_{\gamma d})$ at photon decoupling (scale factor $a_{\gamma d}$) as

$$\theta_s(a_{\gamma d}) = a_{\gamma d}\frac{r_s(a_{\gamma d})}{D_A(a_{\gamma d})}, \tag{4.32}$$

since the angle θ_s is small. The angular diameter distance is

$$D_A(a) = a\int_a^{a_0} da'\,[a'^2 H(a')]^{-1}. \tag{4.33}$$

The quantity $D_A(a_{\gamma d})$ depends on the vacuum (dark) energy equation of state, which is not very well understood. Our approach will eliminate dependence on this poorly constrained component of the energy density.

We can write an expression for the comoving sound horizon in terms of the conformal time as:

$$r_s = \int_0^{\eta} c_s d\eta', \tag{4.34}$$

where c_s is the speed of sound. If p is pressure, the speed of sound is defined as:

$$c_s^2 = \frac{\partial p}{\partial \rho}. \tag{4.35}$$

At and before photon decoupling, only photons and baryons interact with one another acoustically, to a first approximation. Therefore, we can write the sound speed as:

$$c_s^2 = \frac{\partial p}{\partial \rho_\gamma}\frac{d\rho_\gamma}{d\rho} + \frac{\partial p}{\partial \rho_b}\frac{d\rho_b}{d\rho}. \tag{4.36}$$

We make the approximation that matter exhibits no pressure, implying that the second term vanishes. To determine $\partial p/\partial\rho_\gamma \times d\rho_\gamma/d\rho$, note the following:

$$\rho = \rho_\gamma + \rho_b \implies \frac{d\rho}{d\rho_\gamma} = 1 + \frac{d\rho_b}{d\rho_\gamma} \tag{4.37}$$

. ρ_b and ρ_γ are related to the scale factor as implied above:

$$\rho_b \sim a^{-3} \implies \frac{d\rho_b}{da} = -3\frac{\rho_b}{a} \tag{4.38}$$

$$\rho_\gamma \sim a^{-4} \implies \frac{d\rho_\gamma}{da} = -4\frac{\rho_\gamma}{a}. \tag{4.39}$$

Thus:

$$\frac{d\rho_b}{d\rho_\gamma} = \frac{3\rho_b}{4\rho_\gamma} = R \implies \frac{d\rho_\gamma}{d\rho} = (1+R)^{-1}. \tag{4.40}$$

The equation of state for radiation is $p = \rho/3$. This gives the following expression for the sound speed:

$$c_s = \frac{1}{\sqrt{3(1+R)}}, \tag{4.41}$$

where R is a function of a. Rewriting the comoving sound horizon in terms of the scale factor:

$$r_s = \int_0^{a_\star} \frac{da}{a^2 H\sqrt{3(1+R)}}, \tag{4.42}$$

recovering Eq.(4.30).

We need to write R and H in terms of a. R is the following:

$$R = \frac{3}{4}\frac{\rho_b}{\rho_\gamma} = \frac{3}{4}\frac{\rho_{b,\mathrm{eq}}(\frac{a_\mathrm{eq}}{a})^3}{\rho_{\gamma,\mathrm{eq}}(\frac{a_\mathrm{eq}}{a})^4} = R_\mathrm{eq}\frac{a}{a_\mathrm{eq}}. \tag{4.43}$$

Note that $R_\mathrm{eq} \neq 3/4$ since there are other forms of matter (e.g. Dark Matter) and other forms of radiation (e.g. active neutrinos). Furthermore, R_eq can be parameterized using

N_{eff}:

$$R_{\text{eq}} = \frac{3}{4}\frac{\rho_{b,\text{eq}}}{\rho_{\gamma,\text{eq}}} \tag{4.44}$$

$$= \frac{3}{4}\frac{\rho_{b,0}\left(\frac{a_0}{a_{\text{eq}}}\right)^3}{\rho_{\gamma,0}\left(\frac{a_0}{a_{\text{eq}}}\right)^4} \tag{4.45}$$

$$= \frac{3}{4}\frac{\rho_{b,0}}{\rho_{\gamma,0}}\frac{a_{\text{eq}}}{a_0} \tag{4.46}$$

$$= \frac{3}{4}\frac{\Omega_b \rho_{c,0}}{\frac{\pi^2}{15}T_{\gamma,0}^4}\frac{a_{\text{eq}}}{a_0} \tag{4.47}$$

$$= \frac{3}{4}\frac{\Omega_b \frac{3H_0^2}{8\pi G}}{\frac{\pi^2}{15}T_{\gamma,0}^4}\frac{\left(1+\frac{7}{8}\left(\frac{4}{11}\right)^{4/3}N_{\text{eff}}\right)8\pi^3 G T_{\gamma,0}^4}{45H_0^2\Omega_m} \tag{4.48}$$

$$= \frac{3}{4}\frac{\Omega_b}{\Omega_m}(1+0.2271N_{\text{eff}}). \tag{4.49}$$

In addition, we write H using the same expression as above:

$$H = \left[\frac{8\pi G}{3}\rho_{m,\text{eq}}\left(\frac{a_{\text{eq}}}{a}\right)^4\left(1+\frac{a}{a_{\text{eq}}}\right)\right]^{1/2}. \tag{4.50}$$

We are now able to compute the comoving sound horizon:

$$r_s = \int_0^{a_\star}\frac{da}{a^2 H\sqrt{3(1+R)}} \tag{4.51}$$

$$= \int_0^{a_\star}\frac{da}{a^2\sqrt{3}}\left[\frac{8\pi G}{3}\rho_{m,\text{eq}}\left(\frac{a_{\text{eq}}}{a}\right)^4\left(1+\frac{a}{a_{\text{eq}}}\right)\right]^{-1/2}\left(1+R_{\text{eq}}\frac{a}{a_{\text{eq}}}\right)^{-1/2} \tag{4.52}$$

$$= \frac{1}{a_{\text{eq}}^2}\sqrt{\frac{3}{8\pi G\rho_{m,\text{eq}}}}\frac{1}{\sqrt{3R_{\text{eq}}}}\int_0^{a_\star}\left(1+\frac{a}{a_{\text{eq}}}\right)^{-1/2}\left(\frac{1}{R_{\text{eq}}}+\frac{a}{a_{\text{eq}}}\right)^{-1/2}da \tag{4.53}$$

$$= \frac{1}{a_{\text{eq}}}\sqrt{\frac{3}{8\pi G\rho_{m,\text{eq}}}}\frac{1}{\sqrt{3R_{\text{eq}}}}\int_0^{u_\star}(1+u)^{-1/2}\left(\frac{1}{R_{\text{eq}}}+u\right)^{-1/2}du. \tag{4.54}$$

Recall for positive numbers α and β:

$$\int \frac{dx}{\sqrt{\alpha+x}\sqrt{\beta+x}} = 2\ln\left(\sqrt{\alpha+x}+\sqrt{\beta+x}\right)+C. \tag{4.55}$$

Thus:

$$\begin{aligned}
r_s &= \frac{2}{a_{\rm eq}}\sqrt{\frac{3}{8\pi G\rho_{m,\rm eq}}}\frac{1}{\sqrt{3R_{\rm eq}}}\ln\left(\sqrt{1+\frac{a}{a_{\rm eq}}}+\sqrt{\frac{1}{R_{\rm eq}}+\frac{a}{a_{\rm eq}}}\right)\Bigg|_0^{a_\star} && (4.56)\\
&= \frac{2}{a_{\rm eq}}\sqrt{\frac{3}{8\pi G\rho_{m,\rm eq}}}\frac{1}{\sqrt{3R_{\rm eq}}}\ln\left[\frac{1}{R_{\rm eq}}\left(\sqrt{R_{\rm eq}+R_{\rm eq}\frac{a}{a_{\rm eq}}}+\sqrt{1+R_{\rm eq}\frac{a}{a_{\rm eq}}}\right)\right]\Bigg|_0^{a_\star} && (4.57)\\
&= \frac{2}{a_{\rm eq}}\sqrt{\frac{3}{8\pi G\rho_{m,\rm eq}}}\frac{1}{\sqrt{3R_{\rm eq}}}\ln\left[\frac{1}{R_{\rm eq}}\left(\sqrt{R_{\rm eq}+R}+\sqrt{1+R}\right)\right]\Bigg|_0^{R_\star} && (4.58)\\
&= \frac{2}{a_{\rm eq}}\sqrt{\frac{3}{8\pi G\rho_{m,\rm eq}}}\frac{1}{\sqrt{3R_{\rm eq}}}\ln\left(\frac{\sqrt{R_{\rm eq}+R_\star}+\sqrt{1+R_\star}}{1+\sqrt{R_{\rm eq}}}\right). && (4.59)
\end{aligned}$$

Define $k_{\rm eq}$ such that:

$$\begin{aligned}
k_{\rm eq} &\equiv a_{\rm eq}H(a_{\rm eq}) && (4.60)\\
&= a_{\rm eq}\sqrt{\frac{8\pi G}{3}\rho_{\rm eq}} = a_{\rm eq}\sqrt{\frac{8\pi G}{3}2\rho_{m,\rm eq}} && (4.61)\\
&= a_{\rm eq}\sqrt{\frac{8\pi G}{3}2\rho_{m,0}\left(\frac{a_0}{a_{\rm eq}}\right)^3} = a_{\rm eq}\sqrt{\frac{H_0^2}{\rho_{c,0}}2\rho_{m,0}\left(\frac{a_0}{a_{\rm eq}}\right)^3} && (4.62)\\
&= a_0\sqrt{2H_0^2\Omega_m\frac{a_0}{a_{\rm eq}}}, && (4.63)
\end{aligned}$$

and we write r_s as:

$$\begin{aligned}
r_s &= \frac{2}{a_{\rm eq}}\sqrt{\frac{3}{8\pi G\rho_{m,\rm eq}}}\frac{1}{\sqrt{3R_{\rm eq}}}\ln\left(\frac{\sqrt{R_{\rm eq}+R_\star}+\sqrt{1+R_\star}}{1+\sqrt{R_{\rm eq}}}\right) && (4.64)\\
&= \frac{2}{3k_{\rm eq}}\sqrt{\frac{6}{R_{\rm eq}}}\ln\left(\frac{\sqrt{R_{\rm eq}+R_\star}+\sqrt{1+R_\star}}{1+\sqrt{R_{\rm eq}}}\right) && (4.65)
\end{aligned}$$

Eq.(4.65) gives the comoving sound horizon at $R_\star$ in terms of Ω_b, Ω_m, h, and $N_{\rm eff}$ and agrees with Ref.[23]. Fig.4.3 shows a plot of the comoving sound horizon versus $N_{\rm eff}$ at photon decoupling.

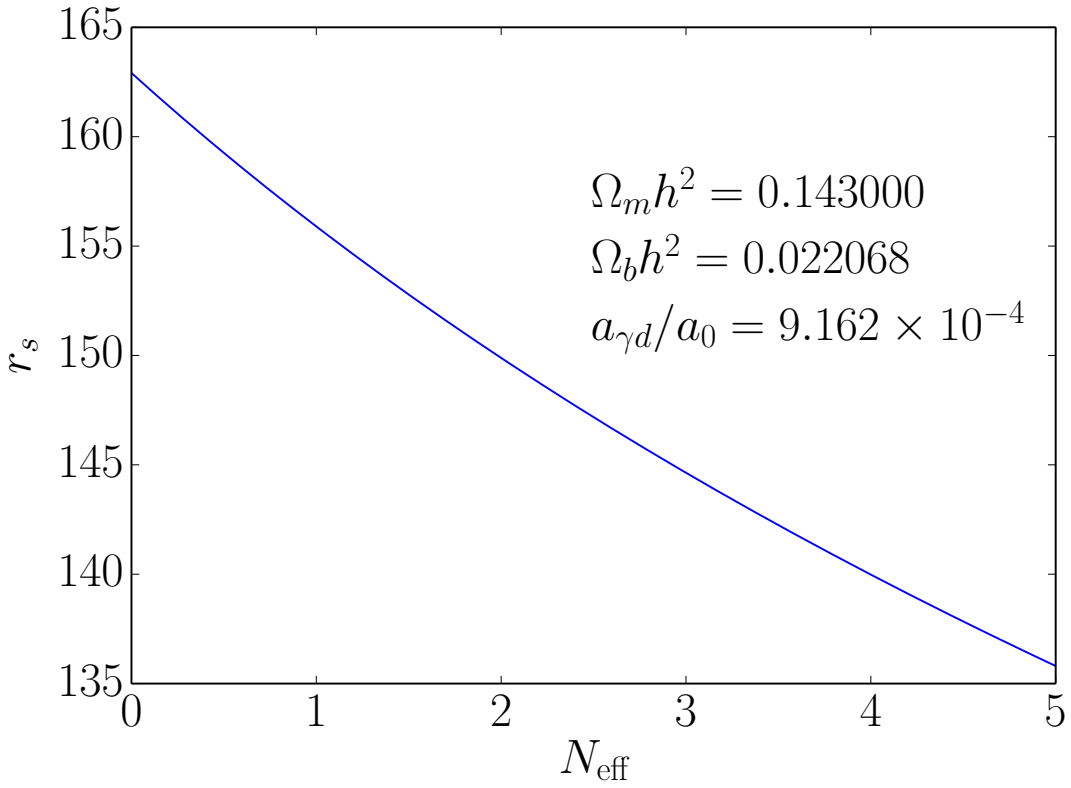

Figure 4.3: Comoving sound horizon versus $N_{\rm eff}$.

4.4 Diffusion length and free–electron fraction

4.4.1 Definition of diffusion length

In the tightly coupled limit, photon diffusion damping is characterized through the damping wave number [47, 48, 49, 50]

$$k_d^{-2} = \int_0^{a_{\gamma d}} \frac{da}{a^2 H(a)} \frac{1}{a n_e(a) \sigma_T} \frac{R^2(a) + \frac{16}{15}(1+R(a))}{6(1+R(a))^2}, \tag{4.66}$$

where σ_T is the Thomson cross section, and n_e is the free–electron proper number density. Here, we have assumed that moments of the temperature fluctuation higher than the quadrupole make a negligible contribution in the linearized Boltzmann equation for the photon distribution.

Equation (4.66) requires the free–electron fraction, $n_e(a)$, determined in the recombination history, as discussed below. The free–electron fraction, over the course of the recombination history, depends strongly on the primordial helium mass fraction Y_P. The point that BBN and recombination are related is well known [11] but has not been implemented self-consistently as a constraint for general, BSM physics model cosmologies. We return to it after describing the relation between r_s and k_d to directly observable quantities given by the CMB power spectrum.

The observed diffusion angle $\theta_d(a_{\gamma d})$ [2] is related to the diffusion damping length, $r_d = \pi/k_d$ as

$$\theta_d(a_{\gamma d}) = a_{\gamma d} \frac{r_d(a_{\gamma d})}{D_A(a_{\gamma d})}, \tag{4.67}$$

with the same stipulation regarding the smallness of the angle in Eq.(4.32).

4.4.2 Step–function method

An analytic expression to Eq.(4.66) exists in the approximation that $R = 0$:

$$k_d^{-2} = \frac{8}{45}\int_0^{\eta} \frac{d\eta^{'}}{n_e \sigma_T a} = \frac{8}{45}\int_0^{a_\star} \frac{da}{n_e \sigma_T a^3 H}. \tag{4.68}$$

We will take the universe to be fully ionized until the sharp transition at $a_{\gamma d}$, as a simplifying assumption. When we work with this specific assumption, we will call it the"step–function method". If electrons are assumed to be non-relativistic, then:

$$n_e = \begin{cases} n_{e,0}\left(\frac{a_0}{a}\right)^3 & \text{if } a < a_{\gamma d} \\ 0 & \text{if } a > a_{\gamma d} \end{cases}. \tag{4.69}$$

Obviously the comoving number density of electrons has changed since photon decoupling because of other astrophysical processes. We are using the expression for n_e to show the scaling prior to photon decoupling. We use:

$$H^2 = \frac{8\pi G}{3}\left(\frac{a_{\rm eq}}{a}\right)^4 \rho_{m,\rm eq}\left(1 + \frac{a}{a_{\rm eq}}\right) \tag{4.70}$$

for the Hubble rate which we derived above. Our expression for k_d becomes:

$$k_d^{-2} = \frac{8}{45}\frac{1}{n_{e,0}\sigma_T a_0^3 a_{\rm eq}^2}\sqrt{\frac{3}{8\pi G \rho_{m,\rm eq}}}\int_0^{a_\star} \frac{a^2 da}{\left(1+\frac{a}{a_{\rm eq}}\right)^{1/2}} \tag{4.71}$$

$$= \frac{8}{45}\frac{a_{\rm eq}}{n_{e,0}\sigma_T a_0^3}\sqrt{\frac{3}{8\pi G \rho_{m,\rm eq}}}\int_0^{u_\star} \frac{u^2 du}{(1+u)^{1/2}}, \tag{4.72}$$

where we have assumed $a_\star < a_{\gamma d}$. Using the substitution $u+1=x \implies du=dx$:

$$k_d^{-2} = \frac{8}{45}\frac{a_{\rm eq}}{n_{e,0}\sigma_T a_0^3}\sqrt{\frac{3}{8\pi G\rho_{m,\rm eq}}}\int_{x(0)}^{x(u_\star)}\frac{(x-1)^2dx}{\sqrt{x}} \tag{4.73}$$

$$= \frac{8}{45}\frac{a_{\rm eq}}{n_{e,0}\sigma_T a_0^3}\sqrt{\frac{3}{8\pi G\rho_{m,\rm eq}}}\int_{x(0)}^{x(u_\star)}\frac{(x^2-2x+1)dx}{\sqrt{x}} \tag{4.74}$$

$$= \frac{8}{45}\frac{a_{\rm eq}}{n_{e,0}\sigma_T a_0^3}\sqrt{\frac{3}{8\pi G\rho_{m,\rm eq}}}\int_{x(0)}^{x(u_\star)}(x^{3/2}-2x^{1/2}+x^{-1/2})dx \tag{4.75}$$

$$= \frac{8}{45}\frac{a_{\rm eq}}{n_{e,0}\sigma_T a_0^3}\sqrt{\frac{3}{8\pi G\rho_{m,\rm eq}}}\left[\frac{2}{5}x^{5/2}-\frac{4}{3}x^{3/2}+2x^{1/2}\right]_{x(0)}^{x(u_\star)} \tag{4.76}$$

$$= \frac{8}{45}\frac{a_{\rm eq}}{n_{e,0}\sigma_T a_0^3}\sqrt{\frac{3}{8\pi G\rho_{m,\rm eq}}}\left[\frac{2}{5}(1+u)^{5/2}-\frac{4}{3}(1+u)^{3/2}+2(1+u)^{1/2}\right]_0^{u_\star} \tag{4.77}$$

$$= \frac{8}{45}\frac{a_{\rm eq}}{n_{e,0}\sigma_T a_0^3}\sqrt{\frac{3}{8\pi G\rho_{m,\rm eq}}}$$
$$\times\left[\frac{2}{5}\left(1+\frac{a}{a_{\rm eq}}\right)^{5/2}-\frac{4}{3}\left(1+\frac{a}{a_{\rm eq}}\right)^{3/2}+2\left(1+\frac{a}{a_{\rm eq}}\right)^{1/2}\right]_0^{a_\star} \tag{4.78}$$

$$= \frac{16}{225}\frac{a_{\rm eq}}{n_{e,0}\sigma_T a_0^3}\sqrt{\frac{3}{8\pi G\rho_{m,\rm eq}}}$$
$$\times\left[\left(1+\frac{a}{a_{\rm eq}}\right)^{5/2}-\frac{10}{3}\left(1+\frac{a}{a_{\rm eq}}\right)^{3/2}+5\left(1+\frac{a}{a_{\rm eq}}\right)^{1/2}\right]_0^{a_\star} \tag{4.79}$$

$$= \frac{16}{225}\frac{a_{\rm eq}}{n_{e,0}\sigma_T a_0^3}\sqrt{\frac{3}{8\pi G\rho_{m,\rm eq}}}$$
$$\times\left[\left(1+\frac{a_\star}{a_{\rm eq}}\right)^{5/2}-\frac{10}{3}\left(1+\frac{a_\star}{a_{\rm eq}}\right)^{3/2}+5\left(1+\frac{a_\star}{a_{\rm eq}}\right)^{1/2}-\frac{8}{3}\right]. \tag{4.80}$$

The end result is:

$$k_d^{-2} = \frac{16}{225}\frac{a_\star^{5/2}}{a_{\rm eq}^{3/2} n_{e,0}\sigma_T a_0^3}\sqrt{\frac{3}{8\pi G\rho_{m,\rm eq}}}\times \left[\left(1+\frac{a_{\rm eq}}{a_\star}\right)^{5/2} - \frac{10}{3}\frac{a_{\rm eq}}{a_\star}\left(1+\frac{a_{\rm eq}}{a_\star}\right)^{3/2} + 5\left(\frac{a_{\rm eq}}{a_\star}\right)^2\left(1+\frac{a_{\rm eq}}{a_\star}\right)^{1/2} - \frac{8}{3}\left(\frac{a_{\rm eq}}{a_\star}\right)^{5/2}\right] \tag{4.81}$$

Writing the electron number density in terms of the baryon mass density:

$$n_e = n_{p^+} = n_H + 2n_{He} = \frac{\rho_b}{m_b}\left(\frac{m_b n_H}{\rho_b} + \frac{4m_b n_{He}}{2\rho_b}\right) = \frac{\rho_b}{m_b}\left(X_p + \frac{Y_p}{2}\right) \tag{4.82}$$

$$= \frac{\rho_b}{m_b}\left(1 - Y_p + \frac{Y_p}{2}\right) = \frac{\rho_b}{m_b}\left(1 - \frac{Y_p}{2}\right) \tag{4.83}$$

where X_p and Y_p are the primordial hydrogen and helium mass fractions, respectively, and m_b is the baryon mass. For the purposes of recombination, we assume that BBN only produces hydrogen and helium. At the current epoch:

$$\rho_{b,0} = \Omega_b \rho_{c,0} = \Omega_b \frac{3H_0^2}{8\pi G} \tag{4.84}$$

$$\implies n_{e,0} = \frac{3\Omega_b H_0^2}{8\pi m_b G}\left(1 - \frac{Y_p}{2}\right) \tag{4.85}$$

Using a similar expression from above:

$$\rho_{m,\rm eq} = \Omega_m \frac{3H_0^2}{8\pi G}\left(\frac{a_0}{a_{\rm eq}}\right)^3. \tag{4.86}$$

Putting these expressions into our damping wavenumber expression:

$$
\begin{aligned}
k_d^{-2} =& \frac{16}{225}\frac{a_\star^{5/2}}{a_{\rm eq}^{3/2}\sigma_T a_0^3}\sqrt{\frac{a_{\rm eq}^3}{\Omega_m H_0^2 a_0^3}}\frac{8\pi m_b G}{3\Omega_b H_0^2}\left(1-\frac{Y_p}{2}\right)^{-1}\times \\
& \left[\left(1+\frac{a_{\rm eq}}{a_\star}\right)^{5/2}-\frac{10}{3}\frac{a_{\rm eq}}{a_\star}\left(1+\frac{a_{\rm eq}}{a_\star}\right)^{3/2}\right. \\
& \left.+5\left(\frac{a_{\rm eq}}{a_\star}\right)^2\left(1+\frac{a_{\rm eq}}{a_\star}\right)^{1/2}-\frac{8}{3}\left(\frac{a_{\rm eq}}{a_\star}\right)^{5/2}\right] \qquad (4.87) \\
=& \frac{128\pi}{675}\frac{m_b G}{\sigma_T a_0^2}\left(\frac{a_\star}{a_0}\right)^{5/2}(\Omega_m H_0^2)^{-1/2}(\Omega_b H_0^2)^{-1}\left(1-\frac{Y_p}{2}\right)^{-1}\times \\
& \left[\left(1+\frac{a_{\rm eq}}{a_\star}\right)^{5/2}-\frac{10}{3}\frac{a_{\rm eq}}{a_\star}\left(1+\frac{a_{\rm eq}}{a_\star}\right)^{3/2}\right. \\
& \left.+5\left(\frac{a_{\rm eq}}{a_\star}\right)^2\left(1+\frac{a_{\rm eq}}{a_\star}\right)^{1/2}-\frac{8}{3}\left(\frac{a_{\rm eq}}{a_\star}\right)^{5/2}\right] \qquad (4.88)
\end{aligned}
$$

Writing $H_0 = h\times 10^2$ km/s/Mpc, and inserting factors of $\hbar$ and c:

$$
\begin{aligned}
k_d^{-2} =& 9.108\times 10^6\left(\frac{\rm Mpc}{a_0}\right)^2\left(\frac{a}{a_0}\right)^{5/2}(\Omega_m h^2)^{-1/2}(\Omega_b h^2)^{-1}\left(1-\frac{Y_p}{2}\right)^{-1}\times \\
& \left[\left(1+\frac{a_{\rm eq}}{a}\right)^{5/2}-\frac{10}{3}\frac{a_{\rm eq}}{a}\left(1+\frac{a_{\rm eq}}{a}\right)^{3/2}\right. \\
& \left.+5\left(\frac{a_{\rm eq}}{a}\right)^2\left(1+\frac{a_{\rm eq}}{a}\right)^{1/2}-\frac{8}{3}\left(\frac{a_{\rm eq}}{a}\right)^{5/2}\right], \qquad (4.89)
\end{aligned}
$$

where we have dropped the $\star$ notation on the scale factor for ease.

Fig.4.4 shows the evolution of the comoving diffusion length with the scale factor for both the above approximation expression with $R = 0$ and a numerical solution using the step–function method, denoted by the superscript (step). We obtain the numerical solution by integrating the expression for the diffusion damping wave number while not setting $R = 0$, but maintaining the same model–parameter forms of ρ_m, ρ_r, and n_e. The approximation holds at early epochs and breaks down at late epochs when clearly $R \neq 0$.

Fig.4.5 shows plots of r_d for the $R = 0$ approximation and the numerical integra-

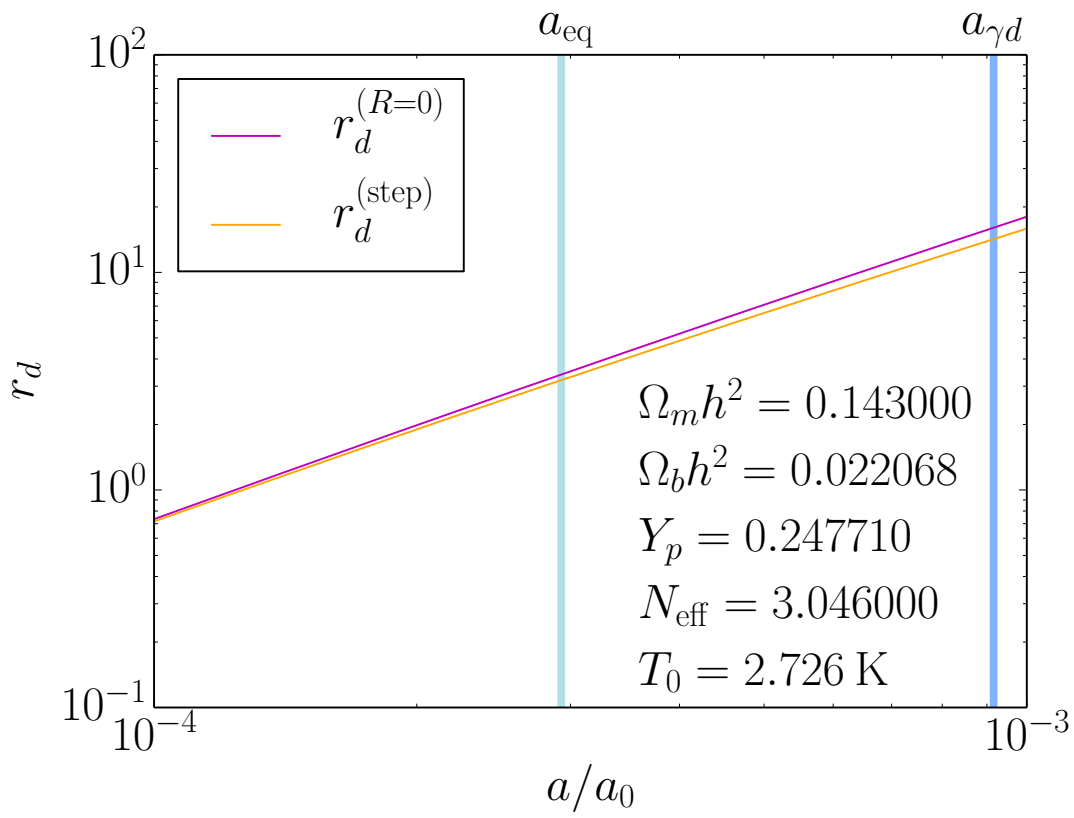

Figure 4.4: Comoving diffusion length r_d versus scale factor ratio a/a_0. $r_d^{(R=0)}$ is the comoving diffusion length using the approximation in Eq.(4.89). $r_d^{(\rm step)}$ is the comoving diffusion length using the step–function method. We highlight certain epochs of interest at $a_{\rm eq}$ and $a_{\gamma d}$.

tion for the step–function method at the epoch of photon decoupling. In addition, we include a plot of the damping wavenumber k_d versus $N_{\rm eff}$ in Fig.4.6.

4.4.3 Saha equilibrium approximation

The step–function method does not accurately depict phsical reality. The ionization fraction does not change discontinuously. Rather, the free electrons recombine gradually onto nuclei to form bound states. If the step–function method is a first approximation to recombination physics, then a second approximation is to assume that the free–electron fraction X_e stays in equilibrium. We call this the equilibrium method.

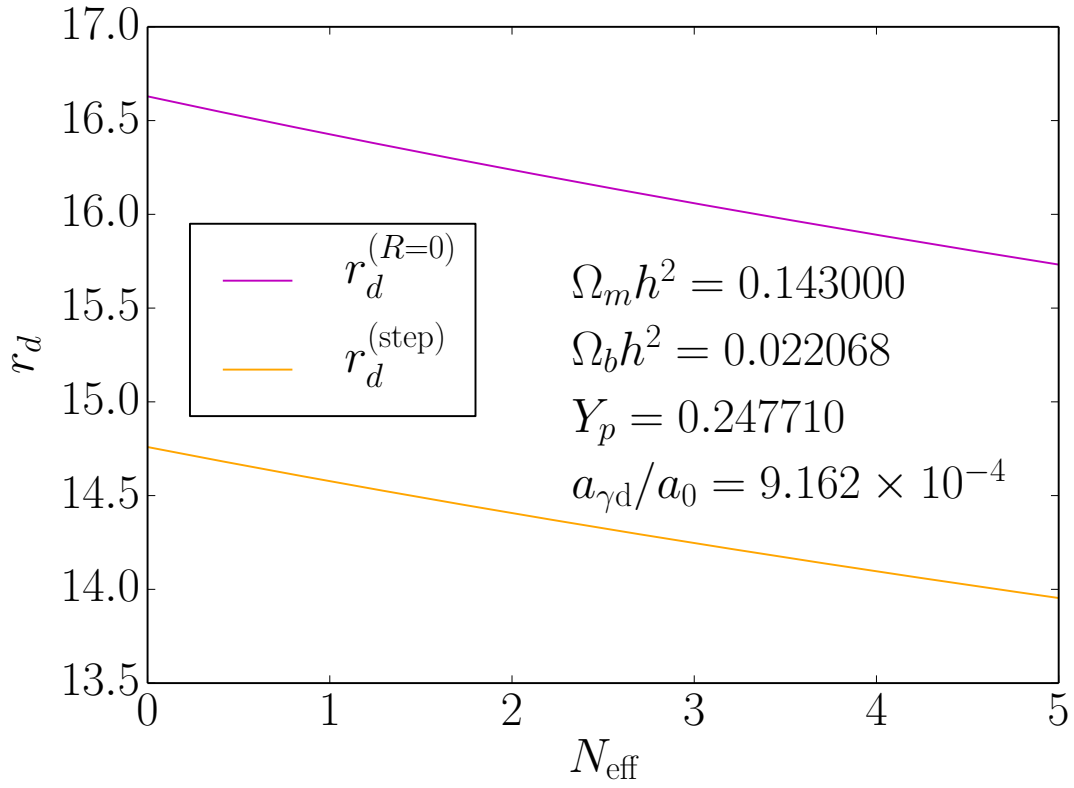

Figure 4.5: Comoving diffusion length versus $N_{\rm eff}$. The superscript notation is the same as in Fig.4.4.

The universe contains hydrogen, helium, and trace amounts of other nuclei. For simplicity, we assume the baryons are only hydrogen nuclei, i.e. protons, unless otherwise noted. The relevant chemical reaction is:

$$p^+ + e^- \leftrightarrow \mathrm{H}^0 + \gamma. \tag{4.90}$$

In equilibirum:

$$\mu_p + \mu_e = \mu_H, \tag{4.91}$$

where μ_i is the chemical potential of the $i^{\rm th}$ species. The argument to find the equilibrium free–electron fraction is similar to that made in Sec.2.4. We repeat it here because of the

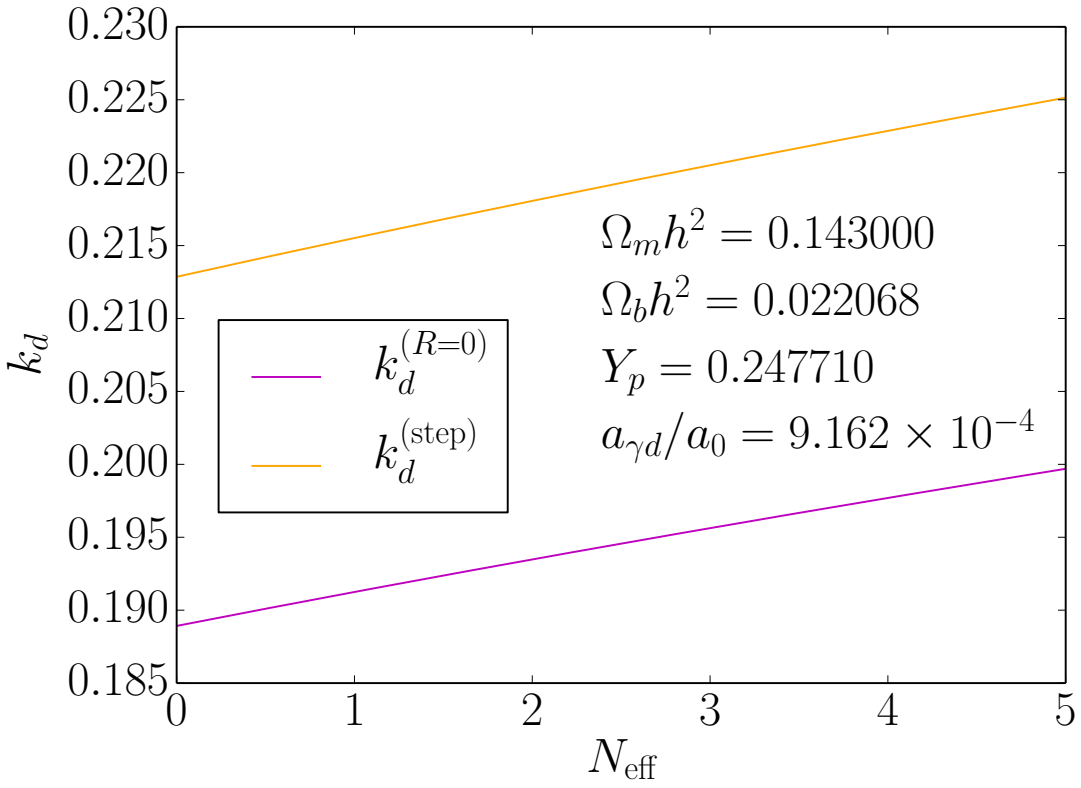

Figure 4.6: Diffusion damping wave number versus $N_{\rm eff}$. The superscript notation is the same as in Fig.4.4.

intricacies of the atomic partition function.

Since there is no constraint fixing the total number of photons, the photon chemical potential is identically zero and does not contribute in Eq. [4.91]. The expression for the chemical potential is the following:

$$\mu_i = \left(\frac{\partial F}{\partial N_i}\right)_{T,V,N_j}, \tag{4.92}$$

where F is the free energy, and the derivative is done with respect to the number of particles N_i while keeping the number of particles of other species N_j constant. The free

energy is related to the partition function Z as follows:

$$F = -T \ln Z = -T \sum_i \ln Z_i = -T \sum_i \ln \frac{\zeta_i^{N_i}}{N_i!}, \tag{4.93}$$

where ζ_i is the partition function of a single gas particle of species i and independent of N_i. Thus, the chemical potential becomes (dropping the i subscript):

$$\mu = -T \ln \frac{\zeta}{N}, \tag{4.94}$$

where we used Stirling's formula to simplify the factorial notation, namely: $\ln N! \simeq N \ln N - N$. To calculate the single-particle partition function, observe:

$$\begin{aligned}
\zeta &= Z_{\text{int}} \int d^3x \int \frac{d^3p}{(2\pi)^3} e^{-p^2/2mT} && (4.95)\\
&= \frac{Z_{\text{int}} V}{2\pi^2} \int_0^\infty p^2 e^{-p^2/2mT} dp && (4.96)\\
&= \frac{Z_{\text{int}} V}{2\pi^2} (2mT)^{3/2} \int_0^\infty x^2 e^{-x^2} dx && (4.97)\\
&= \frac{Z_{\text{int}} V}{2\pi^2} (2mT)^{3/2} \frac{\sqrt{\pi}}{4} && (4.98)\\
&= Z_{\text{int}} V \left(\frac{mT}{2\pi} \right)^{3/2}, && (4.99)
\end{aligned}$$

where Z_{int} is the internal partition function and we have assumed $m \gg T$. Thus, we can now write the chemical potential as:

$$\mu = -T \ln \left[\frac{Z_{\text{int}} V}{N} \left(\frac{mT}{2\pi} \right)^{3/2} \right] = -T \ln \left[\frac{Z_{\text{int}}}{n} \left(\frac{mT}{2\pi} \right)^{3/2} \right], \tag{4.100}$$

where n is the number density. For the electron and proton, the internal partition function is simply the spin degrees of freedom, i.e. $Z_{\text{int}}^{\{e,p\}} = g_{\{e,p\}}$. For hydrogen, the partition

function is the following:

$$Z_{\rm int}^{(H)} = g_H \sum_{\text{bound states}} e^{-\varepsilon/T}. \tag{4.101}$$

Bohr's formula for the energy of a bound state with principal quantum–number n is $E_n = -\Delta Q/n^2$ with degeneracy n^2 for positive integer n. This sum is infinite, so we will take only the first term. In other words, we assume that the excited states are not in equilibrium with the plasma. Thus:

$$Z_{\rm int}^{(H)} = g_H \sum_{n=1}^{\infty} n^2 e^{\Delta Q/n^2 T} \to g_H e^{\Delta Q/T} \tag{4.102}$$

Substituting Eq.(4.102) into Eq. [4.91]:

$$-T\ln\left[\frac{g_p}{n_p}\left(\frac{m_p T}{2\pi}\right)^{3/2}\right] - T\ln\left[\frac{g_e}{n_e}\left(\frac{m_e T}{2\pi}\right)^{3/2}\right] = -T\ln\left[\frac{g_H e^{\Delta Q/T}}{n_H}\left(\frac{m_H T}{2\pi}\right)^{3/2}\right] \tag{4.103}$$

$$\implies \frac{n_H}{n_e n_p} = \frac{g_H}{g_e g_p}\left(\frac{m_H}{m_e m_p}\right)^{3/2}\left(\frac{2\pi}{T}\right)^{3/2} e^{\Delta Q/T} \equiv C(T), \tag{4.104}$$

which serves to define the function $C(T)$. Since the universe is only protons and electrons (in this approximation), the total number of baryons is equal to the sum of hydrogen atoms and free protons, and the number of electrons is equal to the number of protons by charge neutrality:

$$n_p = n_e \text{ and } n_b = n_H + n_p \implies n_H = n_b - n_e. \tag{4.105}$$

Thus, we are left with the following algebraic equation:

$$\frac{n_b - n_e}{n_e^2} = C \implies n_e^2 + \frac{n_e}{C} - \frac{n_b}{C} = 0 \tag{4.106}$$

$$\implies n_e = -\frac{1}{2C} + \frac{1}{2}\sqrt{\frac{1}{C^2} + 4n_b/C} \tag{4.107}$$

$$= n_b \frac{\sqrt{1+4n_bC} - 1}{2n_bC} \tag{4.108}$$

We will now introduce a correction to the leading n_b (while preserving the function C and other n_b terms) to reflect the fact that there is also helium in the universe:

$$n_e = n_{e,0}\left(\frac{a_0}{a}\right)^3 \frac{\sqrt{1+4n_bC} - 1}{2n_bC} \equiv n_{e,0}\left(\frac{a_0}{a}\right)^3 X_e. \tag{4.109}$$

We can again integrate Eq.(4.66), but now with the correction from Eq.(4.109). Fig.4.7 shows a plot of r_d versus scale factor. Clearly, $X_e \sim 1$ in equilibrium at high temperatures. Thus, the step function-method is a valid approximation at high temperatures. At the epoch of photon decoupling, the approximation breaks down rapidly and the two curves in Fig.4.7 diverge. Also included is a plot of k_d versus $N_{\rm eff}$ at the epoch of photon decoupling in Fig.4.8.

4.4.4 Boltzmann–equation approximation

The equilibrium method is only a second approximation. A further refinement is to use the Boltzmann equation to solve for X_e, which we call the Boltzmann–equation method. If we consider a reaction with two reactants and two products, such as $1+2 \rightarrow$

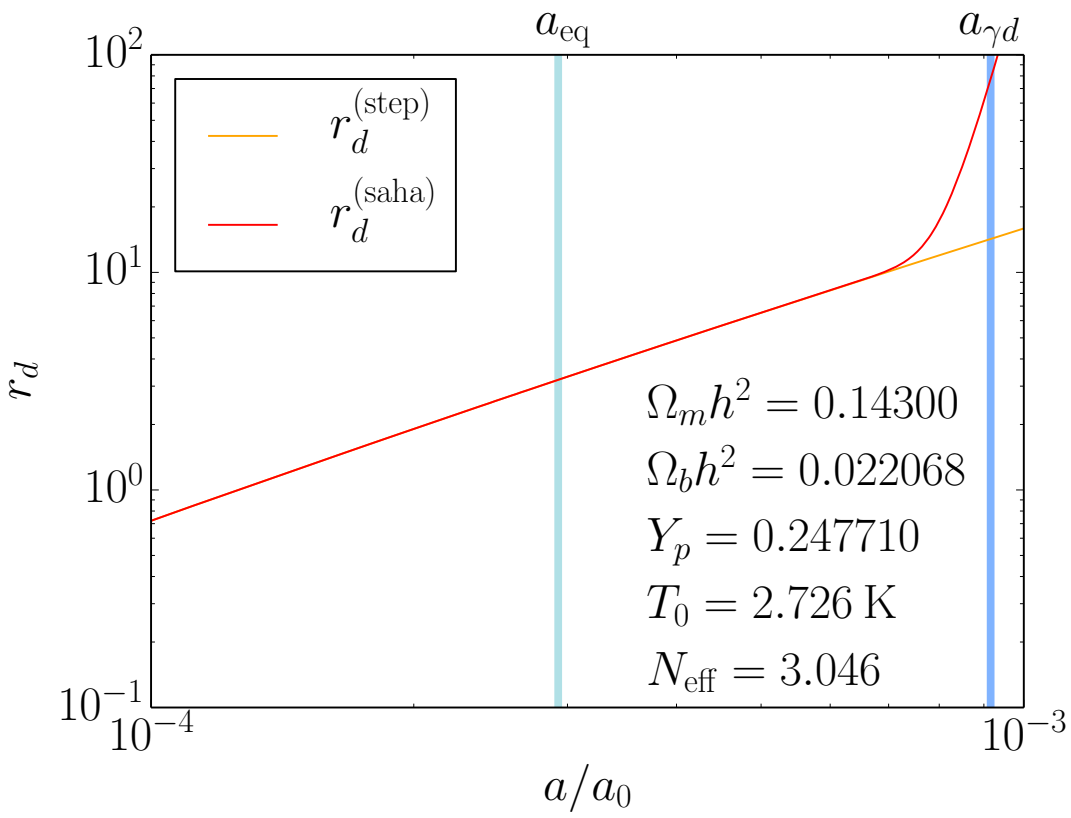

Figure 4.7: Comoving diffusion length versus scale factor. $r_d^{(\rm step)}$ is the comoving diffusion length using the step–function method. $r_d^{(\rm saha)}$ is the same quantity using the equilibrium method.

$3+4$, then the interaction rate of species 1 follows the Boltzmann equation:

$$a^{-3}\frac{d(n_1 a^3)}{dt} = \int \Pi_1\Pi_2\Pi_3\Pi_4 (2\pi)^4 \delta^4(P_1+P_2-P_3-P_4)\times$$
$$[f_3 f_4(1\pm f_1)(1\pm f_2)|\mathcal{M}|^2_{34\to 12} - f_1 f_2(1\pm f_3)(1\pm f_4)|\mathcal{M}|^2_{12\to 34}] \tag{4.110}$$

Eq.(4.110) contains many implicit assumptions, chief among them being conservation of particle number. We will still use Eq.(4.110) even when one of the species is a photon.

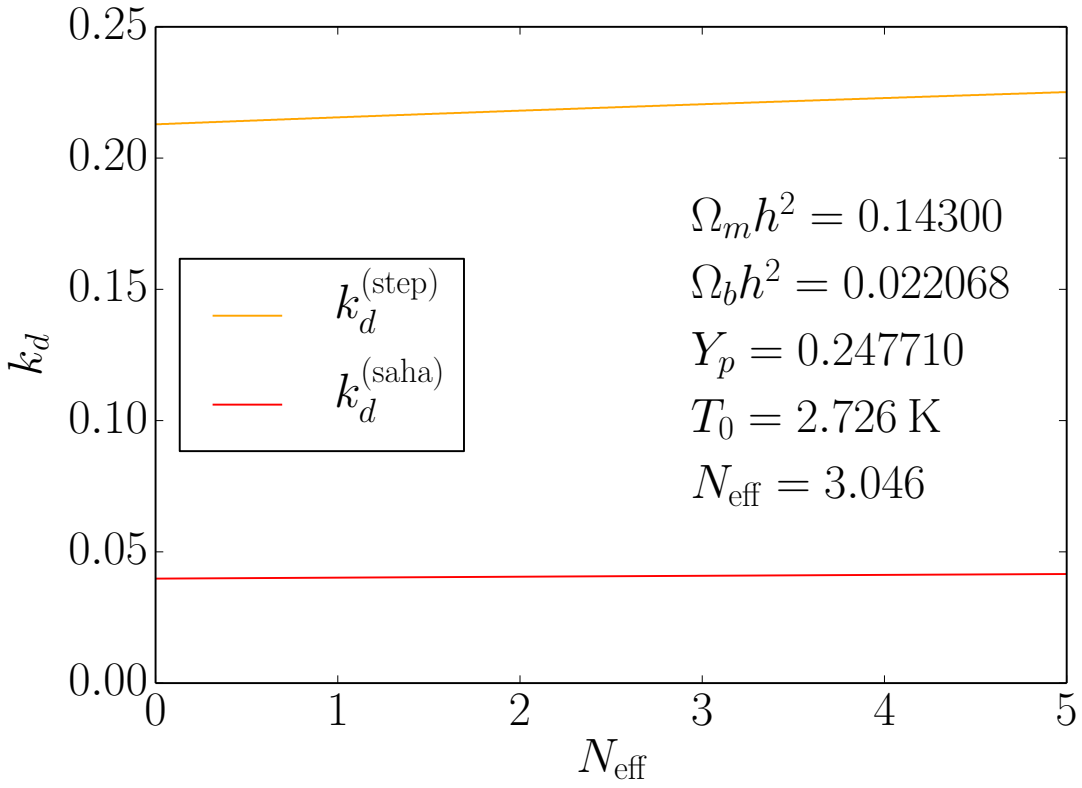

Figure 4.8: Damping diffusion wave number versus $N_{\rm eff}$. The superscript notation is the same as in Fig.4.7

We define the "pseudo"–phase–space factor Π as:

$$\Pi = \frac{g}{(2\pi)^3}\frac{d^3p}{2E}. \tag{4.111}$$

The delta function in Eq.(4.110) ensures conservation of four–momentum P. The occupation fraction f is the probability of finding a particle in the momentum state between $\mathbf{p}$ and $\mathbf{p}+\mathbf{dp}$. In isotropic conditions, $f(\vec{p},t) = f(p,t)$. A $(1-f)$ factor corresponds to fermions, while a $(1+f)$ factor corresponds to bosons. $|\mathcal{M}|^2_{i\to f}$ is the summed-squared amplitude and corresponds to the probability the system evolves from initial state i to

final state f. Assuming CP invariance, we can write:

$$|\mathcal{M}|^2_{i\to f} = |\mathcal{M}|^2_{f\to i} \equiv |\mathcal{M}|^2. \tag{4.112}$$

Eq.(4.110) is an integral–differential equation. We will make further approximations to convert Eq.(4.110) into a strictly differential equation. We begin by making the Boltzmann approximation, assuming that the system is close to equilibrium and dilute enough that Maxwell–Boltzmann statistics apply. Hence:

$$f(p,t) = f(E,t) \simeq e^{-(E-\mu)/T} \text{ and } (1-f) \simeq 1. \tag{4.113}$$

Thus, Eq.(4.110) becomes:

$$\begin{aligned} a^{-3}\frac{d(n_1a^3)}{dt} = \int \Pi_1\Pi_2\Pi_3\Pi_4(2\pi)^4\delta^4(P_1+P_2-P_3-P_4)|\mathcal{M}|^2\times \\ e^{-(E_1+E_2)/T}(e^{\mu_3/T}e^{\mu_4/T} - e^{\mu_1/T}e^{\mu_2/T}), \end{aligned} \tag{4.114}$$

where we have used energy conservation to write $E_3+E_4 = E_1+E_2$. The expression involving the chemical potentials in Eq.(4.114) is independent of the pseudo–phase–space factors and comes outside the integral, which we call I. We can arrange the remaining terms in I as follows:

$$I = \int \Pi_1\Pi_2\Pi_3\Pi_4(2\pi)^4\delta^4(P_1+P_2-P_3-P_4)|\mathcal{M}|^2 e^{-(E_1+E_2)/T} \tag{4.115}$$

$$\begin{aligned} =& g_1g_2\int \frac{d^3p_1}{(2\pi)^3}e^{-E_1/T}\frac{d^3p_2}{(2\pi)^3}e^{-E_2/T}\times \\ & \frac{\int \Pi_1 e^{-E_1/T}\Pi_2 e^{-E_2/T}\Pi_3\Pi_4(2\pi)^4\delta^4(P_1+P_2-P_3-P_4)|\mathcal{M}|^2}{g_1g_2\int \frac{d^3p_1}{(2\pi)^3}e^{-E_1/T}\frac{d^3p_2}{(2\pi)^3}e^{-E_2/T}} \end{aligned} \tag{4.116}$$

$$\equiv g_1g_2\int \frac{d^3p_1}{(2\pi)^3}e^{-E_1/T}\frac{d^3p_2}{(2\pi)^3}e^{-E_2/T}\times\langle\sigma v\rangle, \tag{4.117}$$

where $\langle \sigma v \rangle$ is the thermally–averaged product of cross section and relative speed. Clearly, $\langle \sigma v \rangle$ is not a strict average. We can now write Eq.(4.114) as:

$$a^{-3}\frac{d(n_1 a^3)}{dt} = \langle \sigma v \rangle g_1 g_2 \left[\int \frac{d^3 p_1}{(2\pi)^3} e^{-E_1/T} \frac{d^3 p_2}{(2\pi)^3} e^{-E_2/T} \right] (e^{\mu_3/T} e^{\mu_4/T} - e^{\mu_1/T} e^{\mu_2/T}) \tag{4.118}$$

$$= \langle \sigma v \rangle g_1 g_2 \left[\frac{T^3}{(2\pi)^3} (m_1 m_2)^{3/2} \right] (e^{\mu_3/T} e^{\mu_4/T} - e^{\mu_1/T} e^{\mu_2/T}). \tag{4.119}$$

At this point, we will drop the generality of the two-body expression $1+2 \leftrightarrow 3+4$ and use Eq.(4.90) with species 1 as an electron. Species 4 is then a photon with vanishing chemical potential. Since we are still assuming approximate equilibrium, we can use Eq.(4.100) for the chemical potential expression in Eq.(4.119):

$$e^{\mu_H/T} - e^{\mu_e/T} e^{\mu_p/T} = \frac{n_H}{g_H} \left(\frac{2\pi}{m_H T} \right)^{3/2} e^{-\Delta Q/T} - \frac{n_e n_p}{g_e g_p} \left(\frac{2\pi}{T} \right)^3 \frac{1}{(m_e m_p)^{3/2}}. \tag{4.120}$$

We can now write Eq.(4.119) as:

$$\begin{aligned} a^{-3}\frac{d(n_e a^3)}{dt} =& \langle \sigma v \rangle g_e g_p \left[\frac{T^3}{(2\pi)^3} (m_e m_p)^{3/2} \right] \times \\ & \left[\frac{n_H}{g_H} \left(\frac{2\pi}{m_H T} \right)^{3/2} e^{-\Delta Q/T} - \frac{n_e n_p}{g_e g_p} \left(\frac{2\pi}{T} \right)^3 \frac{1}{(m_e m_p)^{3/2}} \right] \end{aligned} \tag{4.121}$$

$$= \langle \sigma v \rangle \left[n_H \frac{g_e g_p}{g_H} \left(\frac{m_e m_p T}{2\pi m_H} \right)^{3/2} e^{-\Delta Q/T} - n_e n_p \right]. \tag{4.122}$$

Recall that in a hydrogen–only universe: $n_p = n_e$ and $n_b = n_H + n_e$. Thus, Eq.(4.122)

becomes:

$$a^{-3}\frac{d(n_e a^3)}{dt} = \langle\sigma v\rangle\left[n_H\frac{g_e g_p}{g_H}\left(\frac{m_e m_p T}{2\pi m_H}\right)^{3/2} e^{-\Delta Q/T} - n_e n_p\right] \tag{4.123}$$

$$= \langle\sigma v\rangle\left[(n_b - n_e)\left(\frac{m_e T}{2\pi}\right)^{3/2} e^{-\Delta Q/T} - n_e^2\right] \tag{4.124}$$

$$= \langle\sigma v\rangle n_b\left[(1-X_e)\left(\frac{m_e T}{2\pi}\right)^{3/2} e^{-\Delta Q/T} - X_e^2 n_b\right] \tag{4.125}$$

$$\implies \frac{1}{n_b a^3}\frac{d(n_e a^3)}{dt} = \langle\sigma v\rangle\left[(1-X_e)\left(\frac{m_e T}{2\pi}\right)^{3/2} e^{-\Delta Q/T} - X_e^2 n_b\right] \tag{4.126}$$

$$\implies \frac{dX_e}{dt} = \langle\sigma v\rangle\left[(1-X_e)\left(\frac{m_e T}{2\pi}\right)^{3/2} e^{-\Delta Q/T} - X_e^2 n_b\right], \tag{4.127}$$

where we have taken the proton mass to be equivalent to the hydrogen mass. Changing variables from t to a, let us write Eq.(4.127) in a more compact form:

$$\frac{dX_e}{da} = \frac{dX_e}{dt}\frac{1}{aH} = \frac{1}{aH}\left[(1-X_e)\beta - X_e^2 n_b \alpha^{(2)}\right], \tag{4.128}$$

where β is the ionization rate:

$$\beta \equiv \alpha^{(2)}\left(\frac{m_e T}{2\pi}\right)^{3/2} e^{-\Delta Q/T}, \tag{4.129}$$

and $\alpha^{(2)}$ is the recombination rate:

$$\alpha^{(2)} \equiv \langle\sigma v\rangle = \begin{cases} 9.78\dfrac{\alpha^2}{m_e^2}\left(\dfrac{\Delta Q}{T}\right)^{1/2}\ln\dfrac{\Delta Q}{T} & \text{if } T \leq \Delta Q \\ 0 & \text{otherwise} \end{cases}. \tag{4.130}$$

Eq.(4.128) is the final version of the Boltzmann equation which we can solve numerically. Fig.4.9 shows a plot of the comoving diffusion length versus scale factor. We solved Eq.(4.128) using an explicit RK4 scheme. The non-equilibrium solution falls

between the two extreme approximations of the step–function and equilibrium methods. However, the Boltzmann–method is nearly identical to the assumption of equilibrium.

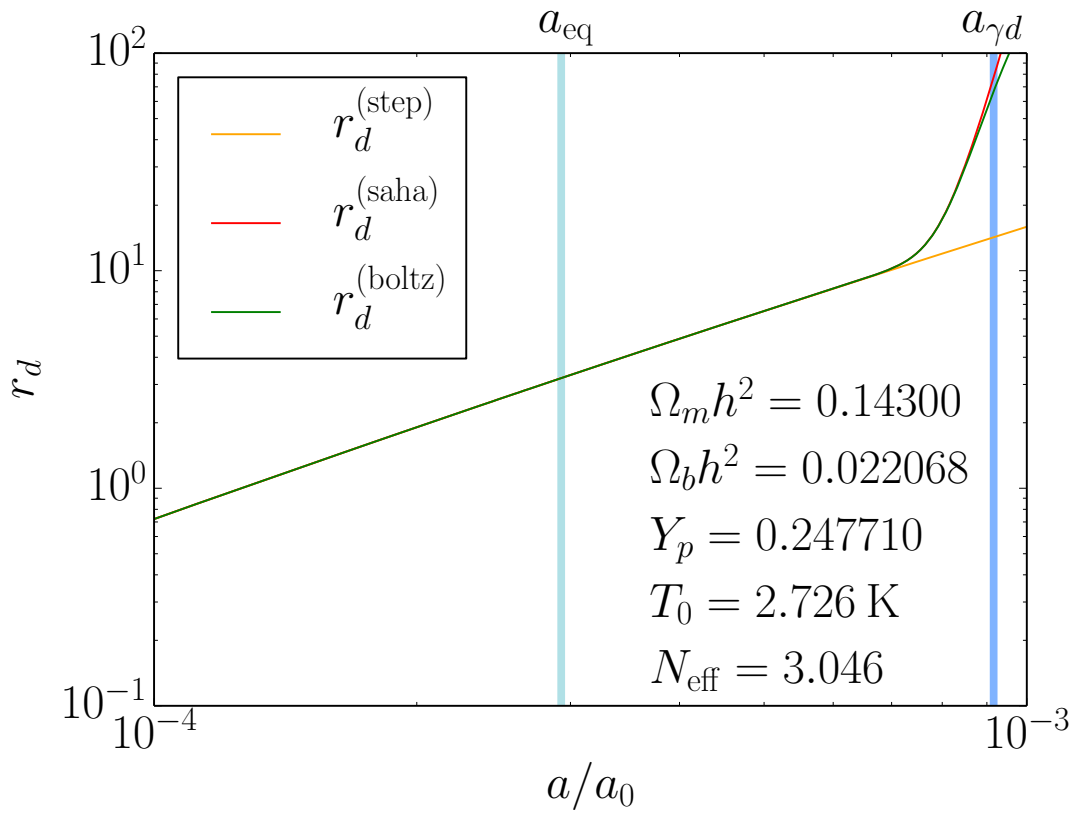

Figure 4.9: Comoving diffusion length versus a/a_0. The superscript notation is the same as in Fig.4.7 with the addition of $r_d^{(\rm boltz)}$ being the comoving diffusion length with the applied Boltzmann–equation method.

4.4.5 Boltzmann–equation correction

Ref.[51] argued that Eq.(4.128) over–estimates the rate of change of X_e. The author derived a different equation by ignoring recombination onto the $n = 1$ level and only considering recombination for levels with $n \geq 2$. Remarkably, Ref.[51] arrived at Eq.(4.128) multiplied by an overall correction factor. We shall refer to this as the Bolzmann–correction method. We will again ignore the presence of helium and assume a hydrogen–only universe.

Recombination onto the ground state

To begin, we need to know how much ionizing radiation is present at a given temperature. To do this, we will resort to a Boltzmann equation for radiation:

$$\frac{\partial}{\partial t}\left(p\frac{d\tilde{N}}{dp}\right)+\frac{dp}{dt}\frac{\partial}{\partial p}\left(p\frac{d\tilde{N}}{dp}\right)=p\frac{dJ}{dp}. \tag{4.131}$$

$\tilde{N}$ is the number of photons as a function of photon-momentum p and time t. J is the net–photon–production rate. The derivatives, $d\tilde{N}/dp$ and dJ/dp are the relevant quantity $\tilde{N}$ or J per unit momentum interval. The photon momenta redshift, so the derivative $dp/dt=-pH$. The product $n_b a^3$ is independent of time and photon momentum, so if we divide Eq.(4.131) by $n_b a^3$, we have:

$$\frac{\partial}{\partial t}\left(\frac{p}{n_b a^3}\frac{d\tilde{N}}{dp}\right)=pH\frac{\partial}{\partial p}\left(\frac{p}{n_b a^3}\frac{d\tilde{N}}{dp}\right)+\frac{p}{n_b a^3}\frac{dJ}{dp}. \tag{4.132}$$

If we define $\tilde{n}=\tilde{N}/a^3$ and $j=J/a^3$, Eq.(4.132) becomes:

$$\frac{\partial}{\partial t}\left(\frac{p}{n_b}\frac{d\tilde{n}}{dp}\right)=pH\frac{\partial}{\partial p}\left(\frac{p}{n_b}\frac{d\tilde{n}}{dp}\right)+\frac{p}{n_b}\frac{dj}{dp}. \tag{4.133}$$

At first, we will concern ourselves with photon production and photo–ionization of the ground state. To wit, we write dj/dp as:

$$\frac{dj}{dp}=\sigma(p)\left[\frac{2p^2}{\pi}\left(\frac{2\pi}{m_e T}\right)^{3/2}e^{-(p-\Delta Q)/T}n_e^2-\frac{d\tilde{n}}{dp}n_{1s}\right], \tag{4.134}$$

where $\sigma(p)$ is the momentum–dependent cross–section for photo–ionization of hydrogen and n_{1s} is the number density of hydrogen atoms in the ground state. For momenta above the binding energy of hydrogen, the photon spectrum is in near equilibrium and Maxwell–Boltzmann–like. If $\tilde{n}_I$ is the number density of photons with momenta above

ΔQ, then we can write:

$$\frac{d\tilde{n}}{dp} = \frac{\tilde{n}_I}{T} e^{-(p-\Delta Q)/T} \text{ for } p > \Delta Q. \tag{4.135}$$

Substituting Eq.(4.135) and Eq.(4.134) into Eq.(4.133) gives (for $p > \Delta Q$):

$$\begin{aligned}\frac{\partial}{\partial t}\left(\frac{p}{n_b}\frac{\tilde{n}_I}{T}e^{-(p-\Delta Q)/T}\right) = {} & pH\frac{\partial}{\partial p}\left(\frac{p}{n_b}\frac{\tilde{n}_I}{T}e^{-(p-\Delta Q)/T}\right) + \frac{p}{n_b}\sigma(p) \\ & \times\left[\frac{2p^2}{\pi}\left(\frac{2\pi}{m_e T}\right)^{3/2} e^{-(p-\Delta Q)/T} n_e^2 - \frac{\tilde{n}_I}{T} e^{-(p-\Delta Q)/T} n_{1s}\right]\end{aligned} \tag{4.136}$$

$$\begin{aligned}\implies \frac{p}{T}e^{-(p-\Delta Q)/T}\frac{\partial}{\partial t}\left(\frac{\tilde{n}_I}{n_b}\right) = {} & \frac{pH\tilde{n}_I}{Tn_b}\frac{\partial}{\partial p}\left(pe^{-(p-\Delta Q)/T}\right) + \frac{p}{n_b}\sigma(p) \\ & \times\left[\frac{2p^2}{\pi}\left(\frac{2\pi}{m_e T}\right)^{3/2} e^{-(p-\Delta Q)/T} n_e^2 - \frac{\tilde{n}_I}{T} e^{-(p-\Delta Q)/T} n_{1s}\right].\end{aligned} \tag{4.137}$$

Dividing Eq.(4.137) by p and integrating for $p \geq \Delta Q$ gives:

$$\begin{aligned}\frac{\partial}{\partial t}\left(\frac{\tilde{n}_I}{n_b}\right) = {} & -H\frac{\tilde{n}_I}{n_b}\frac{\Delta Q}{T} + \frac{n_e^2}{n_b}\left(\frac{2\pi}{m_e T}\right)^{3/2}\int_{\Delta Q}^{\infty}\frac{2p^2}{\pi}\sigma(p)e^{-(p-\Delta Q)/T}dp \\ & - \frac{\tilde{n}_I n_{1s}}{n_b}\frac{1}{T}\int_{\Delta Q}^{\infty}\sigma(p)e^{-(p-\Delta Q)/T}dp.\end{aligned} \tag{4.138}$$

We define the recombination coefficient for transitions direct to the ground state as:

$$\alpha_{1s} = \left(\frac{2\pi}{m_e T}\right)^{3/2}\int_{\Delta Q}^{\infty}\frac{2p^2}{\pi}\sigma(p)e^{-(p-\Delta Q)/T}dp. \tag{4.139}$$

Due to the rapid decay of the exponential $e^{-(p-\Delta Q)/T}$, we will approximate the last integral in Eq.(4.138) as:

$$\sigma_I \simeq \frac{1}{T}\int_{\Delta Q}^{\infty} \sigma(p) e^{-(p-\Delta Q)/T} dp, \tag{4.140}$$

where $\sigma_I \equiv \sigma(p = \Delta Q)$. Thus, Eq. [4.138] becomes:

$$\frac{\partial}{\partial t}\left(\frac{\tilde{n}_I}{n_b}\right) = -H\frac{\tilde{n}_I}{n_b}\frac{\Delta Q}{T} + \alpha_{1s}\frac{n_e^2}{n_b} - \sigma_I \frac{\tilde{n}_I n_{1s}}{n_b}. \tag{4.141}$$

The lhs of Eq.(4.141) is of order $\sim H\tilde{n}_I/n_b$. The first term on the rhs of Eq.(4.141) is of order $\sim H\tilde{n}_I\Delta Q/(n_b T)$. At the temperatures of interest, $\Delta Q/T \sim 50$. Thus, we will make the approximation that the lhs of Eq.(4.141) is zero, producing:

$$0 = -H\frac{\tilde{n}_I}{n_b}\frac{\Delta Q}{T} + \alpha_{1s}\frac{n_e^2}{n_b} - \sigma_I \frac{\tilde{n}_I n_{1s}}{n_b} \tag{4.142}$$

$$\implies \tilde{n}_I = \frac{\alpha_{1s} n_e^2}{\sigma_I n_{1s} + \frac{Q}{T}H}. \tag{4.143}$$

Substituting Eq.(4.143) into the integrated form of the photon–production Eq.(4.134) yields:

$$j = \int_{\Delta Q}^{\infty} \frac{dj}{dp} dp \tag{4.144}$$

$$= \alpha_{1s} n_e^2 - \sigma_I \tilde{n}_I n_{1s} \tag{4.145}$$

$$= \alpha_{1s} n_e^2 - \sigma_I n_{1s} \frac{\alpha_{1s} n_e^2}{\sigma_I n_{1s} + \frac{Q}{T} H} \tag{4.146}$$

$$= \alpha_{1s} n_e^2 \frac{\frac{Q}{T} H}{\sigma_I n_{1s} + \frac{Q}{T} H} \tag{4.147}$$

$$= \alpha_{1s} n_e^2 \frac{1}{\frac{\sigma_I n_{1s} T}{QH} + 1}. \tag{4.148}$$

The factor $\sigma_I n_{1s} T/(QH) \sim 10^7$ at the decoupling epoch. Therefore, ground-state recombination is suppressed by a factor of 10^7, and we can ignore this process[51].

Recombination onto the excited states

We now move on to recombination onto higher states. Using Eq.(4.128) as a standard Boltzmann equation, our modified Boltzmann equation becomes:

$$\frac{dX_e}{dt} = \sum_{q>1} \left(\frac{\beta_q n_q}{n_b} - \alpha_q X_e^2 n_b \right). \tag{4.149}$$

Here we use the symbol q for principal quantum number so as not to confuse it with the symbol n for number density. The sum is for $q > 1$ because we neglect recombination onto the ground state due to the argument in the previous section. We make no distiniction in recombination to states of same q but differing quantum numbers l and m. In other words, the degeneracy of the excited states is built into the coefficients. To solve Eq.(4.149),

we need expressions for the ionization, β_q, and recombination, α_q, coefficients and the number densities of the excited hydrogen states, n_q. We will make some simplifying assumptions.

First, we will assume that the recombination and ionization rates are related to one another through the Saha equation:

$$\frac{\beta_q}{\alpha_q} = \frac{1}{q^2}\left(\frac{m_e T}{2\pi}\right)^{3/2} e^{-E_q/T}, \tag{4.150}$$

where E_q is the binding energy of the q^{th} state and the $1/q^2$ factor is due to the degeneracy of the q^{th} state, i.e. there are more ways to recombine then there is to ionize. Accounting for the electron spin quantum number, there should be another factor of 2 in the denominator of the above expression. However, that factor is already taken care of in the Saha expression.

Second, the ratio of number densities is also in equilibrium:

$$\frac{n_q}{n_2} = \frac{q^2}{4} e^{-(E_2 - E_q)/T}, \tag{4.151}$$

where the factor $q^2/4$ is the ratio of degeneracy factors for the two states. We will define the quantity $\mathcal{R} \equiv n_2/4n_1$. From the previous discussion, $\mathcal{R}$ is not in equilibrium. Thus:

$$n_q = n_1 q^2 \mathcal{R} e^{-(E_2 - E_q)/T}. \tag{4.152}$$

We define the summed quantity α_c as:

$$\alpha_c \equiv \sum_{q>1} \alpha_q. \tag{4.153}$$

With this definition, we can manipulate the expression with β_q in the following manner:

$$\sum_{q>1} \frac{\beta_q n_q}{n_b} = \frac{1}{n_b} \sum_{q>1} \alpha_q \frac{1}{q^2} \left(\frac{m_e T}{2\pi} \right)^{3/2} e^{-E_q/T} n_1 q^2 \mathcal{R} e^{-(E_2 - E_q)/T} \tag{4.154}$$

$$= \frac{n_1 \mathcal{R}}{n_b} \left(\frac{m_e T}{2\pi} \right)^{3/2} e^{-E_2/T} \sum_{q>1} \alpha_q \tag{4.155}$$

$$= \frac{n_1 \mathcal{R}}{n_b} \left(\frac{m_e T}{2\pi} \right)^{3/2} e^{-E_1/T} e^{-(E_2 - E_1)/T} \alpha_c \tag{4.156}$$

$$\equiv \beta_c \frac{n_1 \mathcal{R}}{n_b} e^{-(E_2 - E_1)/T}. \tag{4.157}$$

With the new expressions for α_c and β_c, we can simplify Eq.(4.149) to:

$$\frac{dX_e}{dt} = \beta_c \mathcal{R} \frac{n_1}{n_b} e^{-(E_2 - E_1)/T} - \alpha_c X_e^2 n_b. \tag{4.158}$$

We will make the assumption that most of the neutral hydrogen is in the ground state when recombination occurs, implying $n_1 \sim n_H = n_b - n_e$. Furthermore, the summed coefficients β_c and α_c are simply the coefficients of Eqs.(4.129) and (4.130), namely $\beta_c = \beta$ and $\alpha_c = \alpha^{(2)}$. We now write Eq.(4.158) as:

$$\frac{dX_e}{dt} = \beta \mathcal{R} (1 - X_e) e^{-(E_2 - E_1)/T} - \alpha^{(2)} X_e^2 n_b. \tag{4.159}$$

We must determine an expression for $\mathcal{R}$ before we proceed to solve Eq.(4.159). Let us return to the Boltzmann equation we derived for photons, Eq.(4.133):

$$\frac{\partial}{\partial t} \left(\frac{p}{n_b} \frac{d\tilde{n}}{dp} \right) = pH \frac{\partial}{\partial p} \left(\frac{p}{n_b} \frac{d\tilde{n}}{dp} \right) + \frac{p}{n_b} \frac{dj}{dp} \tag{4.160}$$

We are going to integrate this equation in a small region centered around the momentum

of the Lyman–α photon, which we call $p_\alpha \equiv 3\Delta Q/4$:

$$\int_{p_\alpha-\delta p}^{p_\alpha+\delta p} dp \frac{\partial}{\partial t}\left(\frac{p}{n_b}\frac{d\tilde{n}}{dp}\right) = \int_{p_\alpha-\delta p}^{p_\alpha+\delta p} dp\, pH \frac{\partial}{\partial p}\left(\frac{p}{n_b}\frac{d\tilde{n}}{dp}\right) + \int_{p_\alpha-\delta p}^{p_\alpha+\delta p} dp \frac{p}{n_b}\frac{dj}{dp} \tag{4.161}$$

$$\Longrightarrow \frac{\partial}{\partial t}\left(\frac{p_\alpha}{n_b}\left.\frac{d\tilde{n}}{dp}\right|_{p_\alpha} 2\delta p\right) = \frac{p_\alpha H}{n_b}\left(p\frac{d\tilde{n}}{dp}\right)\Big|_{p_\alpha-\delta p}^{p_\alpha+\delta p} + \frac{p_\alpha}{n_b}\left.\frac{dj}{dp}\right|_{p_\alpha} 2\delta p \tag{4.162}$$

$$\Longrightarrow \frac{p_\alpha 2\delta p}{n_b}\frac{\partial}{\partial t}\left(\left.\frac{d\tilde{n}}{dp}\right|_{p_\alpha}\right) = \frac{p_\alpha H}{n_b}\left(\left.\frac{d\tilde{n}}{dp}\right|_{p_\alpha} 2\delta p + p_\alpha \left.\frac{d^2\tilde{n}}{dp^2}\right|_{p_\alpha} 2\delta p\right) + \frac{p_\alpha}{n_b}\left.\frac{dj}{dp}\right|_{p_\alpha} 2\delta p \tag{4.163}$$

$$\Longrightarrow \frac{\partial}{\partial t}\left(\left.\frac{d\tilde{n}}{dp}\right|_{p_\alpha}\right) = H\left.\frac{d\tilde{n}}{dp}\right|_{p_\alpha} + p_\alpha H\left.\frac{d^2\tilde{n}}{dp^2}\right|_{p_\alpha} + \left.\frac{dj}{dp}\right|_{p_\alpha}. \tag{4.164}$$

The term on the lhs of Eq.(4.164) is nearly identical to the first term on the rhs of the same equation. After we subtract those terms, we have:

$$-\left.\frac{dj}{dp}\right|_{p_\alpha} = p_\alpha H\left.\frac{d^2\tilde{n}}{dp^2}\right|_{p_\alpha} \tag{4.165}$$

$$\Longrightarrow -\frac{1}{p_\alpha H}\left.\frac{dj}{dp}\right|_{p_\alpha} 2\delta p = \left.\frac{d^2\tilde{n}}{dp^2}\right|_{p_\alpha} 2\delta p = \left.\frac{d\tilde{n}}{dp}\right|_{p_\alpha+\delta p} - \left.\frac{d\tilde{n}}{dp}\right|_{p_\alpha-\delta p} \tag{4.166}$$

$$\Longrightarrow -\frac{2\pi^2}{g_\gamma p_\alpha^3 H}\left.\frac{dj}{dp}\right|_{p_\alpha} 2\delta p = \frac{2\pi^2}{g_\gamma p_\alpha^2}\left.\frac{d\tilde{n}}{dp}\right|_{p_\alpha+\delta p} - \frac{2\pi^2}{g_\gamma p_\alpha^2}\left.\frac{d\tilde{n}}{dp}\right|_{p_\alpha-\delta p}. \tag{4.167}$$

The dimensionless factor $(2\pi/g_\gamma p^2)(dn_i/dp)$ is a phase-space probability for species i to occupy the state with momentum p. The first term on the rhs of Eq.(4.167) represents the photons blueward of the Lyman–α line. These photons have a high enough energy to excite an electron from the $q = 1$ state to the $q = 2$ state, thereby reducing the number of photons. The second term on the rhs of Eq.(4.167) represents the photons redward of the Lyman–α line. These photons do not have the requisite energy for the excitation, thereby preserving the number of photons. As we have stressed before, the Lyman–α excitation

is not in equilibrium. Thus, a large

$$\frac{2\pi^2}{g_\gamma p_\alpha^2}\left.\frac{d\tilde{n}}{dp}\right|_{p_\alpha+\delta p}, \tag{4.168}$$

induces a negative photon–production rate. Therefore the difference of these two terms in Eq.(4.167) represents the difference between the equilibrium ratio to the out–of–equilibrium ratio. In terms of an equation:

$$\left.\frac{\pi^2}{p_\alpha^2}\frac{d\tilde{n}}{dp}\right|_{p_\alpha+\delta p} - \left.\frac{\pi^2}{p_\alpha^2}\frac{d\tilde{n}}{dp}\right|_{p_\alpha-\delta p} \simeq e^{-(E_1-E_2)/T} - \frac{n_2}{4n_1} \tag{4.169}$$

$$= e^{-(E_1-E_2)/T} - \mathcal{R}, \tag{4.170}$$

where $g_\gamma = 2$. There is no restriction on the sign of the above quantity, and indeed the above quantity is negative. Furthermore, the single term on the lhs of Eq.(4.167) is representative of Lyman–α production, which is the difference between recombination, ionization, and two-photon decay of the $q = 2$ state:

$$j(p_\alpha) = \alpha^{(2)} n_e^2 - \frac{\beta e^{(E_1-E_2)/T}}{4} n_2 - \Lambda_{2\gamma}\left(\frac{n_2}{4} - n_1 e^{-(E_1-E_2)/T}\right) \tag{4.171}$$

$$= \alpha^{(2)} n_e^2 - \beta e^{(E_1-E_2)/T}\mathcal{R} n_1 - n_1\Lambda_{2\gamma}(\mathcal{R} - e^{-(E_1-E_2)/T}) \tag{4.172}$$

$$\simeq \alpha^{(2)} n_e^2 - \beta e^{(E_1-E_2)/T}\mathcal{R} n_H - n_H\Lambda_{2\gamma}(\mathcal{R} - e^{-(E_1-E_2)/T}). \tag{4.173}$$

If we take the limit as $\delta p \to 0$ of Eq.(4.167), we are left with:

$$\lim_{\delta p\to 0}\left(-\frac{\pi^2}{p_\alpha^3 H}\right)\left.\frac{dj}{dp}\right|_{p_\alpha} 2\delta p = e^{-(E_1-E_2)} - \mathcal{R} \tag{4.174}$$

$$-\frac{\pi^2}{p_\alpha^3 H}\lim_{\delta p\to 0}\left.\frac{dj}{dp}\right|_{p_\alpha} 2\delta p = \tag{4.175}$$

$$-\frac{\pi^2}{p_\alpha^3 H} j(p_\alpha) = \tag{4.176}$$

$$\implies j(p_\alpha) = \frac{p_\alpha^3 H}{\pi^2}(\mathcal{R} - e^{-(E_1-E_2)}). \tag{4.177}$$

We substitute Eq.(4.177) into Eq.(4.173):

$$\frac{p_\alpha^3 H}{\pi^2}(\mathcal{R} - e^{-(E_1-E_2)/T}) = \alpha^{(2)} n_e^2 - \beta e^{(E_1-E_2)/T}\mathcal{R} n_H - n_H \Lambda_{2\gamma}(\mathcal{R} - e^{-(E_1-E_2)/T}) \tag{4.178}$$

$$\implies \mathcal{R}\left(\frac{p_\alpha^3 H}{\pi^2} + \beta e^{(E_1-E_2)/T} n_H + \Lambda_{2\gamma} n_H\right) = \alpha^{(2)} n_e^2 + e^{-(E_1-E_2)/T}\left(\frac{p_\alpha^3 H}{\pi^2} + \Lambda_{2\gamma} n_H\right). \tag{4.179}$$

If we solve for $\mathcal{R}$, we find:

$$\mathcal{R} = e^{-(E_1-E_2)/T}\frac{\alpha^{(2)} n_e^2 e^{(E_1-E_2)/T} + \left(\frac{p_\alpha^3 H}{\pi^2} + \Lambda_{2\gamma} n_H\right)}{\frac{p_\alpha^3 H}{\pi^2} + \beta e^{(E_1-E_2)/T} n_H + \Lambda_{2\gamma} n_H} \tag{4.180}$$

$$= e^{-(E_1-E_2)/T}\frac{\alpha^{(2)}\frac{X_e^2 n_b}{(1-X_e)} e^{(E_1-E_2)/T} + \left(\frac{p_\alpha^3 H}{\pi^2 n_H} + \Lambda_{2\gamma}\right)}{\frac{p_\alpha^3 H}{\pi^2 n_H} + \beta e^{(E_1-E_2)/T} + \Lambda_{2\gamma}} \tag{4.181}$$

$$= e^{-(E_1-E_2)/T}\frac{\alpha^{(2)}\frac{X_e^2 n_b}{(1-X_e)} e^{(E_1-E_2)/T} + \left(\Lambda_\alpha + \Lambda_{2\gamma}\right)}{\Lambda_\alpha + \beta^{(2)} + \Lambda_{2\gamma}}, \tag{4.182}$$

where

$$\Lambda_\alpha \equiv \frac{p_\alpha^3 H}{\pi^2 n_H} = \frac{(3\Delta Q)^3 H}{4^3\pi^2 n_H} = \frac{(3\Delta Q)^3 H}{(8\pi)^2 n_H}, \tag{4.183}$$

$$\beta^{(2)} \equiv \beta e^{(E_1-E_2)/T} = \beta e^{3\Delta Q/4T}. \tag{4.184}$$

Finally, we substitute Eq.(4.182) into Eq.(4.159):

$$\frac{dX_e}{dt} = \beta\frac{\alpha^{(2)}\frac{X_e^2 n_b}{(1-X_e)}e^{(E_1-E_2)/T} + \left(\Lambda_\alpha + \Lambda_{2\gamma}\right)}{\left(\Lambda_\alpha + \beta^{(2)} + \Lambda_{2\gamma}\right)}(1-X_e) - \alpha^{(2)}X_e^2 n_b \tag{4.185}$$

$$= \beta\frac{\Lambda_\alpha + \Lambda_{2\gamma}}{\Lambda_\alpha + \beta^{(2)} + \Lambda_{2\gamma}}(1-X_e) - \left[\alpha^{(2)}X_e^2 n_b - \beta\frac{\alpha^{(2)}X_e^2 n_b e^{(E_1-E_2)/T}}{\Lambda_\alpha + \beta^{(2)} + \Lambda_{2\gamma}}\right] \tag{4.186}$$

$$= \beta(1-X_e)\frac{\Lambda_\alpha + \Lambda_{2\gamma}}{\Lambda_\alpha + \beta^{(2)} + \Lambda_{2\gamma}} - \alpha^{(2)}X_e^2 n_b\frac{\Lambda_\alpha + \beta^{(2)} - \beta e^{(E_1-E_2)/T}) + \Lambda_{2\gamma}}{\Lambda_\alpha + \beta + \Lambda_{2\gamma}} \tag{4.187}$$

$$\equiv \left[\beta(1-X_e) - \alpha^{(2)}X_e^2 n_b\right]C \tag{4.188}$$

$$\Longrightarrow \frac{dX_e}{da} = \frac{1}{aH}\left[\beta(1-X_e) - \alpha^{(2)}X_e^2 n_b\right]C, \tag{4.189}$$

where C is the correction of Ref.[51]:

$$C = \frac{\Lambda_\alpha + \Lambda_{2\gamma}}{\Lambda_\alpha + \Lambda_{2\gamma} + \beta^{(2)}}. \tag{4.190}$$

Obviously there are other processes which can excite atoms, most notably collisional excitations. We ignore those processes in the correction factor above. Eq.(4.189) is Eq.(4.128) with the rhs multiplied by C from Eq.(4.190). We can integrate Eq.(4.189) using the RK4 scheme. The results are in Fig.4.10. Also included is Fig.4.11: a plot of how X_e evolves with scale factor for a cosmology with no helium and a slightly higher $N_{\rm eff}$ than standard. The last plot of this section is Fig.4.12 and shows how k_d changes with $N_{\rm eff}$ for the Boltzmann–equation and the Boltzmann–correction method.

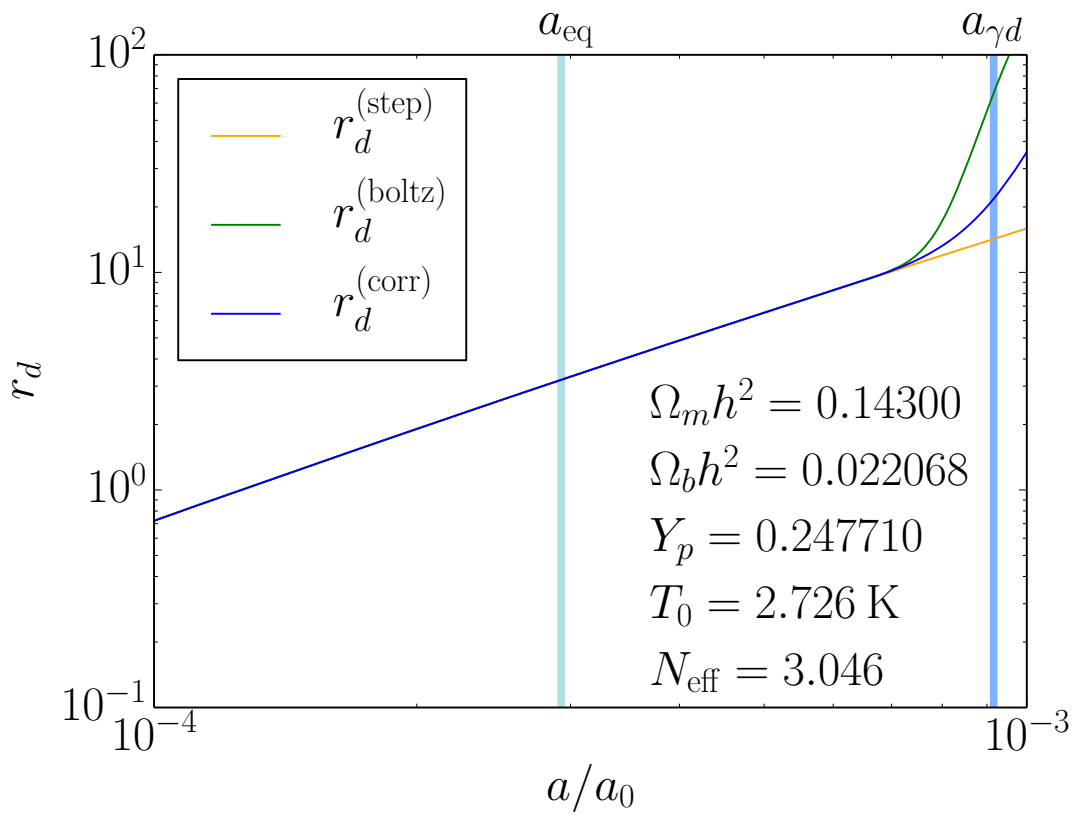

Figure 4.10: Comoving diffusion length vs. a/a_0. The superscript notation is the same as in Fig.4.9 with the addition of $r_d^{(\rm corr)}$ being the comoving diffusion length with the applied Boltzmann–correction method.

When calculating the diffusion lengths, we stated that we were working under the simplification of no helium in the universe. This is not quite true, since we made sure our expression for the electron–density at the current epoch included corrections for the presence of neutrons in helium. However, our evolution of the free–electron fraction in the equilibrium, Boltzmann–equation, and Boltzmann–corrections methods did not account for any helium. We made the assumption the helium recombination is identical to hydrogen recombination and the two processes happen in concert together. We now discard that false persumption and include a separate Boltzmann equation for helium.

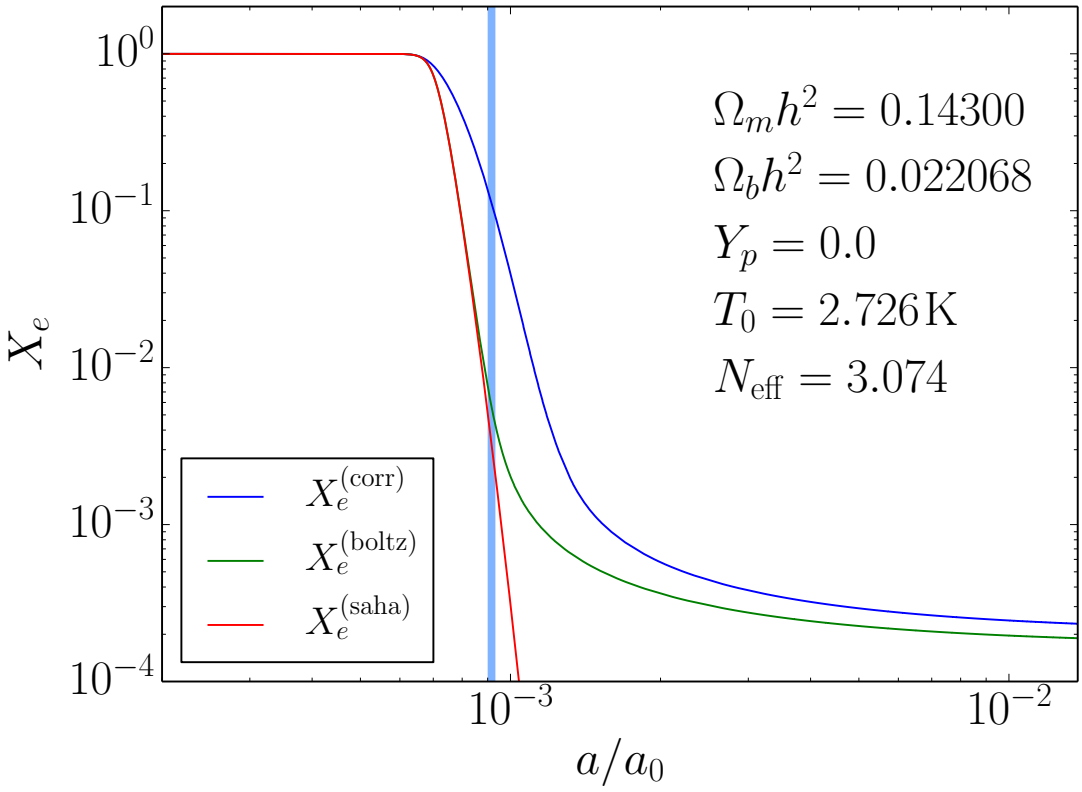

Figure 4.11: Free–electron fraction X_e vs. a/a_0. The superscript notation is consistent with all previous plots.

4.4.6 Inclusion of helium

We have written an independent code to calculate the free–electron fraction, X_e. The results agree well with Ref. [52] (RECFAST). In fact, the agreement is within 2% for most of the range $10^{-4} \lesssim a/a_0 \lesssim 10^{-3}$ ($10^4 \gtrsim z \gtrsim 10^3$). We have not included additional fit parameters, as in Ref. [52], that modify recombination and ionization terms of the three-level treatment to obtain agreement with the full 300-level computation [53]. The code allows significant deviations from the model parameters of ΛCDM; it should be used with caution, however, since the effective three-level treatments for helium and hydrogen recombination have been optimized for near-standard model parameters.

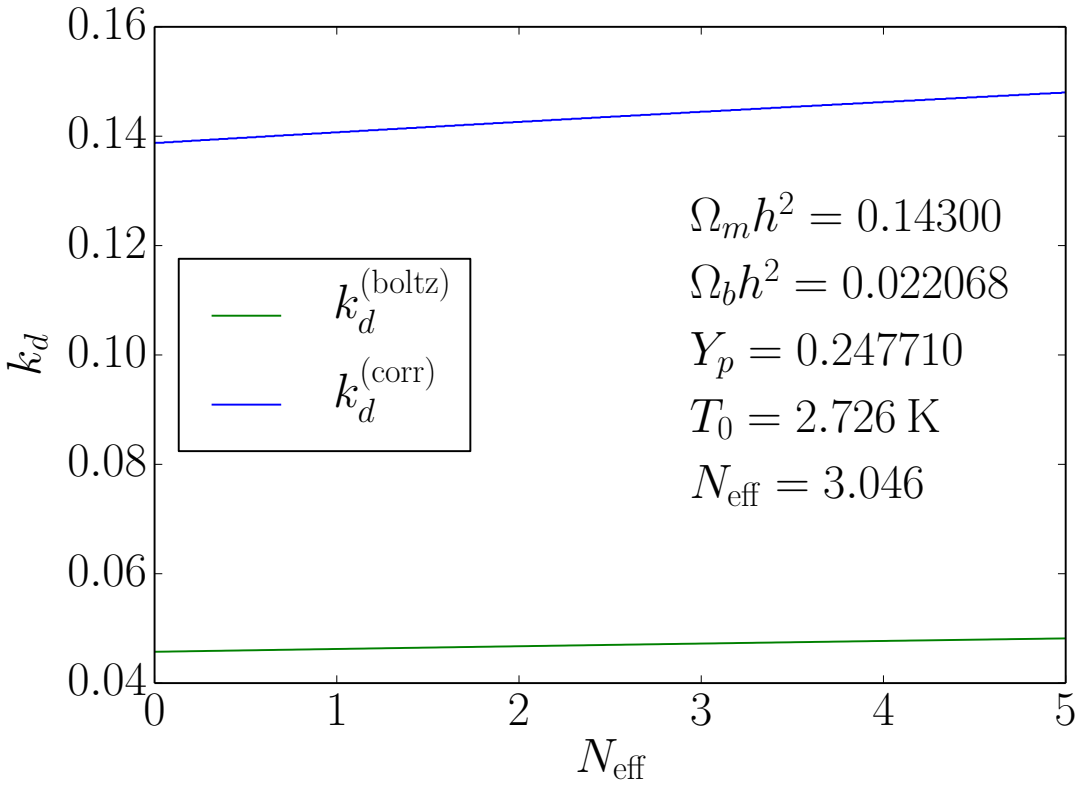

Figure 4.12: Damping diffusion wave number vs. $N_{\rm eff}$. The superscript notation is consistent with all previous plots.

The number density of free and total electrons is

$$n_e^{(\rm free)} = n_p + n_{\rm He\,II} + 2n_{\rm He\,III}, \tag{4.191}$$

$$n_e^{(\rm tot)} = n_b \left(1 - \frac{Y_P}{2}\right), \tag{4.192}$$

where n_b, n_p, $n_{\rm He\,II}$, $n_{\rm He\,III}$ are the proper number densities for baryons, protons, singly- and doubly-ionized helium, respectively. We write the free–electron fraction as

$$X_e \equiv \frac{n_e^{(\rm free)}}{n_e^{(\rm tot)}} \equiv X_p + X_{\rm He\,II} + 2X_{\rm He\,III}, \tag{4.193}$$

so defined to take values in the range $0 \leq X_e \leq 1$.

We follow Refs. [51, 54] and consider the simplification of the multi-level hydrogen and helium atoms to that of an effective three-level system which includes the ground $n = 1$ state, the first excited $n = 2$ states, and the continuum. All other excited states are assumed to be in equilibrium with the $2s$ state. We treat He II recombination approximately [53] (via the Saha equation) since it is essentially complete at the advent of the epoch of He I recombination. The He III contribution, therefore, in the Boltzmann equation for He II is negligible.

Boltzmann equations for H II and He II contain a thermally-averaged cross section and relative velocity $\langle \sigma v \rangle$. We use Case B recombination coefficients for the $\langle \sigma v \rangle$ of both neutral hydrogen [55] and helium [56]. Along with a Saha equation for He III, the Boltzmann equations for H II and He II are a coupled set of ordinary differential equations constituting a recombination network to model the ionization history of the universe prior to photon decoupling.

Fig. 4.13 shows the evolution of the free–electron fraction with scale factor for various values of ω_b and concomitant values of Y_P. The vertical shaded bar is centered on $a_{\gamma d}$, the scale factor at photon decoupling, given by Ref. [2] for a best-fit-value $\omega_b = 0.022068$. The recombination rate increases with increasing ω_b which results in a lower freeze-out value of the free–electron fraction at large a/a_0. The recombination history is largely insensitive to the helium fraction but we calculate Y_P for each value of ω_b to maintain self-consistency between BBN and recombination. The values of Y_P are $Y_P = 0.220, 0.238, 0.243, 0.246$ for increasing ω_b.

4.5 r_s/r_d as a proxy for $N_{\rm eff}$

In this section we describe our method for determining $N_{\rm eff}$ in detail. We introduce two variants of $N_{\rm eff}$. When referring to the radiation energy density equation (4.1), which

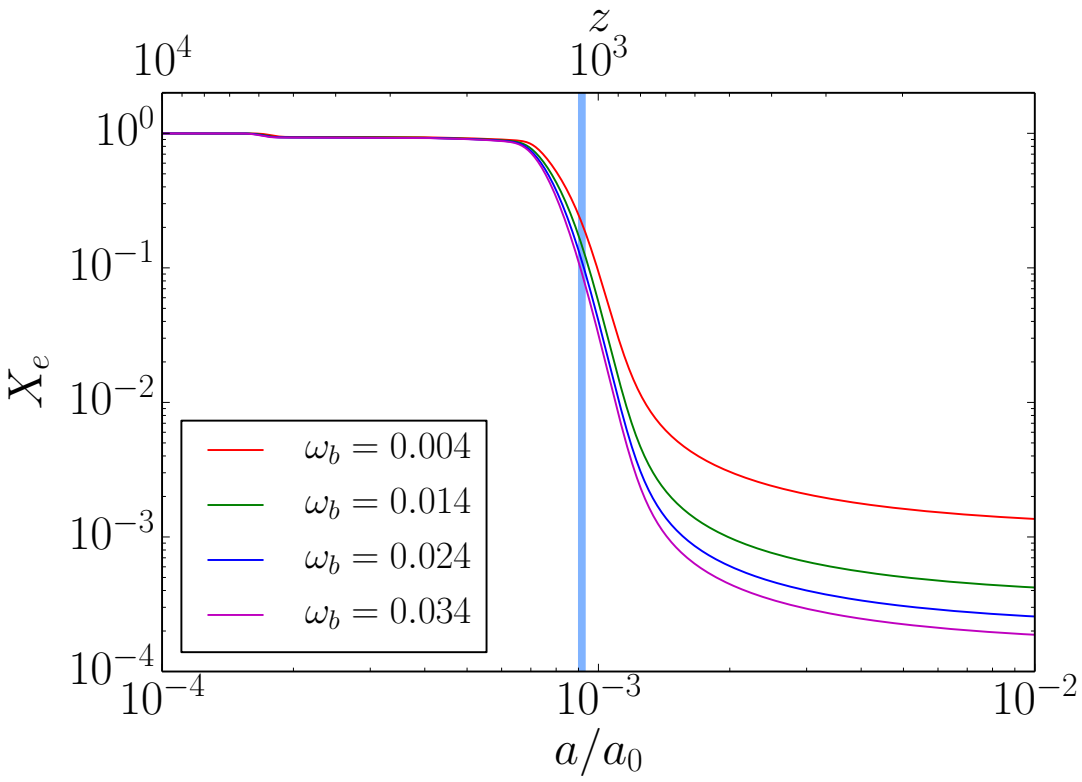

Figure 4.13: Free-electron fraction X_e as a function of scale factor a/a_0 and redshift z (at top.) The different curves correspond to various values of ω_b. The cold dark matter contribution is held fixed at $\omega_c = 0.12029$. The vertical shaded bar is the scale factor at photon decoupling, $a_{\gamma d}$ given by Ref. [2].

takes as an input the quantity $N_{\rm eff}$, we designate $N_{\rm eff}$ as $N_{\rm eff}^{\rm (th)}$. When considering general cosmologies, perhaps with BSM physics, we deduce the value of $N_{\rm eff}$ from the observable quantity $r_s/r_d = \theta_s/\theta_d$, described in this section, and designate it as $\tilde{N}_{\rm eff}$. The simplest cosmologies for which Eq. (4.1) obtains, having negligible neutrino mass, standard model constituents and no energy transfer between species have $N_{\rm eff}^{\rm (th)} = \tilde{N}_{\rm eff}$.

We consider a test input cosmology that is non-standard yet substantively similar to ΛCDM. We proceed by determining Y_P at temperature $T \sim 0.1$ MeV using the BBN network of BURST [31]. The principal observational cosmological input at this time is ω_b. Also input and incorporated into the BBN subroutine is any neutrino and BSM

physics that constitute the test cosmology. Subsequently, we compute the recombination history of the universe from early times ($a/a_0 \sim 10^{-7}$) to the current epoch. Specific observational inputs include ω_b, ω_c (where for cold dark matter $\omega_c \equiv \Omega_c h^2$), Y_P, and H_0 (the Hubble constant, $H_0 = H(a_0)$). For the purposes of the present discussion, other inputs of particular importance include neutrino occupation probabilities (as output from a neutrino transport calculation of weak decoupling that is fully coupled to BBN) and neutrino rest masses. The neutrino energy density of the neutrino seas is calculated by writing the occupation probabilities in the mass eigenbasis [57]. We emphasize the fact that $N_{\rm eff}^{\rm (th)}$ is *not* input as a base parameter; this is of paramount import in the present approach. The recombination history, $n_e(a)$ determines the optical depth as a function of scale factor:

$$\tau(a) \equiv \int_a^{a_0} \frac{da'}{a'^2}\, a' n_e(a') \sigma_T \tag{4.194}$$

We define the scale factor at photon decoupling $a_{\gamma d}$ such that $\tau(a_{\gamma d}) \equiv 1$. In this definition, we do not include the effects of cosmic reionization when calculating $n_e(a)$ for use in Eq. (4.194) [2]. We apply $a_{\gamma d}$ and the input cosmology to equations (4.30) and (4.66) to compute the sound horizon and photon diffusion length, respectively. We arrive in this way at a ratio $(r_s/r_d)^{\rm (inp)}$ for our input cosmology.

Our immediate objective is to determine a value of $N_{\rm eff}$ (here termed $\tilde{N}_{\rm eff}$) corresponding to this value for $(r_s/r_d)^{\rm (inp)}$. We map out a range of values of r_s/r_d that correspond to the same input cosmology as that used in calculating $(r_s/r_d)^{\rm (inp)}$, with one significant difference. We parametrize all of the neutrino and BSM physics into the single $N_{\rm eff}^{\rm (th)}$ parameter. We then use $N_{\rm eff}^{\rm (th)}$ to calculate the radiation energy density in Eq.

(4.1) to determine the Hubble rate. We vary $N_{\rm eff}^{\rm (th)}$ to compute the function

$$r_s/r_d = r_s/r_d[\omega_b, \omega_c, Y_P, \ldots; N_{\rm eff}^{\rm (th)}], \tag{4.195}$$

shown in Fig. 4.14. Since r_s/r_d is a one-to-one function of $N_{\rm eff}^{\rm (th)}$, we may invert Eq. (4.195) to obtain $N_{\rm eff}^{\rm (th)} = N_{\rm eff}^{\rm (th)}[r_s/r_d]$. The final step is to evaluate the previous function with our input cosmology ratio, *i.e.* $\tilde{N}_{\rm eff} = N_{\rm eff}^{\rm (th)}[r_s/r_d = (r_s/r_d)^{\rm (inp)}]$, to obtain a value of $\tilde{N}_{\rm eff}$. As an example, we take the best-fit values from Ref. [2] combined with WMAP Polarization data ($100\theta_s = 1.04136$ & $100\theta_d = 0.161375$) to obtain $(r_s/r_d)^{\rm (inp)} = 100\theta_s/100\theta_d = 6.45304$. This corresponds to a value $\tilde{N}_{\rm eff} = 3.31$ on Fig. 4.14, in line with the best-fit value $N_{\rm eff} = 3.25$ ($3.51^{+0.80}_{-0.74}$ at 95% limits) [2]. We again note that for the simplest cosmologies the two generally distinct functions $N_{\rm eff}^{\rm (th)}[r_s/r_d]$ and $\tilde{N}_{\rm eff}[r_s/r_d]$ reduce to the same function and have $N_{\rm eff}^{\rm (th)} = \tilde{N}_{\rm eff}$.

Figure 4.14, which shows the function $r_s/r_d[N_{\rm eff}^{\rm (th)}]$, demonstrates an important constraint between phenomena occurring during the epochs of BBN and recombination/photon decoupling. For a given input cosmology $(\omega_b, \omega_c, \ldots)$, the graph of r_s/r_d as a function of $N_{\rm eff}^{\rm (th)}$ requires a computation of $n_e(a)$ to obtain r_d for each value of $N_{\rm eff}^{\rm (th)}$.

We can understand Fig. 4.14 qualitatively by a simple scaling argument. We expect that, as the radiation energy density increases with increasing $N_{\rm eff}^{\rm (th)}$, the sound horizon and the diffusion length will decrease with the increasing Hubble rate $H(a)$. The sound horizon decreases due to the increased energy density driving a more rapid expansion and a decrease in the sound speed, $c_s = [3(1+R(a))]^{-1/2}$. The diffusion length increases, naively, due to a decrease in the scattering rate driven by the reduced Hubble time. Caution should be taken when using such naive scaling arguments. For example, the non-trivial dependence of the recombination history leads to counterintuitive effects in the $\tilde{N}_{\rm eff}$ dependence on $\sum m_\nu$ [58]. Ref. [58] demonstrates that where a naive

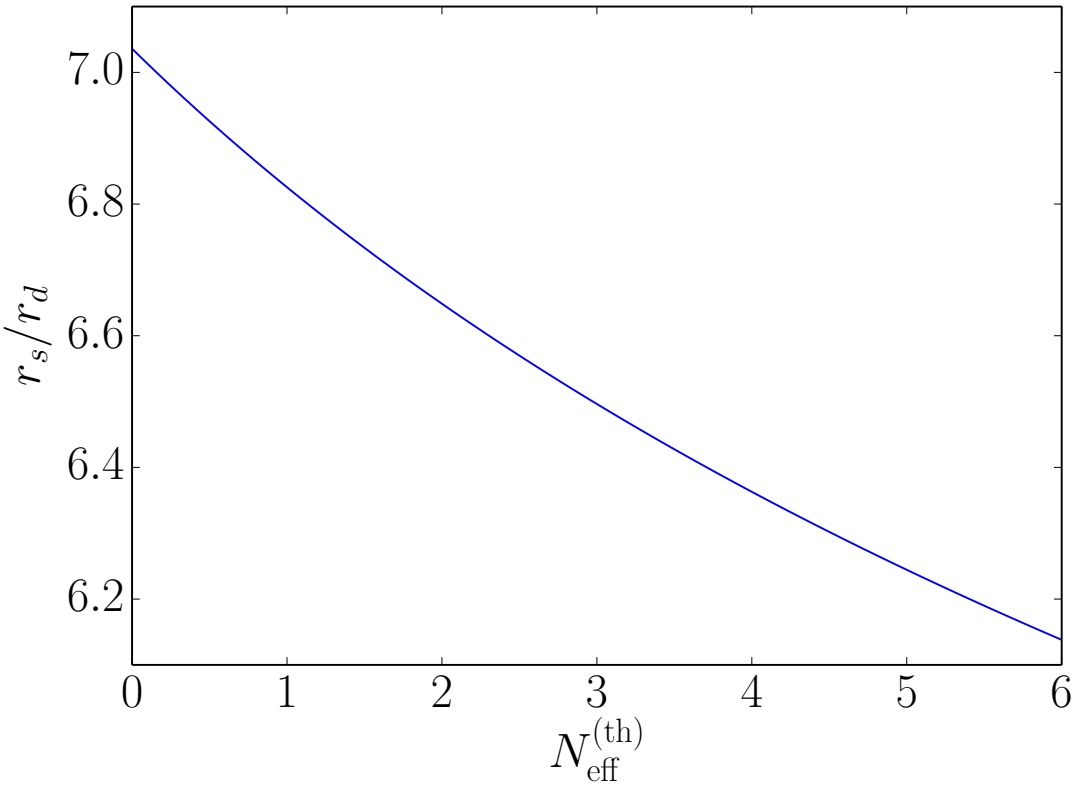

Figure 4.14: Ratio of the comoving coordinate of the sound horizon radius r_s to that of the photon diffusion length r_d as a function of $N_{\rm eff}^{\rm (th)}$ for cosmological parameter values $Y_P = 0.2425$, $\omega_b = 0.22068$, and $\omega_c = 0.12029$.

scaling argument would suggest an increase in $\tilde{N}_{\rm eff}$ with increasing $\sum m_\nu$, the non-trivial dependence of the recombination history on $\sum m_\nu$ implies $\tilde{N}_{\rm eff}$ decreases monotonically and rapidly with increasing $\sum m_\nu$ (see Ch.5).

4.6 Conclusion

Our procedure for $\tilde{N}_{\rm eff}$ is an attempt to delineate the physics of BBN from that of the CMB. The sound horizon is largely insensitive to the processes involved in BBN. The photon diffusion length is indeed sensitive to BBN through the necessary inclusion of Y_p in recombination. Therefore, our procedure does not relieve the degeneracy between

$N_{\rm eff}$ and Y_p. To maintain self-consistency, we always calculate the primordial abundances when adding in BSM physics. We will use $\tilde{N}_{\rm eff}$ to show how the presence of BSM physics would affect CMB observables in later chapters.

We thank Amit Yadav and JJ Cherry for useful conversations with respect to cosmology and the CMB.

Section 4.3, in part, section 4.4.1, section 4.4.6, and section 4.5 are reprints of some of the material as it appears in "Probing neutrino physics with a self-consistent treatment of the weak decoupling, nucleosynthesis, and photon decoupling epochs." Grohs, E.; Fuller, G. M.; Kishimoto, C. K.; Paris, M. W., J. Cosmology Astropart., 5 (May 2015) 17. The dissertation author was the primary investigator and author of this paper.

Chapter 5

Neutrino–mass recombination effect

We show how small neutrino rest masses can increase the expansion rate near the photon decoupling epoch in the early universe, causing an earlier, higher temperature freeze-out for ionization equilibrium compared to the massless neutrino case. This yields a larger free-electron fraction, thereby affecting the photon diffusion length differently than the sound horizon at photon decoupling. This neutrino-mass/recombination effect depends strongly on the neutrino rest masses. Though below current sensitivity, this effect could be probed by next-generation cosmic microwave background experiments, giving another observational handle on neutrino rest mass.

In this Letter, we show that the earlier epoch of ionization freeze-out caused by neutrino rest mass affects the deduced radiation energy density in a novel way. The physics of this freeze-out and its relation to observations of the cosmic microwave background (CMB) is a well studied issue [59, 60, 61, 30, 10, 18, 62, 63]. Here we focus on the influence of the recombination history on the CMB parameter $N_{\rm eff}$ and a subsequent counterintuitive result on its deduced value.

The theoretical definition of $N_{\rm eff}$ arises from a parametrization of radiation energy

density, $\rho_{\rm rad}$, in terms of the photon temperature at decoupling, T_γ, given by:

$$\rho_{\rm rad} = \left(1 + \frac{7}{8}\left(\frac{4}{11}\right)^{4/3} N_{\rm eff}^{\rm (th)}\right)\frac{\pi^2}{15} T_\gamma^4. \tag{5.1}$$

(We set $\hbar = c = k_{\rm b} = 1$ throughout this work.) We adorn $N_{\rm eff}$ with a superscript $({\rm th})$ to distinguish the theoretical version of $N_{\rm eff}$, an *input* parameter in public Boltzmann codes [64], from the CMB *inferred* value of $N_{\rm eff}$ described below. Calculations which include non-equilibrium processes in the early universe suggest $N_{\rm eff}^{\rm (th)} = 3.046$ [60, 59, 61, 30].

Since active neutrinos decouple from the plasma with ultra-relativistic kinematics, their energy densities do not behave like Fermi-Dirac distributions at photon decoupling. The energy density of neutrinos with rest masses m_{ν_i} and neutrino temperature T_ν is:

$$\rho_\nu(m_{\nu_i}, T_\nu) = \sum_i \int \frac{d^3p}{(2\pi)^3} E_i f_\nu(p, T_\nu) \tag{5.2}$$

$$= \frac{1}{2\pi^2}\sum_i \int_0^\infty dp\, p^2 \frac{\sqrt{p^2 + m_{\nu_i}^2}}{e^{p/T_\nu} + 1}, \tag{5.3}$$

where the sum is over active neutrino mass eigenstates, ν_i and the second expression follows from an assumption of decoupled neutrinos. With this assumption, the behavior of the neutrino energy density is a sum of ultra-relativistic Fermi-Dirac occupation probabilities, $f_\nu = (\exp(p/T_\nu) + 1)^{-1}$, but with a general energy dispersion relation, $E_i = \sqrt{p^2 + m_{\nu_i}^2}$. Therefore, the energy density in the presence of a massive-neutrino species is larger than in the massless case and becomes increasingly significant at later times; it does not scale as $T^4 \sim a^{-4}$ as in Eq.(5.1).

The cosmological constraint (at the level of 2σ) on the sum of the light neutrino masses is $\sum m_\nu \leq 0.23$ eV [2]. If we take $\sum m_\nu$ to be at this upper limit and assume degenerate mass eigenvalues, each neutrino has an associated mass $\sim 0.08\,$eV. We see that the neutrino rest masses and temperatures at photon decoupling ($T_\gamma \approx 0.2\,$eV,

$T_\nu \approx 0.15\,\mathrm{eV}$) are coincidentally at the same scale, meaning that neutrinos can not be treated either as pure matter or pure radiation. An individual neutrino has an average momentum of $\sim 0.5\,\mathrm{eV}$ at photon decoupling. As a consequence, we expect fractional corrections to the relativistic neutrino energy density stemming from neutrino rest mass to be $\sim m^2/2p^2 \sim 0.01$, with a concomitant change to $N_{\mathrm{eff}}^{(\mathrm{th})}$ of $\sim 3 \times 0.01 \sim +0.03$. If we were to unphysically classify the entire neutrino energy density into ρ_{rad} the corresponding change to $N_{\mathrm{eff}}^{(\mathrm{th})}$ would be $\Delta N_{\mathrm{eff}}^{(\mathrm{th})} \equiv N_{\mathrm{eff}}^{(\mathrm{th})} - 3 \simeq \frac{5}{7\pi^2}\left(\frac{11}{4}\right)^{2/3} \sum_{i=1}^{3} \left(\frac{m_i}{T_\gamma}\right)^2$. We arrive then at $\Delta N_{\mathrm{eff}}^{(\mathrm{th})} \simeq 0.04$ for $\sum m_\nu = 0.23\,\mathrm{eV}$, a change consistent with the simple kinematic estimate above, and not to be confused with $\Delta N_{\mathrm{eff}}^{(\mathrm{th})} \approx 0.046$ stemming from non-equilibrium neutrino scattering and quantum-electrodynamic effects inherent in Refs.[59, 60, 61].

The radiation energy density is not directly measured by observation of the CMB. References [18] and [63], however, have shown that the ratio of the sound horizon to the photon diffusion length at the photon decoupling epoch is sensitive to the radiation energy density. Consequently, we distinguish between $N_{\mathrm{eff}}^{(\mathrm{th})}$, the input parameter that determines the radiation energy density in Eq.(5.1), and a measure of radiation energy density inferred from observations of the CMB, which we shall term $\tilde{N}_{\mathrm{eff}}$. We determine $\tilde{N}_{\mathrm{eff}}$ by computing the sound horizon, r_s and the photon diffusion length, r_d at the photon decoupling epoch in the manner described below.

The quantities r_s and r_d are given in terms of integrals over the scale factor a [2]:

$$r_s = \int_0^{a_{\gamma d}} \frac{da}{a^2 H} \frac{1}{\sqrt{3(1+R)}}, \tag{5.4}$$

$$r_d^2 = \pi^2 \int_0^{a_{\gamma d}} \frac{da}{a^2 H} \frac{1}{a n_e(a) \sigma_T} \frac{R^2 + \frac{16}{15}(1+R)}{6(1+R)^2}, \tag{5.5}$$

where $H = H(a)$ is the Hubble expansion rate, σ_T is the Thomson cross section, $n_e(a)$ is the free-electron number density, and $R(a) \equiv 3\rho_b/(4\rho_\gamma)$ is a ratio involving the baryon

rest mass and photon energy densities, ρ_b and ρ_γ, respectively. The integrals span the early history of the universe, ending at $a_{\gamma d}$, the epoch of photon decoupling at a redshift $z = 1090.43$ [2]. In the analysis to follow, we ignore the small dependence of the value of $a_{\gamma d}$ on $\sum m_\nu$. This is not entirely self-consistent but we will demonstrate that a consistent treatment changes the decoupling redshift from $z = 1090$ to $z = 1091$. The associated change in $a_{\gamma d}$ has negligible effect on r_s and r_d; this is similar to the finding in Ref.[18]. We should note that Eq.(5.5) is approximate and a more complete analysis would include effects beyond the tight-coupling approximation[65].

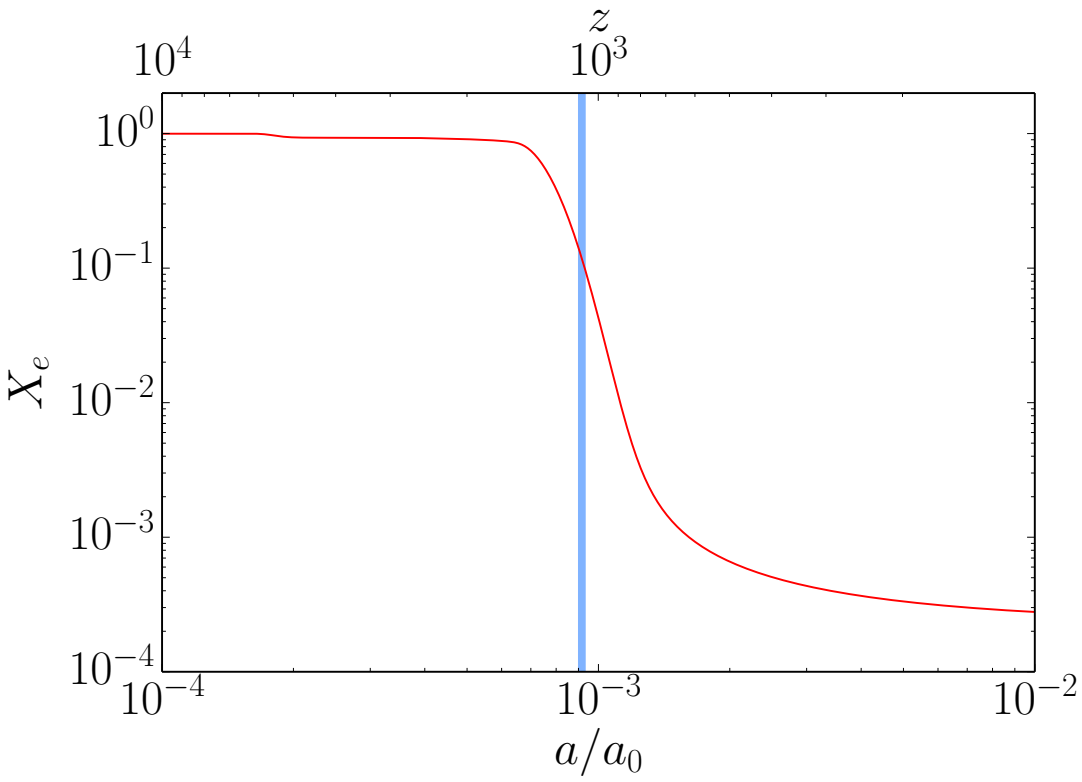

Figure 5.1: The free-electron fraction, X_e, is given as a function of scale factor ratio, a/a_0 ($\equiv 1$ at current epoch), and redshift, z, (at top). The primordial helium mass fraction is taken to be $Y_P = 0.242$. The shaded, vertical bar corresponds to the epoch of photon decoupling given by Ref.[2].

Using Eq.(5.3) with neutrino masses taken as described above for a given value

of $\sum m_\nu$ and the known relations for ρ_γ and ρ_b we compute the quantities r_s and r_d from Eqs.(5.4) and (5.5), respectively. We choose $N_{\rm eff}^{\rm (th)}$ in Eq.(5.1) to reproduce this ratio of r_s/r_d, which is a monotonically decreasing function of $N_{\rm eff}^{\rm (th)}$. The quantity so determined is termed $\tilde{N}_{\rm eff}$ and it reduces to $N_{\rm eff}^{\rm (th)}$ for massless neutrinos. It has been motivated here by the need to characterize massive neutrinos but it is applicable to non-standard cosmic constituents that may have non-equilibrium distributions. Using the ratio r_s/r_d in the determination of $\tilde{N}_{\rm eff}$ avoids any reference to the angular diameter distance to last scattering and, therefore, dependence on the dark energy equation of state. In contrast to Ref.[18] we do not change the value of the primordial helium abundance, Y_P to keep θ_d fixed.

A scaling analysis, similar to that of Ref.[18], demonstrates the approximate relation between the sound horizon, the diffusion length, and the Hubble rate. Consider a scale transformation to the Hubble rate, $H \to \lambda H$, and the corresponding alteration to r_s and r_d. If we neglect the dependence of $R(a)$ and $n_e(a)$ on λ we have

$$r_s \propto \frac{1}{\lambda} \text{ and } r_d \propto \frac{1}{\sqrt{\lambda}} \implies \frac{r_s}{r_d} \propto \frac{1}{\sqrt{\lambda}}. \tag{5.6}$$

These relations suggest that a larger Hubble rate ($\lambda > 1$) results in a smaller value of the ratio r_s/r_d. This fact and $\Delta(r_s/r_d) \sim -\Delta\tilde{N}_{\rm eff}$ (since r_s/r_d is monotonically decreasing with $\tilde{N}_{\rm eff}$) means that a larger Hubble rate would imply a larger value of $\tilde{N}_{\rm eff}$. In fact, as we will show, the λ-scale dependence of $n_e(a)$ leads to the consequence that a larger Hubble rate results in a *larger* ratio of r_s/r_d.

The photon diffusion length r_d depends on the number density of free electrons n_e. To calculate n_e, we follow the competition between ionization and recombination in an expanding universe. The hydrogen contribution to the free-electron fraction,

$X_e^{(\mathrm{H})} \equiv n_{e,\mathrm{H}}^{(\mathrm{free})}/n_e^{(\mathrm{total})}$, follows from the Boltzmann equation [51, 54]:

$$\frac{dX_e^{(\mathrm{H})}}{da} = \frac{1}{aH}\left(\Gamma_{\mathrm{H}(\gamma,e^-)\mathrm{H}^+} - \Gamma_{\mathrm{H}^+(e^-,\gamma)\mathrm{H}}\right), \tag{5.7}$$

where $\Gamma_{\mathrm{H}(\gamma,e^-)\mathrm{H}^+}$ is the ionization rate and $\Gamma_{\mathrm{H}^+(e^-,\gamma)\mathrm{H}}$ is the recombination rate. There is a similar Boltzmann equation for the contribution of helium to the free-electron fraction, $X_e^{(\mathrm{He})} \equiv n_{e,\mathrm{He}}^{(\mathrm{free})}/n_e^{(\mathrm{total})}$.

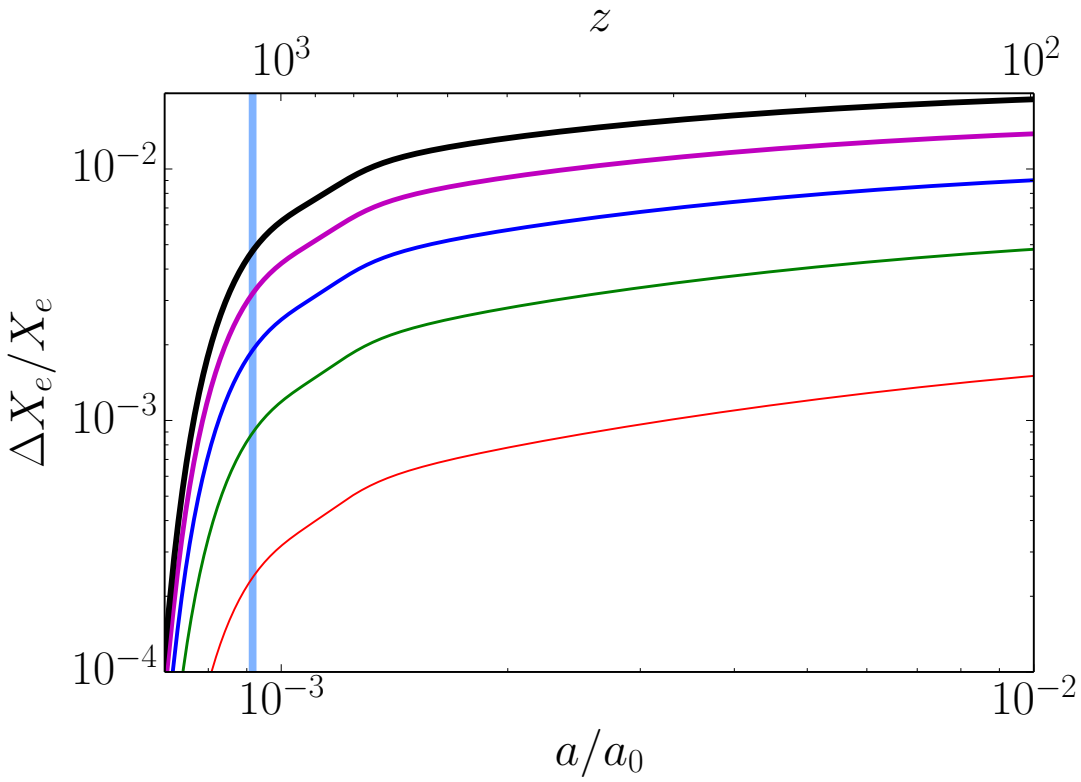

Figure 5.2: The relative change in the free-electron fraction, $\Delta X_e/X_e$ given as a function of scale factor ratio, a/a_0, and redshift, z, (at top). The primordial helium mass fraction and vertical bar are identical to Fig. 5.1. Each curve corresponds to a different non-zero $\sum m_\nu$. The curves are in equal increments of $\Delta\Sigma m_\nu = 0.2$ eV, starting with the smallest change for $\sum m_\nu = 0.2$ eV and ending with the largest change for $\sum m_\nu = 1.0$ eV.

We employ a recombination reaction network that includes hydrogen and helium and which is similar to, but independent of, the code `recfast`[52]. Figure 5.1 shows a

calculation of the free-electron fraction, $X_e \equiv X_e^{(\mathrm{H})} + X_e^{(\mathrm{He})}$, as a function of scale factor ratio a/a_0 ($\equiv 1$ at current epoch), where we have taken $\sum m_\nu = 0$. We neglect effects due to reionization processes at low redshift, $z \sim O(1)$. We evolve the free-electron fraction through the photon decoupling epoch to show the freeze-out of ionization equilibrium. Note the drop from the initial value of $X_e = 1$ near $a/a_0 \simeq 2 \times 10^{-4}$. This is a consequence of the recombination onto He III.

Similarly, in Fig. 5.2 we plot the change in X_e for non-zero values of $\sum m_\nu$ relative to the case with $\sum m_\nu = 0$. Non-zero $\sum m_\nu$ has a discernible effect on the freeze-out of X_e. A larger $\sum m_\nu$ implies a larger Hubble rate which implies an earlier epoch for X_e freeze-out. In a study of the expansion rate during recombination, Ref.[66] observed that scaling the Hubble rate affects the recombination history. Here we build on this argument to explicitly consider the role of neutrino rest mass on recombination. The curve describing the largest change corresponds to $\sum m_\nu = 1.0$ eV, whereas the smallest change corresponds to $\sum m_\nu = 0.2$ eV; consecutive curves are spaced by $\Delta\Sigma m_\nu = 0.2$ eV. The larger X_e at $a_{\gamma d}$ produces a smaller r_d, opposite to the expectation from Eq.(5.6) based solely on the λ-scale dependence of the Hubble rate.

In order to investigate physics beyond the standard models of particle physics and cosmology, we have formulated a self-consistent approach that is not constrained to minimal extensions to the standard model. To do so, we simulate the early universe from weak decoupling through Big Bang Nucleosynthesis (BBN) to photon decoupling using the `BURST` code[67]. This treatment self-consistently incorporates binned, general, momentum occupation probabilities for each of six neutrino species (ν_e, $\bar{\nu}_e$, ν_μ, $\bar{\nu}_\mu$, ν_τ, and $\bar{\nu}_\tau$) and a Boltzmann treatment of neutrino scattering, absorption and emission processes to evolve the early universe.

In this treatment, neutrinos decouple from the γ, $e^\pm$ plasma at high temperatures, $1 \lesssim T \lesssim 3$ MeV, ensuring that their kinematics are ultra-relativistic [57, 68]. Addition-

ally, the computation of Y_P in this treatment may be more nuanced than in the standard cosmology. For general cosmologies, Y_P is not simply a function of $N_{\rm eff}^{\rm (th)}$ and ω_b. Assuming zero lepton numbers and an adopted world-average neutron lifetime of 886 s, our calculations give a ^{4}He primordial mass fraction $Y_P = 0.242$ taking the baryon number $\Omega_b h^2 \equiv \omega_b = 0.022068$ from the Ref.[2] best-fit. This is consistent with the observationally inferred primordial helium abundance [8, 1]. Although we take the neutrinos to decouple in weak eigenstates, i.e. flavor states, we write their occupation probabilities in the mass eigenbasis. Since we are assuming the neutrinos have identical thermal spectra with zero-chemical potential in the weak eigenstates, we can use the same occupation probabilities for the mass eigenstates at a given momentum p [69, 57].

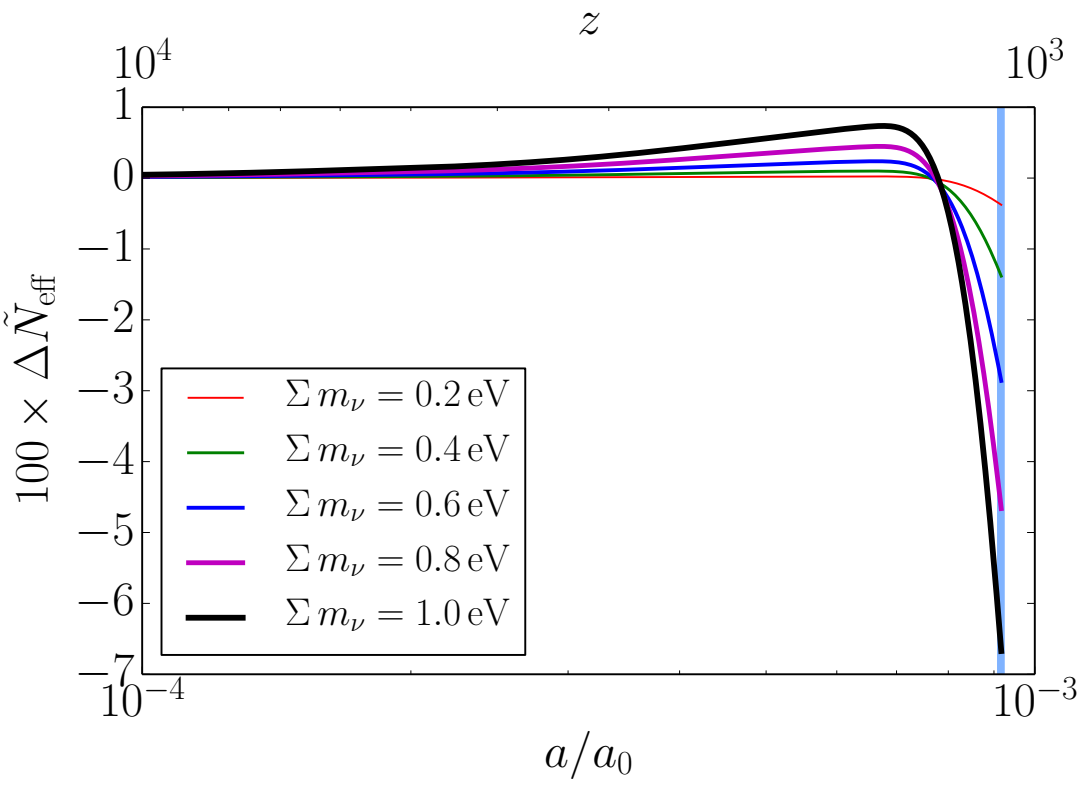

Figure 5.3: The change in $\tilde{N}_{\rm eff}$, $\Delta\tilde{N}_{\rm eff}$, is given as a function of scale factor ratio, a/a_0, and redshift, z, (at top). The primordial helium mass fraction and vertical bar are identical to Fig. 5.1. For each value of $\sum m_\nu$, $\Delta\tilde{N}_{\rm eff}$ is initially positive. $\Delta\tilde{N}_{\rm eff}$ becomes negative once the recombination histories of Fig. 5.2 differ from the massless case.

Figure 5.3 shows the evolution of $\tilde{N}_{\rm eff}$ with scale factor. Here for illustrative purposes, we treat $\Delta\tilde{N}_{\rm eff}$ as a quantity to be determined at any epoch, whereas it is only observed at photon decoupling. The neutrino rest mass has no discernible effect on $\tilde{N}_{\rm eff}$ at early epochs, at small a/a_0. At larger values of $a/a_0\,(\sim 5\times10^{-4})$, the extra energy density from the neutrino rest masses produces a larger $\tilde{N}_{\rm eff}$ in accordance with Eq.(5.6) before the neutrino-mass/recombination (νMR) effect is significant. If we were to extrapolate this evolution trend to the epoch of photon decoupling, we would find a value of $\Delta\tilde{N}_{\rm eff} > 0$. The νMR effect intervenes to modify this extrapolation and results in $\Delta\tilde{N}_{\rm eff} < 0$ at $a_{\gamma d}$.

Each evolution curve for $\Delta\tilde{N}_{\rm eff}$ in Fig. 5.3 corresponds to an evolution curve for $X_e(a)$ in Fig. 5.2 for various values of $\sum m_\nu$. The smallest value of $\sum m_\nu$ produces the smallest change in X_e, which subsequently changes $\Delta\tilde{N}_{\rm eff}$ the least. Conversely, the largest value of $\sum m_\nu$ produces the largest change in X_e, which changes $\Delta\tilde{N}_{\rm eff}$ the most. From the curves in Fig. 5.3, it is clear that the effect of neutrino rest mass in producing a higher X_e at freeze-out overwhelms the effect of the extra energy density, thereby decreasing $\tilde{N}_{\rm eff}$ at photon decoupling, i.e. at $a = a_{\gamma d}$, the vertical bar in Figs. 5.2 & 5.3.

There are several interesting features to note in Fig. 5.3. Each curve in Fig. 5.3 goes through $\Delta\tilde{N}_{\rm eff} = 0$ near the value $a/a_0 \sim (7.65 \pm 0.10)\times10^{-4}$. The larger the value of $\sum m_\nu$, the higher the curvature of the function $\Delta\tilde{N}_{\rm eff}(a)$. For values of a/a_0 above $\Delta\tilde{N}_{\rm eff} = 0$, the slope of $\Delta\tilde{N}_{\rm eff}(a)$ is an extremely rapidly decreasing function of $\sum m_\nu$. We note that for $\sum m_\nu = 0.23$ eV, the preferred upper limit from Ref.[2], we find $\Delta\tilde{N}_{\rm eff} = -0.005$. This effect is certainly below present sensitivities of CMB observations. Next-generation CMB measurements, however, aspire to percent level accuracy in determinations of the relativistic energy density[70]. The exquisite sensitivity of the νMR effect on $\Delta\tilde{N}_{\rm eff}(a_{\gamma d})$ suggests that it may be an important component in future precision determinations of cosmological parameters.

As mentioned earlier, we do not constrain $a_{\gamma d}$ to maintain a uniform optical depth $\tau(a_{\gamma d})$

$$\tau(a_{\gamma d}) = \int_{a_{\gamma d}}^{a_0} \frac{da}{a^2 H} a\, n_e(a)\, \sigma_T \equiv 1, \tag{5.8}$$

when comparing different values for $\sum m_\nu$. Note that this definition of $\tau(a_{\gamma d})$ does not include reionization effects on $n_e(a)$. We should emphasize that each curve in Figs. 5.2 and 5.3 is calculated using the same value for the scale factor of last scattering $a_{\gamma d} = 9.162 \times 10^{-4}$ (corresponding to $z = 1090.43$). This is not self consistent, strictly speaking, but we have verified that the effect on $\tilde{N}_{\rm eff}$, due to the differences in n_e and H, is negligible. If we impose the constraint in Eq.(5.8), we find $a_{\gamma d}$ decreases by a few parts in 10^4 for $\sum m_\nu = 0.23$ eV, which has an insignificant effect on $\tilde{N}_{\rm eff}$.

Up to this point in the present analysis we have not considered variation of the primordial helium mass fraction Y_P since BBN occurs at high enough temperatures that the neutrinos are effectively massless. If we consider, however, cosmological parameters that affect Y_P we can examine the dependence of ionization freeze-out (and subsequent alteration of $\tilde{N}_{\rm eff}$) on both $\sum m_\nu$ and Y_P simultaneously. A direct way to vary Y_P is to consider changes to the baryon number ω_b. In the range of values of ω_b that we're interested in, Y_P is a monotonically increasing function of ω_b.

Figure 5.4 shows a contour plot of $\Delta\tilde{N}_{\rm eff}$ in the $\sum m_\nu$ versus ω_b parameter space; contours correspond to constant values of $-\Delta\tilde{N}_{\rm eff}$. Varying ω_b requires new computations of Y_P from BBN and $X_e(a)$ from recombination. Changing $\sum m_\nu$ requires a new computation of X_e but no new computation of Y_P. As a consequence, we compute BBN with the `BURST` code only once for a given ω_b, and compute the recombination history for each pair (ω_b, $\sum m_\nu$). Holding $\sum m_\nu$ fixed, the change in $|\Delta\tilde{N}_{\rm eff}|$ increases with increasing ω_b due to the different recombination histories effecting a change in r_d. Note that the change

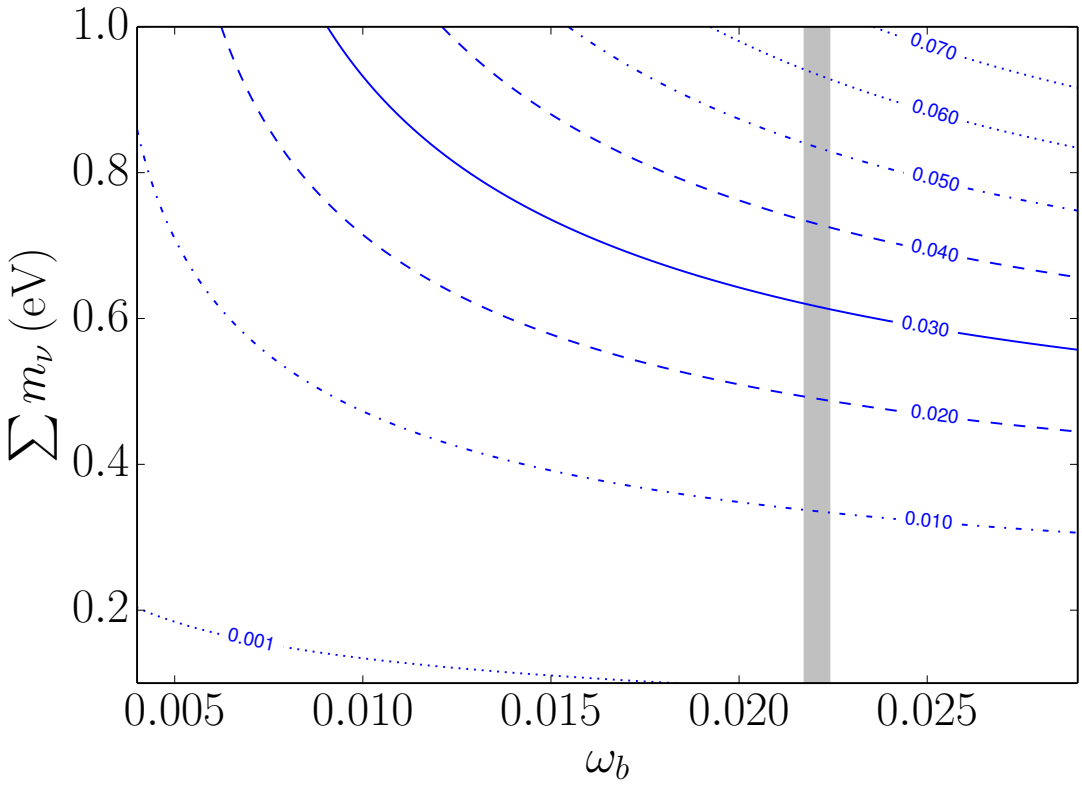

Figure 5.4: Contours of constant $-\Delta\tilde{N}_{\rm eff}$ in the $\sum m_\nu$ vs. ω_b parameter space. The shaded, vertical bar corresponds to the 1σ error for ω_b [2].

in r_s does not completely compensate for the change in r_d. The shaded vertical region in Fig. 5.4 is the 1σ range of ω_b given by Ref.[2], but we explore a larger range in the ω_b parameter space to illustrate the dependence of $\tilde{N}_{\rm eff}$ on $\sum m_\nu$ and ω_b. An interesting feature of these curves is their increasing curvature with decreasing ω_b and increasing $\sum m_\nu$. This is a consequence of an enhancement of the νMR effect with increasing ω_b: as $\sum m_\nu$ increases, the change in $\tilde{N}_{\rm eff}$ is faster for higher values of ω_b.

We have discussed two ways in which neutrino rest mass affects measurable quantities at photon decoupling. First, neutrino rest mass drives an earlier recombination freeze-out resulting in a higher free-electron fraction. Second, this effect is enhanced with increasing ω_b stemming from a self-consistently calculated recombination history. As radiation energy density is not a directly measurable quantity, we use observable

quantities to indirectly arrive at the radiation energy density. For this purpose, we choose the ratio of the sound horizon to the photon diffusion length. Photon diffusion is sensitive to the recombination history, which requires a Boltzmann-equation treatment. We find a non-trivial evolution of $\Delta\tilde{N}_{\rm eff}$ with scale factor, as shown in Fig. 5.3. Note that the evolution of $\tilde{N}_{\rm eff}$ shown in this figure does not reflect a *kinematical* evolution of the radiation energy density with a massive component. The trends evidenced in this figure are a consequence of the νMR effect.

Self-consistency is a primary motivation for defining the radiation energy density parameter $\tilde{N}_{\rm eff}$ in terms of the ratio r_s/r_d; it generalizes the $N_{\rm eff}^{\rm (th)}$ parameter to the massive neutrino case. Further, $\tilde{N}_{\rm eff}$ is defined for arbitrary energy densities and arbitrary distribution functions. Moreover, $\tilde{N}_{\rm eff}$ makes no assumption regarding the underlying cosmological model. We use $\tilde{N}_{\rm eff}$ to relate the sound horizon and photon diffusion length to predictions made by the standard cosmological model via the parameter $N_{\rm eff}^{\rm (th)}$.

The νMR effect is an example of a recurring phenomenon in cosmology: an increase in the expansion rate leads to an earlier epoch of freeze-out. This effect was revealed in the present context by using $\tilde{N}_{\rm eff}$ to *infer* the cosmic radiation energy content from observable CMB data, rather than treating $N_{\rm eff}^{\rm (th)}$ as an *input*. The procedure we describe here differs from that adopted by the public Boltzmann codes. CAMB[64], for example, includes options to evolve massive neutrino energy density through the epoch of recombination and requires $N_{\rm eff}^{\rm (th)}$ to be provided as an input.

Depending on $\sum m_\nu$, the concomitant changes in ionization equilibrium and $\tilde{N}_{\rm eff}$ discussed here may be within the sensitivity of the next generation CMB experiments when polarization effects are taken into account[2, 43, 71, 70]. CMB precision is planned to be increased to the $\tilde{N}_{\rm eff} \sim 1\%$ level which would probe both massive active neutrinos and other possible components of dark radiation. Scenarios with sterile neutrinos and other very weakly coupled light massive species with masses larger than those associated

with the active neutrinos could enhance the effects discussed here. However, depending on their masses and their flavor mixing with active species, sterile neutrinos could have number densities and energy spectra which differ from those of active neutrinos [72, 73, 74, 75, 76, 77], complicating the analysis given here.

We would like to acknowledge the Institutional Computing Program at Los Alamos National Laboratory for use of their HPC cluster resources. This work was supported in part by NSF grant PHY-1307372 at UC San Diego, by the Los Alamos National Laboratory Institute for Geophysics, Space Sciences and Signatures subcontract 257842, and the National Nuclear Security Administration of the U.S. Department of Energy at Los Alamos National Laboratory under Contract No. DE-AC52-06NA25396. We thank J.J. Cherry, Amit Yadav, and Lloyd Knox for helpful discussions. We would also like to thank the anonymous referees for their useful comments.

Chapter 5, in full, is a reprint of the material as submitted for publication: Grohs, E.; Fuller, G. M.; Kishimoto, C. K.; Paris, M. W. “Effects of neutrino rest mass on $N_{\rm eff}$ and ionization equilibrium freeze-out”. The dissertation author was the primary investigator and author of this paper.

Chapter 6

Examples for neutrino sector beyond–standard–model physics

We describe three examples of unresolved issues in BSM/CSM physics, which require the fully self-consistent parameter determination described in previous sections. We consider, in turn, models incorporating neutrino rest mass, sterile neutrinos, and non-zero lepton numbers. We use, throughout this section, the observationally-inferred definition of $N_{\rm eff}$, $\tilde{N}_{\rm eff}$.

6.1 Neutrino rest mass

Section 2.5 details a self-consistent treatment of the BBN observables Y_P, D/H, $\tilde{N}_{\rm eff}$, and ω_b. The sum of the light neutrino masses, denoted $\sum m_\nu$, has no bearing on the determination of primordial abundances in BBN calculations due to the high temperatures relevant there. Here, however, we explore the epochs and energy scales in the history of the universe associated with the $\sum m_\nu$ energy scale in order to investigate the relationship between $\sum m_\nu$ and the other four observables of interest (ω_b, $\tilde{N}_{\rm eff}$, Y_P and D/H). Specific

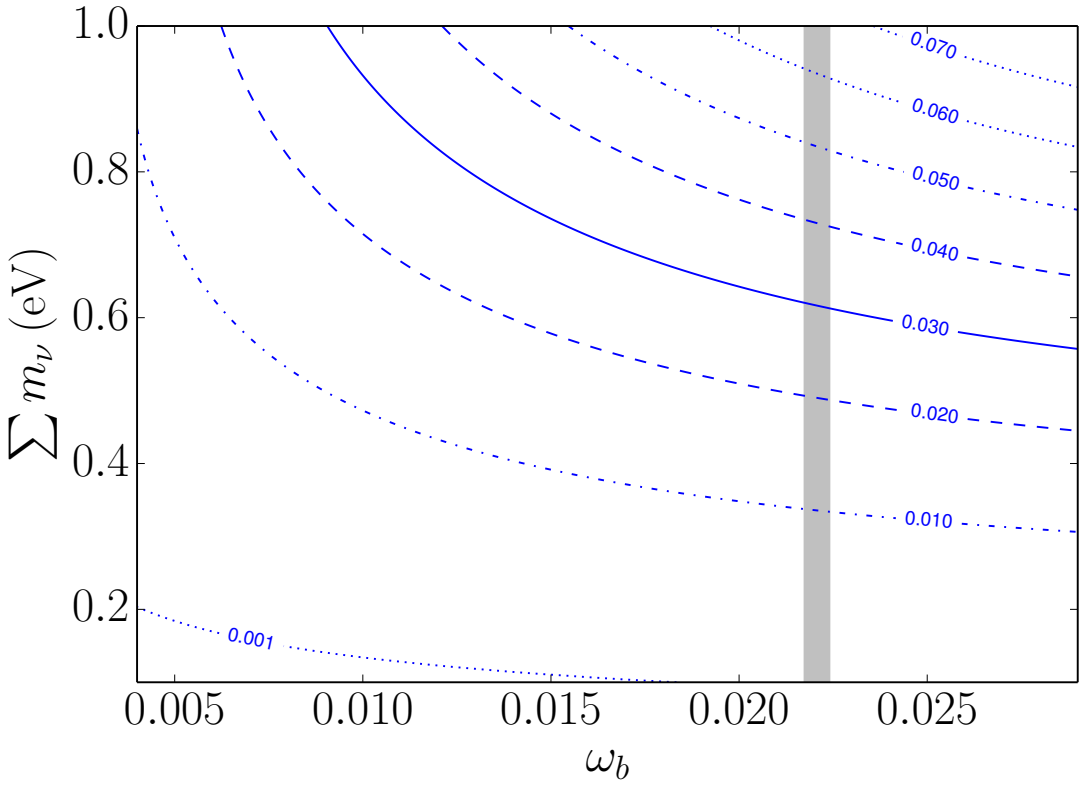

Figure 6.1: Determination of $\sum m_\nu$ plotted against ω_b at constant $\Delta\tilde{N}_{\rm eff}$. The contours are spaced by ≈ 0.01 in values of $\Delta\tilde{N}_{\rm eff}$. All contours correspond to $\Delta\tilde{N}_{\rm eff} < 0$.

examples of such epochs that we might consider include the surface of last scattering ($z \sim 1100$) and the advent of LSS ($z \lesssim 10$). We focus on the surface of last scattering and implications for the CMB in this paper.

Reference [58] (hereafter GFKPI) investigates the effect of neutrino rest mass on $\tilde{N}_{\rm eff}$ using the BURST suite of codes. Conventional estimates based on the energy density added by non-zero neutrino rest masses suggest an increase in $N_{\rm eff}^{\rm (th)}$. However, using the method outlined in Sec. 4.5, GFKPI shows a decrease in $\tilde{N}_{\rm eff}$. The decrease is due to an effect on the recombination history stemming from an increase in the Hubble rate, which results in a larger free-electron fraction. This counterintuitive result is termed the "neutrino-mass/recombination (νMR) effect." The νMR effect manifests itself only in a self-consistent treatment, such as that employed by GFKPI.

In addition, GFKPI investigates the dependence of the νMR effect on ω_b. We revisit this physics here in preparation for a discussion on the effect of non-zero lepton number L_ν later, in Sec. 6.3.2. Increasing ω_b leads to an enhancement of the νMR effect when $\sum m_\nu$ is held constant, as is evident by the curvature of the contours in Fig. 6.1. The enhancement is a consequence of the effect that changing ω_b has on the the recombination history. We might naively expect a larger change in the Hubble rate relative to the massless neutrino case resulting in an enhanced νMR effect for the smaller ω_b case. This is opposite to that observed in Fig. 6.1. This result also is counterintuitive based on expectations from a simple scaling of the energy density and the resulting change in the recombination history [58].

The origin of the enhancement of the νMR effect can be understood by considering a simplification of the Boltzmann equation that determines the recombination history [Eq. (4.193)]. We take $Y_P = 0$ for the purposes of this argument since the νMR enhancement is insensitive to Y_P, as we have verified numerically for the ranges of parameters we are considering. In this simple scenario, $X_e = X_p$ and we obtain an expression for the

change in the free-electron fraction:

$$\frac{dX_e}{dt} = (1 - X_e)\beta - X_e^2 n_e^{(\mathrm{tot})} \alpha^{(2)}, \tag{6.1}$$

where $\beta \equiv \alpha^{(2)} (m_e T/2\pi)^{3/2} e^{-\Delta Q/T}$ is the ionization coefficient and $\alpha^{(2)}$ is the recombination coefficient with $\Delta Q = 13.6$ eV.

Equation (6.1) for the recombination history shows that the free-electron disappearance rate is proportional to the total electron number density, which in turn is proportional to ω_b through Eq. (4.192). Equation (4.192) also shows how $n_e^{(\mathrm{tot})}$ relates to Y_P. Note that ω_b and Y_P affect $n_e^{(\mathrm{tot})}$ differently. However, due to the relative insensitivity of Y_P to ω_b, the ω_b dependence dominates in Eq. (4.192). The increase in energy density from $\sum m_\nu \neq 0$ and the increase in the free-electron disappearance rate combine to alter the recombination history so as to enhance the νMR effect for increasing ω_b.

6.2 Sterile neutrinos

We next consider the possibility that there exists either single or multiple sterile-neutrino species, which could have profound implications in cosmology. We entertain two possibilities of either light or heavy sterile neutrinos.

6.2.1 Light sterile neutrinos

Observations of neutrino events in large scintillating detectors may have revealed anomalies that could be interpreted as sterile neutrinos with rest masses $m_{\nu_s} \sim 1$ eV [78, 79, 80]. We investigate the presence of a single sterile neutrino in the early universe by employing a model where the sterile state populates a thermal Fermi-Dirac shaped distribution with temperature parameter T_s, possibly through flavor mixing. The sterile

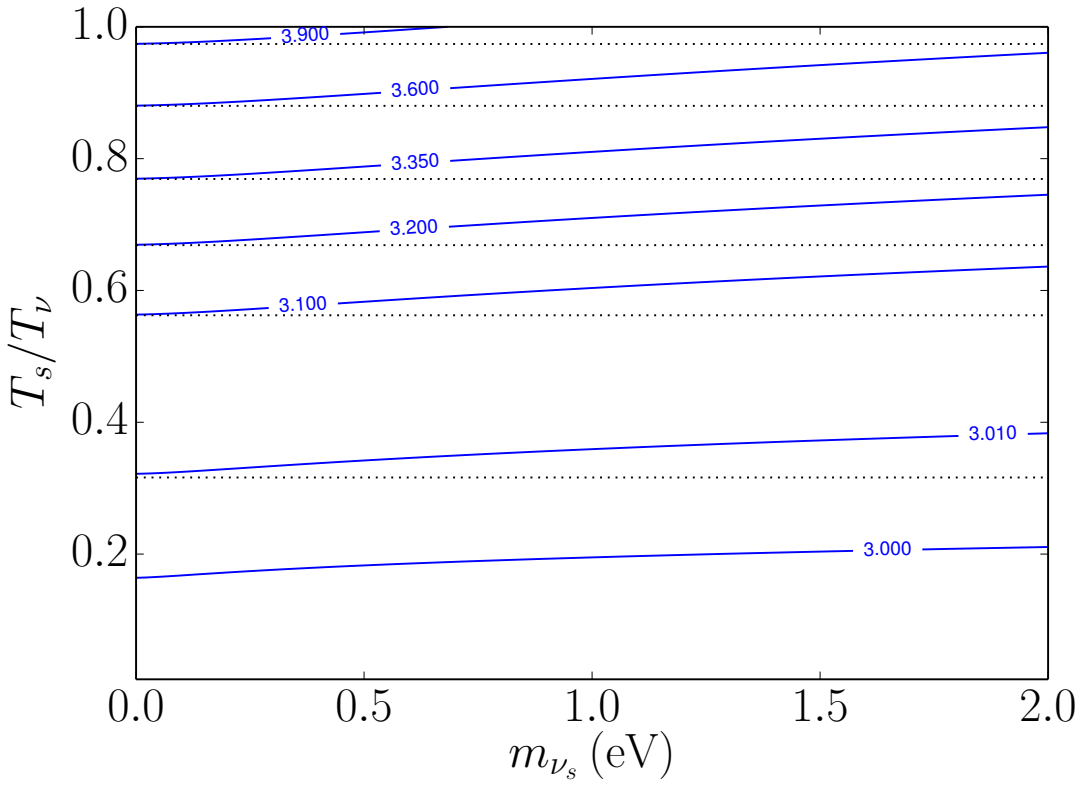

Figure 6.2: Ratio of the sterile to active neutrino temperatures, T_s/T_ν, plotted against m_{ν_s} for contours of constant $\tilde{N}_{\rm eff}$ for $\sum m_\nu = 0.06$ eV. Horizontal dotted lines show the prediction if the sterile neutrino was massless, i.e. $m_{\nu_s} = 0$

neutrino temperature, T_s is taken to be less than or equal to the active neutrino temperature T_ν. The ratio T_s/T_ν is assumed to be the same throughout weak decoupling, BBN, and recombination. For this analysis, we do not investigate smaller active-sterile neutrino mixing angles with resultant non Fermi-Dirac-shaped energy spectra [81, 57]. Future work will consider such physics [82].

Figure 6.2 displays contours of constant $\tilde{N}_{\rm eff}$. The vertical axis is the ratio T_s/T_ν and the horizontal axis the sterile neutrino rest mass m_{ν_s}. We maintain the ratio $T_\nu/T = (4/11)^{1/3}$, assuming covariant conservation of entropy, starting at the end of the epoch of $e^\pm$-annihilation and continuing throughout the remainder of the history of the universe. The dotted lines show the expectation from the dark radiation analysis of

Sec. 2.5 without employing the self-consistent, iterative approach developed in Sec. 4.5. The deviation of the contours from the dotted lines is again due to an effect similar to the νMR effect but, in this instance, due to the sterile state. Fig. 6.2 takes the sum of the active neutrino masses to be 0.06 eV. This is inconsequential for large $T_s/T_\nu \lesssim 1$. For $T_s/T_\nu \lesssim 0.1$, $\Delta\tilde{N}_{\rm eff} < 0$ due to the νMR effect in the active neutrino sector. As a consequence, the contour for $\tilde{N}_{\rm eff} = 3$ is not coincident with the m_{ν_s} axis. Since m_{ν_s} is too small to be of any significant kinematic effect during BBN, we need only compute BBN once for a given value of T_s/T_ν. During recombination, m_{ν_s} is kinematically important and affects the Hubble rate. Hence, for every point in the T_s/T_ν-m_{ν_s} plane of Fig. 6.2 we calculate recombination. This figure clearly emphasizes the need for a self-consistent treatment between BBN and recombination when considering this BSM physics.

6.2.2 Heavy sterile neutrinos

Heavy sterile neutrinos that decay out of equilibrium in the early universe can affect weak decoupling and, as a consequence, primordial nucleosynthesis [69, 16, 83]. Sterile neutrinos in the rest mass range 0.1 GeV $\leq m_{\nu_s} \leq$ 1.0 GeV, with lifetimes $\gtrsim 1$ s decaying during the weak decoupling, weak freeze-out, and/or BBN epochs can have constrainable, sometimes dramatic, cosmological effects.

Such sterile neutrinos have mass and vacuum mixings with ν_e, ν_μ, ν_τ constrained by accelerator and other laboratory oscillation experiments/observations [84, 85, 86, 87, 88, 89, 90, 91], beta-decay experiments [92], and cosmological considerations, including constraints on $\sum m_\nu$ and $N_{\rm eff}$ [93, 94, 95, 96, 97, 98, 99, 100]. In fact, stringent constraints can be obtained from $N_{\rm eff}$ limits alone [16], as sterile neutrinos decaying out of equilibrium can lead to dilution (entropy production) which, in the weak decoupling epoch, can lead to distortions in the relic neutrino energy spectrum, affecting $\sum m_\nu$, and have significant impact on the relativistic energy content and, hence, $N_{\rm eff}$. A sophisticated

theoretical and computational treatment of dilution physics is a challenging endeavor. We have developed BURST to address this specific problem. BURST employs individual neutrino spectra for each species, binned according to the co-moving quantity $\varepsilon \equiv E/T_\nu$. The binned-spectra evolve with the universe as heavy particles decay, injecting entropy into the neutrino seas, and subsequently equilibrate by scattering on background neutrinos and electrons and positrons. We track multiple decades of ε values over many Hubble times. Our Boltzmann solver calculates the rates for each individual scattering process so we can decipher the contributions of each process to the shape of the neutrino spectra. Even though these heavy sterile neutrinos may decay away before an epoch where $T \sim 10$ keV, they can nevertheless alter the relationship between Y_P, D/H, $N_{\rm eff}$, $\sum m_\nu$, and ω_b, necessitating the need for a self-consistent treatment between the weak decoupling, weak freeze-out, BBN, recombination, photon decoupling, and advent of LSS epochs [101].

6.3 Lepton numbers

We examine how lepton numbers affect the primordial abundances and $\tilde{N}_{\rm eff}$. We define the lepton number L_ν for a neutrino species ν in a flavor eigenstate as

$$L_\nu \equiv \frac{n_\nu - n_{\bar{\nu}}}{n_\gamma}, \tag{6.2}$$

where n_ν is the number density of neutrino species ν, $n_{\bar{\nu}}$ is the number density of anti-neutrino species $\bar{\nu}$, and n_γ is the number density of photons. Here, for illustrative purposes, we take $L_{\nu_e} = L_{\nu_\mu} = L_{\nu_\tau} \equiv L_\nu$. The efficiency of neutrino oscillations in equating lepton numbers is approximate, and indeed dependent on neutrino physics [102, 103, 104]. In fact, Ref. [103] shows that oscillations with solar mass-splitting scales cause disparate lepton numbers in e, μ, τ neutrinos to equilibrate to within an order of magnitude of one

another. The limitations of existing calculations revolve around how quantum damping and neutrino energy dependence are handled.

We use the comoving-invariant neutrino degeneracy parameter $\xi_\nu \equiv \mu_\nu/T_\nu$, where μ_ν is the chemical potential of neutrino ν, to compute L_ν. The present model assumes that the lepton number evolves through the epoch of $e^\pm$ annihilation only in response to the relative increase in n_γ. We do not consider any BSM physics which could alter the difference $n_\nu - n_{\bar{\nu}}$; that is, we fix ξ_ν throughout weak decoupling, BBN, and photon decoupling. We relate the degeneracy parameter to the lepton number using the following expression [105, 19, 81]:

$$L_\nu = \frac{4}{11}\frac{1}{12\zeta(3)}\left(\pi^2\xi_\nu + \xi_\nu^3\right), \tag{6.3}$$

where $\zeta(3) \approx 1.202$. The factor $4/11$ in Eq.(6.3) implies that our lepton numbers refer to the post $e^\pm$ annihilation epoch, where $T_\nu/T = (4/11)^{1/3}$.

6.3.1 Effect on nucleosynthesis

The helium mass fraction is sensitive to the neutron-to-proton ratio, n/p. We determine n/p by calculating the weak rates associated with neutrino-nucleon reactions, namely:

$$\nu_e + n \rightleftharpoons e^- + p^+ \tag{6.4}$$

$$\bar{\nu}_e + p^+ \rightleftharpoons e^+ + n \tag{6.5}$$

and in addition, neutron and inverse neutron decay:

$$n \rightleftharpoons e^- + \bar{\nu}_e + p^+ \tag{6.6}$$

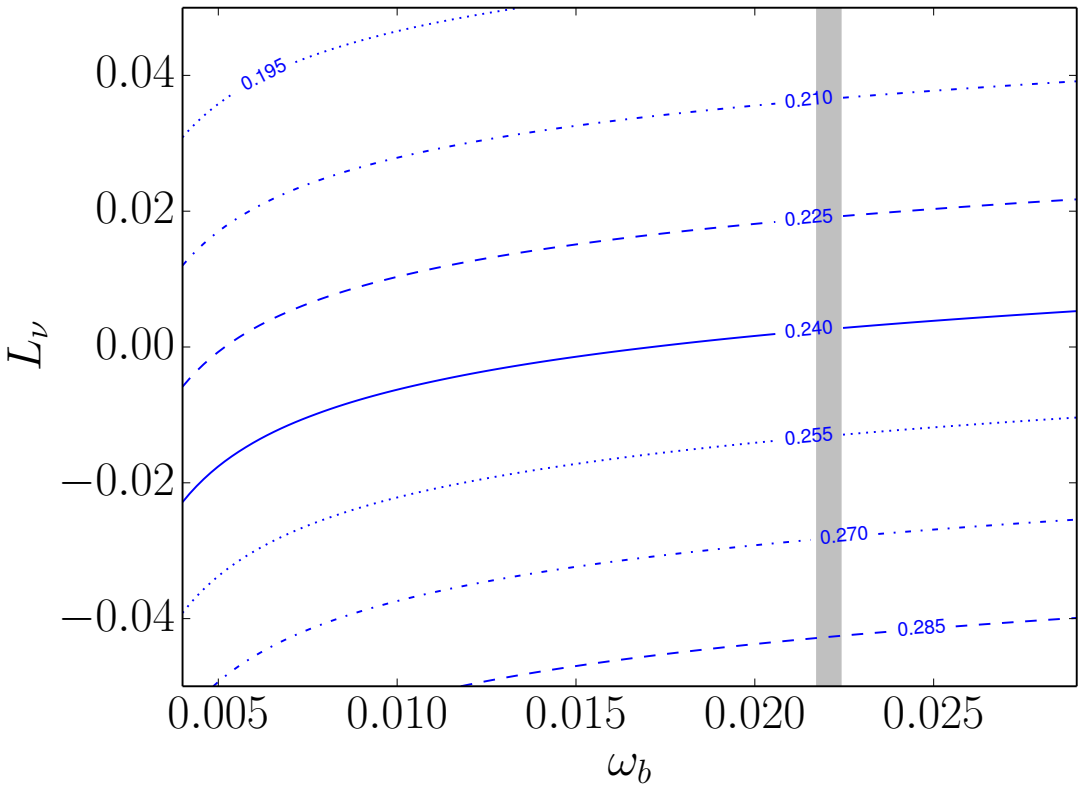

Figure 6.3: Lepton asymmetry L_ν [Eq.(6.2)] plotted against ω_b for contours of constant Y_P. The contours are spaced by $\Delta Y_P = 0.015$.

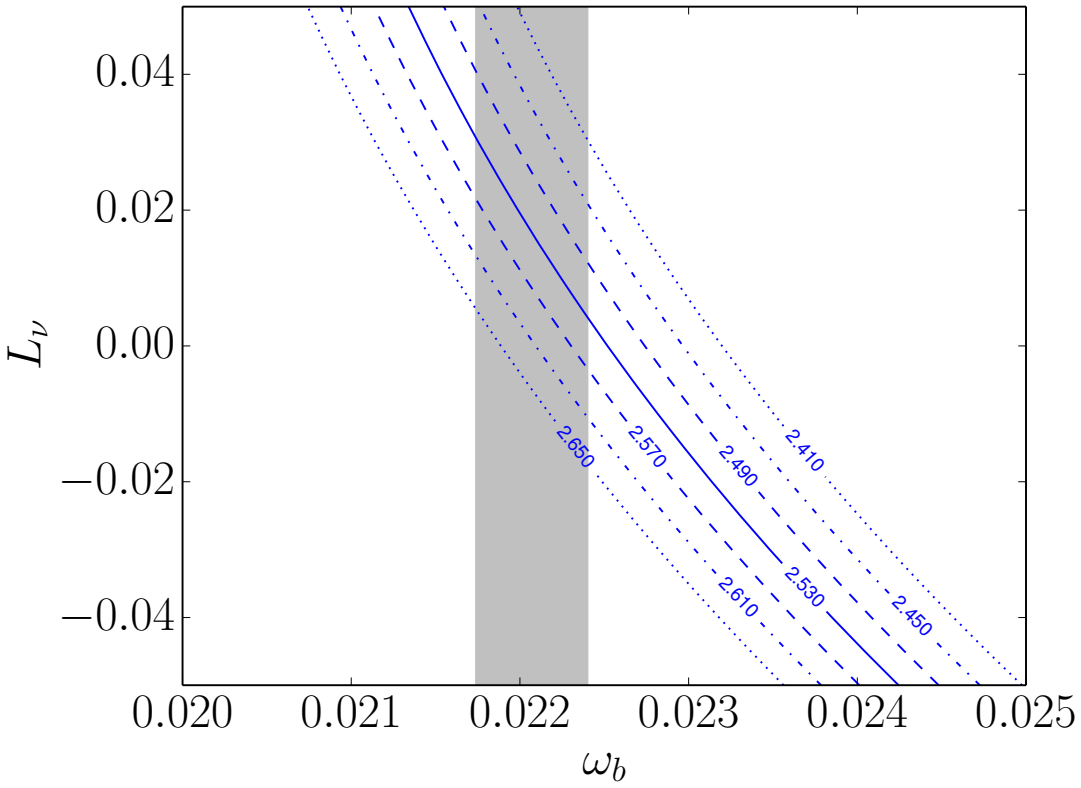

Figure 6.4: Lepton asymmetry L_ν plotted against ω_b for contours of constant $10^5 \times$ D/H. The solid curve is the preferred value of Ref. [3]. The contours are spaced by $\Delta(10^5 \times \mathrm{D/H}) = 0.04$.

The net rates in reactions (6.4) and (6.5) fall below the Hubble rate at the epoch of weak freeze-out. Weak freeze-out largely precedes the alpha-particle formation process in BBN, though unlike the brief time/temperature range of α-formation, weak freeze-out occurs over several Hubble times at this epoch. The rates in reactions (6.4) through (6.6) are sensitive to the neutrino and $e^{\pm}$ distributions. We follow Ref. [27] to evolve T and the electron chemical potential in order to maintain equilibrium between the electrons, positrons and photons. For the electron-flavor neutrinos, we use the comoving invariants aT_ν and ξ_{ν_e} to compute the neutrino distributions. We set $\sum m_\nu = 0$ as neutrinos of sub-eV rest mass remain ultra-relativistic throughout weak freeze-out.

Figures 6.3 and 6.4 show the helium mass fraction and the relative deuterium abundance, respectively. Each plot is in the L_ν-ω_b plane for contours of constant primordial abundance. The relationships between lepton number and nucleosynthesis are well known [106, 41]. Increasing L_{ν_e} leads to an overabundance of neutrinos compared to anti-neutrinos. The forward rate of reaction (6.4) freezes-out after the forward rate of reaction (6.5). The imbalance lowers n/p which lowers Y_P as seen in Fig. 6.3. The decrease in n/p also leads to a decrease in D/H, although deuterium is not as sensitive to L_ν as helium. However, D/H is known to much higher precision than is Y_P.

Comparing with recent observations [1, 3], the two light element abundances achieve consistency at 2σ. Y_P prefers a value of $L_\nu < 0$ whereas D/H prefers a positive value of L_ν. If future observations of the light-element abundances were to show a larger disagreement than 2σ, lepton numbers of identical value could not solely rectify the tension. Future analyses will consider scenarios with multiple facets of BSM physics including non-zero lepton numbers [107]. This analysis will use $\tilde{N}_{\rm eff}$ as a discriminating factor.

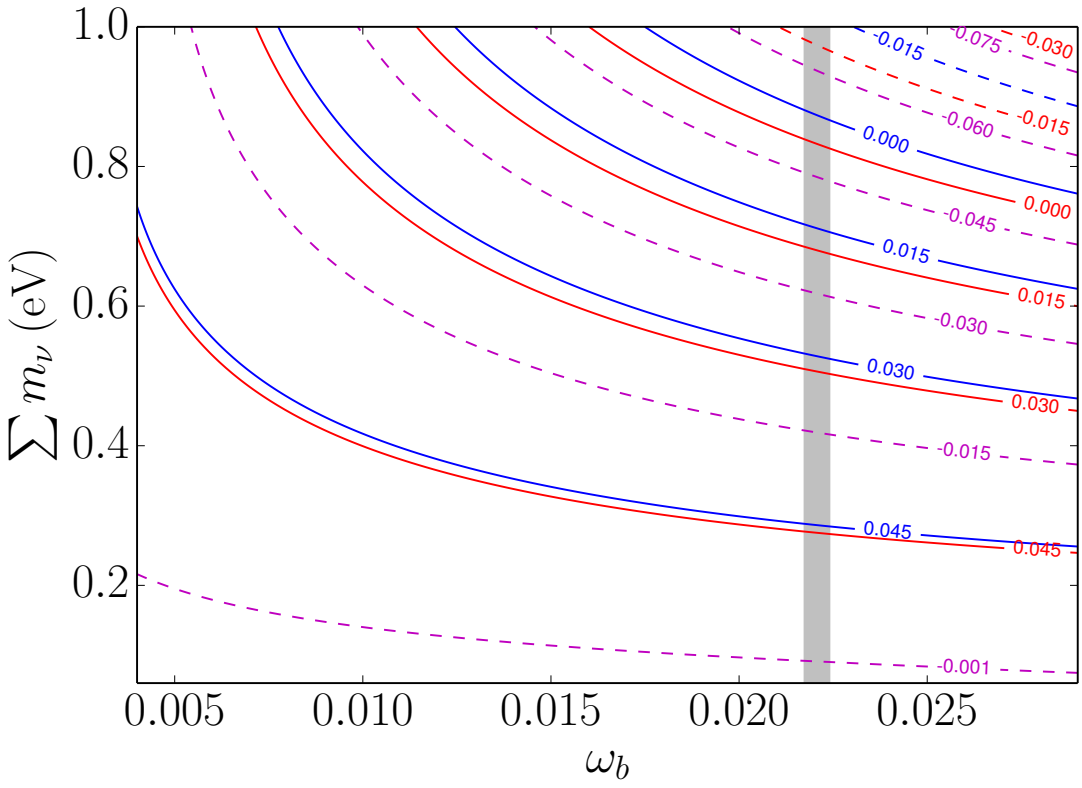

Figure 6.5: $\sum m_\nu$ plotted against ω_b for contours of constant $\Delta\tilde{N}_{\rm eff}$. The blue contours are for $L_\nu = -0.05$. The magenta contours are for $L_\nu = 0$. The red contours are for $L_\nu = 0.05$. Solid contours are for positive values; dashed contours are for negative values.

6.3.2 Effect on $N_{\rm eff}$

We consider how two aspects of non-CSM/BSM physics ($L_\nu \neq 0$ and/or $\sum m_\nu \neq 0$) modify $\tilde{N}_{\rm eff}$. If we set the neutrino rest mass to $\sum m_\nu \neq 0$, we can investigate whether the νMR effect still applies with non-zero L_ν. Figure 6.5 shows the changes to $\tilde{N}_{\rm eff}$ in the $\sum m_\nu$-ω_b plane for three values of $L_\nu = -0.05, 0, 0.05$ corresponding to blue, magenta, and red contours, respectively. The non-zero lepton number increases $\tilde{N}_{\rm eff}$ for small values of $\sum m_\nu$ in accordance with Ref.[10]. However, for values of $\sum m_\nu \sim 1.0$ eV, the νMR effect overwhelms the extra energy density from more particles to lower $\tilde{N}_{\rm eff}$ below three.

Figure 6.5 also shows that, despite the total energy density being insensitive to the sign of L_ν, the contours for non-zero values of L_ν with opposite sign do not overlap because Y_P depends sensitively on its value. Y_P is largest for the blue contours, so more helium suppresses the νMR effect.

Note that taking $L_\nu \neq 0$ conflates the interpretation that the effect of $\sum m_\nu$ is identical to perturbations in the matter power spectrum, which are used in calculating the suppression of power on small scales. This is borne out by the present model where the $\sum m_\nu$ statistic cannot be equated to the cosmological measurement. In our model, $\sum m_\nu$ is simply the sum of the active vacuum neutrino mass eigenvalues. The observationally determined value of $\sum m_\nu$ depends on quantities other than the sum of the active neutrino masses such as their energy distributions.

6.4 Conclusion

We have shown that the parameters $N_{\rm eff}$ and $\sum m_\nu$ are inadequate to fully cover the neutrino sector when considering BSM physics. Active neutrino rest mass, sterile neutrinos, and lepton numbers modify predictions of $N_{\rm eff}$ and $\sum m_\nu$. The characterization of this physics (and undoubtedly other phenomena) requires a self–consistent treatment of the universe from early times (weak decoupling) to late times (the advent of LSS).

Chapter 6, in full, is a reprint of some of the material as it appears in "Probing neutrino physics with a self-consistent treatment of the weak decoupling, nucleosynthesis, and photon decoupling epochs." Grohs, E.; Fuller, G. M.; Kishimoto, C. K.; Paris, M. W., J. Cosmology Astropart., 5 (May 2015) 17. The dissertation author was the primary investigator and author of this paper. We thank Lauren Gilbert, Jeremy Ariche, Amit Yadav, and JJ Cherry for useful discussions.

Chapter 7

Transport

7.1 Introduction

Above a temperature of a few MeV, the neutrinos efficiently exchange energy with the electrons and positrons. Besides cold–dark–matter, all of the constiuents of the universe are in close thermal contact until weak decoupling in the standard cosmology. In our work so far, we have assumed an instantaneous decoupling of the neutrinos from the electromagnetic plasma. We abandon this approximation in this chapter.

Ref.[28] (hereafter called DHS) confronted the problem of the non-sharp transition of weak decoupling. In their seminal work, the authors used a non-perturbative method to calculate the collision integrals in the Boltzmann equation, Eq.(1.170):

$$\frac{df(\varepsilon)}{dt} = \hat{C}[f(\varepsilon)], \tag{7.1}$$

We define the independent variable $\varepsilon = E/T_{\rm cm}$ from Eq.(1.72), where we have equated the energy and the magnitude of the three–momentum, and used the comoving temperature $T_{\rm cm}$. $f(\varepsilon)$ is the phase–space occupation probability (or simply occupation probability) of the neutrinos and the input into the collision integral of Eq.(7.1). For the processes

relevant to weak decoupling, it is necessary to calculate the occupation probabilities for the charged leptons. We assume FD equilibrium spectra, using a chemical potential and temperature, for the electron and positron occupation probabilities:

$$f_{e^{\pm}}(E) = \frac{1}{e^{(E\pm\mu)/T}+1} \equiv \frac{1}{\exp\left(\frac{E}{T}\pm\phi_e\right)+1}, \tag{7.2}$$

where we have defined the electron degeneracy parameter, ϕ_e. The finite mass of the electron complicates the expression in Eq.(7.2). We use a temperature–scaled mass m_ε, which we define as:

$$m_\varepsilon \equiv \frac{m_e}{T_{\rm cm}}. \tag{7.3}$$

We do not use the plasma temperature T in our definition of m_ε, opting instead to use the comoving temperature.

The calculation of the collision integral in Eq.(7.1) is non-trivial. However, the integrations are easily parallelizable. Therefore, we execute our computations on a supercomputer. We have written our code BURST in Fortran 90/95, using OPENMPI for message passing. We have not used any publicly available Boltzmann–collision–term calculators in BURST. Our code is tuned for the specific problem of the weak–decoupling collision terms. We always consider speed and accuracy when modifying the parallel version of our code. The efficiency of the parallel structure reduces the run time by nearly a factor of the number of cores. Calculations involving the neutrino Quantum Kinetic Equations (QKEs, see Ref.[12]) mandate the use of sophisticated numerical techniques for speed and accuracy. With the QKE problem in mind, we designed BURST to calculate the collision integrals as efficiently as possible.

We define δf at a given time and ε to be the relative change in the occupation

probabilities with respect to (wrt) a FD occupation probability:

$$\delta f \equiv \frac{f(\varepsilon,t) - f^{(\mathrm{eq})}(\varepsilon)}{f^{(\mathrm{eq})}(\varepsilon)} \quad \text{where} \quad f^{(\mathrm{eq})}(\varepsilon) = \frac{1}{e^{\varepsilon}+1}. \tag{7.4}$$

$f^{(\mathrm{eq})}$ is independent of time or temperature. To encapsulate the total change in the neutrino spectrum, we encode the neutrino energy density into N_{eff}, the so–called effective number of neutrinos. The standard definition of N_{eff} is the following:

$$\rho_r = \left[2 + \frac{7}{4}\left(\frac{4}{11}\right)^{4/3} N_{\mathrm{eff}}\right] \frac{\pi^2}{30} T^4. \tag{7.5}$$

If we equate the radiation–energy density to the sum of the photon and neutrino energy densities, we find:

$$\rho_\gamma + \rho_\nu = \left[1 + \frac{7}{8}\left(\frac{4}{11}\right)^{4/3} N_{\mathrm{eff}}\right] \rho_\gamma \tag{7.6}$$

$$\implies N_{\mathrm{eff}} = \frac{8}{7}\left(\frac{11}{4}\right)^{4/3} \frac{\rho_\nu}{\rho_\gamma}. \tag{7.7}$$

We use Eq.(7.7) when calculating N_{eff}. The calculation of the photon energy density is straight–forward. To calculate the neutrino energy density, we use Boole's rule[108] when integrating the neutrino spectra over ε to obtain a dimensionless number. We multiply the dimensionless number by T_{cm}^4 to determine the energy density.

The outline of this chapter is as follows. In Sec.7.2, we briefly give an overview of past approaches to solving the weak–decoupling problem. Sec.7.3 lists the summed–squared–amplitudes needed in calculating the collision term in Eq.(7.1). We follow DHS and do not include finite–temperature QED effects when calculating the collision terms. In Sec.7.4, we outline our non-perturbative approach. Sec.7.5 discusses the quantization of error in the coupled Ordinary Differential Equation (ODE) network of the occupation

probabilities. Secs.7.3, 7.4, and 7.5 lay the framework for an actual weak–decoupling calculation, which we present in Sec.7.6. We conclude in Sec.7.7

7.2 Overview of past approaches

The problem we consider in this chapter is the departure from equilibrium in weak decoupling. Such a problem can be treated perturbatively, as was done by Refs.[30, 109]. DHS and Ref.[29] treated the same problem, but used a non-perturbative approach by binning the neutrino spectra.

Different research groups estimated the correction to the neutrino spectra without using a set of Boltzmann equations. Ref.[110] examined the effect of finite–temperature radiative corrections on the production of helium. In addition, the authors of Ref.[110] estimated the effect of incomplete weak decoupling by assuming thermal equilibrium is maintained in a single neutrino species and using a constant, average cross section. They found relative changes in the ν_e temperature of $\sim 3\times10^{-3}$ and the $\nu_{\mu,\tau}$ temperature of $\sim 1\times10^{-3}$ when only considering positron–electron annihilation. Refs.[111, 112] also looked at changes in the neutrino temperatures and found similar results to within an order of magnitude. Refs.[113, 114, 115] all used coupled sets of Boltzmann equations for their treatment of the weak decoupling problem. Refs.[113, 114] used a Boltzmann approximation for their Boltzmann equations. Ref.[115] did not make the Boltzmann approximation, and found relative changes in the energy densities of:

$$\delta\rho_{\nu_e} \equiv \frac{\Delta\rho_{\nu_e}}{\rho_\nu^{(\mathrm{eq})}} = 0.83\%, \tag{7.8}$$

$$\delta\rho_{\nu_\mu} = 0.41\%. \tag{7.9}$$

DHS assumes a baryon-free, FLRW universe. The independent variable is $x \equiv m\,a$,

where a is the scale factor, and m is a generic mass scale. x is normalized such that the comoving temperature is:

$$T_{\rm cm} = \frac{1\ {\rm MeV}}{x}. \tag{7.10}$$

DHS evolves, in x, three sets of quantities. The first quantity is the total energy density, deduced from covariant energy conservation:

$$x\frac{d\rho}{dx} = -3(\rho + p), \tag{7.11}$$

where ρ is the total energy density and p is the total pressure. The total energy density includes photons, charged leptons, and the partially decoupled neutrino species. From Eq.(7.11), DHS deduces a plasma temperature. The electron and positron chemical potential is identically zero since there is no baryon asymmetry. Therefore, the degeneracy parameter ϕ_e is not an evolution variable. With Eq.(7.11), DHS evolves the sets of Boltzmann equations for ν_e and ν_μ. The Boltzmann equations are indexed by the dimensionless quantity $y \equiv p_j a$. The ν_τ spectrum is identical to ν_μ, and the anti-neutrinos have identical spectra to the corresponding neutrino.

The number of bins in y is either 100 or 200, although DHS achieves acceptable convergence at 100 bins. The bins are linearly-spaced from $y = 0$ to $y = 20.0$. There is a point at zero which is evolved with different collision integrals. DHS executes two different, but in theory identical, procedures (called FD). The first FD procedure evolves the occupation probabilities directly. The second procedure evolves the changes $\delta(x,y)$, where $f(x,y) = f^{(\rm eq)}(x,y)(1+\delta(x,y))$. $f^{(\rm eq)}(x,y)$ is a FD occupation probability at coordinate x. The two procedures should give identical results. Differences arise due to machine precision; however, the two procedures produce similar results for convergence. In addition to the two FD procedures outlined above, DHS solves the neutrino Boltzmann equations by employing the Boltzmann approximation. Within this approximation, there

are an additional two procedures (called MB). The first MB procedure integrates the scattering integrals exactly the same way as the procedures for $f(x,y)$ and $\delta(x,y)$ except using the Boltzmann approximation, where $1-f \to 1$. The second procedure uses two different integrals for the forward and reverse rates. The forward rate is the same as the first procedure. The reverse rate explicitly integrates the integrals over the phase space of the third particle, since $1-f_3 \to 1$ and so $\int dp_3$ is analytic. Both MB procedures are approximations to the FD procedures outlined first, and are not expected to converge with the FD results. However, the MB procedures supply a method to check for coding or computational errors. The authors claim complete agreement between the two MB procedures.

For the FD procedures, the authors initiate the computation at three points, denoted $x_{in} = 0.1, 0.2,$ and 0.5. The last initialization point (equivalent to $T_{\rm cm} = 2$ MeV) does not converge with the first two points. The authors use 4000 points in x. The computation ends at $x = 60.0$ once freeze-out has occured. There are two ODE integration algorithms: a simple time evolution (presumably Eulerian); and a Bulirsch-Stoer routine similar to that of Ref.[108], except written in C. The Bulirsch-Stoer routine agrees well with the simple time evolution for 4000 points in x. Convergence is most sensitive to the number of points in x, as compared to the number of bins, the initial x, the FD procedure, or the ODE algorithm. DHS accepts the following values for the relative changes in the neutrino energy densities:

$$\delta\rho_{\nu_e} = 0.94\%, \tag{7.12}$$

$$\delta\rho_{\nu_\mu} = 0.40\%, \tag{7.13}$$

and the final ratio of photon to comoving temperatures:

$$\frac{T}{T_{\rm cm}} = 1.3991. \tag{7.14}$$

This would imply:

$$N_{\rm eff} = \left(\frac{11/4}{1.3991^3}\right)^{4/3} (3 + 0.0094 + 2 \times 0.0040) = 3.034. \tag{7.15}$$

The authors published an addendum[59] where they improved the accuracy of the code, and still found the same value for $N_{\rm eff}$.

Ref.[29] also treated the problem with a binned spectrum. However, their binning scheme was pseudo-logarithmic; it consisted of 40 linear-spaced bins per decade, ranging from $10^{-5.5} \leq \zeta \leq 10^{1.7}$, for a total of 289 points (in Ref.[29] $\zeta = p/T_{\rm cm}$.) The authors began their integration at $T = 10$ MeV and terminated it at $T = 1$ keV, while maintaining a relative accuracy of 10^{-7} at each time step. The authors assumed zero asymmetry between the electrons and positrons. For the integration, the authors employ a unique numerical scheme which does not require the calculation of the full Jacobian matrix. Their scheme is more efficient than the standard adaptive RK5 scheme by a factor of 20-60. The authors find $N_{\rm eff} = 3.022$, lower than DHS.

Departing from the bin schemes, Ref.[30] adopts a perturbative approach using orthogonal polynomials weighted by the Fermi-Dirac expression for occupation probability. They employ a Fortran code developed by Ref.[116]. In Ref.[30], the orthogonal

polynomials P_i are defined such that:

$$f_{\nu_\alpha}(x,y) = \frac{1}{e^y+1}\left[1+\sum_{i=0}^{\infty} b_i^{(\alpha)}(x)\,P_i(y)\right], \tag{7.16}$$

$$\int_0^\infty dy \frac{P_i(y)P_j(y)}{e^y+1} = \delta_{ij}, \tag{7.17}$$

where $x \equiv m_e\,a$ and $y \equiv p\,a$. The coefficients $b_i^{(\alpha)}$ are different for ν_e compared to ν_μ, and evolve according to the Boltzmann equation:

$$\frac{db_i^{(\alpha)}}{dx} = \frac{1}{xH}\int_0^\infty dy_1 P_i(y_1) I_{\nu_\alpha}[f_{\nu_e}, f_{\nu_\mu}], \tag{7.18}$$

where I_{ν_α} is the collision integral. The summation in Eq.(7.16) is truncated at $i = 3$. Ref.[116] describes the integration method of Eq.(7.18) as backward differentiation using Newton's method and an adaptive step–size. Ref.[30] determines $N_{\rm eff}$ to be 3.0345, in agreement with DHS. In addition, Ref.[30] does another calculation with QED corrections. The corrections renormalize the masses of the photon and electron. Along with the Boltzmann solution, Ref.[30] determines $N_{\rm eff}$ to be 3.0395. A later paper by many of the same authors of Ref.[30], finds $N_{\rm eff} = 3.046$[117]. Ref.[117] included an improved numerical technique over Ref.[30] to calculate the derivative of the plasma temperature.

Ref.[109] also used a perturbative method to determine $N_{\rm eff}$. Their approach assumes the neutrino spectra are close to thermal equilibrium, but need not be in chemical equilibrium. They use the weight function:

$$w_\Upsilon(z) \equiv \frac{z^2}{\Upsilon^{-1}e^z+1}, \tag{7.19}$$

and find orthogonal polynomials based on that weight. For the weak-decoupling problem, Ref.[109] uses two modes, and finds $N_{\rm eff} = 3.044$, including the finite temperature QED

corrections.

7.3 Weak Interactions

7.3.1 Summed–squared amplitudes

Table 7.1 gives the summed–squared amplitudes for the two–body processes we consider in weak decoupling. The numbering scheme for the four–momenta in Tb.7.1 is:

$$1 + 2 \leftrightarrow 3 + 4, \tag{7.20}$$

where particle 1 is always a neutrino (or anti-neutrino). We use four-momenta P for massless particles (neutrinos), and four-momenta Q for massive particles (charged leptons at all temperatures under consideration).

The summed–squared–amplitudes are different for the electron–flavor neutrinos compared to the mu or tau–flavor neutrinos. The addition of a charged–current diagram for the electron–flavor only, changes the factors of $2\sin^2\theta_W - 1$ to $2\sin^2\theta_W + 1$.

Notice the difference between Tb.7.1 and Tbs.(1) and (2) in DHS. Row 11 of Tb.7.1 corresponds to Row 6 of Tb.(1) in DHS. The expressions for column 2 are the same. However, particle 3 of Row 11 is an electron, and particle 3 of Row 6 is a positron. The discrepancy also occurs between Row 12 of Tb.7.1 and Row 6 of Tb.(2) in DHS. Our expression does agree with Row 7 of Tb.(1) in Ref.[115].

Table 7.1: Table of summed-squared scattering amplitudes $\langle|\mathcal{M}|^2\rangle$. i is always different than j. Not included are scatterings involving one anti-neutrino and one charged lepton. Those matrix elements are identical to the corresponding parity conjugate reactions of rows 6–10. S is the symmetrization factor and is unity for all processes except the process in row 1, where $S = 1/2$.

Process	$G_F^{-2} S \langle\|\mathcal{M}\|^2\rangle$
$\nu_i + \nu_i \leftrightarrow \nu_i + \nu_i$	$2^6 (P_1 \cdot P_2)(P_3 \cdot P_4)$
$\nu_i + \nu_j \leftrightarrow \nu_i + \nu_j$	$2^5 (P_1 \cdot P_2)(P_3 \cdot P_4)$
$\nu_i + \overline{\nu}_i \leftrightarrow \nu_i + \overline{\nu}_i$	$2^7 (P_1 \cdot P_4)(P_2 \cdot P_3)$
$\nu_i + \overline{\nu}_j \leftrightarrow \nu_i + \overline{\nu}_j$	$2^5 (P_1 \cdot P_4)(P_2 \cdot P_3)$
$\nu_i + \overline{\nu}_i \leftrightarrow \nu_j + \overline{\nu}_j$	$2^5 (P_1 \cdot P_4)(P_2 \cdot P_3)$
$\nu_e + e^- \leftrightarrow e^- + \nu_e$	$2^5[(2\sin^2\theta_W + 1)^2 (P_1 \cdot Q_2)(Q_3 \cdot P_4)$ $+4\sin^4\theta_W (P_1 \cdot Q_3)(Q_2 \cdot P_4)$ $-2\sin^2\theta_W (2\sin^2\theta_W + 1) m_e^2 (P_1 \cdot P_4)]$
$\nu_{\mu(\tau)} + e^- \leftrightarrow e^- + \nu_{\mu(\tau)}$	$2^5[(2\sin^2\theta_W - 1)^2 (P_1 \cdot Q_2)(Q_3 \cdot P_4)$ $+4\sin^4\theta_W (P_1 \cdot Q_3)(Q_2 \cdot P_4)$ $-2\sin^2\theta_W (2\sin^2\theta_W - 1) m_e^2 (P_1 \cdot P_4)]$
$\nu_e + e^+ \leftrightarrow e^+ + \nu_e$	$2^5[(2\sin^2\theta_W + 1)^2 (P_1 \cdot Q_3)(Q_2 \cdot P_4)$ $+4\sin^4\theta_W (P_1 \cdot Q_2)(Q_3 \cdot P_4)$ $-2\sin^2\theta_W (2\sin^2\theta_W + 1) m_e^2 (P_1 \cdot P_4)]$
$\nu_{\mu(\tau)} + e^+ \leftrightarrow e^+ + \nu_{\mu(\tau)}$	$2^5[(2\sin^2\theta_W - 1)^2 (P_1 \cdot Q_3)(Q_2 \cdot P_4)$ $+4\sin^4\theta_W (P_1 \cdot Q_2)(Q_3 \cdot P_4)$ $-2\sin^2\theta_W (2\sin^2\theta_W - 1) m_e^2 (P_1 \cdot P_4)]$
$\nu_e + \overline{\nu}_e \leftrightarrow e^- + e^+$	$2^5[(2\sin^2\theta_W + 1)^2 (P_1 \cdot Q_4)(P_2 \cdot Q_3)$ $+4\sin^4\theta_W (P_1 \cdot Q_3)(P_2 \cdot Q_4)$ $+2\sin^2\theta_W (2\sin^2\theta_W + 1) m_e^2 (P_1 \cdot P_2)]$
$\nu_{\mu(\tau)} + \overline{\nu}_{\mu(\tau)} \leftrightarrow e^- + e^+$	$2^5[(2\sin^2\theta_W - 1)^2 (P_1 \cdot Q_4)(P_2 \cdot Q_3)$ $+4\sin^4\theta_W (P_1 \cdot Q_3)(P_2 \cdot Q_4)$ $+2\sin^2\theta_W (2\sin^2\theta_W - 1) m_e^2 (P_1 \cdot P_2)]$

7.3.2 Collision integrals

With the summed–squared–amplitudes in Tb.7.1, we can calculate the collision integral for Eq.(1.170) from Ch.1:

$$\hat{C}[f_1(p_1)] = \frac{1}{2E_1}\sum\int \frac{d^3p_2}{(2\pi)^3 2E_2}\frac{d^3p_3}{(2\pi)^3 2E_3}\frac{d^3p_4}{(2\pi)^3 2E_4} \times (2\pi)^4\delta^{(4)}(P_1+P_2-P_3-P_4)S\langle|\mathcal{M}|^2\rangle F(p_1,p_2,p_3,p_4), \quad (7.21)$$

where S is the symmetrization factor for identical particles, and:

$$F(p_1,p_2,p_3,p_4) \equiv f_3(p_3)f_4(p_4)[1-f_1(p_1)][1-f_2(p_2)] - f_1(p_1)f_2(p_2)[1-f_3(p_3)][1-f_4(p_4)], \quad (7.22)$$

for occupation probabilities only dependent on the magnitude of the three momentum. In Eq.(7.21), the sum is over all processes involving f_1. $\delta^{(4)}(P_1+P_2-P_3-P_4)$ is a four–momentum conserving delta function. The factor $1/2E_1$ is put in by hand so that the integral over d^3p_1 of the collision integral for f_1 vanishes in number–conserving processes. All of the amplitudes in Tb.7.1 are proportional to G_F^2, the square of the Fermi–coupling constant. We take that factor outside of the integral in Eq.(7.21), along with $T_{\rm cm}^5$. The remainder of the integral is unit–less and in terms of ε, our binning parameter for the occupation probabilities. The product $G_F^2\,T_{\rm cm}^5$ has dimensions of energy, and so we divide by $\hbar$ to obtain a time derivative.

In general for two-body processes, Eq.(7.21) is a nine–dimensional integral over the phase–spaces of particles 2, 3, and 4. The delta function reduces the collision integral to five dimensions. Homogeneity and isotropy further reduce Eq.(7.21) to a two–dimensional expression in terms of single–particle energies of either species 2 and 3, or 2 and 4, or 3 and 4. The reduction from five to two–dimensions is non-trivial and

depends on the specific process in Tb.7.1. Appendix D details a comparison between a three–dimensional and a two–dimensional expression for the process in the first row of Tb.7.1. App.E shows how to obtain a three–dimensional expression for the process in the fifth row of Tb.7.1. Apps.F, G, and H contain the algebra for the reduction of the collision integrals to two dimensions for the processes involving the charged leptons.

7.4 Non-perturbative approach

7.4.1 Binning

We employ a linear binning scheme for the occupation probabilities in terms of the comoving invariant quantity $\varepsilon = p/T_{\rm cm}$. For the energy scales we consider during weak decoupling, the neutrinos are ultra-relativistic, implying the energy is equal to the momentum and so $\varepsilon = E_\nu/T_{\rm cm}$. We partition the interval from $\varepsilon = 0$ to $\varepsilon = \varepsilon_{\rm max}$ into $N_{\rm bins}$ number of equal–length bins. $\varepsilon_{\rm max}$ should be large enough to encompass the most–actively–evolving bins, yet still small enough to ensure high resolution. For a linear binning scheme, we use $N_{\rm bins}+1$ abscissas and place an abscissa at $\varepsilon = 0$. We do not integrate this point in order to avoid division by zero. However, the limit of the scattering integrals is zero as $\varepsilon \to 0$. The abscissa at zero also helps in interpolation accuracy.

7.4.2 Integration methods

The scattering integrals are over two dimensions in ε. We use the terms "inner" to refer to the first integration, and the term "outer" to refer to the second integration. It makes no difference to use momentum or energy if a given one–dimensional integral is over a neutrino kinematic variable. We simply divide the energy/momentum variable by $T_{\rm cm}$ to obtain an ε quantity. If the integral is over a charged–lepton kinematic variable,

we choose to use energy. For example, the occupation probability for an electron is:

$$f_{e^-} = \left[\exp\left(\frac{E-\mu}{T}\right)+1\right]^{-1} \tag{7.23}$$

$$= \left[\exp\left(\frac{E}{T}-\phi_e\right)+1\right]^{-1} \tag{7.24}$$

$$= \left[\exp\left(\frac{E}{T_{\rm cm}}\frac{T_{\rm cm}}{T}-\phi_e\right)+1\right]^{-1} \tag{7.25}$$

$$= \left[\exp\left(\varepsilon\frac{T_{\rm cm}}{T}-\phi_e\right)+1\right]^{-1}. \tag{7.26}$$

The summed–squared–amplitude expressions require both energies and three–momenta, so we can determine dimensionless momenta using:

$$\frac{p}{T_{\rm cm}} = \frac{\sqrt{E^2-m_e^2}}{T_{\rm cm}} = \sqrt{\left(\frac{E}{T_{\rm cm}}\right)^2-\left(\frac{m_e}{T_{\rm cm}}\right)^2} = \sqrt{\varepsilon^2-m_\varepsilon^2}, \tag{7.27}$$

where m_ε will continuously increase with decreasing $T_{\rm cm}$.

Depending on the specific process in Tb.7.1, the epsilon dimension may be over a neutrino or a charged lepton. For the inner integral, regardless of the species, the integration method is always a Gauss quadrature method. We modified the publicly–available software of Ref.[118] to calculate the quadrature weights and abscissas within BURST. If the limits of the inner integral are finite, we usually use a Gauss–Legendre quadrature method. For large finite intervals ($\Delta\varepsilon > 200$), we use a Gauss–Laguerre quadrature method. For semi-infinite limits, we always use Gauss–Laguerre.

If the outer integral is over an ε-value of a charged lepton, we use either a Gauss–Legendre or Gauss–Laguerre method, depending on the integration limits. If it is over a neutrino energy, we use Boole's rule with absicssas aligned with the bin points in order to avoid an interpolation of the occupation probabilities for the neutrino energy of the outer integral.

7.4.3 Interpolation and Extrapolation

As detailed in the appendices, we have the freedom to pick which single–particle ε-values to use in calculating the collision integral. The 2×2 processes in Tb.7.1 have at least two neutrinos in the combined initial and final states. We always use three of the four dimensions of the delta function to eliminate an integral over the phase space of one of the neutrino species. This procedure requires an interpolation over the ε-value of that species to determine the occupation probability. For processes that involve four neutrinos or anti-neutrinos, we do another interpolation over ε for the occupation probability of the inner–integration–variable species. The outer–integration is either a Gauss–quadrature method over a charged lepton, or a Boole's rule method over the bin points. In either case, no interpolation is required. There is no situation in which we need to interpolate the occupation probabilities for the charged leptons. We always use exact FD expressions for electrons and positrons.

We use a polynomial interpolator[108] for the neutrino occupation probabilities, if the energy of the third or fourth neutrino does not fall on an abscissa. We have found the interpolation is more accurate if we interpolate on the logarithms of the occupation probabilities, as opposed to the occupation probabilities themselves. For ε-values larger than $\varepsilon_{\max}$, we have to extrapolate. If the ε-value is larger than 300.0, we set the occupation probability to be $f = e^{-300}$. For $\varepsilon_{\max} < \varepsilon < 300.0$, we use the following expression:

$$\log[f(\varepsilon)] = \log[f(\varepsilon_{\max})] + \log\left[\frac{f^{(\mathrm{eq})}(\varepsilon)}{f^{(\mathrm{eq})}(\varepsilon_{\max})}\right]. \tag{7.28}$$

If we solve for the relative change in $f(\varepsilon)$ using Eq.(7.28), we find:

$$\delta f(\varepsilon) = \frac{f(\varepsilon) - f^{(\mathrm{eq})}(\varepsilon)}{f^{(\mathrm{eq})}(\varepsilon)} \tag{7.29}$$

$$= \frac{f^{(\mathrm{eq})}(\varepsilon)\dfrac{f(\varepsilon_{\max})}{f^{(\mathrm{eq})}(\varepsilon_{\max})} - f^{(\mathrm{eq})}(\varepsilon)}{f^{(\mathrm{eq})}(\varepsilon)} \tag{7.30}$$

$$= \frac{f(\varepsilon_{\max})}{f^{(\mathrm{eq})}(\varepsilon_{\max})} - 1 \tag{7.31}$$

$$= \delta f(\varepsilon_{\max}) \quad \text{if} \quad \varepsilon_{\max} < \varepsilon < 300.0. \tag{7.32}$$

Figure 7.5 suggests Eq.(7.32) is an inaccurate extrapolation.

7.4.4 Acceptance tolerance for rates

FD occupation probabilities guarantee the collision integral is zero, regardless of the summed–squared amplitude. Numerical integration, interpolation, and finite machine precision engender non-zero values of the collision integrals when calculated in equilibrium conditions. Therefore, during an actual computation, the need arises to set a tolerance to accept a collision–integral value as non-zero, or conversely reject a value as the result of imprecision. To accomplish this task, we use the net rate and forward–reverse–summed (frs) rate. The net rate is simply the value produced by the collision integral in Eq.(7.21). As the label indicates, the frs rate is the same as the net rate, except that instead of a difference in Eq.(7.22), the equation uses a sum.

We calculate the net and frs rates for each neutrino species, in each bin, for each process in Tb.7.1, assuming strict thermal and chemical equilibrium between the three flavors of neutrinos, anti-neutrinos, positrons and electrons. We sum over all of the processes to obtain the collision integral for the net rate, and a modified collision integral for the frs rate. For each neutrino species and each bin, we calculate the precision ratio,

defined as:

$$\mathcal{R}_{\nu_i}(\varepsilon) \equiv \frac{|\hat{C}[f_i^{(\mathrm{eq})}(\varepsilon)]|}{\hat{C}[f_i^{(\mathrm{eq})}(\varepsilon)]_{\mathrm{frs}}}. \tag{7.33}$$

The frs rate is strictly positive. We take the absolute value of the net rate to obtain a positive precision ratio. Eq.(7.33) is independent of temperature, except for the electron and positron quantity m_ε. When calculating the collision integrals in Eq.(7.33), we set $m_\varepsilon = 0$.

During our actual computation of weak decoupling, we calculate the collision integrals for both the net and frs rates at each time step. We then take a ratio of ratios and compare to a dimensionless tolerance $(\mathrm{net}/\mathrm{frs})^{(\mathrm{tol})}$:

$$\left\{ \frac{|\hat{C}[f_i(\varepsilon)]|}{\hat{C}[f_i(\varepsilon)]_{\mathrm{frs}}} \right\} \Big/ \mathcal{R}_{\nu_i}(\varepsilon) \sim (\mathrm{net}/\mathrm{frs})^{(\mathrm{tol})}. \tag{7.34}$$

If the lhs of Eq.(7.34) is larger than the tolerance threshold, we accept the collision integral as non-zero and use it in our time derivative of the occupation probability $f_i(\varepsilon)$. If the lhs of Eq.(7.34) is smaller than the threshold, we set the collision integral to zero.

7.5 Sum rule tests

We define the total scaled errors in the number and energy densities as:

$$\delta\left(\frac{dn}{dt}\right) = \frac{\sum_{\nu=1}^{6} \int d\varepsilon \varepsilon^2 \left.\frac{df_\nu}{dt}\right|_{\mathrm{net}}}{\sum_{\nu} \int d\varepsilon \varepsilon^2 \left.\frac{df_\nu}{dt}\right|_{\mathrm{frs}}} \quad (\mathrm{number}) \tag{7.35}$$

$$\delta\left(\frac{d\rho}{dt}\right) = \frac{\sum_{\nu} \int d\varepsilon \varepsilon^3 \left.\frac{df_\nu}{dt}\right|_{\mathrm{net}}}{\sum_{\nu} \int d\varepsilon \varepsilon^3 \left.\frac{df_\nu}{dt}\right|_{\mathrm{frs}}} \quad (\mathrm{energy}). \tag{7.36}$$

The summation over ν is for the three flavors of neutrinos and anti-neutrinos. We choose to use a ratio of sums as opposed to a sum of ratios. The ratio of sums gives a total error in the neutrino seas. We use a scaled error where the denominator in expressions (7.35) and (7.36) is always non-zero. In thermal equilibrium, the total scaled errors are $\sim 10^{-12}$ for both the number and energy sum rules for 100 bins. The total scaled errors do not change for non-zero m_ε or ϕ_e.

We introduce a test to monitor error in the sum rules in an out–of–equilibrium scenario. Within ε space, we add a Gaussian distribution to the FD occupation probabilities:

$$\bar{\varepsilon} = 3.0, \tag{7.37}$$

$$A = \frac{9.0}{e^{\bar{\varepsilon}} + 1}, \tag{7.38}$$

$$\sigma_\varepsilon = 0.2, \tag{7.39}$$

$$f(\varepsilon) = \frac{1}{e^{\varepsilon} + 1} + A e^{-(\varepsilon - \bar{\varepsilon})^2 / 2\sigma_\varepsilon^2}. \tag{7.40}$$

To monitor the sum rules, we only investigate the processes isolated within the neutrino seas. We do not follow the spectra of the charged leptons, so scattering processes involving electrons and positrons will not preserve the sum rules. In effect, we do not calculate the collision terms involving charged leptons in this test.

Figure 7.1 shows the total scaled error for both the number and energy densities as a function of the number of bins, N_{bins}. The calculation occurs in an infinite homogeneous and isotropic slab for a single time step. The rates depend on a temperature–like parameter. However, the total scaled errors for the sum rules are independent of temperature, and so we do not mandate a temperature for Fig.7.1. We only include data points for $N_{\text{bins}} \geq 300$. The calculations for 100 and 200 bins give total scaled errors of $\sim 10^{-3}$ and 10^{-4}, respectively, for both sum rules.

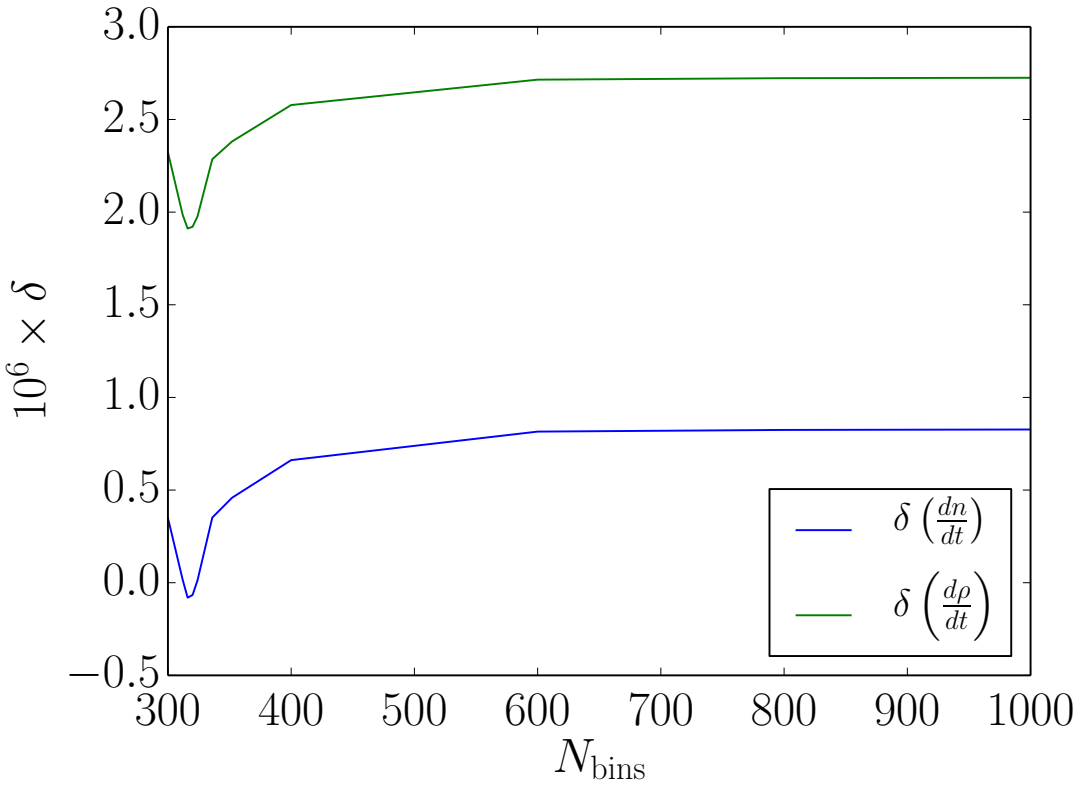

Figure 7.1: The total scaled error in the sum rules as a function of the number of bins in a homogeneous, isotropic, infinite slab for one time step.

7.6 Weak decoupling calculations

We use BURST to do a self-consistent calculation of weak decoupling and BBN. The neutrinos are in thermal equilibrium with the electrons and positrons until a user–defined temperature, which we label the input temperature T_{in}. The comoving temperature and plasma temperature are equal for all temperatures greater than the input temperature: $T = T_{\text{cm}} \geq T_{\text{in}}$. At T_{in}, we turn on the collision integrals and evolve the neutrino occupation probabilities. We end the transport calculation once the relict electron–positron pairs have annihilated, leaving only the surplus electrons to maintain charge neutrality. The terminal temperature is $T \sim 12$ keV, or $T_{\text{cm}} \sim 9$ keV. For all the plots shown in this section, the run parameters are $\varepsilon_{\text{max}} = 20.0$, $N_{\text{bins}} = 100$, $T_{\text{in}} = 8$ MeV, and $(\text{net/frs})^{(\text{tol})} = 30.0$.

7.6.1 Convergence tests

Table 7.2 shows a summary of preliminary transport runs. The first column ($N_{\rm bins}$) gives the number of bins used in the run for the neutrino spectra. The second column ($\varepsilon_{\rm max}$) gives the maximum value of ε used for the neutrino binning. The third column ($T_{\rm in}$) gives the input temperature when the transport rates are turned on. The fourth column ($(\mathrm{net}/\mathrm{frs})^{(\mathrm{tol})}$) gives the tolerance threshold. The fifth column ($N_{\rm eff}$) gives the calculation of $N_{\rm eff}$ at $T_{\rm cm} \sim 1\,\mathrm{keV}$ using Eq.(7.7). The sixth column ($T_{\rm cm}/T$) gives the ratio of the comoving to plasma temperatures. The seventh colmn gives the final entropy–per–baryon. Columns eight and nine give the nucleosynthesis calculations for helium and deuterium.

Table 7.2: Changing $N_{\rm eff}$ and temperature–ratio values for different weak–decoupling runs. For column five reference, $(4/11)^{1/3} = 0.7138$.

$N_{\rm bins}$	$\varepsilon_{\rm max}$	$T_{\rm in}$ (MeV)	$({\rm net/frs})^{\rm (tol)}$	$N_{\rm eff}$	$T_{\rm cm}/T$	s	Y_P	D/H
100	20.0	8.0	30.0	3.043	0.7146	5.929×10^9	0.2426	2.628×10^{-5}
100	20.0	5.0	30.0	3.043	0.7146	5.930×10^9	0.2426	2.628×10^{-5}
100	20.0	2.0	30.0	3.045	0.7153	5.936×10^9	0.2426	2.634×10^{-5}

7.6.2 Error Monitoring

To monitor the errors in the collision integrals, we use the sum rules from Sec.7.5. Fig.7.2 shows the number and energy sum rules plotted against comoving temperature. As in Equations (7.35) and (7.36), the sum rules are wrt the processes of Tb.7.1 only involving neutrinos. We maintain accuracy to better than one part in 10^6 over the entire run. Both sum rules seem to exhibit discontinuities at the same temperatures in the form of steps in Fig.7.2. Actually, the scaled errors in the sum rules are both continuous over the entire temperature range. However, at certain temperatures, for example $T_{\rm cm} = 0.53$ MeV, the scaled errors change rapidly and cause a step–like feature when drawing the plot. We speculate that the rapid changes are only numerical, and due to the ε-values falling into different cases with changing m_ε (see Apps.F, G, and H). Future work will investigate the errors in more detail.

7.6.3 Neutrino spectra

Figures 7.3 to 7.6 show relative changes in the neutrino spectra. Fig.7.3 shows δf plotted against $T_{\rm cm}$ for $\varepsilon = 3, 5, 7$, while Fig.7.5 shows δf plotted against ε at a comoving temperature $T_{\rm cm} = 9.221$ keV. Fig.7.6 shows the normalized change in the differential energy density:

$$\frac{\Delta\left(\frac{d\rho}{d\varepsilon}\right)}{\rho} = \frac{\left[\frac{\varepsilon^3}{2\pi^2} f(\varepsilon) - \frac{\varepsilon^3}{2\pi^2} f^{(\rm eq)}(\varepsilon)\right]}{\frac{1}{2\pi^2}\int dx\, x^3 f^{(\rm eq)}(x)} \tag{7.41}$$

$$= \frac{\frac{\varepsilon^3}{2\pi^2}[f(\varepsilon) - f^{(\rm eq)}(\varepsilon)]}{\frac{7}{8}\frac{\pi^2}{30}} \tag{7.42}$$

$$= \frac{240}{14\pi^4}\varepsilon^3[f(\varepsilon) - f^{(\rm eq)}(\varepsilon)]. \tag{7.43}$$

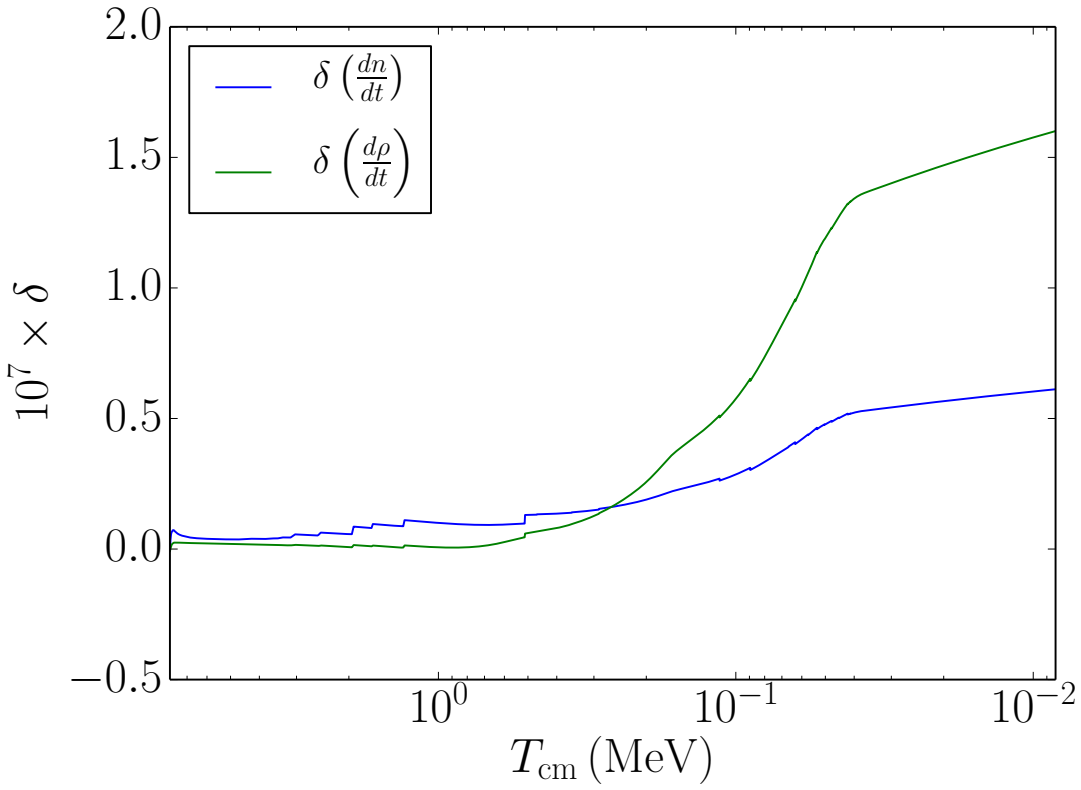

Figure 7.2: The total error in each sum rule plotted against the comoving temperature. The notation corresponds to Equations (7.35) and (7.36). For this run, $\varepsilon_{\rm max} = 20.0$, $N_{\rm bins} = 100$, $T_{\rm in} = 8$ MeV, and $({\rm net/frs})^{\rm (tol)} = 30.0$.

We only show curves for the electron and muon–flavor neutrinos. The tau flavor is identical to the muon flavor. The anti-neutrino behavior is nearly identical to the neutrino behavior for all flavors. Fig.7.4 show plots of the difference in relative change for neutrinos and anti-neutrinos:

$$\delta\overline{f} \equiv \delta f_{\nu} - \delta f_{\bar{\nu}} = \frac{f_{\nu} - f_{\bar{\nu}}}{f^{\rm (eq)}}. \tag{7.44}$$

For each ε-value in Fig.7.3, the relative change in the electron–flavor (ν_e) is larger than the relative change in the muon–flavor (ν_μ) neutrino sea. The annihilation and scattering rates with electrons and positrons are faster due to the addition of the charged–

current diagrams for ν_e over ν_μ. In addition to the larger perturbation of the spectra, the charged–current processes keep ν_e in thermal contact with the charged leptons longer than ν_μ. We see this by noticing the crossing of the $\varepsilon = 5$, ν_e curve with the $\varepsilon = 7$, ν_μ curve at $T_{\rm cm} \sim 0.8$ MeV. Although the curves are for different ε-values, the ν_μ freeze–out is occuring at a slightly earlier epoch than the ν_e freeze–out. The $\varepsilon = 5$ ν_e curve continues to rise at a more rapid rate and crosses the $\varepsilon = 7$, ν_μ curve. Fig.(4) of Ref.[116] also exhibits a crossing between the $\varepsilon = 5$, ν_e curve and the $\varepsilon = 7$, ν_μ curve. Comparing Fig.7.3 with Figs.(3a) and (3b) of DHS, we see a similar behavior between BURST and DHS. Our relative changes are larger for both ν_e and ν_μ.

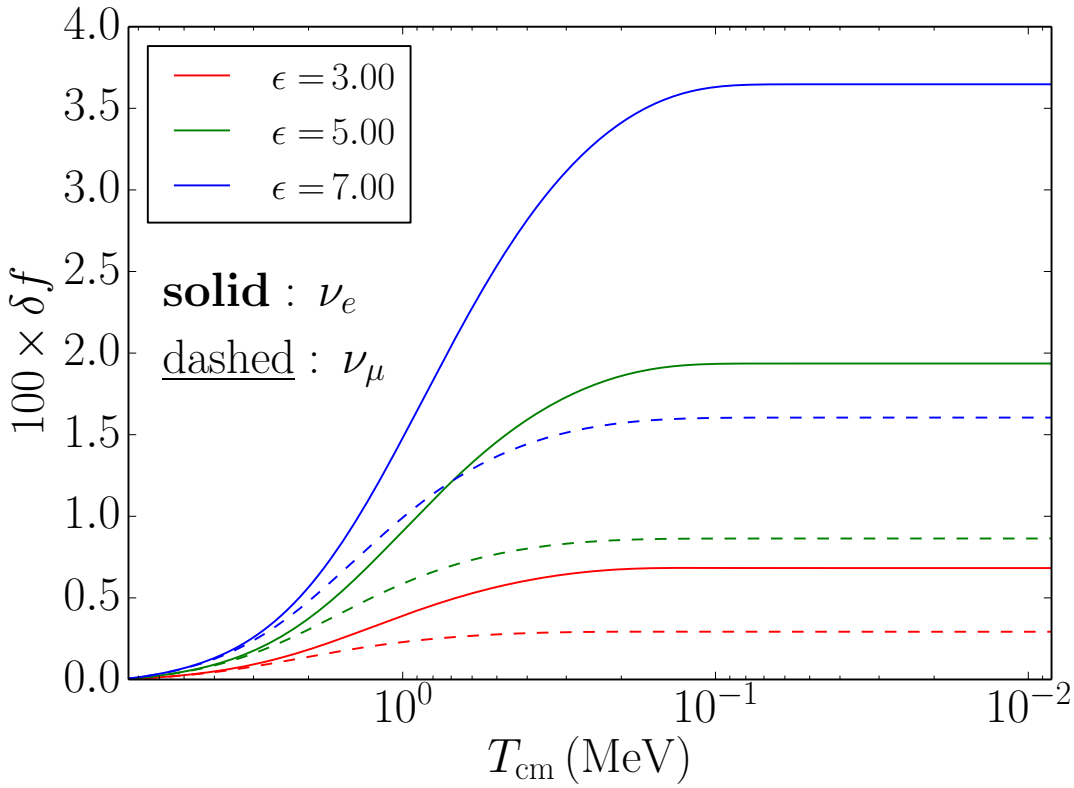

Figure 7.3: The relative change in the occupation probabilitiy plotted against comoving temperature $T_{\rm cm}$. Three abscissas are plotted: at $\varepsilon = 3, 5, 7$. The solid lines are for electron–flavor neutrinos, and the dashed lines are for muon–flavor neutrinos. For this run, $\varepsilon_{\rm max} = 20.0$, $N_{\rm bins} = 100$, $T_{\rm in} = 8$ MeV, and $({\rm net/frs})^{\rm (tol)} = 30.0$.

The asymmetry between neutrinos and anti-neutrinos is small. The non-zero baryon number induces a slight excess of electrons over positrons to compensate for the presence of protons. Fig.7.4 shows the difference in relative change of ν_e and $\bar{\nu}_e$, and also ν_μ and $\bar{\nu}_\mu$. The electron–flavor shows an enhanced effect over the muon–flavor for all ε-values. For both flavors at all ε-values in Fig.7.4, the relative changes are positive. The negative differences for $\varepsilon = 3$ indicate there is an abundance of anti-neutrinos over neutrinos, independent of flavor.

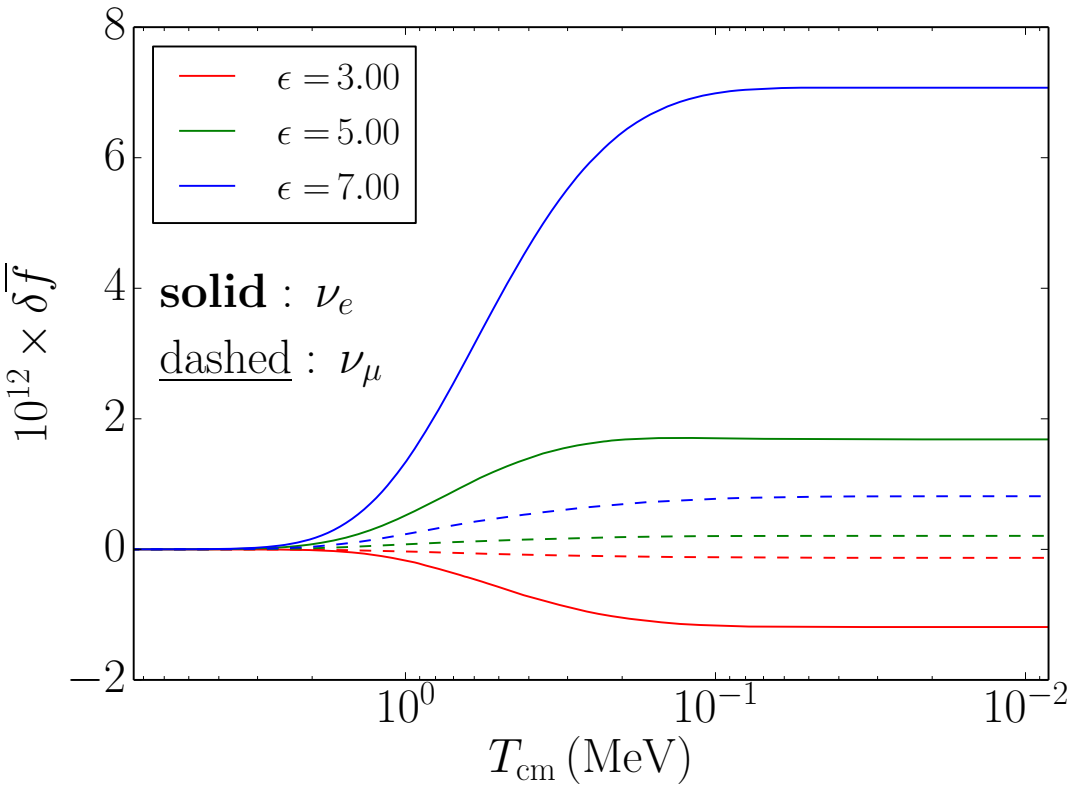

Figure 7.4: The difference in relative changes in the occupation probabilities of ν and $\bar{\nu}$ plotted against comoving temperature $T_{\rm cm}$. Three abscissas are plotted: at $\varepsilon = 3, 5, 7$. The solid lines are for electron–flavor neutrinos, and the dashed lines are for muon–flavor neutrinos. The ν_e experience a larger change than the ν_μ. For this run, $\varepsilon_{\rm max} = 20.0$, $N_{\rm bins} = 100$, $T_{\rm in} = 8$ MeV, and $(\text{net/frs})^{(\rm tol)} = 30.0$.

Fig.7.5 also shows that the ν_e have a larger relative change than the ν_μ. The spectra are plotted at a temperature of $T_{\rm cm} = 9.221$ keV, after the end of weak decoupling.

An interesting artifact of Fig.7.5 is the negative relative change for $\varepsilon \lesssim 1$. We make a conjecture that the elastic–scattering processes in rows 6 – 10 of Tb.7.1 deplete the low–energy occupation probabilities by upscattering. Fig.(5) of Ref.[116] also seems to show a negative value in the relative change from equilibrium at small ε-values. This is not explicitly mentioned by the authors of DHS, but Fig.(5) of DHS seems to show the same phenomenon for small ε-values. We mention that again, our relative changes are larger than those of DHS for both ν_e and ν_μ.

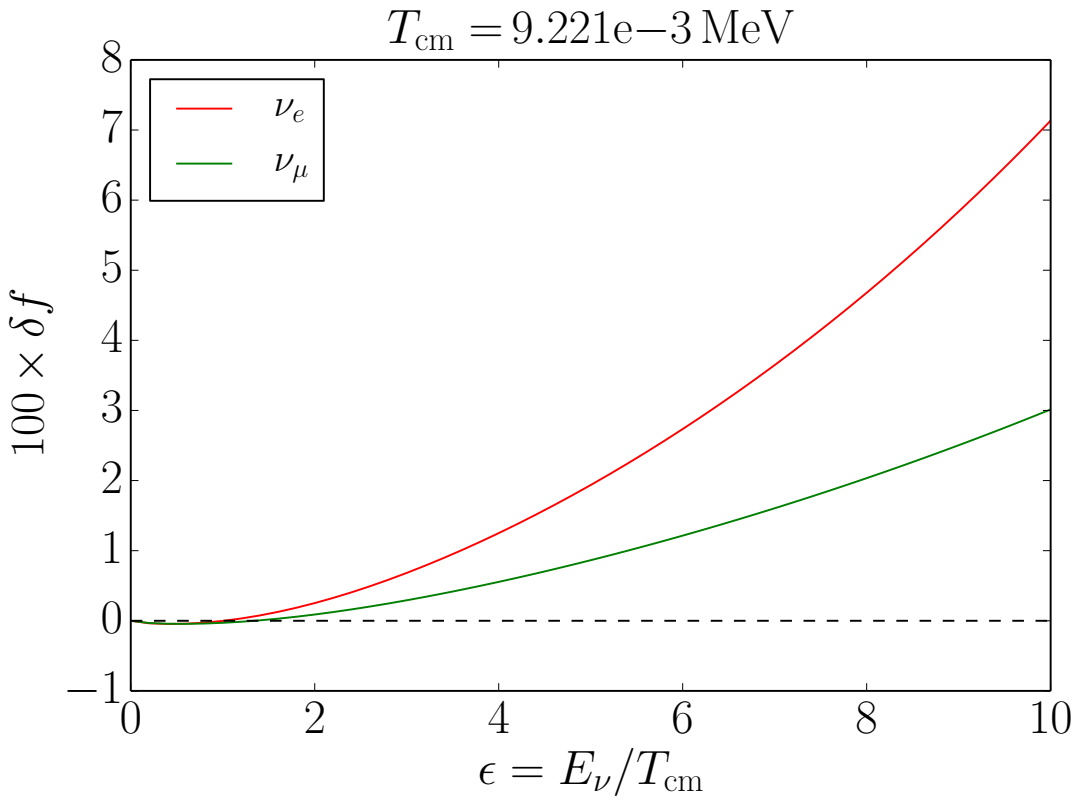

Figure 7.5: The relative change in the occupation probabilitiy plotted against ε. The larger change is the electron–flavor neutrinos, over the muon–flavor neutrinos. The anti-neutrino evolution is nearly identical to the neutrino evolution for all flavors. For this run, $\varepsilon_{\rm max} = 20.0$, $N_{\rm bins} = 100$, $T_{\rm in} = 8$ MeV, and $(\text{net/frs})^{(\text{tol})} = 30.0$.

The last spectra we show is in Fig.7.6. The comoving temperature in Fig.7.6 is the same as in Fig.7.5. Although Fig.7.5 shows the divergence from equilibrium of the

occupation probabilities increases for increasing ε-values, the probability is so small in the high–ε bins that the large changes from equilibrium have little effect on the total energy density. Fig.7.6 shows where the largest change in the energy–density spectrum occurs. In effect, Fig.7.6 is Fig.7.5 multiplied by ε^3. The peak of the normalized change in the differential energy density is located at $\varepsilon \sim 5$, for both ν_e and ν_μ. Fig.(6) of Ref.[116] also shows a peak at an $\varepsilon \sim 5$.

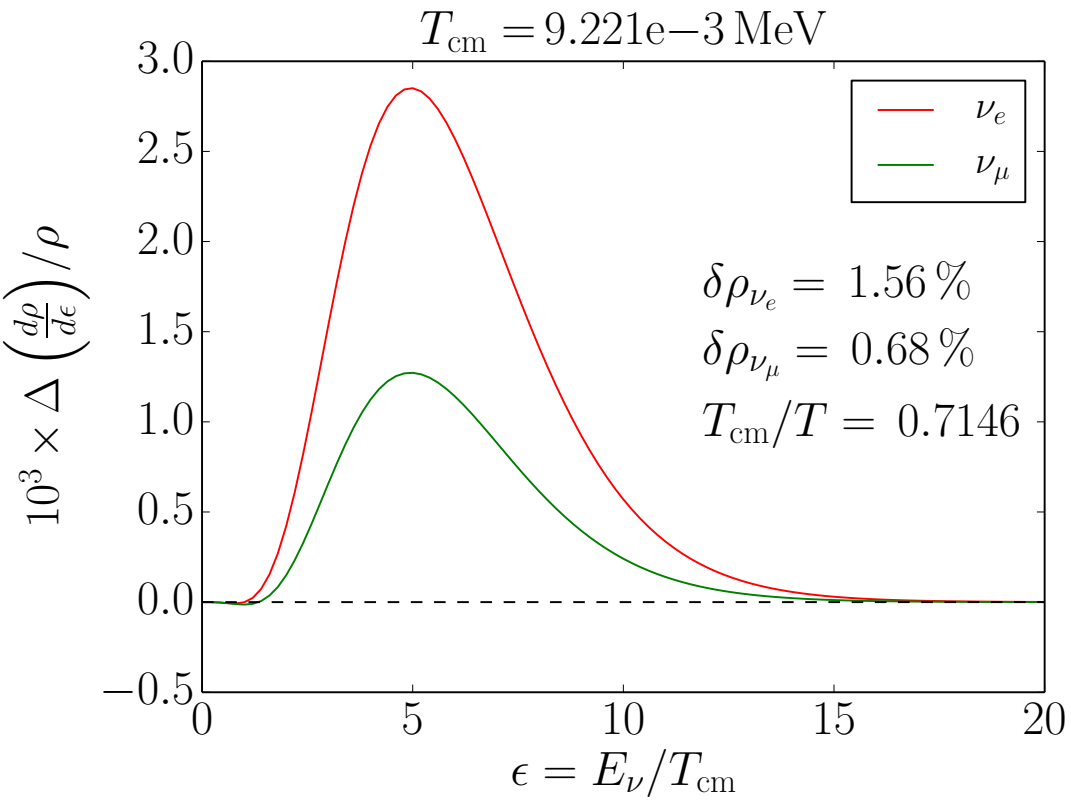

Figure 7.6: The normalized change in the differential energy density as a function of ε. The larger change is the electron–flavor neutrinos, over the muon–flavor neutrinos. The anti-neutrino evolution is nearly identical to the neutrino evolution for all flavors. For this run, $\varepsilon_{\rm max} = 20.0$, $N_{\rm bins} = 100$, $T_{\rm in} = 8$ MeV, and $(\text{net/frs})^{(\text{tol})} = 30.0$.

7.6.4 Entropy and $N_{\rm eff}$

The baryons and plasma constituents only interact with the neutrinos via gravitation at temperatures below the weak–decoupling and weak freeze–out scales. Therefore, we take the entropy–per–baryon, s, to be only the entropy in the plasma constituents which are thermally–coupled to the baryons. In the early universe, the entropy is dominated by relativistic species. The entropy is equivalent to the baryon density, which we obtain from CMB measurements of the temperature power spectrum. At photon decoupling, the only relativistic species coupled to the baryons is the photons. Ref.[2] gives the baryon density as $\omega_b = 0.022068$, equivalent to $s = 5.929 \times 10^9$. For the temperatures we investigate at weak decoupling, photons, electrons, and positrons are all present. Although the charged leptons are not ultra-relativistic, both species carry entropy. To first order, when electron–positron pairs begin to annihilate (the epoch of $e^{\pm}$–annihilation), the heat produced from the annihilations stays within the plasma – thereby maintaining the same value of the entropy. This is true to first order, ignoring the effects of weak–decoupling and nucleosynthesis.

The non-sharp weak–decoupling epoch precipitates a flow of heat from the elctromagnetic plasma to the neutrino seas. The heat flow $(\partial\rho_\nu/\partial t)|_{a,T}$ is directly proportional to the change in the entropy via the classical thermodynamic relation:

$$dS = \frac{dQ}{T} \implies \frac{ds}{dt} = \frac{1}{n_b T}\frac{\partial \rho_\nu}{\partial t}\bigg|_{a,T}. \tag{7.45}$$

There is also a heat flow due to nucleosynthesis, which we are ignoring. To reiterate, the change in energy density of the charged leptons stays within the plasma by heating the photons, and does not change the entropy. Fig.7.7 shows the temperature ranges spanning both the weak–decoupling and $e^{\pm}$–annihilation epochs. The curve labeled Entropy is the evolution of s wrt $T_{\rm cm}$. The curve labeled Ratio is the evolution of the temperature ratio

$T_{\rm cm}/T$ wrt $T_{\rm cm}$. The entropy curve illuminates the weak–decoupling epoch. The ratio curve illuminates the $e^{\pm}$–annihilation epoch.

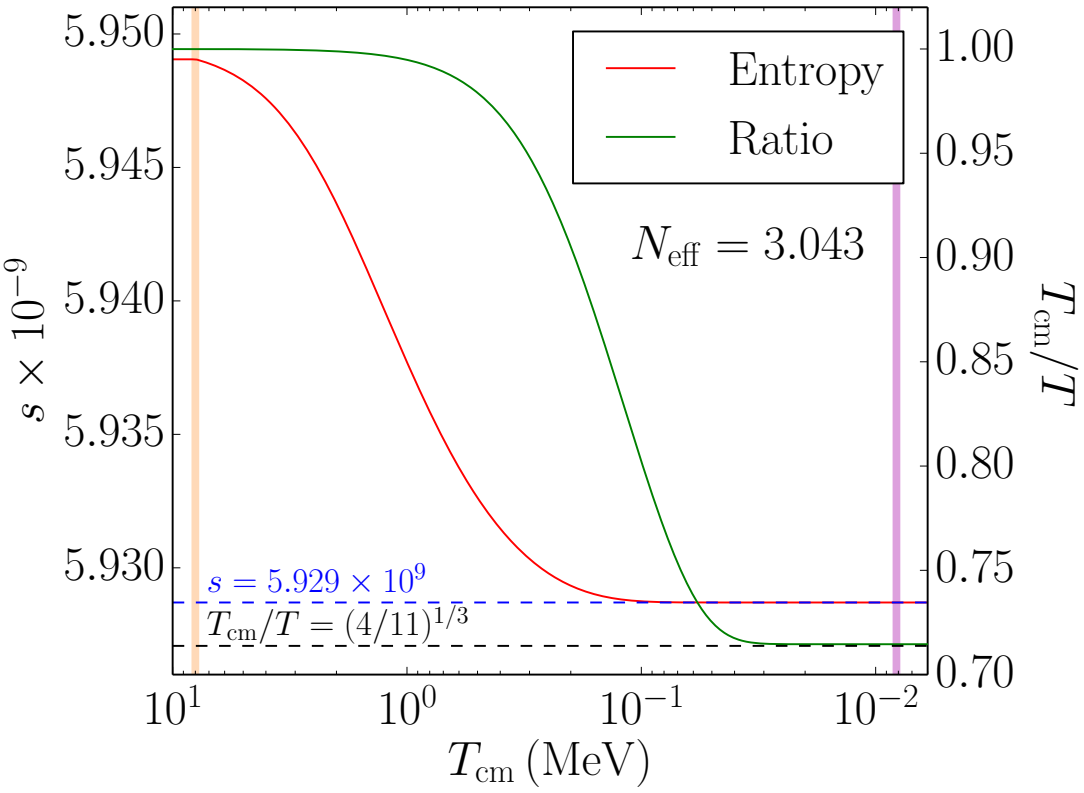

Figure 7.7: The entropy and temperature ratio as functions of comoving temperature. The red line is the evolution of the entropy per baryon, s, in the plasma as a function of comoving temperature, $T_{\rm cm}$. The green line is the evolution of the ratio of comoving temperature to plasma temperature, $T_{\rm cm}/T$ as a function of $T_{\rm cm}$. The blue dashed line is the entropy value as given by Ref.[2]. The black dashed line is the temperature ratio $T_{\rm cm}/T = (4/11)^{1/3}$. The first shaded line at high temperature corresponds to $T_{\rm in}$. The final temperature where the transport code finished is at the second shaded line. For this run, $\varepsilon_{\rm max} = 20.0$, $N_{\rm bins} = 100$, $T_{\rm in} = 8$ MeV, and $({\rm net/frs})^{\rm (tol)} = 30.0$.

Clearly the curves of Fig.7.7 are not coincident. However, there is a non-zero overlap between the two epochs, with weak decoupling beginning prior to $e^{\pm}$–annihilation. Furthermore, the weak–freeze–out and BBN epochs overlap both curves in Fig.7.7. The treatment of all four epochs requires a self-consistent calculation of the Boltzmann equations for weak, electromagnetic, and nuclear processes.

If we integrate the curves of Fig.7.6, we find relative changes in the energy density of:

$$\delta\rho_{\nu_e} = 0.0156, \tag{7.46}$$

$$\delta\rho_{\nu_\mu} = 0.0068. \tag{7.47}$$

The relative change in the neutrino energy density is:

$$\delta\rho_\nu = 0.0156 + 2 \times 0.0068 = 0.0292, \tag{7.48}$$

where we have multiplied $\delta\rho_{\nu_\mu}$ by 2 to account for the changes in the tau–flavor of neutrinos, and have not included anti-neutrinos. The value 0.0292 is wrt the equilibrium energy density for a temperature ratio $T_{\rm cm}/T = 0.7146$. If we want the relative change wrt an equilibrium energy density for a temperature ratio $T_{\rm cm}/T = (4/11)^{1/3}$, labeled as $\delta\rho_{(4/11)^{1/3}}$, we need to add 1 to each neutrino species, multiply by the ratio of temperature ratios to the fourth power, and subtract 1 for each neutrino species to yield:

$$\delta\rho_{(4/11)^{1/3}} = [(1+0.0156) + 2 \times (1+0.0068)] \times \left(\frac{0.7146}{(4/11)^{1/3}}\right)^4 - 3 = 0.0427. \tag{7.49}$$

Eq.(7.49) is equivalent to the change in $N_{\rm eff}$ as defined by Eq.(7.7). We use $\Delta N_{\rm eff} = 0.043$ to quantify the change in the radiation energy density from weak decoupling.

7.6.5 Nucleosynthesis

Assuming a sharp weak–decoupling epoch, the values for the primordial mass fraction of helium and relative abundance of deuterium (wrt to hydrogen) are:

$$Y_P = 0.2425, \tag{7.50}$$

$$\mathrm{D/H} = 2.615 \times 10^{-5}, \tag{7.51}$$

as calculated with the BBN network detailed in Ch.2. From our neutrino–energy–transport calculations, we find altered abundances of:

$$Y_P = 0.2426 \quad \Longrightarrow \delta(Y_P) \simeq 4 \times 10^{-4}, \tag{7.52}$$

$$\mathrm{D/H} = 2.628 \times 10^{-5} \Longrightarrow \delta(\mathrm{D/H}) \simeq 5 \times 10^{-3}. \tag{7.53}$$

Helium is sensitive to the neutron–to–proton ratio which is being altered by the presence of high–energy, electron–flavor, anti-neutrinos. Deuterium is sensitive to the baryon number which is changing due to heat flow out of the plasma during neutrino transport. Our preliminary calculations indicate that deuterium is more sensitive to weak–decoupling than helium.

7.7 Conclusion

The calculations detailed in Sec.7.6 are preliminary. The changes from $N_{\mathrm{eff}} = 3$ do not include the finite temperature QED effects from renormalization of the electron and photon masses as given in Refs.[30, 117]. In addition, other plasma effects, such as electron–positron screening, may also affect a small change in N_{eff}. The ultimate goal will be to include the QED effects, and then to expand the current Boltzmann–

solver code into a quantum–mechanical code using the QKEs of Ref.[12]. If the QKEs lead to an equilibration between ν_e and ν_μ (as highlighted in Figures 7.3 to 7.6), we would expect a decrease in $N_{\rm eff}$ due to the lack of a charged–current diagram in the ν_μ scattering processes. However, the QKE problem is inherently non-linear and requires a sophisticated calculation to verify quantitative and qualitative predictions.

BURST is a non-perturbative Boltzmann–solver code, similar to the code used in DHS. DHS calculated $N_{\rm eff} = 3.034$, while we obtained $N_{\rm eff} = 3.043$, a difference of $\sim 30\%$. We conclude this chapter with possible reasons for disagreement between DHS and BURST.

BBN makes a difference. BURST includes the heat density from nucleosynthesis, and a non-zero electron chemical potential. The inclusion of these terms may alter $N_{\rm eff}$. The binding–energy release from the formation of helium heats the plasma, and lowers the temperature ratio $T_{\rm cm}/T$. The lower ratio would decrease $N_{\rm eff}$. However, the higher plasma temperature leads to more scattering as the charged leptons are more energetic. This has the opposite effect and raises $N_{\rm eff}$. Therefore, we cannot determine how the binding–energy release from nucleosynthesis would alter $N_{\rm eff}$ a priori. We can perhaps glean the magnitude of the effect by examining the electron chemical potential. A non-zero chemical potential implies a larger total charged–lepton energy density. Fig.7.4 shows that the induced asymmetry between neutrinos and anti-neutrinos is orders of magnitude smaller than the changes from equilibrium, and therefore much too small to account for a 30% change. We opine that the changes from nucleosnythesis would be roughly the same order of magnitude as the changes from the charged–lepton asymmetry, and hence believe the inclusion of BBN is unlikely to be the cause of our high value of $N_{\rm eff}$.

The ODE driver is inadequate. Our driver to integrate the integral–differential, Boltzmann equations of Eq.(7.1) is similar to Ref.[26]. The algorithm is based off of an

explicit RK2 method, and the driver uses an adaptive time step. The author of Ref.[26] realized that the explicit RK2 method would not be adequate for the nuclear–reaction Boltzmann equations with a reasonable time step size constrained by the technology of the era. Although the nuclear reactions are non-linear, Ref.[26] linearized the Boltzmann equations and used the Jacobian matrix to recast the explicit RK2 method as a semi-implicit method. The neutrino-transport Boltzmann equations are also non-linear, yet have similar forms to the nuclear reactions which are 2×2. However, the task at hand is to determine the departures from FD equilibrium, not the flavor content of thermal–equilibrium neutrinos, which is the analog of the nucleosynthesis problem. Therefore, the linearization procedure of Ref.[26] is inadequate for our purposes. We therefore must devolve our algorithm to the explicit RK2 method, used to integrate the plasma temperature, scale factor, and electron chemical potential. DHS specifically mentions that their results are sensitive to the number of grid points in x, equivalent to the number of steps in time. DHS uses on order 4K points in x, where BURST uses on order 40K steps in time to maintain accuracy. The number of time steps may still not be enough, suggesting that we should use a different ODE driver.

Mistakes in the collision–integral coding. The coding of the collision terms of Eq.(7.21) is a major undertaking. It is quite possible that there could be mistakes in the code. Fig.7.2 shows errors much smaller than 30%. The errors in Fig.7.2 are at a specific time step and thus not cumulative. There are roughly 40K time steps in the weak–decoupling calculation. If we take the fractional error in the second sum rule for each time step to be $\sim 2 \times 10^{-7}$, and assume the errors add incoherently at each time step, the cumulative error is about 1%, smaller than the discrepancy with DHS by an order of magnitude. In addition, the curves of Figures 7.3, 7.5 and 7.6 all have the same shape as DHS and Ref.[116]. It would be highly unlikely that mistakes in the collision integrals of BURST produce results which are scaled versions of the accepted behavior.

Imprecision in the temperature derivative from Bessel functions. When we evolve the plasma temperature derivative through the weak–decoupling epoch, we can neither treat the charged leptons as ultra-relativistic nor ultra-massive. To compute the integrals of energy density and pressure for the charged leptons, we use modified Bessel functions of the second kind. We use two limits to calculate the Bessel functions: $m_\varepsilon > 2$; and $m_\varepsilon < 2$. For weak decoupling, $m_\varepsilon \sim 2$, the value where our approximations are the least accurate.

Errors in extrapolation. As mentioned in Sec.7.4.3, we have underestimated the occupation probabilities when extrapolating for $\varepsilon_{\rm max} < \varepsilon < 300.0$. There is very little energy density above $\varepsilon_{\rm max} = 20$. We use Boole's rule to integrate the neutrino energy density, and ignore the occupation probabilities for $\varepsilon > \varepsilon_{\rm max}$. The correct extrapolation would only be relevant during the calculation of the collision integrals and would lead to upscattering of the neutrinos. In the first case, the scattering would raise the energy density if the neutrino upscattered to an ε-value smaller than $\varepsilon_{\rm max}$. In the second case, the upscattering would lower the energy density if the neutrino upscattered to an ε-value larger than $\varepsilon_{\rm max}$. The vanishing amount of probability density with increasing ε would suggest this is a small error in either case.

Not enough runs to exhibit convergence. We have only included the results of three runs, identical to one another except for different input temperatures. We attempted to use the same computational parameters as DHS. We used an input temperature $T_{\rm in} = 8$ MeV, whereas DHS used $T_{\rm in} = 10$ MeV as the highest input temperature. The number of bins and maximum ε-value used in the binning are the same between us and DHS. We used a tolerance threshold of $({\rm net/frs})^{\rm (tol)} = 30.0$. DHS does not explicitly mention a tolerance threshold. Our value for $N_{\rm eff}$ will most likely change when we do more runs.

We thank Lauren Gilbert, Eric Michelsen, JJ Cherry, Vincenzo Cirigliano, and Daniel Plaschke for useful conversations with respect to cosmology, neutrino physics,

Fortran 90, and parallel computing. We acknowledge the Integrated Computing Network at Los Alamos National Laboratory for supercomputer time.

Chapter 7, in full, is a reprint of the material being prepared for submission of publication: Fuller, G. M.; Grohs, E.; Kishimoto, C. K.; Paris, M. W.; Vlasenko, A. “Energy transport in neutrino decoupling and big bang nucleosynthesis”. The dissertation author is the primary investigator and author of this paper.

Chapter 8

Conclusion

8.1 Summary

Our work included analysis on BBN, dilution, recombination, the νMR effect, BSM physics, and neutrino energy transport. We used a nuclear reaction network to study the departures from NSE so we can make predictions of the primordial abundances. We showed that the predictions made by our codes agree within two–sigma of observations. When investigating dilution, we presented the framework on how to calculate heavy–particle decay during weak decoupling and BBN. We were able to give estimates on changes to the abundances. In addition, dilution and other sectors of sterile neutrino physics challenged the interpretation of the quantity $N_{\rm eff}$. This led to the epiphany of using the sound horizon and photon diffusion length to develop the quantity $\tilde{N}_{\rm eff}$. The calculation of the photon difusion length required an extensive calculation of recombination. We showed how the role of neutrino rest mass in recombination produced counter intuitive effects when considering BSM physics, i.e. the νMR effect. Our results thus far were only revealed when we followed the neutrino spectra. The calculation of the non-thermal distortions to the spectra is a difficult computation in which we have made significant

progress. There is still much work remaining to solve the weak–decoupling problem.

8.2 Outlook

Cosmological considerations are a key route to exploring BSM physics. This is especially true for the neutrino sector, where there are many outstanding questions and where laboratory experiments are limited in what aspects of this physics can be addressed. In this work we have argued that a self consistent treatment of BSM issues, across all epochs from weak decoupling to photon decoupling, is the best way to take advantage of the expected coming increase in precision of CMB measurements and observationally-inferred primordial abundances of the light elements. We employ a limited prescription to link the salient features of self consistency between early-time neutrino dynamics and the surface of last scattering. We couple the weak decoupling and nucleosynthesis of early times to CMB observables, including baryon-to-photon ratio (equivalently ω_b), sound horizon, and photon diffusion length.

We have shown that such a self consistent treatment is necessary, in part because new neutrino physics can alter the relationships between different cosmological epochs. For example, ω_b and other CMB observables affect the calculated yields of deuterium and helium. In addition, the calculated relic neutrino energy spectra after weak decoupling affects the predicted value of $\tilde{N}_{\rm eff}$ at photon decoupling. The principal tool in our analysis is the suite of BURST codes for nucleosynthesis and neutrino interactions and energy transport.

A case in point is our investigation of the relationship between neutrino rest masses, i.e. $\sum m_\nu$, and the four potential observables ω_b, $\tilde{N}_{\rm eff}$, Y_P, and D/H. This analysis reveals the "neutrino-mass/recombination" (νMR) effect first described in Ref. [58]. The νMR effect is below the threshold of current CMB capabilities, but may not be in future

observations [70].

There have been spectacular advances in the measurements/observations of neutrino properties. We know the neutrino mass-squared differences and three of the four parameters in the unitary transformation between the energy eigenstates (mass states) and the weak interaction eigenstates (flavor states) of the three active neutrinos (only the *CP*-violating phase remains unmeasured). As active neutrinos mix in vacuum and have non-zero rest masses, the question indubitably arises of whether there exist "sterile" neutrino states. If indeed sterile neutrinos do exist, we acknowledge that the parameter space of mass, vacuum mixing angle, and number is enormous. However, sterile neutrinos could have profound effects in all of the epochs under study in this work. This possibility makes a self consistent treatment of these effects a powerful basis for constraining sterile neutrino states.

In this work we have considered scenarios for both "light" (mass $\sim 1\,\mathrm{eV}$) and "heavy" (mass $\sim 0.1 - 1\,\mathrm{GeV}$) sterile neutrinos. In the former case we consider cases where the sterile neutrino relic energy spectra are Fermi-Dirac black-body shaped, though with a temperature parameter T_s differing from that characterizing the relic energy spectra of active neutrino species. We show here that the νMR effect has interesting consequences and that this case *demands* a self consistent treatment of recombination and BBN. Additionally, heavy sterile neutrino decay out of equilibrium can lead to dilution and high energy relic active neutrinos, and both of these features potentially can have dramatic and constrainable effects on CMB-epoch observables. This implies that CMB observations can indirectly probe the CνB and explore active-sterile mass/vacuum-mixing parameter space unavailable to current accelerator-based experiments.

We have also studied the effects of non-zero lepton numbers on the relationship between CMB observables, nucleosynthesis, and neutrino physics. Our conclusion is that the primordial deuterium abundance is a potentially powerful probe of lepton number.

However, an eventual CMB-*only* measurement of the primordial helium abundance Y_P will be the most powerful probe of lepton number and many other issues. Determining Y_P from CMB observables will require a sophisticated self-consistent approach to BBN, neutrino physics, and photon decoupling transport physics.

Finally, our study has revealed a potential tension between $\tilde{N}_{\rm eff}$, ω_b, and the primordial deuterium abundance, D/H, inferred from high redshift QSO absorption systems. In fact, if the advent of 30-m class telescopes in the near future allows for a decrease in errors in observationally-inferred D/H to the $\sim 1\,\%$ level, while observed ω_b and $\tilde{N}_{\rm eff}$ maintain their respective current central values, then tension is unavoidable. This may signal BSM or non-CSM physics, likely in the neutrino sector, or it could point to not understanding systematics in the damped Lyman-α cloud measurements of the isotope-shifted hydrogen absorption lines. We advocate using future instruments to explore the rich physics of weak decoupling, nucleosynthesis, and photon decoupling to discover what role BSM neutrino physics has in these epochs.

8.3 Future Work

The BURST code is still under development. The goal is to have a version of BURST suitable for public release in the Fall of 2018. BURST will include the following physics:

1. A unitary nuclear reaction network.
2. A neutrino energy and flavor transport network.
3. An independent three–level computation of recombination.
4. A Boltzmann–equation treatment of the advent of LSS in BSM physics scenarios.
5. A call to a CMB Boltzmann code to calculate power spectra.

It will be available to members of the community who wish to test BSM physics in the cosmological laboratory. The code is a modular architecture using Fortran90/95 and OPENMPI.

With BURST, we will be able to investigate multiple physical phenomena. We now know the QKEs in an analytical form. Ref.[12] presents the QKEs in a general context, but also with the goal of applying the techniques to the core–collapse supernova (CCSN) problem. Coding the QKEs into a CCSN computation has not been done, and is a daunting undertaking. However, the early universe provides a medium with a high degree of symmetry, simplifying the problem immensely. Once we have a working QKE code, we will have the ability to follow the evolution of active–neutrino lepton numbers, and sterile–neutrino–phase–space occupation probabilities. An early universe QKE code will provide the proof of concept that the QKEs are indeed solvable. We can further develop our methods to employ QKE techniques in other exotic environments which have much less symmetry, such as CCSN and neutron star mergers.

Work on neutrino magnetic moments[119] has shown intriguing possibilities for postponement of weak decoupling and alteration of primordial abundances and $N_{\rm eff}$. The summed–squared–amplitudes for neutrino–electron interactions through a magnetic moment are similar to Klein–Nishina amplitudes. BURST will be able to integrate those Boltzmann equations to calculate scattering rates and give accurate predictions of Y_P, D/H, $N_{\rm eff}$, and $\sum m_\nu$. A self-consistent treatment of heavy–particle decay has implications for sterile–neutrino[16] and axion[120] dark matter. BURST is suitable for ΛCDM. However, the code has the flexibility to study significant deviations of the fundamental constants from their accepted values. Theories of the multiverse predict an infinite number of alternate universes where the fundamental constants could differ from the values of our universe[121, 122].

Section 8.2 is a reprint of some of the material as it appears in "Probing neutrino physics with a self-consistent treatment of the weak decoupling, nucleosynthesis, and photon decoupling epochs." Grohs, E.; Fuller, G. M.; Kishimoto, C. K.; Paris, M. W., J. Cosmology Astropart., 5 (May 2015) 17. The dissertation author was the primary investigator and author of this paper.

Appendix A

Nucleosynthesis linearization procedure

The reaction of interest is:

$$N_i({}^{A_i}X_{z_i}) + N_j({}^{A_j}X_{z_j}) \leftrightarrow N_k({}^{A_k}X_{z_k}) + N_l({}^{A_l}X_{z_l}). \tag{A.1}$$

The symbols in Eq.(A.1) have the following meaning:

$$N_m : \text{The number of nuclides of species } m \text{ in the reaction} \tag{A.2}$$

$$A_m : \text{The atomic mass number of species } m \tag{A.3}$$

$$z_m : \text{The atomic number of species } m. \tag{A.4}$$

We adopt the convention in Eq.(A.1) that $A_i \geq A_j$ and $A_l \geq A_k$. The rate of destruction/creation of nuclide i is:

$$\left.\frac{dn_i}{dt}\right|_{ij\to kl} = -N_i \frac{n_i^{N_i} n_j^{N_j}}{N_i! N_j!} R_{kl,ij} \text{ (destruction)} \tag{A.5}$$

$$\left.\frac{dn_i}{dt}\right|_{kl\to ij} = N_i \frac{n_k^{N_k} n_l^{N_l}}{N_k! N_l!} R_{ij,kl} \text{ (creation)}, \tag{A.6}$$

where n_m is the number density of species m, $R_{kl,ij}$ is the reaction coefficient for projectile j on target i synthesizing products k and l, and $R_{ij,kl}$ is the same quantity as the previous except with opposite projectile, target, and products. The overall N_i factor corresponds to how many i particles the reaction creates/destroys, and the factorial terms are symmetrization factors. We have already made the Boltzmann approximation in Eqs.(A.5) and (A.6). In the case that $N_i = N_j = 1$, the reaction coefficient $R_{kl,ij} = \langle \sigma v \rangle_{kl,ij}$, the thermally averaged product of cross section and relative velocity for projectile j and target i. In terms of abundances, the net rate for the change in Y_i for the specific Rxn.(A.1) is:

$$\left.\frac{dY_i}{dt}\right|_{ij\leftrightarrow kl} = N_i \left(-\frac{Y_i^{N_i} Y_j^{N_j}}{N_i! N_j!} [ij]_{kl} + \frac{Y_l^{N_l} Y_k^{N_k}}{N_l! N_k!} [lk]_{ij} \right), \tag{A.7}$$

where $[ij]_{kl}$ is the reaction coefficient multiplied by the proper amount of factors of n_b, the baryon density. It is customary to call $[ij]_{kl}$ the reaction rate. Eq.(A.7) is for only one specific process, namely $ij \leftrightarrow kl$. To find the total change in the abundance Y_i for all reactions involving Y_i, we sum over the different projectiles and products[26]:

$$\frac{dY_i}{dt} = \sum_{j,k,l} N_i \left(-\frac{Y_i^{N_i} Y_j^{N_j}}{N_i! N_j!} [ij]_{kl} + \frac{Y_l^{N_l} Y_k^{N_k}}{N_l! N_k!} [lk]_{ij} \right). \tag{A.8}$$

Eq.(A.8) is exactly how it appears in Ref.[26]. There are three points to note in Eq.(A.8). First, it is tempting to bring the number N_i outside of the summation because the index

i is a free index. However, N_i is paricular to the reaction $ij \leftrightarrow kl$. In fact, all of the quantities in Eq.(A.8) are particular to the specific reaction, and must remain within the inner summation. Second, Eq.(A.8) assumes that for a set of $\{i, j, k, l\}$ nuclides, there is at most one reaction relating those nuclides. In other words, there is only one set of $\{N_i, N_j, N_k, N_l\}$ for the transmutation $ij \leftrightarrow kl$. Third, it would seem to imply that the summation limits of Eq.(A.8) are from 1 to the number of nuclides, $N_{\rm nuc}$. This is not the case. We explicitly give the limits on the summations:

$$\frac{dY_i}{dt} = \sum_{j=1}^{N_{\rm nuc}} \sum_{k=1}^{N_{\rm nuc}} \sum_{l=k}^{N_{\rm nuc}} N_i \left(-\frac{Y_i^{N_i} Y_j^{N_j}}{N_i! N_j!} [ij]_{kl} + \frac{Y_l^{N_l} Y_k^{N_k}}{N_l! N_k!} [lk]_{ij} \right), \tag{A.9}$$

where the limits are explicit to avoid double-counting. Eq.(A.9) uses the convention when $j = i$, $N_j = 0$ and $N_i \geq 1$. The same applies to $k = l$: $N_k = 0$ and $N_l \geq 1$. There are many impossibilities in Eq.(A.9). For example, the reaction $d + n \leftrightarrow p + {}^7$Be is allowed in Eq.(A.9), but is physically impossible. In this case, $[ij]_{kl} = [lk]_{ij} = 0$. Eq.(A.9) is non-linear. We will linearize it for a specific ODE integration algorithm.

We investigate the linear differential equation:

$$\mathbf{Y}' = -\mathbf{C} \cdot \mathbf{Y}, \tag{A.10}$$

where $\mathbf{Y}$ is a vector of dependent variables, $\mathbf{Y}'$ is the first derivative of $\mathbf{Y}$ with respect to the independent variable, and $\mathbf{C}$ is a positive-definite matrix independent of any of the components of $\mathbf{Y}$. For our purposes, the independent variable is time t, and the dependent variables are the abundances. To numerically integrate Eq.(A.10), we step through time

with index h. To first order, an explicit method gives:

$$\mathbf{Y}^{(h+1)} = \mathbf{Y}^{(h)} + \Delta t \mathbf{Y}^{(h)'} \tag{A.11}$$

$$\mathbf{Y}^{(h+1)} = \mathbf{Y}^{(h)} - \Delta t \mathbf{C} \cdot \mathbf{Y}^{(h)} \tag{A.12}$$

$$= (\mathbf{1} - \Delta t \mathbf{C}) \cdot \mathbf{Y}^{(h)}. \tag{A.13}$$

If the largest eigenvalue of $\mathbf{C}$ is $\lambda_{\max}$, then Eq.(A.13) is unstable if:

$$\Delta t > \frac{2}{\lambda_{\max}}. \tag{A.14}$$

Therefore, we investigate the following implicit equation:

$$\mathbf{Y}^{(h+1)} = \mathbf{Y}^{(h)} + \Delta t \mathbf{Y}^{(h+1)'} \tag{A.15}$$

$$\mathbf{Y}^{(h+1)} = \mathbf{Y}^{(h)} - \Delta t \mathbf{C} \cdot \mathbf{Y}^{(h+1)} \tag{A.16}$$

$$\implies (\mathbf{1} + \Delta t \mathbf{C}) \cdot \mathbf{Y}^{(h+1)} = \mathbf{Y}^{(h)} \tag{A.17}$$

$$\implies \mathbf{Y}^{(h+1)} = (\mathbf{1} + \Delta t \mathbf{C})^{-1} \cdot \mathbf{Y}^{(h)}, \tag{A.18}$$

which is stable for all eigenvalues of $\mathbf{C}$. We must construct the matrix $(\mathbf{1} + \Delta t \mathbf{C})$ and invert it to find the dependent values at the next time step. We will use the symbol $\mathbf{f}$ for the vector of derivatives of Eq.(A.9):

$$f_i(\mathbf{Y}) \equiv \frac{dY_i}{dt}. \tag{A.19}$$

Eq.(A.9) and by extension Eq.(A.19) are non-linear in Y_i. To linearize the derivatives of $\mathbf{Y}$, we use Newton's method[108]:

$$\mathbf{Y}^{(h+1)} = \mathbf{Y}^{(h)} + \Delta t \left[\mathbf{f}(\mathbf{Y}^{(h)}) + \left. \frac{\partial \mathbf{f}}{\partial \mathbf{Y}} \right|_{\mathbf{Y}=\mathbf{Y}^{(h)}} \cdot (\mathbf{Y}^{(h+1)} - \mathbf{Y}^{(h)}) \right]. \tag{A.20}$$

We need to solve for the expression in brackets. Subtracting the bracketed expression from Eq.(A.20) will give us the $(\mathbf{1}+\Delta t\mathbf{C})$ matrix on the left-hand-side. We adopt the following notation:

$$\overline{\mathbf{Y}} = \mathbf{Y}^{(h+1)} \tag{A.21}$$

$$\widetilde{\mathbf{Y}} = \mathbf{Y}^{(h)}. \tag{A.22}$$

Consider a single component, i, of the vector expression in brackets in Eq.(A.20):

$$f_i(\widetilde{\mathbf{Y}}) + \left.\frac{\partial f_i}{\partial \mathbf{Y}}\right|_{\mathbf{Y}=\widetilde{\mathbf{Y}}} \cdot (\overline{\mathbf{Y}} - \widetilde{\mathbf{Y}}) = f_i(\widetilde{\mathbf{Y}}) + \sum_{m=1}^{N_{\text{nuc}}} \left.\frac{\partial f_i}{\partial Y_m}\right|_{\mathbf{Y}=\widetilde{\mathbf{Y}}} (\overline{Y}_m - \widetilde{Y}_m). \tag{A.23}$$

We need to compute the partial derivative:

$$\frac{\partial f_i}{\partial Y_m} = \frac{\partial}{\partial Y_m} \sum_{j=1}^{N_{\text{nuc}}} \sum_{k=1}^{N_{\text{nuc}}} \sum_{l=k}^{N_{\text{nuc}}} \left(-\frac{N_i[ij]_{kl}}{N_i!N_j!} Y_i^{N_i} Y_j^{N_j} + \frac{N_i[lk]_{ij}}{N_l!N_k!} Y_l^{N_l} Y_k^{N_k} \right) \tag{A.24}$$

$$\begin{aligned} &= \sum \left[-\frac{N_i[ij]_{kl}}{N_i!N_j!} (N_i Y_i^{N_i-1} Y_j^{N_j} \delta_{im} + N_j Y_j^{N_j-1} Y_i^{N_i} \delta_{jm}) \right. \\ &\left. + \frac{N_i[lk]_{ij}}{N_l!N_k!} (N_k Y_k^{N_k-1} Y_l^{N_l} \delta_{km} + N_l Y_l^{N_l-1} Y_k^{N_k} \delta_{lm}) \right] \end{aligned} \tag{A.25}$$

The summation in Eq.(A.23) becomes something akin to:

$$\simeq \sum_{m=1}^{N_{\rm nuc}} \sum \left[-\frac{N_i[ij]_{kl}}{N_i!N_j!}(N_i\widetilde{Y}_i^{N_i-1}\widetilde{Y}_j^{N_j}\delta_{im}+N_j\widetilde{Y}_j^{N_j-1}\widetilde{Y}_i^{N_i}\delta_{jm})(\overline{Y}_m-\widetilde{Y}_m) \right.$$
$$\left. + \frac{N_i[lk]_{ij}}{N_l!N_k!}(N_k\widetilde{Y}_k^{N_k-1}\widetilde{Y}_l^{N_l}\delta_{km}+N_l\widetilde{Y}_l^{N_l-1}\widetilde{Y}_k^{N_k}\delta_{lm})(\overline{Y}_m-\widetilde{Y}_m) \right] \quad \text{(A.26)}$$

$$= \sum \sum_{m=1}^{N_{\rm nuc}} \left[-\frac{N_i[ij]_{kl}}{N_i!N_j!}(N_i\widetilde{Y}_i^{N_i-1}\widetilde{Y}_j^{N_j}\delta_{im}+N_j\widetilde{Y}_j^{N_j-1}\widetilde{Y}_i^{N_i}\delta_{jm})(\overline{Y}_m-\widetilde{Y}_m) \right.$$
$$\left. + \frac{N_i[lk]_{ij}}{N_l!N_k!}(N_k\widetilde{Y}_k^{N_k-1}\widetilde{Y}_l^{N_l}\delta_{km}+N_l\widetilde{Y}_l^{N_l-1}\widetilde{Y}_k^{N_k}\delta_{lm})(\overline{Y}_m-\widetilde{Y}_m) \right] \quad \text{(A.27)}$$

$$= \sum \left\{ -\frac{N_i[ij]_{kl}}{N_i!N_j!}[N_i\widetilde{Y}_i^{N_i-1}\widetilde{Y}_j^{N_j}(\overline{Y}_i-\widetilde{Y}_i)+N_j\widetilde{Y}_j^{N_j-1}\widetilde{Y}_i^{N_i}(\overline{Y}_j-\widetilde{Y}_j)] \right.$$
$$\left. + \frac{N_i[lk]_{ij}}{N_l!N_k!}[N_k\widetilde{Y}_k^{N_k-1}\widetilde{Y}_l^{N_l}(\overline{Y}_k-\widetilde{Y}_k)+N_l\widetilde{Y}_l^{N_l-1}\widetilde{Y}_k^{N_k}(\overline{Y}_l-\widetilde{Y}_l)] \right\} \quad \text{(A.28)}$$

$$= \sum \left\{ -\frac{N_i[ij]_{kl}}{N_i!N_j!}[N_i\widetilde{Y}_i^{N_i-1}\widetilde{Y}_j^{N_j}\overline{Y}_i+N_j\widetilde{Y}_j^{N_j-1}\widetilde{Y}_i^{N_i}\overline{Y}_j-(N_i+N_j)\widetilde{Y}_i^{N_i}\widetilde{Y}_j^{N_j}] \right.$$
$$\left. + \frac{N_i[lk]_{ij}}{N_l!N_k!}[N_k\widetilde{Y}_k^{N_k-1}\widetilde{Y}_l^{N_l}\overline{Y}_k+N_l\widetilde{Y}_l^{N_l-1}\widetilde{Y}_k^{N_k}\overline{Y}_l-(N_k+N_l)\widetilde{Y}_k^{N_k}\widetilde{Y}_l^{N_l}] \right\}. \quad \text{(A.29)}$$

We have used the symbol $\simeq$ instead of $=$ on Eq.(A.26) because Eq.(A.26) glosses over an important point. We are linearizing the expression in brackets in Eq.(A.20). We are only looking at the $i^{\rm th}$ component in Eq.(A.23). This process produces terms in the summation that are linear in $\overline{Y}_i$, $\overline{Y}_j$, $\overline{Y}_k$, and $\overline{Y}_l$. If we consider two separate free indicies, i and $i^{'}$, they each have an expression like Eq.(A.29). For the expression for i, the dummy indicies j,k,l may assume the index $i^{'}$ for a specific reaction. We label that reaction $R_{ijkl}=R_{ii^{'}kl}$ where the index j assumed $i^{'}$ in this example. Conversely, in the expression for $i^{'}$, the dummy indicies j,k,l will assume the index i for the reaction $R_{i^{'}ikl}$. This is tantamount to calling i the target and $i^{'}$ the projectile in $R_{ii^{'}kl}$, and vice-versa for $R_{i^{'}ikl}$. There is no difference physically, i.e. $R_{ii^{'}kl}=R_{i^{'}ikl}$ and the terms in the summation are simply index permutations and thus identical. Therefore, we have double-counted in Eq.(A.29). To correct for the double-counting in the i,j indicies, we need to divide each factor in the

first bracketed expression of Eq.(A.29) by $N_i + N_j$. To correct for double-counting in the k,l indicies, we divide each factor in the second bracketed expression of Eq.(A.29) by $N_k + N_l$. leaving us with:

$$
\begin{aligned}
&= \sum \Bigg\{ -\frac{N_i[ij]_{kl}}{N_i!N_j!(N_i+N_j)}[N_i\widetilde{Y}_i^{N_i-1}\widetilde{Y}_j^{N_j}\overline{Y}_i + N_j\widetilde{Y}_j^{N_j-1}\widetilde{Y}_i^{N_i}\overline{Y}_j - (N_i+N_j)\widetilde{Y}_i^{N_i}\widetilde{Y}_j^{N_j}] \\
&+ \frac{N_i[lk]_{ij}}{N_l!N_k!(N_k+N_l)}[N_k\widetilde{Y}_k^{N_k-1}\widetilde{Y}_l^{N_l}\overline{Y}_k + N_l\widetilde{Y}_l^{N_l-1}\widetilde{Y}_k^{N_k}\overline{Y}_l - (N_k+N_l)\widetilde{Y}_k^{N_k}\widetilde{Y}_l^{N_l}] \Bigg\} \qquad \text{(A.30)} \\
&= \sum \Bigg\{ -\frac{N_i[ij]_{kl}}{N_i!N_j!(N_i+N_j)}[N_i\widetilde{Y}_i^{N_i-1}\widetilde{Y}_j^{N_j}\overline{Y}_i + N_j\widetilde{Y}_j^{N_j-1}\widetilde{Y}_i^{N_i}\overline{Y}_j] \\
&+ \frac{N_i[lk]_{ij}}{N_l!N_k!(N_k+N_l)}[N_k\widetilde{Y}_k^{N_k-1}\widetilde{Y}_l^{N_l}\overline{Y}_k + N_l\widetilde{Y}_l^{N_l-1}\widetilde{Y}_k^{N_k}\overline{Y}_l] \Bigg\} \\
&- \sum N_i \left(-\frac{Y_i^{N_i}Y_j^{N_j}}{N_i!N_j!}[ij]_{kl} - \frac{Y_l^{N_l}Y_k^{N_k}}{N_l!N_k!}[lk]_{ij} \right) \qquad \text{(A.31)} \\
&= \sum \Bigg\{ -\frac{N_i[ij]_{kl}}{N_i!N_j!(N_i+N_j)}[N_i\widetilde{Y}_i^{N_i-1}\widetilde{Y}_j^{N_j}\overline{Y}_i + N_j\widetilde{Y}_j^{N_j-1}\widetilde{Y}_i^{N_i}\overline{Y}_j] \\
&+ \frac{N_i[lk]_{ij}}{N_l!N_k!(N_k+N_l)}[N_k\widetilde{Y}_k^{N_k-1}\widetilde{Y}_l^{N_l}\overline{Y}_k + N_l\widetilde{Y}_l^{N_l-1}\widetilde{Y}_k^{N_k}\overline{Y}_l] \Bigg\} - f_i(\overline{\mathbf{Y}}), \qquad \text{(A.32)}
\end{aligned}
$$

implying that the expression for Newton's formula for the $i^{(th)}$ component is:

$$
\begin{aligned}
f_i(\widetilde{\mathbf{Y}}) + \left.\frac{\partial f_i}{\partial \mathbf{Y}}\right|_{\mathbf{Y}=\widetilde{\mathbf{Y}}} \cdot (\overline{\mathbf{Y}} - \widetilde{\mathbf{Y}}) = \sum \Bigg\{ &-\frac{N_i[ij]_{kl}}{N_i!N_j!(N_i+N_j)}[N_i\widetilde{Y}_i^{N_i-1}\widetilde{Y}_j^{N_j}\overline{Y}_i + N_j\widetilde{Y}_j^{N_j-1}\widetilde{Y}_i^{N_i}\overline{Y}_j] \\
&+ \frac{N_i[lk]_{ij}}{N_l!N_k!(N_k+N_l)}[N_k\widetilde{Y}_k^{N_k-1}\widetilde{Y}_l^{N_l}\overline{Y}_k + N_l\widetilde{Y}_l^{N_l-1}\widetilde{Y}_k^{N_k}\overline{Y}_l] \Bigg\}. \qquad \text{(A.33)}
\end{aligned}
$$

Eq.(A.33) is linear in $\overline{\mathbf{Y}}$ and the same expression in Ref.[26].

We acknowledge Mark Paris for useful discussions.

Appendix B

Charged lepton annihilation into photons

B.1 Determining the integral over u

We are interested in the following process:

$$e^-(1) + e^+(2) \to \gamma(3) + \gamma(4). \tag{B.1}$$

The matrix element for this process is the Klein-Nishina matrix element and looks like:

$$\langle |\mathcal{M}|^2 \rangle \sim \lambda (Q_1 \cdot Q_2)(Q_1 \cdot P_3). \tag{B.2}$$

We will adopt the notation that Q_i is the four-momentum of a massive particle and P_j is the four-momentum of a massless particle. λ is a constant and is related to the fine-structure constant and the electron mass. There are other terms in the Klein-Nishina matrix element, but those other terms have a similar form to Eq.B.2. Unfortunately, Eq.B.2 cannot be simplified using conservation of four-momentum like was done when

using neutrino matrix elements. Thus, we will attempt to derive a new expression for the transport rates.

To understand the form of Eq.B.2, we need to define the angles between the three-vectors. Let's define the angle θ_2 such that:

$$Q_1 \cdot Q_2 = E_1 E_2 - q_1 q_2 \cos\theta_2, \tag{B.3}$$

where E_i is the energy and q_i is the magnitude of the three-momentum of particle i. For P_3, let's define θ_3 as the angle between $\vec{q}_1 + \vec{q}_2$ and $\vec{p}_3$:

$$(\vec{q}_1 + \vec{q}_2) \cdot \vec{p}_3 = |\vec{q}_1 + \vec{q}_2| p_3 \cos\theta_3. \tag{B.4}$$

Using Eq.B.4 for our definition of θ_3, we arrive at the following expression for the four-momenta product:

$$Q_1 \cdot P_3 = E_1 p_3 - \frac{q_1 p_3}{|\vec{q}_1 + \vec{q}_2|}[\cos\theta_3(q_1 + q_2\cos\theta_2) + \sin\theta_2 \sin\theta_3 \sin\phi_3 q_2]. \tag{B.5}$$

To see how we got Eq.B.5, let's consider the following geometry. Start with $\vec{q}_1$ pointing along the z-axis. $\vec{q}_2$ makes an angle θ_2 with $\vec{q}_1$, so let's assume that $\vec{q}_2$ is in the z-x plane with no y-component. Hence, $\vec{q}_1 + \vec{q}_2$ lies in the z-x plane with no y-component. We will label the unit vector in the direction of $\vec{q}_1 + \vec{q}_2$ as $\hat{a}$, which is:

$$\hat{a} = \frac{q_1 + \cos\theta_2 q_2}{|\vec{q}_1 + \vec{q}_2|}\hat{z} + \frac{\sin\theta_2 q_2}{|\vec{q}_1 + \vec{q}_2|}\hat{x}. \tag{B.6}$$

Now, $\vec{p}_3$ is rotated an angle θ_3 from $\vec{q}_1 + \vec{q}_2$, so in general $\vec{p}_3$ has non-zero x, y, and z components. Let's decompose $\vec{p}_3$ into components parallel and perpendicular to $\vec{q}_1 + \vec{q}_2$ using the fact that $\vec{p}_3$ makes an angle θ_3 with $\vec{q}_1 + \vec{q}_2$. Define the plane N_a as the plane

normal to $\hat{a}$. Define ϕ_3 to be the angle the projection of $\vec{p}_3$ in the N_a plane makes with the $\hat{y}$ axis. To write the decomposition of $\vec{p}_3$, we need a unit vector which lies in the N_a plane and is perpendicular to $\hat{y}$. We will define that vector as $\hat{b}$:

$$\hat{b} \equiv \frac{\sin\theta_2 q_2}{|\vec{q}_1+\vec{q}_2|}\hat{z} - \frac{q_1+q_2\cos\theta_2}{|\vec{q}_1+\vec{q}_2|}\hat{x}. \tag{B.7}$$

This leaves us with the following expression for $\vec{p}_3$:

$$\begin{aligned}
\vec{p}_3 =& p_3\cos\theta_3\hat{a} + p_3\sin\theta_3\cos\phi_3\hat{y} + p_3\sin\theta_3\sin\phi_3\hat{b} \\
=& \left[\frac{p_3\cos\theta_3(q_1+q_2\cos\theta_2)}{|\vec{q}_1+\vec{q}_2|} + \frac{p_3\sin\theta_3\sin\phi_3 q_2\sin\theta_2}{|\vec{q}_1+\vec{q}_2|}\right]\hat{z} \\
&+ p_3\sin\theta_3\cos\phi_3\hat{y} \\
&+ \left[\frac{p_3\cos\theta_3 q_2\sin\theta_2}{|\vec{q}_1+\vec{q}_2|} - \frac{p_3\sin\theta_3\sin\phi_3(q_1+q_2\cos\theta_2)}{|\vec{q}_1+\vec{q}_2|}\right]\hat{x}
\end{aligned}$$

Thus, after calculating the 3-vector dot product between $\vec{q}_1$ and $\vec{p}_3$, we find:

$$\vec{q}_1\cdot\vec{p}_3 = \frac{q_1 p_3}{|\vec{q}_1+\vec{q}_2|}[\cos\theta_3(q_1+q_2\cos\theta_2) + \sin\theta_2\sin\theta_3\sin\phi_3 q_2], \tag{B.8}$$

which is the result in Eq.B.5. Eq.B.5 is not a simple clean equation. It contains dependencies on q_2 and p_3 which does not present a problem since those will be dummy variables of integration. It contains a non-linear dependence on $\cos\theta_2$. It also has a non-linear dependence on $\cos\theta_3$. We will use a delta function to integrate out the dependence of $\cos\theta_3$, and thus will have to properly use the substitution in the $\sin\theta_3$ terms. The most concerning aspect of Eq.B.5 is the azimuthal dependence on ϕ_3. This cannot be eliminated at this point, suggesting that the rate integral will appear to be four-dimensional. What follows is working through the mathematics to write the scattering integral akin to neutrino–neutrino scattering, but with important modifications.

Our general expression for 2×2 scattering is:

$$\frac{Df_1}{Dt} = \int \frac{s}{2E_1} \frac{d^3q_2}{(2\pi)^3 2E_2} \frac{d^3p_3}{(2\pi)^3 2p_3} \frac{d^3p_4}{(2\pi)^3 2p_4} \times \langle|\mathcal{M}|^2\rangle (2\pi)^4 \delta^4(Q_1 + Q_2 - P_3 - P_4) F(E_1, E_2, p_3, p_4), \tag{B.9}$$

where s is a multiplicity factor and:

$$F(E_1, E_2, p_3, p_4) = (1 - f_1(E_1))(1 - f_2(E_2)) f_3(p_3) f_4(p_4) - f_1(E_1) f_2(E_2)(1 + f_3(p_3))(1 + f_4(p_4)). \tag{B.10}$$

$f_i(E_i)$ is the occupation probability density of species i at energy E_i. Keep in mind the $+$ signs in F are due to the fact that photons are bosons. Eq.B.9 now becomes:

$$\frac{Df_1}{Dt} = \frac{s}{2^4(2\pi)^5 E_1} \int \frac{d^3q_2}{E_2} \int \frac{d^3p_3}{p_3} \int \frac{d^3p_4}{p_4} \langle|\mathcal{M}|^2\rangle \times \delta(E_1 + E_2 - p_3 - p_4) \delta^3(\vec{q}_1 + \vec{q}_2 - \vec{p}_3 - \vec{p}_4) F(E_1, E_2, p_3, p_4). \tag{B.11}$$

Using the spatial component of the delta function over d^3p_4, Eq.B.11 becomes:

$$\frac{Df_1}{Dt} = \frac{s}{2^4(2\pi)^5 E_1} \int \frac{d^3q_2}{E_2} \int \frac{d^3p_3}{p_3} \times \left(\frac{1}{u} \langle|\mathcal{M}|^2\rangle \delta(E_1 + E_2 - p_3 - u) F(E_1, E_2, p_3, u) \right) \Bigg|_{u=|\vec{q}_1 + \vec{q}_2 - \vec{p}_3|}. \tag{B.12}$$

u is a function of $q_1, q_2, p_3, \theta_2, \text{and} \, \theta_3$ in general, but is independent of ϕ_3. There are still six integrals remaining in Eq.B.12. We can eliminate one of the remaining six integrals by using the last remaining delta-function factor. Specifically, let us eliminate $d\cos\theta_3$

by using a u-substitution with the conveniently named function u. Our matrix element depends on $\cos\theta_3$, so we will have to be careful that we do the proper substitution into $\langle|\mathcal{M}|\rangle^2$. Write u as the following:

$$u^2 = |\vec{q}_1 + \vec{q}_2 - \vec{p}_3|^2 = |\vec{q}_1 + \vec{q}_2|^2 + p_3^2 - 2|\vec{q}_1 + \vec{q}_2|p_3\cos\theta_3, \tag{B.13}$$

from how we defined θ_3 in Eq.B.4. Since we are concerned only with the integral over $d\cos\theta_3$, we treat $q_2, p_3,$ and θ_2 as constants. Taking the derivative of u^2:

$$\begin{aligned} 2u\,du &= 0 + 0 - 2|\vec{q}_1 + \vec{q}_2|p_3\,d\cos\theta_3 \\ \implies d\cos\theta_3 &= -\frac{u}{|\vec{q}_1 + \vec{q}_2|p_3}du. \end{aligned}$$

Eq.B.12 now appears as:

$$\begin{aligned} \frac{Df_1}{Dt} &= \frac{s}{2^4(2\pi)^5E_1}\int\frac{d^3q_2}{E_2}\int d\phi_3\int\frac{p_3^2dp_3}{p_3} \\ &\times\int_{-1}^{1} d\cos\theta_3\frac{1}{u}\langle|\mathcal{M}|^2\rangle\delta(E_1+E_2-p_3-u)F(E_1,E_2,p_3,u) \qquad \text{(B.14)} \\ &= \frac{s}{2^4(2\pi)^5E_1}\int\frac{d^3q_2}{E_2}\int d\phi_3\int\frac{p_3^2dp_3}{p_3} \\ &\times\int_{b}^{a}\left(-\frac{u}{|\vec{q}_1+\vec{q}_2|p_3}du\right)\frac{1}{u}\langle|\mathcal{M}|^2\rangle\delta(E_1+E_2-p_3-u)F(E_1,E_2,p_3,u) \qquad \text{(B.15)} \\ &= \frac{s}{2^4(2\pi)^5E_1}\int\frac{d^3q_2}{E_2|\vec{q}_1+\vec{q}_2|}\int d\phi_3\int dp_3 \\ &\times\int_{a}^{b} du\,\langle|\mathcal{M}|^2\rangle\delta(E_1+E_2-p_3-u)F(p_1,p_2,p_3,u). \qquad \text{(B.16)} \end{aligned}$$

From the u-substitution, our expression for $\langle|\mathcal{M}|^2\rangle$ now looks like the following:

$$\begin{aligned}
\langle|\mathcal{M}|^2\rangle \sim & \lambda(E_1E_2 - q_1q_2\cos\theta_2) \\
& \times\left\{E_1p_3 - \frac{q_1p_3}{|\vec{q}_1+\vec{q}_2|}[\cos\theta_3(q_1+q_2\cos\theta_2)+\sin\theta_2\sin\theta_3\sin\phi_3q_2]\right\} \qquad \text{(B.17)} \\
= & \lambda(E_1E_2 - q_1q_2\cos\theta_2) \\
& \times\left\{E_1p_3 - \frac{q_1p_3}{|\vec{q}_1+\vec{q}_2|}\left[\left(\frac{|\vec{q}_1+\vec{q}_2|^2+p_3^2-u^2}{2|\vec{q}_1+\vec{q}_2|p_3}\right)(q_1+\cos\theta_2q_2)\right.\right. \\
& \left.\left. + \sin\theta_2\sqrt{1-\left(\frac{|\vec{q}_1+\vec{q}_2|^2+p_3^2-u^2}{2|\vec{q}_1+\vec{q}_2|p_3}\right)^2}\sin\phi_3q_2\right]\right\} \qquad \text{(B.18)} \\
\equiv & \lambda(E_1E_2 - q_1q_2\cos\theta_2) \\
& \times\left\{E_1p_3 - \frac{q_1p_3}{|\vec{q}_1+\vec{q}_2|}\right. \\
& \left.\times\left[\left(\frac{|\vec{q}_1+\vec{q}_2|^2+p_3^2-u^2}{2|\vec{q}_1+\vec{q}_2|p_3}\right)(q_1+\cos\theta_2q_2)+A\sin\phi_3\right]\right\}, \qquad \text{(B.19)}
\end{aligned}$$

where A is a function dependent on $q_1, q_2, p_3, \text{and}\,\theta_2$, but not on ϕ_3. Everything in the above expression is an input variable or an integration variable, besides u, which we can write as $u = E_1 + E_2 - p_3$. The new limits of $\int du$ are:

$$\begin{aligned}
a &= u(\cos\theta_3 = +1) = ||\vec{q}_1+\vec{q}_2| - p_3|, \\
b &= u(\cos\theta_3 = -1) = |\vec{q}_1+\vec{q}_2| + p_3.
\end{aligned}$$

The $\int dp_3$ is over infinity, but the $\int du$ is over a finite interval. Therefore, there may be (or may not be) values of p_3 which constrain u to be inside (or outside) the range $[a,b]$. Thus, for the overall rate integral to be non-zero: $a < u$ and $u < b$.

B.2 Case 1: $a < u$

B.2.1 Case 1(i): $|\vec{q}_1 + \vec{q}_2| > p_3$

For the delta function to be non-zero, write u as $u = E_1 + E_2 - p_3$. This implies:

$$|\vec{q}_1 + \vec{q}_2| - p_3 < E_1 + E_2 - p_3 \implies |\vec{q}_1 + \vec{q}_2| < E_1 + E_2,$$

which is simply the triangle inequality and the fact that electrons have rest mass. Hence this subcase provides no new information.

B.2.2 Case 1(ii): $p_3 > |\vec{q}_1 + \vec{q}_2|$

We have:

$$\begin{aligned} p_3 - |\vec{q}_1 + \vec{q}_2| &< E_1 + E_2 - p_3 \\ \implies 2p_3 &< E_1 + E_2 + |\vec{q}_1 + \vec{q}_2| \\ \implies p_3 &< \frac{1}{2}(E_1 + E_2 + |\vec{q}_1 + \vec{q}_2|) \equiv p_{\max}, \end{aligned}$$

which defines $p_{\max}$.

B.3 Case 2: $u < b$

We have:

$$\begin{aligned} E_1 + E_2 - p_3 &< |\vec{q}_1 + \vec{q}_2| + p_3 \\ \implies E_1 + E_2 - |\vec{q}_1 + \vec{q}_2| &< 2p_3 \\ \implies p_3 &> \frac{1}{2}(E_1 + E_2 - |\vec{q}_1 + \vec{q}_2|) \equiv p_{\min}. \end{aligned}$$

The triangle inequality and the non-zero rest mass of the electron ensure $p_{\min} > 0$.

B.4 Combining integrals over p_3 and u

Therefore, we can combine $\int dp_3 \int du$ to produce the following expression for our scattering integral:

$$\frac{Df_1}{Dt} = \frac{s}{2^4(2\pi)^5 E_1} \int \frac{d^3q_2}{E_2|\vec{q}_1+\vec{q}_2|} \int d\phi_3 \int_{p_{\min}}^{p_{\max}} dp_3 \langle|\mathcal{M}|^2\rangle F(E_1,E_2,p_3,E_1+E_2-p_3). \tag{B.20}$$

Let $x \equiv \cos\theta_2$, implying $|\vec{q}_1+\vec{q}_2|^2 = q_1^2+q_2^2+2q_1q_2x$. Since there are no identical particles in the final state, let $s=1$:

$$\begin{aligned}\frac{Df_1}{Dt} &= \frac{1}{2^4(2\pi)^5 E_1} \int \frac{q_2^2 dq_2}{E_2} \int \frac{dx}{|\vec{q}_1+\vec{q}_2|} \int d\phi_2 \int d\phi_3 \\ &\quad \times \int_{p_{\min}}^{p_{\max}} dp_3 \langle|\mathcal{M}|^2\rangle F(E_1,E_2,p_3,E_1+E_2-p_3) \qquad \text{(B.21)} \\ &= \frac{1}{2^4(2\pi)^4 E_1} \int \frac{q_2^2 dq_2}{E_2} \int \frac{dx}{\sqrt{q_1^2+q_2^2+2q_1q_2x}} \int d\phi_3 \\ &\quad \times \int_{p_{\min}}^{p_{\max}} dp_3 \langle|\mathcal{M}|^2\rangle F(E_1,E_2,p_3,E_1+E_2-p_3). \qquad \text{(B.22)}\end{aligned}$$

The limits on $\int dp_3$ do not depend on ϕ_3. Thus, we can change the order of $\int d\phi_3$ and $\int dp_3$ so that we can integrate out the ϕ_3 dependence:

$$\frac{Df_1}{Dt} = \frac{1}{2^4(2\pi)^4 E_1}\int \frac{q_2^2 dq_2}{E_2}\int \frac{dx}{\sqrt{q_1^2+q_2^2+2q_1q_2x}}\int_{p_{\min}}^{p_{\max}} dp_3 F(E_1,E_2,p_3,E_1+E_2-p_3)$$
$$\times \int d\phi_3 \langle|\mathcal{M}|^2\rangle \tag{B.23}$$
$$= \frac{\lambda}{2^4(2\pi)^4 E_1}\int \frac{q_2^2 dq_2}{E_2}\int \frac{(E_1E_2-q_1q_2x)dx}{\sqrt{q_1^2+q_2^2+2q_1q_2x}}\int_{p_{\min}}^{p_{\max}} dp_3 F(E_1,E_2,p_3,E_1+E_2-p_3)$$
$$\times \int_0^{2\pi} d\phi_3 \left\{E_1p_3 - \frac{q_1p_3}{|\vec{q}_1+\vec{q}_2|}\left[\left(\frac{|\vec{q}_1+\vec{q}_2|^2+p_3^2-u^2}{2|\vec{q}_1+\vec{q}_2|p_3}\right)(q_1+\cos\theta_2 q_2)+A\sin\phi_3\right]\right\} \tag{B.24}$$
$$= \frac{\lambda}{2^4(2\pi)^4 E_1}\int \frac{q_2^2 dq_2}{E_2}\int \frac{(E_1E_2-q_1q_2x)dx}{\sqrt{q_1^2+q_2^2+2q_1q_2x}}\int_{p_{\min}}^{p_{\max}} dp_3 F(E_1,E_2,p_3,E_1+E_2-p_3)$$
$$\times \left\{E_1p_3 2\pi - \frac{q_1p_3}{|\vec{q}_1+\vec{q}_2|}\left[\left(\frac{|\vec{q}_1+\vec{q}_2|^2+p_3^2-u^2}{2|\vec{q}_1+\vec{q}_2|p_3}\right)(q_1+\cos\theta_2 q_2)2\pi + A\cdot 0\right]\right\} \tag{B.25}$$
$$= \frac{\lambda}{16(2\pi)^3 E_1}\int \frac{q_2^2 dq_2}{E_2}\int \frac{(E_1E_2-q_1q_2x)dx}{\sqrt{q_1^2+q_2^2+2q_1q_2x}}\int_{p_{\min}}^{p_{\max}} dp_3 F(E_1,E_2,p_3,E_1+E_2-p_3)$$
$$\times \left\{E_1p_3 - q_1(q_1+q_2x)\frac{q_1^2+q_2^2+2q_1q_2x+p_3^2-(E_1+E_2-p_3)^2}{2(q_1^2+q_2^2+2q_1q_2x)}\right\} \tag{B.26}$$
$$= \frac{\lambda}{16(2\pi)^3 E_1}\int \frac{q_2^2 dq_2}{E_2}\int \frac{(E_1E_2-q_1q_2x)dx}{\sqrt{q_1^2+q_2^2+2q_1q_2x}}\int_{p_{\min}}^{p_{\max}} dp_3 F(E_1,E_2,p_3,E_1+E_2-p_3)$$
$$\times \left\{E_1p_3 - q_1(q_1+q_2x)\frac{2q_1q_2x-2m_e^2-2E_1E_2+2E_1p_3+2E_2p_3}{2(q_1^2+q_2^2+2q_1q_2x)}\right\}. \tag{B.27}$$

The Klein-Nishina matrix element may have powers of $Q_1\cdot P_3$, or rational expressions involving $Q_1\cdot P_3$. Whatever the form is, it should be possible to integrate out the ϕ_3 dependence because the limits of $\int dp_3$ do not depend on ϕ_3. Thus, the final expression

is a triple integral (and not a quadruple integral).

Appendix C

Dilution decay spectra

C.1 Decay into a charged pion and electron

C.1.1 Spectra for pion decay

To begin, we consider the simultaneous decays:

$$\nu_s \to \pi^+ + e^-, \tag{C.1}$$

$$\pi^+ \to \mu^+ + \nu_\mu. \tag{C.2}$$

We wish to determine the resulting spectrum of the ν_μ. The proper calculation requires a Boltzmann equation. However, we will bypass this route and assume all the species are dilute at the pertinent energies.

To determine the spectrum of ν_μ, we need to know the spectrum of the parent particle (the π^+) and the grandparent particle (the ν_s). We will work in the reference frame of the ν_s, implying a null spectrum with number density n_s and energy m_s. The ν_s particle has an inherent lifetime, which we will write as a rate, namely Γ. ν_s decays into two particles, implying both particles must be monoenergetic. To determine the energy

of the π^+, we use energy and momentum conservation:

$$m_s = E_\pi + E_e \implies E_e = m_s - E_\pi \tag{C.3}$$

$$0 = \vec{p}_\pi + \vec{p}_e \implies p_\pi = p_e = \sqrt{E_e^2 - m_e^2}. \tag{C.4}$$

If we substitute Eq.(C.3) into the square of Eq.(C.4), and solve for E_π, we find:

$$p_\pi^2 = E_\pi^2 - m_\pi^2 = (m_s - E_\pi)^2 - m_e^2 \implies E^{(1)} \equiv \frac{m_s^2 + m_\pi^2 - m_e^2}{2m_s} = E_\pi. \tag{C.5}$$

We can write the π^+ spectrum as:

$$\frac{dn_\pi}{dE_\pi\, d\Omega_\pi\, dt} = \Gamma n_s \frac{\delta(E_\pi - E^{(1)})}{4\pi}. \tag{C.6}$$

Simply put, Eq.(C.6) states that the amount of π^+ coming into energy bin E_π, solid angle Ω_π, per unit time is equal to the creation rate of π^+ (i.e. Γn_s) multiplied by the probability density the π^+ has energy E_π (i.e. $\delta(E_\pi - E^{(1)})$) and solid angle Ω_π (i.e. $1/4\pi$). The decay has no preferred direction, hence why the probability density for the solid angle is independent of Ω_π.

To determine the spectrum of ν_μ, we consider the reference frame where the π^+ is at rest. In this reference frame, the decay particles ν_μ and μ^+ are monoenergetic implying the ν_μ has energy:

$$E^{(2)} \equiv \frac{m_\pi^2 - m_\mu^2}{2m_\pi}. \tag{C.7}$$

We have used analogous equations of Eqs.(C.3) and (C.4) to derive Eq.(C.7), except we have taken the mass of ν_μ to be negligible. The decay spectrum for ν_μ follows from

analogy with Eq.(C.6):

$$\frac{dn_\nu}{dE_\nu^{'}\,d\Omega_\nu^{'}\,dt^{'}} = \frac{dn_\pi}{dt}\frac{dt}{dt^{'}}\frac{\delta(E_\nu^{'}-E^{(2)})}{4\pi}. \tag{C.8}$$

We have intentionally inserted primes on the kinematic variables in Eq.(C.8) to delineate the reference frame where the π^+ is at rest (primed) from the reference frame where the ν_s is at rest (unprimed). For the time variable, we do not use the quantity $dn_\pi/dt^{'}$ because we will assume the π^+ immediately decays in the unprimed frame, implying that the decay rate of the π^+ in the primed frame is infintely fast.

We can combine Eqs.(C.6) and (C.8) if we write the spectrum of ν_μ as the following:

$$\begin{aligned}\frac{dn_\nu}{dE_\nu^{'}\,d\Omega_\nu^{'}\,dE_\pi\,d\Omega_\pi\,dt^{'}} &= \frac{dn_\pi}{dE_\pi\,d\Omega_\pi\,dt}\frac{dt}{dt^{'}}\frac{\delta(E_\nu^{'}-E^{(2)})}{4\pi} \\ &= \Gamma n_s\frac{dt}{dt^{'}}\frac{\delta(E_\pi-E^{(1)})}{4\pi}\frac{\delta(E_\nu^{'}-E^{(2)})}{4\pi}.\end{aligned} \tag{C.9}$$

Both sides of Eq.(C.9) involve multiple reference frames. Let us take the primed reference frame moving with speed v in the unprimed frame of reference such that the π^+ is at rest in the primed frame. If we take the $x^{'}$ and $y^{'}$ axes parallel to the x and y axis, respectively, then the z and $z^{'}$ axes are coincident. By boosting in the z direction, we can relate the energy in the primed reference frame to that in the unprimed frame:

$$E_\nu^{'} = \gamma E_\nu - \gamma v p_\nu^{(z)}, \tag{C.10}$$

where:

$$\gamma = \frac{1}{\sqrt{1-v^2}}, \tag{C.11}$$

and $p_\nu^{(z)}$ is the z component of the ν_μ momentum. We carefully distinguished between

momentum and energy in Eq.(C.10). The neutrino mass is still negligible in the unprimed reference frame, so $E_\nu = p_\nu$. Let us define the angle θ_ν to be the angle between the 3-momentum vector of ν_μ and the z axis, implying $p_\nu^{(z)} = E_\nu \cos\theta_\nu$. We are boosting in the direction of the π^+ which we have assumed is moving along the z axis. In the unprimed frame, the π^+ has energy and momentum:

$$E_\pi = \gamma m_\pi \implies \gamma = \frac{E_\pi}{m_\pi} \tag{C.12}$$

$$p_\pi = \gamma v m_\pi \implies \gamma v = \frac{p_\pi}{m_\pi}. \tag{C.13}$$

Using Eqs.(C.12) and (C.13) in the expression for (C.10) yields:

$$E_\nu^{'} = \frac{E_\pi}{m_\pi} E_\nu - \frac{p_\pi}{m_\pi} E_\nu \cos\theta_\nu = \frac{E_\nu}{m_\pi}(E_\pi - p_\pi \cos\theta_\nu). \tag{C.14}$$

With Eq.(C.14), we can write the argument of $\delta(E_\nu^{'} - E^{(2)})$ in terms of quantities in the unprimed reference frame, implying all of the quantities on the right-hand-side of Eq.(C.9) are in terms of the unprimed frame.

Our expression for the left-hand-side of Eq.(C.9) still involves quantities in terms of the primed frame. We can eliminate those quantities with the proper change of coordinates, i.e.:

$$\frac{dn_\nu}{dE_\nu\, d\Omega_\nu\, dE_\pi\, d\Omega_\pi\, dt} = \frac{dn_\nu}{dE_\nu^{'}\, d\Omega_\nu^{'}\, dE_\pi\, d\Omega_\pi\, dt^{'}} \frac{dE_\nu^{'}}{dE_\nu} \frac{d\Omega_\nu^{'}}{d\Omega_\nu} \frac{dt^{'}}{dt}. \tag{C.15}$$

Using Eq.(C.14):

$$E_\nu^{'} = \frac{E_\nu}{m_\pi}(E_\pi - p_\pi \cos\theta_\nu) \implies \frac{dE_\nu^{'}}{dE_\nu} = \frac{1}{m_\pi}(E_\pi - p_\pi \cos\theta_\nu). \tag{C.16}$$

For the solid angles, let us define $\xi = \cos\theta$ such that:

$$d\Omega = \sin\theta\, d\theta\, d\phi \equiv d\xi\, d\phi. \tag{C.17}$$

The coordinate transformation for $d\Omega_\nu$ becomes:

$$\frac{d\Omega_\nu^{'}}{d\Omega_\nu} = \frac{d\xi_\nu^{'}}{d\xi_\nu}\frac{d\phi_\nu^{'}}{d\phi_\nu} = \frac{d\xi_\nu^{'}}{d\xi_\nu}, \tag{C.18}$$

where $d\phi^{'}/d\phi = 1$ as $\phi, \phi^{'}$ describe angles in the x-y plane and are unaffected by a boost in the z direction. We can write $\xi_\nu^{'}$ as a function of ξ_ν using the following:

$$\xi_\nu^{'} = \cos\theta_\nu^{'} = \frac{p_\nu^{(z)'}}{p_\nu^{'}} = \frac{p_\nu^{(z)'}}{E_\nu^{'}} = \frac{\gamma E_\nu \xi_\nu - \gamma v E_\nu}{\gamma E_\nu - \gamma v E_\nu \xi_\nu} = \frac{E_\pi \xi_\nu - p_\pi}{E_\pi - p_\pi \xi_\nu}, \tag{C.19}$$

where we have used the Lorentz transformation for the momenta in the numerator, the fact that $E_\nu = p_\nu$, and Eqs.(C.12) and (C.13) for γ and γv. Taking the derivative of Eq.(C.19) with respect to ξ_ν yields:

$$\frac{d\xi_\nu^{'}}{d\xi_\nu} = \frac{(E_\pi - p_\pi\xi_\nu)E_\pi - (E_\pi\xi_\nu - p_\pi)(-p_\pi)}{(E_\pi - p_\pi\xi_\nu)^2} = \frac{E_\pi^2 - p_\pi^2}{(E_\pi - p_\pi\xi_\nu)^2} = \frac{m_\pi^2}{(E_\pi - p_\pi\xi_\nu)^2}. \tag{C.20}$$

We can now write Eq.(C.15) as:

$$\frac{dn_\nu}{dE_\nu\, d\Omega_\nu\, dE_\pi\, d\Omega_\pi\, dt} = \frac{dn_\pi}{dE_\pi\, d\Omega_\pi\, dt}\frac{dt}{dt^{'}}\frac{\delta(E_\nu^{'} - E^{(2)})}{4\pi}\frac{dE_\nu^{'}}{dE_\nu}\frac{d\xi_\nu^{'}}{d\xi_\nu}\frac{dt^{'}}{dt} \tag{C.21}$$

$$= \Gamma n_s \frac{\delta(E_\pi - E^{(1)})}{4\pi}\frac{\delta[\frac{E_\nu}{m_\pi}(E_\pi - p_\pi\xi_\nu) - E^{(2)}]}{4\pi} \times \frac{1}{m_\pi}(E_\pi - p_\pi\xi_\nu)\frac{m_\pi^2}{(E_\pi - p_\pi\xi_\nu)^2} \tag{C.22}$$

$$= \Gamma n_s \frac{\delta(E_\pi - E^{(1)})}{4\pi}\frac{\delta[\frac{E_\nu}{m_\pi}(E_\pi - p_\pi\xi_\nu) - E^{(2)}]}{4\pi}\frac{m_\pi}{E_\pi - p_\pi\xi_\nu}. \tag{C.23}$$

Our initial objective was to determine the spectrum of the ν_μ, which we can do by integrating over Eq.(C.23):

$$\frac{dn_\nu}{dE_\nu\, d\Omega_\nu\, dt} = \int dE_\pi \int d\Omega_\pi \frac{dn_\nu}{dE_\nu\, d\Omega_\nu\, dE_\pi\, d\Omega_\pi\, dt} \tag{C.24}$$

$$= \int dE_\pi \int d\Omega_\pi \Gamma n_s \frac{\delta(E_\pi - E^{(1)})}{4\pi} \frac{\delta[\frac{E_\nu}{m_\pi}(E_\pi - p_\pi \xi_\nu) - E^{(2)}]}{4\pi} \frac{m_\pi}{E_\pi - p_\pi \xi_\nu} \tag{C.25}$$

$$= \Gamma n_s \int dE_\pi \delta(E_\pi - E^{(1)}) \frac{\delta[\frac{E_\nu}{m_\pi}(E_\pi - p_\pi \xi_\nu) - E^{(2)}]}{4\pi} \frac{m_\pi}{E_\pi - p_\pi \xi_\nu} \int d\Omega_\pi \frac{1}{4\pi} \tag{C.26}$$

$$= \Gamma n_s \frac{\delta[\frac{E_\nu}{m_\pi}(E^{(1)} - p^{(1)} \xi_\nu) - E^{(2)}]}{4\pi} \frac{m_\pi}{E^{(1)} - p^{(1)} \xi_\nu}, \tag{C.27}$$

where $p^{(1)} = \sqrt{E^{(1)^2} - m_\pi^2}$. We can calculate the spectrum over all solid angles by

integrating Eq.(C.27) over $d\Omega_\nu$:

$$\begin{aligned}
\frac{dn_\nu}{dE_\nu\,dt} &= \int d\Omega_\nu \frac{dn_\nu}{dE_\nu\,d\Omega_\nu\,dt} \qquad \text{(C.28)}\\
&= \int d\Omega_\nu \Gamma n_s \frac{\delta[\frac{E_\nu}{m_\pi}(E^{(1)}-p^{(1)}\xi_\nu)-E^{(2)}]}{4\pi}\frac{m_\pi}{E^{(1)}-p^{(1)}\xi_\nu}\\
&= \Gamma n_s \int \frac{d\phi_\nu}{2\pi}\frac{1}{2}\int d\xi_\nu \delta\left[\frac{E_\nu}{m_\pi}(E^{(1)}-p^{(1)}\xi_\nu)-E^{(2)}\right]\frac{m_\pi}{E^{(1)}-p^{(1)}\xi_\nu}\\
&= \Gamma n_s \frac{1}{2}\int_{-1}^{1} d\xi_\nu \delta\left[\frac{E_\nu}{m_\pi}E^{(1)}-E^{(2)}-\frac{E_\nu p^{(1)}}{m_\pi}\xi_\nu\right]\frac{m_\pi}{E^{(1)}-p^{(1)}\xi_\nu}\\
&= \Gamma n_s \frac{1}{2}\int_{-E_\nu p^{(1)}/m_\pi}^{E_\nu p^{(1)}/m_\pi} du \frac{m_\pi}{E_\nu p^{(1)}}\delta\left[\frac{E_\nu}{m_\pi}E^{(1)}-E^{(2)}-u\right]\frac{m_\pi}{E^{(1)}-p^{(1)}\frac{m_\pi}{E_\nu p^{(1)}}u}\\
&= \Gamma n_s \frac{1}{2}\frac{m_\pi}{E_\nu p^{(1)}}\frac{m_\pi}{E^{(1)}-\frac{m_\pi}{E_\nu}(\frac{E_\nu}{m_\pi}E^{(1)}-E^{(2)})}\\
&\times \theta\left[\frac{E_\nu}{m_\pi}E^{(1)}-E^{(2)}-\left(-\frac{E_\nu p^{(1)}}{m_\pi}\right)\right]\theta\left[\frac{E_\nu p^{(1)}}{m_\pi}-\left(\frac{E_\nu}{m_\pi}E^{(1)}-E^{(2)}\right)\right]\\
&= \Gamma n_s \frac{1}{2}\frac{m_\pi}{E_\nu p^{(1)}}\frac{E_\nu}{E^{(2)}}\theta\left[\frac{E_\nu}{m_\pi}(E^{(1)}+p^{(1)})-E^{(2)}\right]\theta\left[E^{(2)}-\frac{E_\nu}{m_\pi}(E^{(1)}-p^{(1)})\right]\\
&= \Gamma n_s \frac{m_\pi}{2E^{(2)}p^{(1)}}\theta\left[E_\nu - E^{(2)}\frac{m_\pi}{E^{(1)}+p^{(1)}}\right]\theta\left[E^{(2)}\frac{m_\pi}{E^{(1)}-p^{(1)}}-E_\nu\right]\\
&= \Gamma n_s \frac{m_\pi}{2E^{(2)}p^{(1)}}\theta\left[E_\nu - E^{(2)}\frac{E^{(1)}-p^{(1)}}{m_\pi}\right]\theta\left[E^{(2)}\frac{E^{(1)}+p^{(1)}}{m_\pi}-E_\nu\right], \qquad \text{(C.29)}
\end{aligned}$$

where the θ functions are defined as:

$$\theta(x) = \begin{cases} 1 & \text{if } x > 0 \\ 0 & \text{otherwise} \end{cases}. \qquad \text{(C.30)}$$

Finally, we can calculate the total rate by integrating Eq.(C.29) over all energies E_ν:

$$\frac{dn_\nu}{dt} = \int dE_\nu \frac{dn_\nu}{dE_\nu dt} \tag{C.31}$$

$$= \int dE_\nu \Gamma n_s \frac{m_\pi}{2E^{(2)}p^{(1)}} \theta\left[E_\nu - E^{(2)}\frac{E^{(1)}-p^{(1)}}{m_\pi}\right] \theta\left[E^{(2)}\frac{E^{(1)}+p^{(1)}}{m_\pi} - E_\nu\right] \tag{C.32}$$

$$= \Gamma n_s \frac{m_\pi}{2E^{(2)}p^{(1)}} \int dE_\nu \theta\left[E_\nu - E^{(2)}\frac{E^{(1)}-p^{(1)}}{m_\pi}\right] \theta\left[E^{(2)}\frac{E^{(1)}+p^{(1)}}{m_\pi} - E_\nu\right] \tag{C.33}$$

$$= \Gamma n_s \frac{m_\pi}{2E^{(2)}p^{(1)}} \left(E^{(2)}\frac{E^{(1)}+p^{(1)}}{m_\pi} - E^{(2)}\frac{E^{(1)}-p^{(1)}}{m_\pi}\right) \tag{C.34}$$

$$= \Gamma n_s \frac{m_\pi}{2E^{(2)}p^{(1)}} \frac{E^{(2)}}{m_\pi}(2p^{(1)}) \tag{C.35}$$

$$= \Gamma n_s. \tag{C.36}$$

C.1.2 Spectra for muon decay

Eq.(C.29) gives the decay spectrum for the ν_μ integrated over the solid angle. The spectrum for μ^+ is identical with $E_\mu = E^{(1)} - E_\nu$:

$$\frac{dn_\mu}{dE_\mu dt} = \Gamma n_s \frac{m_\pi}{2E^{(2)}p^{(1)}} \theta\left[(E^{(1)}-E_\mu) - E^{(2)}\frac{E^{(1)}-p^{(1)}}{m_\pi}\right] \times \theta\left[E^{(2)}\frac{E^{(1)}+p^{(1)}}{m_\pi} - (E^{(1)}-E_\mu)\right] \tag{C.37}$$

$$= \Gamma n_s \frac{m_\pi}{2E^{(2)}p^{(1)}} \theta\left[E_\mu - \left(E^{(1)} - E^{(2)}\frac{E^{(1)}+p^{(1)}}{m_\pi}\right)\right] \times \theta\left[E^{(1)} - E^{(2)}\frac{E^{(1)}-p^{(1)}}{m_\pi} - E_\mu\right] \tag{C.38}$$

$$\equiv \Gamma n_s \frac{m_\pi}{2E^{(2)}p^{(1)}} \theta\left[E_\mu - E_\mu^{(\min)}\right] \theta\left[E_\mu^{(\max)} - E_\mu\right] \tag{C.39}$$

$$\implies \frac{dn_\mu}{dE_\mu d\Omega_\mu dt} = \Gamma n_s \frac{m_\pi}{2E^{(2)}p^{(1)}} \frac{1}{4\pi} \theta\left[E_\mu - E_\mu^{(\min)}\right] \theta\left[E_\mu^{(\max)} - E_\mu\right] \tag{C.40}$$

$$\tag{C.41}$$

The μ^+ decays into three particles: $\mu^+ \rightarrow \bar{\nu}_\mu + e^+ + \nu_e$. We will focus on the spectrum of the ν_e, which we call:

$$\frac{dn_{\nu_e}}{dE'_{\nu_e} d\Omega'_{\nu_e} dt'} \equiv \frac{dn_\mu}{dt}\frac{dt}{dt'}\frac{1}{4\pi}\frac{df_{\nu_e}}{dE'_{\nu_e}}, \tag{C.42}$$

where dn_μ/dt is the creation rate of μ^+, and df_{ν_e}/dE'_{ν_e} is the probability density of creating a ν_e with energy E'_{ν_e}. We reuse the primed reference frame for the frame where μ^+ is at rest. The unprimed reference frame is the frame where the ν_s is at rest. For μ^+ decay:

$$\frac{df_{\nu_e}}{dE'_{\nu_e}} = \frac{2}{m_\mu G(x_0^2)}\frac{(1-x_0^2-y')^2 y^{2'}}{1-y'}, \tag{C.43}$$

where $y' = 2E'_{\nu_e}/m_\mu$, $x_0 = m_e/m_\mu$, and

$$G(x) = \frac{1}{12}(1-8x-12x^2\ln x+8x^3-x^4). \tag{C.44}$$

We rewrite the spectrum of ν_e as:

$$\frac{dn_{\nu_e}}{dE'_{\nu_e} d\Omega'_{\nu_e} dE_\mu d\Omega_\mu dt'} = \frac{dn_\mu}{dE_\mu d\Omega_\mu dt}\frac{dt}{dt'}\frac{1}{4\pi}\frac{df_{\nu_e}}{dE'_{\nu_e}}, \tag{C.45}$$

and transform into the unprimed frame through:

$$\frac{dn_{\nu_e}}{dE_{\nu_e}\,d\Omega_{\nu_e}\,dE_\mu\,d\Omega_\mu\,dt} = \frac{dn_{\nu_e}}{dE'_{\nu_e}\,d\Omega'_{\nu_e}\,dE_\mu\,d\Omega_\mu\,dt'}\frac{dE'_{\nu_e}}{dE_{\nu_e}}\frac{d\Omega'_{\nu_e}}{d\Omega_{\nu_e}}\frac{dt'}{dt} \tag{C.46}$$

$$= \frac{dn_\mu}{dE_\mu\,d\Omega_\mu\,dt}\frac{dt}{dt'}\frac{1}{4\pi}\frac{df_{\nu_e}}{dE'_{\nu_e}}\frac{dE'_{\nu_e}}{dE_{\nu_e}}\frac{d\Omega'_{\nu_e}}{d\Omega_{\nu_e}}\frac{dt'}{dt} \tag{C.47}$$

$$= \Gamma n_s \frac{m_\pi}{2E^{(2)}p^{(1)}}\frac{1}{4\pi}\theta\left[E_\mu - E_\mu^{(\min)}\right]\theta\left[E_\mu^{(\max)} - E_\mu\right]$$
$$\times \frac{1}{4\pi}\frac{df_{\nu_e}}{dE'_{\nu_e}}\frac{dE'_{\nu_e}}{dE_{\nu_e}}\frac{d\Omega'_{\nu_e}}{d\Omega_{\nu_e}} \tag{C.48}$$

$$= \Gamma n_s \frac{m_\pi}{2E^{(2)}p^{(1)}}\frac{1}{4\pi}\theta\left[E_\mu - E_\mu^{(\min)}\right]\theta\left[E_\mu^{(\max)} - E_\mu\right]$$
$$\times \frac{1}{4\pi}\frac{df_{\nu_e}}{dE'_{\nu_e}}\frac{m_\mu}{E_\mu - p_\mu\xi_{\nu_e}}, \tag{C.49}$$

where we have used the Lorentz transformation $E'_{\nu_e} = \frac{E_{\nu_e}}{m_\mu}(E_\mu - p_\mu\xi_{\nu_e})$. We want the spectrum for the ν_e integrated over solid angle:

$$\frac{dn_{\nu_e}}{dE_{\nu_e}\,dt} = \int d\Omega_\mu \int dE_\mu \int d\Omega_{\nu_e}\frac{dn_{\nu_e}}{dE_{\nu_e}\,d\Omega_{\nu_e}\,dE_\mu\,d\Omega_\mu\,dt}. \tag{C.50}$$

The $\int d\Omega_\mu$ is trivial. The theta functions change the limits of $\int dE_\mu$, implying:

$$\frac{dn_{\nu_e}}{dE_{\nu_e}\,dt} = 4\pi \int_{E_\mu^{(\min)}}^{E_\mu^{(\max)}} dE_\mu\, 2\pi \int_{-1}^{1} d\xi_{\nu_e}\Gamma n_s \frac{m_\pi}{2E^{(2)}p^{(1)}}\frac{1}{4\pi}\frac{1}{4\pi}\frac{df_{\nu_e}}{dE'_{\nu_e}}\frac{m_\mu}{E_\mu - p_\mu\xi_{\nu_e}} \tag{C.51}$$

$$= \Gamma n_s \frac{m_\pi}{2E^{(2)}p^{(1)}} \int_{E_\mu^{(\min)}}^{E_\mu^{(\max)}} dE_\mu \int_{-1}^{1} d\xi_{\nu_e}\frac{df_{\nu_e}}{dE'_{\nu_e}}\frac{m_\mu}{2(E_\mu - p_\mu\xi_{\nu_e})} \tag{C.52}$$

To solve $\int d\xi_{\nu_e}$ in Eq.(C.52), we can use a u-substitution by utilizing the Lorentz transformation:

$$E'_{\nu_e} = \frac{E_{\nu_e}}{m_\mu}(E_\mu - p_\mu\xi_{\nu_e}) \implies d\xi_{\nu_e} = -\frac{m_\mu}{E_{\nu_e}p_\mu}dE'_{\nu_e}. \tag{C.53}$$

Using the substitution in Eq.(C.52), we are left with:

$$\frac{dn_{\nu_e}}{dE_{\nu_e}dt} = \Gamma n_s \frac{m_\pi}{2E^{(2)}p^{(1)}} \int_{E_\mu^{(\min)}}^{E_\mu^{(\max)}} dE_\mu \int_{E_{\nu_e}^{(\max)'}}^{E_{\nu_e}^{(\min)'}} \left(-\frac{m_\mu}{E_{\nu_e}p_\mu}\right) dE'_{\nu_e} \frac{df_{\nu_e}}{dE'_{\nu_e}} \frac{E_{\nu_e}}{2E'_{\nu_e}} \tag{C.54}$$

$$= \Gamma n_s \frac{m_\pi m_\mu}{4E^{(2)}p^{(1)}} \int_{E_\mu^{(\min)}}^{E_\mu^{(\max)}} dE_\mu \frac{1}{p_\mu} \int_{E_{\nu_e}^{(\min)'}}^{E_{\nu_e}^{(\max)'}} dE'_{\nu_e} \frac{df_{\nu_e}}{dE'_{\nu_e}} \frac{1}{E'_{\nu_e}}, \tag{C.55}$$

where:

$$E_{\nu_e}^{(\min)'} = \frac{E_{\nu_e}}{m_\mu}(E_\mu - p_\mu) \tag{C.56}$$

$$E_{\nu_e}^{(\max)'} = \frac{E_{\nu_e}}{m_\mu}(E_\mu + p_\mu). \tag{C.57}$$

By using the u-substitution, we can use Eq.(C.43) without having to write the y' in terms of $E_{\nu_e}, \xi_{\nu_e}, E_\mu$ and p_μ using the Lorentz transformation.

C.2 Decay into a charged pion and muon

The relevant decays are:

$$\nu_s \to \pi^+ + \mu^- \tag{C.58}$$

$$\mu^- \to \nu_\mu + \bar{\nu}_e + e^-. \tag{C.59}$$

We do not consider the decay of the π^+ because that is analogous to the previous section, except for different expressions for $E^{(1)}$ and $p^{(1)}$ involving m_μ instead of m_e. To determine the spectrum of the $\overline{\nu}_e$, we use the same expression for the probability density

of Eq.(C.43):

$$\frac{dn_{\overline{\nu}_e}}{dE'_{\overline{\nu}_e}\,d\Omega'_{\overline{\nu}_e}\,dE_\mu\,d\Omega_\mu\,dt'} = \frac{dn_\mu}{dE_\mu\,d\Omega_\mu\,dt}\frac{dt}{dt'}\frac{1}{4\pi}\frac{df_{\overline{\nu}_e}}{dE'_{\overline{\nu}_e}} \tag{C.60}$$

$$= \Gamma n_s \frac{\delta(E_\mu - (m_s - E^{(1)}))}{4\pi}\frac{dt}{dt'}\frac{1}{4\pi}\frac{df_{\overline{\nu}_e}}{dE'_{\overline{\nu}_e}}, \tag{C.61}$$

where:

$$E^{(1)} = \frac{m_s^2 + m_\pi^2 - m_\mu^2}{2m_s}, \tag{C.62}$$

and Γ is the decay rate of $\nu_s \to \pi^+ + \mu^-$. We use the change of coordinates,

$$\frac{dE'_{\overline{\nu}_e}}{dE_{\overline{\nu}_e}}\frac{d\Omega'_{\overline{\nu}_e}}{d\Omega_{\overline{\nu}_e}} = \frac{m_\mu}{E_\mu - p_\mu \xi_{\overline{\nu}_e}}, \tag{C.63}$$

to write the spectrum of $\overline{\nu}_e$ integrated over solid angle as:

$$\frac{dn_{\overline{\nu}_e}}{dE_{\overline{\nu}_e}\,dt} = \int d\Omega_\mu \int dE_\mu \int d\Omega_{\overline{\nu}_e} \frac{dn_{\overline{\nu}_e}}{dE_{\overline{\nu}_e}\,d\Omega_{\overline{\nu}_e}\,dE_\mu\,d\Omega_\mu\,dt} \tag{C.64}$$

$$= 4\pi \int dE_\mu 2\pi \int_{-1}^{1} d\xi_{\overline{\nu}_e} \Gamma n_s \frac{\delta(E_\mu - (m_s - E^{(1)}))}{4\pi}\frac{1}{4\pi}\frac{df_{\overline{\nu}_e}}{dE'_{\overline{\nu}_e}}\frac{m_\mu}{E_\mu - p_\mu \xi_{\overline{\nu}_e}} \tag{C.65}$$

$$= \Gamma n_s \int dE_\mu\, \delta(E_\mu - (m_s - E^{(1)}))\frac{1}{2}\int_{-1}^{1} d\xi_{\overline{\nu}_e}\frac{df_{\overline{\nu}_e}}{dE'_{\overline{\nu}_e}}\frac{m_\mu}{E_\mu - p_\mu \xi_{\overline{\nu}_e}} \tag{C.66}$$

$$= \Gamma n_s \frac{m_\mu}{2}\int dE_\mu\, \delta(E_\mu - (m_s - E^{(1)}))\frac{1}{p_\mu}\int_{E^{(\mathrm{min})'}_{\overline{\nu}_e}}^{E^{(\mathrm{max})'}_{\overline{\nu}_e}} dE'_{\overline{\nu}_e}\frac{df_{\overline{\nu}_e}}{dE'_{\overline{\nu}_e}}\frac{1}{E'_{\overline{\nu}_e}}, \tag{C.67}$$

where:

$$E^{(\mathrm{min})'}_{\overline{\nu}_e} \equiv \frac{E_{\overline{\nu}_e}}{m_\mu}(E_\mu - p_\mu) \tag{C.68}$$

$$E^{(\mathrm{max})'}_{\overline{\nu}_e} \equiv \frac{E_{\overline{\nu}_e}}{m_\mu}(E_\mu + p_\mu). \tag{C.69}$$

Define $E^{(3)}$ such that:

$$E^{(3)} \equiv m_s - E^{(1)} = \frac{m_s^2 + m_\mu^2 - m_\pi^2}{2m_s} \tag{C.70}$$

$$p^{(3)} \equiv \sqrt{{E^{(3)}}^2 - m_\mu^2}. \tag{C.71}$$

Then Eq.(C.67) becomes:

$$\frac{dn_{\bar{\nu}_e}}{dE_{\bar{\nu}_e}\,dt} = \Gamma n_s \frac{m_\mu}{2} \int dE_\mu\, \delta(E_\mu - E^{(3)}) \frac{1}{p_\mu} \int_{E_{\bar{\nu}_e}^{(\mathrm{min})'}}^{E_{\bar{\nu}_e}^{(\mathrm{max})'}} dE'_{\bar{\nu}_e} \frac{df_{\bar{\nu}_e}}{dE'_{\bar{\nu}_e}} \frac{1}{E'_{\bar{\nu}_e}} \tag{C.72}$$

$$= \Gamma n_s \frac{m_\mu}{2p^{(3)}} \int_{\tilde{E}_{\bar{\nu}_e}^{(\mathrm{min})'}}^{\tilde{E}_{\bar{\nu}_e}^{(\mathrm{max})'}} dE'_{\bar{\nu}_e} \frac{df_{\bar{\nu}_e}}{dE'_{\bar{\nu}_e}} \frac{1}{E'_{\bar{\nu}_e}}, \tag{C.73}$$

where:

$$\tilde{E}_{\bar{\nu}_e}^{(\mathrm{min})'} \equiv \frac{E_{\bar{\nu}_e}}{m_\mu}(E^{(3)} - p^{(3)}) \tag{C.74}$$

$$\tilde{E}_{\bar{\nu}_e}^{(\mathrm{max})'} \equiv \frac{E_{\bar{\nu}_e}}{m_\mu}(E^{(3)} + p^{(3)}). \tag{C.75}$$

We acknowledge Chad Kishimoto for indispensable discussions.

Appendix D

Comparison of integration methods

D.1 CK Method

Begin with the expression for the integral for the $\nu_e\nu_e \leftrightarrow \nu_e\nu_e$ process in the CK method:

$$C = \frac{\kappa}{32\,(2\pi)^3} \int dp_2 p_1 p_2^3 \int_{-1}^{1} dx \frac{(1-x)^2}{\sqrt{p_1^2+p_2^2+2p_1p_2x}} \tag{D.1}$$

$$\times \int_{p_-}^{p_+} dp_3 F\,(p_1,p_2,p_3,p_1+p_2-p_3)\,, \tag{D.2}$$

where $p_\pm = \left(p_1+p_2 \pm \sqrt{p_1^2+p_2^2+2p_1p_2x}\right)/2$. Let's only look at the last two integrals, over x and p_3:

$$I_{\rm CK} \equiv \int_{-1}^{1} dx \frac{(1-x)^2}{\sqrt{p_1^2+p_2^2+2p_1p_2x}} \int_{p_-}^{p_+} dp_3 F\,(p_1,p_2,p_3,p_1+p_2-p_3)\,. \tag{D.3}$$

We will take $F(p_1,p_2,p_3,p_1+p_2-p_3)=1$ so as to make $I_{\rm CK}$ analytical.

$$\begin{aligned} I_{\rm CK} &= \int_{-1}^{1} dx \frac{(1-x)^2}{\sqrt{p_1^2+p_2^2+2p_1p_2x}} \int_{p_-}^{p_+} dp_3 \\ &= \int_{-1}^{1} dx \frac{(1-x)^2}{\sqrt{p_1^2+p_2^2+2p_1p_2x}} (p_+ - p_-) \\ &= \int_{-1}^{1} dx \frac{(1-x)^2}{\sqrt{p_1^2+p_2^2+2p_1p_2x}} \sqrt{p_1^2+p_2^2+2p_1p_2x} \\ &= \int_{-1}^{1} dx\,(1-x)^2 \\ &= \frac{8}{3}. \end{aligned} \tag{D.4}$$

D.2 AV Method

The expression for the collision integral in the AV method is

$$C = \frac{\kappa}{32\,(2\pi)^3} \int_0^\infty dp_2 p_1 p_2^3 \int_0^{p_1+p_2} dp_3\, F(p_1,p_2,p_3,p_1+p_2-p_3)\, W(p_1,p_2,p_3), \tag{D.5}$$

where the weight W is defined as follows:

$$W \equiv \int_{x_0(p_1,p_2,p_3)}^{1} dx \frac{(1-x)^2}{\sqrt{p_1^2+p_2^2+2p_1p_2x}}, \tag{D.6}$$

where $x_0 = \mathrm{Max}\left(-1, 1-\frac{2p_3(p_1+p_2-p_3)}{p_1p_2}\right)$. The exact expression for W in terms of x_0 is:

$$\begin{aligned} W = {} & \frac{p_1+p_2}{15p_1^3p_2^3}\left[2\left(p_1^4+p_2^4\right)+8\left(p_1^3p_2+p_1p_2^3\right)+12p_1^2p_2^2\right] - \frac{\sqrt{p_1^2+p_2^2+2p_1p_2x_0}}{15p_1^3p_2^3} \\ & \times\left[2\left(p_1^4+p_2^4\right)+2\left(p_1^3p_2+p_1p_2^3\right)(5-x_0)+p_1^2p_2^2\left(3x_0^2-10x_0+19\right)\right]. \end{aligned} \tag{D.7}$$

Again, only consider the integral over p_3 and the W function:

$$I_{\mathrm{AV}} \equiv \int_0^{p_1+p_2} dp_3\, F\left(p_1,p_2,p_3,p_1+p_2-p_3\right) W\left(p_1,p_2,p_3\right). \tag{D.8}$$

We do not have an exact expression for x_0. To obtain an exact expression, consider the following argument. Let $x_0 = \mathrm{Max}\left(-1, x_1(p_1,p_2,p_3)\right)$ where $x_1 \equiv 1 - \frac{2p_3(p_1+p_2-p_3)}{p_1 p_2}$. We are integrating over p_3 in I_{AV}, with a lower limit of 0 and an upper limit of p_1+p_2. At both limits, $x_1(p_3=0) = x_1(p_3=p_1+p_2) = 1$. Furthermore, $x_1(p_3=p_1) = x_1(p_3 = p_2) = -1$. x_1 is quadratic in p_3, implying that x_1 can only be equal to -1 in at most two unique p_3 values (assuming fixed p_1 and p_2).

D.2.1 Case 1: $p_1 > p_2$

Since $p_1 > p_2$ and $x_1 = -1$ in only two places, we can write Eq.D.8 as:

$$\begin{aligned} I_{\mathrm{AV}} &= \int_0^{p_2} dp_3\, F\left(p_1,p_2,p_3,p_1+p_2-p_3\right) W\left(x_1\right) \\ &+ \int_{p_2}^{p_1} dp_3\, F\left(p_1,p_2,p_3,p_1+p_2-p_3\right) W\left(-1\right) \\ &+ \int_{p_1}^{p_1+p_2} dp_3\, F\left(p_1,p_2,p_3,p_1+p_2-p_3\right) W\left(x_1\right), \end{aligned} \tag{D.9}$$

where we have written the argument of W as the number to use in the $\mathrm{Max}(-1,x_1)$ expression. Again, to make the integral analytic, we set $F\left(p_1,p_2,p_3,p_1+p_2-p_3\right) = 1$, giving:

$$I_{\mathrm{AV}} = \int_0^{p_2} dp_3\, W\left(x_1\right) + \int_{p_2}^{p_1} dp_3\, W\left(-1\right) + \int_{p_1}^{p_1+p_2} dp_3\, W\left(x_1\right). \tag{D.10}$$

The expression for W involves two terms: a product of polynomials and roots of polynomials of p_3; and a term constant in p_3. Let's call those terms W_p and W_c:

$$W_\mathrm{p}(x_1(p_3)) \equiv -\frac{\sqrt{p_1^2+p_2^2+2p_1p_2x_1}}{15p_1^3p_2^3} \times \left[2\left(p_1^4+p_2^4\right)+2\left(p_1^3p_2+p_1p_2^3\right)(5-x_1)+p_1^2p_2^2\left(3x_1^2-10x_1+19\right)\right], \tag{D.11}$$

$$W_\mathrm{c} \equiv \frac{p_1+p_2}{15p_1^3p_2^3}\left[2\left(p_1^4+p_2^4\right)+8\left(p_1^3p_2+p_1p_2^3\right)+12p_1^2p_2^2\right]. \tag{D.12}$$

Hence:

$$\begin{aligned} I_\mathrm{AV} &= \int_0^{p_2} dp_3\, W_\mathrm{p}(x_1) + \int_{p_2}^{p_1} dp_3\, W_\mathrm{p}(-1) + \int_{p_1}^{p_1+p_2} dp_3\, W_\mathrm{p}(x_1) + \int_0^{p_1+p_2} dp_3\, W_\mathrm{c} \\ &\equiv \quad I_1 \quad + \quad I_2 \quad + \quad I_3 \quad + \quad I_4 \end{aligned} \tag{D.13}$$

I_1 Integral

We use the u-substitution $x_1 = x_1(p_3)$ to simplify the integral:

$$x_1 = 1 - \frac{2p_3(p_1+p_2-p_3)}{p_1p_2} \implies dx_1 = -\frac{2}{p_1p_2}(p_1+p_2-2p_3)dp_3 \tag{D.14}$$

$$\implies dp_3 = \frac{p_1p_2}{2(2p_3-p_1-p_2)}dx_1. \tag{D.15}$$

The limits of the integral over x_1 become: $x_1(p_3 = 0) = 1$ and $x_1(p_3 = p_2) = -1$. We need to solve for p_3 as a function of x_1:

$$x_1 = 1 - \frac{2p_3(p_1 + p_2 - p_3)}{p_1 p_2} \implies 2p_3(p_1 + p_2 - p_3) = p_1 p_2(1 - x_1) \tag{D.16}$$

$$\implies p_3^2 - p_3(p_1 + p_2) + \frac{p_1 p_2}{2}(1 - x_1) = 0 \tag{D.17}$$

$$\implies p_3 = \frac{p_1 + p_2}{2} \pm \frac{1}{2}\sqrt{(p_1 + p_2)^2 + 2p_1 p_2(x_1 - 1)} \tag{D.18}$$

$$\implies p_3 = \frac{p_1 + p_2}{2} \pm \frac{1}{2}\sqrt{p_1^2 + p_2^2 + 2p_1 p_2 x_1}. \tag{D.19}$$

Recall that the limits of integration are $+1$ to -1. To reproduce the original p_3 limits, observe:

$$p_3(x_1 = 1) = 0 = \frac{p_1 + p_2}{2} \pm \frac{1}{2}\sqrt{p_1^2 + p_2^2 + 2p_1 p_2} = \frac{p_1 + p_2}{2} \pm \frac{p_1 + p_2}{2} \tag{D.20}$$

$$p_3(x_1 = -1) = p_2 = \frac{p_1 + p_2}{2} \pm \frac{1}{2}\sqrt{p_1^2 + p_2^2 - 2p_1 p_2} = \frac{p_1 + p_2}{2} \pm \frac{p_1 - p_2}{2}, \tag{D.21}$$

where we are working under the assumption that $p_1 > p_2$. Therefore, we will take the negative sign from the quadratic-formula solution:

$$p_3 = \frac{p_1 + p_2}{2} - \frac{1}{2}\sqrt{p_1^2 + p_2^2 + 2p_1 p_2 x_1} \tag{D.22}$$

$$\implies dp_3 = \frac{p_1 p_2}{2(2p_3 - p_1 - p_2)} dx_1 \tag{D.23}$$

$$= -\frac{p_1 p_2}{2\sqrt{p_1^2 + p_2^2 + 2p_1 p_2 x_1}} dx_1. \tag{D.24}$$

Thus, our expression for I_1 after the u-substitution becomes:

$$I_1 = \int_0^{p_2} dp_3\, W_{\mathrm{p}}(x_1) \tag{D.25}$$

$$= \int_1^{-1} dx_1 \left(-\frac{p_1 p_2}{2\sqrt{p_1^2 + p_2^2 + 2p_1 p_2 x_1}} \right) \left\{ -\frac{\sqrt{p_1^2 + p_2^2 + 2p_1 p_2 x_1}}{15 p_1^3 p_2^3} \right.$$
$$\left. \times \left[2\left(p_1^4 + p_2^4\right) + 2\left(p_1^3 p_2 + p_1 p_2^3\right)(5 - x_1) + p_1^2 p_2^2 \left(3x_1^2 - 10x_1 + 19\right) \right] \right\} \tag{D.26}$$

$$= -\frac{1}{30 p_1^2 p_2^2} \times \int_{-1}^{1} dx_1 \left[2\left(p_1^4 + p_2^4\right) + 2\left(p_1^3 p_2 + p_1 p_2^3\right)(5 - x_1) + p_1^2 p_2^2 \left(3x_1^2 - 10x_1 + 19\right) \right] \tag{D.27}$$

$$= -\frac{1}{30 p_1^2 p_2^2} \times \left[2\left(p_1^4 + p_2^4\right) x_1 + 2\left(p_1^3 p_2 + p_1 p_2^3\right) \left(5x_1 - \frac{1}{2}x_1^2\right) + p_1^2 p_2^2 \left(x_1^3 - 5x_1^2 + 19x_1\right) \right] \Big|_{-1}^{1} \tag{D.28}$$

$$= -\frac{1}{30 p_1^2 p_2^2} \left[4\left(p_1^4 + p_2^4\right) + 20\left(p_1^3 p_2 + p_1 p_2^3\right) + 40 p_1^2 p_2^2 \right] \tag{D.29}$$

$$= -\frac{2}{15 p_1^2 p_2^2} \left[\left(p_1^4 + p_2^4\right) + 5\left(p_1^3 p_2 + p_1 p_2^3\right) + 10 p_1^2 p_2^2 \right]. \tag{D.30}$$

I_3 Integral

We use the same u-substitution and solve for p_3 in the same way as the I_1 integral:

$$I_3 = \int_{p_1}^{p_1+p_2} dp_3\, W_{\rm p}(x_1) \tag{D.31}$$

$$x_1 = 1 - \frac{2p_3(p_1+p_2-p_3)}{p_1 p_2} \tag{D.32}$$

$$dp_3 = \frac{p_1 p_2}{2(2p_3-p_1-p_2)} dx_1 \tag{D.33}$$

$$p_3 = \frac{p_1+p_2}{2} \pm \frac{1}{2}\sqrt{p_1^2+p_2^2+2p_1p_2x_1}. \tag{D.34}$$

Again, the limits of I_3 over x_1 become: $x_1(p_3 = p_1) = -1$ and $x_1(p_3 = p_1+p_2) = 1$. To recover the p_3 limits in Eq.D.34, we need to take the positive sign in the quadratic-formula solution. Thus:

$$dp_3 = \frac{p_1 p_2}{2\sqrt{p_1^2+p_2^2+2p_1p_2x_1}} dx_1 \tag{D.35}$$

$$\implies I_3 = \int_{-1}^{1} \left(\frac{p_1 p_2}{2\sqrt{p_1^2+p_2^2+2p_1p_2x_1}} \right) dx_1 W_{\rm p}(x_1) \tag{D.36}$$

$$= I_1. \tag{D.37}$$

I_2 Integral

$x_0 = -1$ in the I_2 integral. Thus, W_p does not contain any p_3 dependence, implying:

$$I_2 = \int_{p_2}^{p_1} dp_3\, W_\mathrm{p}(-1) \tag{D.38}$$

$$= (p_1 - p_2) \left\{ -\frac{\sqrt{p_1^2 + p_2^2 - 2p_1p_2}}{15p_1^3p_2^3} \right. \tag{D.39}$$

$$\left. \times \left[2\left(p_1^4 + p_2^4\right) + 2\left(p_1^3p_2 + p_1p_2^3\right)(5 - (-1)) + p_1^2p_2^2(3 + 10 + 19)\right] \right\} \tag{D.40}$$

$$= -\frac{(p_1 - p_2)^2}{15p_1^3p_2^3}\left[2\left(p_1^4 + p_2^4\right) + 12\left(p_1^3p_2 + p_1p_2^3\right) + 32p_1^2p_2^2\right] \tag{D.41}$$

I_4 Integral

$$I_4 = \int_0^{p_1+p_2} dp_3\, W_\mathrm{c} \tag{D.42}$$

$$= (p_1 + p_2)\frac{p_1 + p_2}{15p_1^3p_2^3}\left[2\left(p_1^4 + p_2^4\right) + 8\left(p_1^3p_2 + p_1p_2^3\right) + 12p_1^2p_2^2\right] \tag{D.43}$$

$$= \frac{(p_1 + p_2)^2}{15p_1^3p_2^3}\left[2\left(p_1^4 + p_2^4\right) + 8\left(p_1^3p_2 + p_1p_2^3\right) + 12p_1^2p_2^2\right]. \tag{D.44}$$

$I_{\mathbf{AV}}$ Integral

Let's add I_4 to I_2:

$$
\begin{aligned}
I_4 + I_2 = &+ \frac{(p_1+p_2)^2}{15p_1^3p_2^3}\left[2\left(p_1^4+p_2^4\right)+8\left(p_1^3p_2+p_1p_2^3\right)+12p_1^2p_2^2\right] \\
&- \frac{(p_1-p_2)^2}{15p_1^3p_2^3}\left[2\left(p_1^4+p_2^4\right)+12\left(p_1^3p_2+p_1p_2^3\right)+32p_1^2p_2^2\right] && \text{(D.45)} \\
= &+ \frac{p_1^2}{15p_1^3p_2^3}\left[-4\left(p_1^3p_2+p_1p_2^3\right)-20p_1^2p_2^2\right] \\
&+ \frac{p_2^2}{15p_1^3p_2^3}\left[-4\left(p_1^3p_2+p_1p_2^3\right)-20p_1^2p_2^2\right] \\
&+ \frac{2p_1p_2}{15p_1^3p_2^3}\left[4\left(p_1^4+p_2^4\right)+20\left(p_1^3p_2+p_1p_2^3\right)+44p_1^2p_2^2\right] && \text{(D.46)} \\
= &\frac{1}{15p_1^3p_2^3}\left[4p_1^5p_2+20p_1^4p_2^2+80p_1^3p_2^3+20p_1^2p_2^4+4p_1p_2^5\right] && \text{(D.47)} \\
= &\frac{4}{15p_1^2p_2^2}\left[p_1^4+5p_1^3p_2+20p_1^2p_2^2+5p_1p_2^3+p_2^4\right]. && \text{(D.48)}
\end{aligned}
$$

I_3 is equal to I_1, so let's add $2I_1$ to Eq.D.48, which is Eq.D.13:

$$
\begin{aligned}
I_{\mathrm{AV}} = I_4 + I_2 + 2I_1 = &\frac{4}{15p_1^2p_2^2}\left[p_1^4+5p_1^3p_2+20p_1^2p_2^2+5p_1p_2^3+p_2^4\right] \\
&+2\left\{-\frac{2}{15p_1^2p_2^2}\left[\left(p_1^4+p_2^4\right)+5\left(p_1^3p_2+p_1p_2^3\right)+10p_1^2p_2^2\right]\right\} && \text{(D.49)} \\
= &+\frac{4}{15p_1^2p_2^2}\left[10p_1^2p_2^2\right] && \text{(D.50)} \\
= &\frac{8}{3}, && \text{(D.51)}
\end{aligned}
$$

which agrees with Eq.D.4.

D.2.2 Case 2: $p_2 > p_1$

The expressions above are symmetric between p_1 and p_2 except for a few $p_1 - p_2$ expressions from square roots. Those expressions would become $p_2 - p_1$ if $p_2 > p_1$. The result is the same in both cases.

D.2.3 Case 3: $p_1 = p_2$

In this case, $I_1 = I_3$, and I_4 have all of the same values as in Case 1. $I_2 = 0$ in this case. Thus:

$$\begin{aligned} I_{\mathrm{AV}} = I_4 + 2I_1 = &+ \frac{(p_1+p_2)^2}{15p_1^3p_2^3}\left[2\left(p_1^4+p_2^4\right)+8\left(p_1^3p_2+p_1p_2^3\right)+12p_1^2p_2^2\right] \\ &+ 2\left\{-\frac{2}{15p_1^2p_2^2}\left[\left(p_1^4+p_2^4\right)+5\left(p_1^3p_2+p_1p_2^3\right)+10p_1^2p_2^2\right]\right\} \quad \text{(D.52)} \\ = &+ \frac{4p_1^2}{15p_1^6}\left[2\left(2p_1^4\right)+8\left(2p_1^4\right)+12p_1^4\right] \\ &- \frac{4}{15p_1^4}\left[\left(2p_1^4\right)+5\left(2p_1^4\right)+10p_1^4\right] \quad \text{(D.53)} \\ = &\frac{8}{3}. \quad \text{(D.54)} \end{aligned}$$

We acknowledge Chad Kishimoto and Alexey Vlasenko for useful discussions.

Appendix E

Neutrino annihilation into other neutrinos

E.1 Finding integral limits over u

To find the matrix element for neutrino-neutrino annihilation into other neutrinos, we begin with elastic scattering of neutrinos of differing flavor: $\nu_i(1)+\nu_j(2)\rightarrow\nu_i(3)+\nu_j(4)$ where $i\neq j$. The matrix element for this process is:

$$\langle|M|^2\rangle=\lambda(P_1\cdot P_2)(P_3\cdot P_4)$$

P_i is the 4-momentum of each particle. λ is a constant and equal to $32G_F^2$. If we permute the second and third particles, we get the pertinent reaction: $\nu_i(1)+\bar{\nu}_i(2)\rightarrow\bar{\nu}_j(3)+\nu_j(4)$ with matrix element:

$$\langle|M|^2\rangle=\lambda(P_1\cdot P_3)(P_2\cdot P_4)$$

Conservation of linear momentum and energy imply: $P_1 + P_2 = P_3 + P_4$. Taking the inner product of both sides with themselves gives:

$$P_1^2 + P_2^2 + 2P_1 \cdot P_2 = P_3^2 + P_4^2 + 2P_3 \cdot P_4$$

$P_i^2 = m_i^2 = 0$ in the limit that the neutrinos are ultra-relativistic. Thus, we are left with $P_1 \cdot P_2 = P_3 \cdot P_4$.

To simplify the matrix element expression, observe the following:

$$\begin{aligned} P_2 \cdot P_4 &= P_2 \cdot (P_1 + P_2 - P_3) \\ &= P_2 \cdot P_1 + P_2^2 - P_2 \cdot P_3 \\ &= P_3 \cdot P_4 + 0 - P_2 \cdot P_3 \\ &= P_3 \cdot P_4 + P_3^2 - P_3 \cdot P_2 \\ &= P_3 \cdot (P_4 + P_3 - P_2) \\ &= P_3 \cdot P_1 \end{aligned}$$

So we can now simplify the matrix element as:

$$\langle |M|^2 \rangle = \lambda (P_1 \cdot P_3)^2$$

Keep in mind the following prescription when labeling indicies:

$$P_1 : \nu_i$$

$$P_2 : \bar{\nu}_i$$

$$P_3 : \bar{\nu}_j$$

$$P_4 : \nu_j$$

What follows is working through the mathematics to write the scattering integral akin to neutrino-antineutrino scattering.

Our general expression for 2×2 scattering is:

$$\frac{Df_1}{Dt} = \int \frac{s}{2E_1} \frac{d^3p_2}{(2\pi)^3 2E_2} \frac{d^3p_3}{(2\pi)^3 2E_3} \frac{d^3p_4}{(2\pi)^3 2E_4} \times \langle |M|^2 \rangle (2\pi)^4 \delta^4(P_1 + P_2 - P_3 - P_4) F(E_1, E_2, E_3, E_4), \tag{E.1}$$

where s is a multiplicity factor and

$$F(E_1, E_2, E_3, E_4) = (1 - f_1(E_1))(1 - f_2(E_2)) f_3(E_3) f_4(E_4) - f_1(E_1) f_2(E_2)(1 - f_3(E_3))(1 - f_4(E_4)). \tag{E.2}$$

$f_i(E_i)$ is the occupation probability density of species i at energy E_i. As an example, for fermions in thermal and chemical equilibrium:

$$f(E) = \frac{1}{e^{(E-\mu)/T} + 1}$$

$\delta^4(P_1 + P_2 - P_3 - P_4)$ is a four-dimensional delta function denoting conservation of

energy and linear momentum, i.e.:

$$\delta^4(P_1+P_2-P_3-P_4)=\delta(E_1+E_2-E_3-E_4)\delta^3(\vec{p}_1+\vec{p}_2-\vec{p}_3-\vec{p}_4)$$

Our scattering integral now becomes:

$$\begin{aligned}\frac{Df_1}{Dt}&=\frac{s\lambda}{2^4(2\pi)^5 p_1}\int\frac{d^3p_2}{p_2}\int\frac{d^3p_3}{p_3}(P_1\cdot P_3)^2\\&\times\int\frac{d^3p_4}{p_4}\delta(p_1+p_2-p_3-p_4)\delta^3(\vec{p}_1+\vec{p}_2-\vec{p}_3-\vec{p}_4)F(p_1,p_2,p_3,p_4)\end{aligned}\tag{E.3}$$

Since neutrinos are ultra-relativistic, we have dropped the distinction between energy and the magnitude of the linear momentum. Using the spatial component of the delta function over d^3p_4:

$$\begin{aligned}\frac{Df_1}{Dt}&=\frac{s\lambda}{2^4(2\pi)^5 p_1}\int\frac{d^3p_2}{p_2}\\&\times\int\frac{d^3p_3}{p_3}(P_1\cdot P_3)^2\frac{1}{u}\delta(p_1+p_2-p_3-u)F(p_1,p_2,p_3,u)\Big|_{u=|\vec{p}_1+\vec{p}_2-\vec{p}_3|}\end{aligned}\tag{E.4}$$

u is a function of $p_1, p_2, p_3, \theta_2, \text{and}\,\theta_3$ in general. There are still six integrals remaining in our scattering integral. Two of the integrals are trivial integrations around the azimuthal angles ϕ_2 and ϕ_3. We can eliminate one of the remaining four integrals by using the last remaining delta-function factor. Specifically, let us eliminate $d\cos\theta_2$ by using a u-substitution with the conveniently named function u. First, write u as the following:

$$u^2=|\vec{p}_1+\vec{p}_2-\vec{p}_3|^2=|\vec{p}_1-\vec{p}_3|^2+p_2^2+2|\vec{p}_1-\vec{p}_3|p_2\cos\theta_2$$

where we pick θ_2 to be the angle between $\vec{p}_2$ and $\vec{p}_1-\vec{p}_3$. Since we are concerned only with the integral over $d\cos\theta_2$, we treat $p_2, p_3, \text{and}\,\theta_3$ as constants. Taking the derivative

of u^2:

$$2u\,du = 0+0+2|\vec{p}_1-\vec{p}_3|p_2\,d\cos\theta_2$$
$$\implies d\cos\theta_2 = \frac{u}{|\vec{p}_1-\vec{p}_3|p_2}du$$

Our scattering integral now appears as:

$$\begin{aligned}\frac{Df_1}{Dt} &= \frac{s\lambda}{2^4(2\pi)^5 p_1}\int\frac{d^3p_3}{p_3}(P_1\cdot P_3)^2\int d\phi_2\int\frac{p_2^2 dp_2}{p_2}\\ &\times\int_{-1}^{1} d\cos\theta_2\frac{1}{u}\delta(p_1+p_2-p_3-u)F(p_1,p_2,p_3,u) \qquad \text{(E.5)}\\ &= \frac{s\lambda}{2^4(2\pi)^5 p_1}\int\frac{d^3p_3}{p_3}(P_1\cdot P_3)^2(2\pi)\int p_2\,dp_2\\ &\times\int_a^b\frac{u}{|\vec{p}_1-\vec{p}_3|p_2}du\frac{1}{u}\delta(p_1+p_2-p_3-u)F(p_1,p_2,p_3,u) \qquad \text{(E.6)}\\ &= \frac{s\lambda}{2^4(2\pi)^4 p_1}\int\frac{d^3p_3}{p_3|\vec{p}_1-\vec{p}_3|}(P_1\cdot P_3)^2\int dp_2\\ &\times\int_a^b du\,\delta(p_1+p_2-p_3-u)F(p_1,p_2,p_3,u), \qquad \text{(E.7)}\end{aligned}$$

where the new limits of $\int du$ are:

$$a = u(\cos\theta_2=-1) = ||\vec{p}_1-\vec{p}_3|-p_2|, \qquad \text{(E.8)}$$

$$b = u(\cos\theta_2=1) = |\vec{p}_1-\vec{p}_3|+p_2 \qquad \text{(E.9)}$$

The $\int dp_2$ is over infinity, but the $\int du$ is over a finite interval. Therefore, there may be (or may not be) values of p_2 which constrain u to be inside (or outside) the range $[a,b]$. Thus, for the integral to be non-zero: $a<u$ and $u<b$.

E.2 Case 1: $a < u$

E.2.1 Case 1(i): $|\vec{p}_1 - \vec{p}_3| > p_2$

For the delta function to be non-zero, write u as $u = p_1 + p_2 - p_3$. This implies:

$$|\vec{p}_1 - \vec{p}_3| - p_2 < p_1 + p_2 - p_3.$$

Solving for p_2 yields:

$$p_2 > \frac{1}{2}(|\vec{p}_1 - \vec{p}_3| - (p_1 - p_3)) \equiv p_{min}.$$

By the triangle inequality: $|\vec{p}_1 - \vec{p}_3| \geq p_1 - p_3 \implies p_{min} \geq 0$.

E.2.2 Case 1(ii): $p_2 > |\vec{p}_1 - \vec{p}_3|$

In this case, we have:

$$\begin{aligned} & p_2 - |\vec{p}_1 - \vec{p}_3| < p_1 + p_2 - p_3 \\ \implies & -|\vec{p}_1 - \vec{p}_3| < p_1 - p_3 \\ \implies & |\vec{p}_1 - \vec{p}_3| > p_3 - p_1 \end{aligned}$$

The last expression is the triangle inequality. Thus, this sub-case provides no new information.

E.2.3 Case 2: $u < b$

In this case, we have:

$$p_1 + p_2 - p_3 < |\vec{p}_1 - \vec{p}_3| + p_2$$
$$\implies p_1 - p_3 < |\vec{p}_1 - \vec{p}_3|.$$

The last expression is the triangle inequality. Thus, this case provides no new information.

E.3 Combining the integrals over p_2 and u

We can combine $\int dp_2 \int du$ to produce the following expression for our scattering integral:

$$\frac{Df_1}{Dt} = \frac{s\lambda}{2^4(2\pi)^4 p_1} \int \frac{d^3p_3}{p_3|\vec{p}_1 - \vec{p}_3|}(P_1 \cdot P_3)^2 \int_{p_{min}}^{\infty} dp_2 F(p_1, p_2, p_3, p_1 + p_2 - p_3).$$

Let θ_3 be the angle between $\vec{p}_1$ and $\vec{p}_3$. This implies that:

$$|\vec{p}_1 - \vec{p}_3| = \sqrt{p_1^2 + p_3^2 - 2p_1p_3\cos\theta_3},$$

and

$$P_1 \cdot P_3 = p_1p_3 - \vec{p}_1 \cdot \vec{p}_3 = p_1p_3(1 - \cos\theta_3).$$

Let $x \equiv \cos\theta_3$:

$$\frac{Df_1}{Dt} = \frac{s\lambda}{2^4(2\pi)^4 p_1} \int \frac{p_3^2\, dp_3}{p_3} \int \frac{p_1^2 p_3^2 (1-x)^2}{\sqrt{p_1^2 + p_3^2 - 2p_1 p_3 x}} dx \int d\phi_3 \times \int_{p_{min}}^{\infty} dp_2 F(p_1, p_2, p_3, p_1 + p_2 - p_3). \tag{E.10}$$

Since there are no identical particles in the final state, let $s = 1$. Thus:

$$\frac{Df_1}{Dt} = \frac{\lambda}{16(2\pi)^3} p_1 \int p_3^3\, dp_3 \int \frac{(1-x)^2}{\sqrt{p_1^2 + p_3^2 - 2p_1 p_3 x}} dx \times \int_{p_{min}}^{\infty} dp_2 F(p_1, p_2, p_3, p_1 + p_2 - p_3). \tag{E.11}$$

We thank Chad Kishimoto for useful discussions.

Appendix F

First integral of elastic scattering

The reaction of interest is annihilation of electron neutrino and anti-neutrino into an $e^{\pm}$ pair:

$$\nu_e(1) + e^-(2) \rightarrow e^-(3) + \nu_e(4) \tag{F.1}$$

The numbering scheme ensures the fourth particle is massless. We will use q's to denote the magnitude of three-momenta for massive particles, E's to denote energies of massive particles, and p's to denote the energy/momentum magnitude for massless particles.

We start with the three-dimensional integral expression for the process in Eq.(H.1):

$$R_1 \equiv \frac{1}{16(2\pi)^3} \int_{m_e}^{\infty} dE_2 \frac{q_2}{p_1} \int_{-1}^{1} dx \frac{M_1(p_1E_2 - p_1q_2x)}{\sqrt{p_1^2 + q_2^2 + 2p_1q_2x}} \int_{E_{\min}}^{E_{\max}} dE_3 F[p_1, E_2, E_3, p_1 + E_2 - E_3]. \tag{F.2}$$

Eq.(F.36) uses the following defitnitions:

$$M_1(\xi) \equiv 32G_F^2(1+2\sin^2\theta_W)^2\left(\xi^2 - \frac{2\sin^2\theta_W}{1+2\sin^2\theta_W}m_e^2\xi\right) \tag{F.3}$$

$$E_{\min,\max} \equiv \frac{1}{2}\left(p_1+E_2 \mp |\vec{p}_1+\vec{q}_2| + \frac{m_e^2}{p_1+E_2\mp|\vec{p}_1+\vec{q}_2|}\right) \tag{F.4}$$

$$\begin{aligned} F[p_1,E_2,E_3,p_4] \equiv{}& (1-f_1(p_1))(1-f_2(E_2))f_3(E_3)f_4(p_4) \\ & - f_1(p_1)f_2(E_2)(1-f_3(E_3))(1-f_4(p_4)), \end{aligned} \tag{F.5}$$

where G_F is the Fermi coupling constant, θ_W is the Weinberg angle, m_e is the electron rest mass, and $f_i(E_i)$ is the occupation probability of species i at energy E_i.

We use the method of AV to write the third integral of Eq.(F.36) in terms of step functions θ:

$$\begin{aligned} R_1 = {}& \frac{1}{16(2\pi)^3}\int_{m_e}^{\infty} dE_2\frac{q_2}{p_1}\int_{-1}^{1} dx \frac{M_1(p_1E_2-p_1q_2x)}{\sqrt{p_1^2+q_2^2+2p_1q_2x}} \\ & \times \int_{m_e}^{\infty} dE_3 F[p_1,E_2,E_3,p_1+E_2-E_3]\theta(E_3-E_{\min})\theta(E_{\max}-E_3) \end{aligned} \tag{F.6}$$

$$\begin{aligned} = {}& \frac{1}{16(2\pi)^3}\int_{m_3}^{\infty} dE_2\frac{q_2}{p_1}\int_{m_e}^{p_1+E_2} dE_3 F[p_1,E_2,E_3,p_1+E_2-E_3] \\ & \times \int_{-1}^{1} dx \frac{M_1(p_1E_2-p_1q_2x)}{\sqrt{p_1^2+q_2^2+2p_1q_2x}}\theta(E_3-E_{\min})\theta(E_{\max}-E_3). \end{aligned} \tag{F.7}$$

At this point, we will use a change of variables to simplify the integrand in the integral over x:

$$y \equiv |\vec{p}_1+\vec{q}_2| = \sqrt{p_1^2+q_2^2+2p_1q_2x} \tag{F.8}$$

$$\implies dx = dy\frac{y}{p_1q_2} \tag{F.9}$$

The argument in M_1 changes to:

$$p_1E_2 - p_1q_2x = p_1E_2 - \frac{1}{2}(y^2 - p_1^2 - q_2^2) \tag{F.10}$$

$$= \frac{1}{2}(p_1^2 + 2p_1E_2 + q_2^2) - \frac{1}{2}y^2 \tag{F.11}$$

$$= \frac{1}{2}[(p_1 + E_2)^2 - m_e^2] - \frac{1}{2}y^2 \tag{F.12}$$

Eq.(F.7) becomes:

$$R_1 = \frac{1}{16(2\pi)^3}\int_{m_e}^{\infty} dE_2 \frac{q_2}{p_1} \int_{m_e}^{p_1+E_2} dE_3 F[p_1, E_2, E_3, p_1 + E_2 - E_3] \tag{F.13}$$

$$\times \int_{|p_1-q_2|}^{p_1+q_2} \frac{y\,dy}{p_1q_2} \frac{M_1\{\frac{1}{2}[(p_1+E_2)^2 - m_e^2] - \frac{1}{2}y^2\}}{y} \theta(E_3 - E_{\min})\theta(E_{\max} - E_3)$$

(F.14)

$$= \frac{1}{16(2\pi)^3}\int_{m_e}^{\infty} dE_2 \frac{1}{p_1^2} \int_{m_e}^{p_1+E_2} dE_3 F[p_1, E_2, E_3, p_1 + E_2 - E_3] \tag{F.15}$$

$$\times \int_{|p_1-q_2|}^{p_1+q_2} dy M_1\{\frac{1}{2}[(p_1+E_2)^2 - m_e^2] - \frac{1}{2}y^2\}\theta(E_3 - E_{\min})\theta(E_{\max} - E_3).$$

(F.16)

Let's focus on the first θ function, $\theta(E_3 - E_{\min})$. The argument must be positive to have a non-trivial integrand:

$$E_3 - E_{\min} > 0 \tag{F.17}$$

$$\Longrightarrow E_3 - \frac{1}{2}\left(p_1 + E_2 - y + \frac{m_e^2}{p_1 + E_2 - y}\right) > 0 \tag{F.18}$$

$$\Longrightarrow (2E_3 - p_1 - E_2 + y)(p_1 + E_2 - y) - m_e^2 > 0 \tag{F.19}$$

$$\Longrightarrow y^2 - 2y(p_1 + E_2 - E_3) + (p_1 + E_2)^2 - 2E_3(p_1 + E_2) + m_e^2 < 0 \tag{F.20}$$

We can solve for y if we set Eq.(G.54) equal to zero:

$$y = p_1 + E_2 - E_3 \pm \frac{1}{2}\sqrt{4(p_1+E_2-E_3)^2 - 4[(p_1+E_2)^2 - 2E_3(p_1+E_2) + m_e^2]} \quad \text{(F.21)}$$

$$= p_1 + E_2 - E_3 \pm \sqrt{E_3^2 - m_e^2} \quad \text{(F.22)}$$

$$= p_1 + E_2 - E_3 \pm q_3 \quad \text{(F.23)}$$

Thus:

$$y < p_1 + E_2 - E_3 + q_3 \;\; \& \;\; y > p_1 + E_2 - E_3 - q_3. \quad \text{(F.24)}$$

For the second θ function, we have:

$$E_{\max} - E_3 > 0 \quad \text{(F.25)}$$

$$\implies \frac{1}{2}\left(p_1 + E_2 + y + \frac{m_e^2}{p_1 + E_2 + y}\right) - E_3 > 0 \quad \text{(F.26)}$$

$$\implies (p_1 + E_2 + y - 2E_3)(p_1 + E_2 + y) + m_e^2 > 0 \quad \text{(F.27)}$$

$$\implies y^2 + 2y(p_1 + E_2 - E_3) + (p_1 + E_2)^2 - 2E_3(p_1 + E_2) + m_e^2 > 0 \quad \text{(F.28)}$$

Solving for y by setting Eq.(G.61) to zero:

$$y < E_3 - q_3 - p_1 - E_2 \;\; \& \;\; y > E_3 + q_3 - p_1 - E_2. \quad \text{(F.29)}$$

$y \geq 0$ so the first inequality of Eq.(G.62) is extraneous. Eq.(G.58) and Eq.(G.62) imply:

$$y < p_1 + E_2 - E_3 + q_3 \;\; \& \;\; y > |p_1 + E_2 - E_3 - q_3|. \quad \text{(F.30)}$$

The limits of Eq.(F.30) change Eq.(F.16) to:

$$R_1 = \frac{1}{16(2\pi)^3}\int_{m_e}^{\infty} dE_2 \frac{1}{p_1^2}\int_{m_e}^{p_1+E_2} dE_3 F[p_1, E_2, E_3, p_1+E_2-E_3] \times \int_{y_{\min}}^{y_{\max}} dy M_1\{\frac{1}{2}[(p_1+E_2)^2 - m_e^2] - \frac{1}{2}y^2\} \tag{F.31}$$

where:

$$y_{\min} = \max(|p_1 - q_2|, |p_1 + E_2 - E_3 - q_3|) \tag{F.32}$$

$$y_{\max} = \min(p_1 + q_2, p_1 + E_2 - E_3 + q_3). \tag{F.33}$$

It will prove useful to consider two different cases for p_1:

$$\frac{p_1}{m_e} < \frac{1}{2} \tag{F.34}$$

$$\frac{p_1}{m_e} > \frac{1}{2} \tag{F.35}$$

In addition, when writing R_1, we will drop the integrands and overall multiplicative factor for notational simplicity, yielding:

$$R_1 = \int_{m_e}^{\infty} dE_2 \int_{m_e}^{p_1+E_2} dE_3 \int_{y_{\min}}^{y_{\max}} dy \tag{F.36}$$

F.1 Case 1: $\frac{p_1}{m_e} < \frac{1}{2}$

Our goal is to determine the transition points on $\int dE_3$ when the limits change for $\int dy$. The expression for R_1 is:

$$R_1^{(1)} = \int_{m_e}^{E_{\text{cut}}^{(3)}} dE_2 \int_{m_e}^{p_1+E_2} dE_3 \int_{b_1}^{y_{\max}} dy + \int_{E_{\text{cut}}^{(3)}}^{\infty} dE_2 \int_{m_e}^{p_1+E_2} dE_3 \int_{b_2}^{y_{\max}} dy, \tag{F.37}$$

where:

$$\begin{cases} b_1 = \max(p_1 - q_2, |p_1 + E_2 - E_3 - q_3|) \\ b_2 = \max(q_2 - p_1, |p_1 + E_2 - E_3 - q_3|) \end{cases}. \tag{F.38}$$

We begin by investigating the transition point for the top limit $y_{\max}$:

$$p_1 + q_2 = p_1 + E_2 - E_3 + q_3 \tag{F.39}$$

$$\implies E_3 = E_2 \tag{F.40}$$

$$\implies y_{\max} = \begin{cases} p_1 + E_2 - E_3 + q_3 & \text{if } E_3 < E_2 \\ p_1 + q_2 & \text{if } E_3 > E_2 \end{cases}. \tag{F.41}$$

For b_1, we have the first possibility:

$$p_1 - q_2 = p_1 + E_2 - E_3 - q_3 \tag{F.42}$$

$$\implies E_3 = E_2 \tag{F.43}$$

and a second possibility:

$$p_1 - q_2 = E_3 + q_3 - p_1 - E_2 \tag{F.44}$$

$$\implies 2p_1 + E_2 - q_2 - E_3 = q_3. \tag{F.45}$$

For Eq.(F.45) to be valid, $2p_1 + E_2 - q_2 > m_e$. If $\frac{p_1}{m_e} < \frac{1}{2}$, then:

$$2p_1 + E_2 - q_2 = m_e \tag{F.46}$$

$$\implies 2p_1 + E_2 - m_e = q_2 \tag{F.47}$$

$$\implies 4p_1^2 + 4p_1(E_2 - m_e) + E_2^2 - 2E_2 m_e + m_e^2 = E_2^2 - m_e^2 \tag{F.48}$$

$$\implies 4p_1^2 - 4p_1 m_e + 2m_e^2 = E_2(2m_e - 4p_1) \tag{F.49}$$

$$\implies \frac{4p_1^2 - 4p_1 m_e + 2m_e^2}{2m_e - 4p_1} = E_2 \tag{F.50}$$

$$\implies E_{\text{cut}}^{(1)} \equiv m_e + \frac{2p_1^2}{m_e - 2p_1} = E_2 \tag{F.51}$$

$$\implies \begin{cases} 2p_1 + E_2 - q_2 > m_e \text{ if } E_2 < E_{\text{cut}}^{(1)} \\ 2p_1 + E_2 - q_2 < m_e \text{ if } E_2 > E_{\text{cut}}^{(1)} \end{cases}. \tag{F.52}$$

$E_{\text{cut}}^{(1)}$ provides a cut point on $\int dE_2$. Comparing $E_{\text{cut}}^{(1)}$ to $E_{\text{cut}}^{(3)}$:

$$E_{\text{cut}}^{(1)} \sim E_{\text{cut}}^{(3)} \tag{F.53}$$

$$\implies m_e + \frac{2p_1^2}{m_e - 2p_1} \sim \sqrt{p_1^2 + m_e^2} \tag{F.54}$$

$$\implies m_e^2 + \frac{2p_1^2 m_e}{m_e - 2p_1} + \frac{4p_1^4}{(m_e - 2p_1)^2} \sim p_1^2 + m_e^2 \tag{F.55}$$

$$\implies 2p_1^2 m_e(m_e - 2p_1) + 4p_1^4 \sim p_1^2(m_e - 2p_1)^2 \tag{F.56}$$

$$\implies 4p_1^2 - 4p_1 m_e + 2m_e^2 \sim 4p_1^2 - 4p_1 m_e + m_e^2. \tag{F.57}$$

Thus, $E_{\text{cut}}^{(1)} > E_{\text{cut}}^{(3)}$ for $\frac{p_1}{m_e} < \frac{1}{2}$. For $E_2 < E_{\text{cut}}^{(1)}$, Eq.(F.45) gives:

$$2p_1 + E_2 - q_2 - E_3 = \sqrt{E_3^2 - m_e^2} \tag{F.58}$$

$$\implies (2p_1 + E_2 - q_2)^2 - 2E_3(2p_1 + E_2 - q_2) + E_3^2 = E_3^2 - m_e^2 \tag{F.59}$$

$$\implies E_{\text{trans}}^{(2)} \equiv \frac{1}{2}\left(2p_1 + E_2 - q_2 + \frac{m_e^2}{2p_1 + E_2 - q_2}\right) = E_3 \tag{F.60}$$

. We need to compare $E_{\text{trans}}^{(2)}$ to the other transition point, i.e. $E_3 = E_2$:

$$E_{\text{trans}}^{(2)} \sim E_2 \tag{F.61}$$

$$\implies \frac{1}{2}\left(2p_1 + E_2 - q_2 + \frac{m_e^2}{2p_1 + E_2 - q_2}\right) \sim E_2 \tag{F.62}$$

$$\implies 2p_1 - q_2 + \frac{m_e^2}{2p_1 + E_2 - q_2} \sim E_2 \tag{F.63}$$

$$\implies (2p_1 - q_2)(2p_1 + E_2 - q_2) + m_e^2 \sim E_2(2p_1 + E_2 - q_2) \tag{F.64}$$

$$\implies 4p_1^2 + 2p_1E_2 - 4p_1q_2 - E_2q_2 + q_2^2 + m_e^2 \sim 2p_1E_2 + E_2^2 - E_2q_2 \tag{F.65}$$

$$\implies 4p_1^2 - 4p_1q_2 \sim 0 \tag{F.66}$$

$$\implies E_{\text{cut}}^{(3)} \sim E_2 \tag{F.67}$$

$$\implies \begin{cases} E_2 < E_{\text{trans}}^{(2)} \text{ if } E_2 < E_{\text{cut}}^{(3)} \\ E_2 > E_{\text{trans}}^{(2)} \text{ if } E_2 > E_{\text{cut}}^{(3)} \end{cases} \tag{F.68}$$

We also need to compare $E^{(2)}_{\text{trans}}$ to $p_1 + E_2$, the top limit of $\int dE_3$:

$$E^{(2)}_{\text{trans}} \sim p_1 + E_2 \tag{F.69}$$

$$\implies \frac{1}{2}\left(2p_1 + E_2 - q_2 + \frac{m_e^2}{2p_1 + E_2 - q_2}\right) \sim p_1 + E_2 \tag{F.70}$$

$$\implies -q_2 + \frac{m_e^2}{2p_1 + E_2 - q_2} \sim E_2 \tag{F.71}$$

$$\implies -q_2(2p_1 + E_2 - q_2) + m_e^2 \sim E_2(2p_1 + E_2 - q_2) \tag{F.72}$$

$$\implies -2p_1q_2 - E_2q_2 + q_2^2 + m_e^2 \sim 2p_1E_2 + E_2^2 - E_2q_2 \tag{F.73}$$

$$\implies -2p_1q_2 \sim 2p_1E_2. \tag{F.74}$$

$E^{(2)}_{\text{trans}} < p_1 + E_2$ in all cases. Therefore, for $E_2 < E^{(3)}_{\text{cut}}$:

$$b_1 = \begin{cases} p_1 + E_2 - E_3 - q_3 & m_e < E_3 < E_2 \\ p_1 - q_2 & E_2 < E_3 < E^{(2)}_{\text{trans}} \\ E_3 + q_3 - p_1 - E_2 & E^{(2)}_{\text{trans}} < E_3 \end{cases}. \tag{F.75}$$

We can write down the integral expression for $R^{(1)}_1$ if we know the terminus of $\int dE_3$. We determine this point by equating the bottom and top limits of $\int dy$:

$$E_3 + q_3 - p_1 - E_2 = p_1 + q_2 \tag{F.76}$$

$$\implies q_3 = 2p_1 + E_2 + q_2 - E_3 \tag{F.77}$$

$$\implies E_3^2 - m_e^2 = (2p_1 + E_2 + q_2)^2 - 2E_3(2p_1 + E_2 + q_2) + E_3^2 \tag{F.78}$$

$$\implies E_3 = \frac{1}{2}\left(2p_1 + E_2 + q_2 + \frac{m_e^2}{2p_1 + E_2 + q_2}\right) \equiv E^{(1)}_{\text{lim}} \tag{F.79}$$

We need to compare $E_{\rm lim}^{(1)}$ to p_1+E_2:

$$E_{\rm lim}^{(1)} \sim p_1+E_2 \tag{F.80}$$

$$\Longrightarrow \frac{1}{2}\left(2p_1+E_2+q_2+\frac{m_e^2}{2p_1+E_2+q_2}\right) \sim p_1+E_2 \tag{F.81}$$

$$\Longrightarrow q_2+\frac{m_e^2}{2p_1+E_2+q_2} \sim E_2 \tag{F.82}$$

$$\Longrightarrow q_2(2p_1+E_2+q_2)+m_e^2 \sim E_2(2p_1+E_2+q_2) \tag{F.83}$$

$$\Longrightarrow 2p_1q_2+E_2q_2+q_2^2+m_e^2 \sim 2p_1E_2+E_2^2+E_2q_2 \tag{F.84}$$

$$\Longrightarrow 2p_1q_2 \sim 2p_1E_2 \tag{F.85}$$

$$\tag{F.86}$$

Thus, $E_{\rm lim}^{(1)} < p_1+E_2$ always. At this point, the expression for $R_1^{(1)}$ is:

$$\begin{aligned} R_1^{(1)} = &\int_{m_e}^{E_{\rm cut}^{(3)}} dE_2 \left(\int_{m_e}^{E_2} dE_3 \int_{p_1+E_2-E_3-q_3}^{p_1+E_2-E_3+q_3} dy + \int_{E_2}^{E_{\rm trans}^{(2)}} dE_3 \int_{p_1-q_2}^{p_1+E_2-E_3+q_3} dy \right. \\ &\left. + \int_{E_{\rm trans}^{(2)}}^{E_{\rm lim}^{(1)}} dE_3 \int_{E_3+q_3-p_1-E_2}^{p_1+q_2} dy \right) \\ &+ \int_{E_{\rm cut}^{(3)}}^{E_{\rm cut}^{(1)}} dE_2 \int_{m_e}^{p_1+E_2} dE_3 \int_{b_2}^{y_{\rm max}} dy \\ &+ \int_{E_{\rm cut}^{(1)}}^{\infty} dE_2 \int_{m_e}^{p_1+E_2} dE_3 \int_{b_3}^{y_{\rm max}} dy. \end{aligned} \tag{F.87}$$

where we have broken up the interval $E_2 > E_{\rm cut}^{(3)}$ into two intervals to anticipate when Eq.(F.45) is no longer valid.

To determine the transition point for b_2, we start with:

$$q_2 - p_1 = p_1 + E_2 - E_3 - q_3 \tag{F.88}$$

$$\Longrightarrow q_3 = 2p_1 + E_2 - q_2 - E_3 \tag{F.89}$$

Eq.(F.89) is identical to Eq.(F.45), implying:

$$\begin{cases} p_1 + E_2 - E_3 - q_3 > q_2 - p_1 \text{ if } E_3 < E_{\text{trans}}^{(2)} \\ p_1 + E_2 - E_3 - q_3 < q_2 - p_1 \text{ if } E_3 > E_{\text{trans}}^{(2)} \end{cases} \tag{F.90}$$

The transition point E_2 also holds, and $E_{\text{trans}}^{(2)} < E_2$ for b_2. For $E_2 > E_{\text{cut}}^{(1)}$, there is no $E_{\text{trans}}^{(2)}$. We investigate where the initial starting value of $\int dE_2$ is, by equating the bottom and top limits of the first $\int dy$:

$$p_1 + E_2 - E_3 + q_3 = q_2 - p_1 \tag{F.91}$$

$$\Longrightarrow q_3 = E_3 - 2p_1 - E_2 + q_2 \tag{F.92}$$

$$\Longrightarrow E_3 = \frac{1}{2}\left(2p_1 + E_2 - q_2 + \frac{m_e^2}{2p_1 + E_2 - q_2}\right) \equiv E_{\text{lim}}^{(2)} \tag{F.93}$$

We need to ensure that $E_{\text{lim}}^{(2)}$ is larger than m_e. To begin, we consider the derivative of $E_{\text{lim}}^{(2)}$ with respect to E_2:

$$\frac{\partial E_{\text{lim}}^{(2)}}{\partial E_2} = \frac{1}{2}\left[1 - \frac{E_2}{q_2} - \frac{m_e^2}{(2p_1 + E_2 - q_2)^2}\left(1 - \frac{E_2}{q_2}\right)\right] = 0 \tag{F.94}$$

$$\Longrightarrow (2p_1 + E_2 - q_2)^2 = m_e^2 \tag{F.95}$$

$$\Longrightarrow 2p_1 + E_2 - m_e = q_2 \tag{F.96}$$

$$\Longrightarrow E_{\text{cut}}^{(1)} = E_2 \tag{F.97}$$

$E_{\text{cut}}^{(1)}$ is a local min. Calculating the momentum when $E_2 = E_{\text{cut}}^{(1)}$ yields:

$$q_2(E_2 = E_{\text{cut}}^{(1)}) = \left[\left(m_e + \frac{2p_1^2}{m_e - 2p_1}\right) - m_e^2\right]^{1/2} \tag{F.98}$$

$$= \left[m_e^2 + \frac{4p_1^2 m_e}{m_e - 2p_1} + \frac{4p_1^4}{(m_e - 2p_1)^2} - m_e^2\right]^{1/2} \tag{F.99}$$

$$= \frac{2p_1}{m_e - 2p_1}\left[m_e(m_e - 2p_1) + p_1^2\right] \tag{F.100}$$

$$= \frac{2p_1(m_e - p_1)}{m_e - 2p_1} \tag{F.101}$$

which implies the difference between E_2 and q_2 when $E_2 = E_{\text{cut}}^{(1)}$ is:

$$(E_2 - q_2)(E_2 = E_{\text{cut}}^{(1)}) = m_e + \frac{2p_1^2}{m_e - 2p_1} - \frac{2p_1(m_e - p_1)}{m_e - 2p_1} \tag{F.102}$$

$$= \frac{m_e(m_e - 2p_1) + 2p_1^2 - 2p_1(m_e - p_1)}{m_e - 2p_1} \tag{F.103}$$

$$= \frac{m_e^2 - 4p_1 m_e + 4p_1^2}{m_e - 2p_1} \tag{F.104}$$

$$= m_e - 2p_1. \tag{F.105}$$

Finally, the value of $E_{\text{lim}}^{(2)}$ when $E_2 = E_{\text{cut}}^{(1)}$ is:

$$E_{\text{lim}}^{(2)}(E_2 = E_{\text{cut}}^{(1)}) = \frac{1}{2}\left(2p_1 + m_e - 2p_1 + \frac{m_e^2}{2p_1 + m_e - 2p_1}\right) = m_e \tag{F.106}$$

Therefore, $E_{\text{lim}}^{(2)} > m_e$. We are left with the following equation for $R_1^{(1)}$:

$$
\begin{aligned}
R_1^{(1)} = & \int_{m_e}^{E_{\text{cut}}^{(3)}} dE_2 \left(\int_{m_e}^{E_2} dE_3 \int_{p_1+E_2-E_3-q_3}^{p_1+E_2-E_3+q_3} dy \right. \\
& \left. + \int_{E_2}^{E_{\text{trans}}^{(2)}} dE_3 \int_{p_1-q_2}^{p_1+q_2} dy + \int_{E_{\text{trans}}^{(2)}}^{E_{\text{lim}}^{(1)}} dE_3 \int_{E_3+q_3-p_1-E_2}^{p_1+q_2} dy \right) \\
& + \int_{E_{\text{cut}}^{(3)}}^{E_{\text{cut}}^{(1)}} dE_2 \left(\int_{m_e}^{E_{\text{trans}}^{(2)}} dE_3 \int_{p_1+E_2-E_3-q_3}^{p_1+E_2-E_3+q_3} dy \right. \\
& \left. + \int_{E_{\text{trans}}^{(2)}}^{E_2} dE_3 \int_{q_2-p_1}^{p_1+E_2-E_3+q_3} dy + \int_{E_2}^{E_{\text{lim}}^{(1)}} dE_3 \int_{E_3+q_3-p_1-E_2}^{p_1+q_2} dy \right) \\
& + \int_{E_{\text{cut}}^{(1)}}^{\infty} dE_2 \left(\int_{E_{\text{lim}}^{(2)}}^{E_2} dE_3 \int_{q_2-p_1}^{p_1+E_2-E_3+q_3} dy + \int_{E_2}^{E_{\text{lim}}^{(1)}} dE_3 \int_{E_3+q_3-p_1-E_2}^{p_1+q_2} dy \right) . \qquad \text{(F.107)}
\end{aligned}
$$

F.2 Case 2: $\frac{p_1}{m_e} > \frac{1}{2}$

$E_{\text{cut}}^{(1)}$ is not relevant in this case because $2p_1 + E_2 - q_2 > m_e$ for all E_2. Therefore, $E_{\text{lim}}^{(2)}$ is not applicable and we can just change the limit on the second $\int dE_2$ of Eq.(F.107)

to find $R_1^{(2)}$:

$$
\begin{aligned}
R_1^{(2)} = \int_{m_e}^{E_{\text{cut}}^{(3)}} dE_2 \Bigg(& \int_{m_e}^{E_2} dE_3 \int_{p_1+E_2-E_3-q_3}^{p_1+E_2-E_3+q_3} dy \\
& + \int_{E_2}^{E_{\text{trans}}^{(2)}} dE_3 \int_{p_1-q_2}^{p_1+E_2-E_3+q_3} dy + \int_{E_{\text{trans}}^{(2)}}^{E_{\text{lim}}^{(1)}} dE_3 \int_{E_3+q_3-p_1-E_2}^{p_1+q_2} dy \Bigg) \\
& + \int_{E_{\text{cut}}^{(3)}}^{\infty} dE_2 \Bigg(\int_{m_e}^{E_{\text{trans}}^{(2)}} dE_3 \int_{p_1+E_2-E_3-q_3}^{p_1+E_2-E_3+q_3} dy \qquad \text{(F.108)} \\
& + \int_{E_{\text{trans}}^{(2)}}^{E_2} dE_3 \int_{q_2-p_1}^{p_1+E_2-E_3+q_3} dy + \int_{E_2}^{E_{\text{lim}}^{(1)}} dE_3 \int_{E_3+q_3-p_1-E_2}^{p_1+q_2} dy \Bigg) . \qquad \text{(F.109)}
\end{aligned}
$$

Appendix G

Second integral of elastic scattering

G.1 Determining triple integral involving $M_2(P_1 \cdot Q_3)$

The reaction of interest is elastic scattering of electron neutrinos with electrons:

$$\nu_e(1) + e^-(2) \rightarrow e^-(3) + \nu_e(4) \tag{G.1}$$

The numbering scheme ensures the fourth particle is massless. We will use q's to denote the magnitude of three-momenta for massive particles, E's to denote energies of massive particles, and p's to denote the energy/momentum magnitude for massless particles. We use capital P and Q to denote four-momenta of massless and massive particles, respectively. After using the three-dimensional delta function to reduce the $\int d^3p_4$ and the u substitution $u = p_4$, CK finds:

$$R_2 = \frac{1}{16(2\pi)^4} \int \frac{q_2 dq_2 d^3q_3}{p_1 E_2 E_3 |\vec{p}_1 - \vec{q}_3|} M_2(P_1 \cdot Q_3) \int_a^b du\, \delta(p_1 + E_2 - E_3 - u) F(p_1, E_2, E_3, u), \tag{G.2}$$

with limits of integration:

$$a = ||\vec{p}_1 - \vec{q}_3| - q_2| \tag{G.3}$$

$$b = |\vec{p}_1 - \vec{q}_3| + q_2, \tag{G.4}$$

summed-squared-matrix element:

$$M_2(\xi) \equiv 128 G_F^2 \sin^4\theta_W \left(\xi^2 + \frac{1+2\sin^2\theta_W}{2\sin^2\theta_W} m_e^2 \xi\right), \tag{G.5}$$

and occupation probability expression:

$$\begin{aligned} F(p_1, E_2, E_3, p_4) \equiv & (1-f_1(p_1))(1-f_2(E_2))f_3(E_3)f_4(p_4) \\ & - f_1(p_1)f_2(E_2)(1-f_3(E_3))(1-f_4(p_4)). \end{aligned} \tag{G.6}$$

G_F is the Fermi coupling constant, θ_W is the Weinberg angle, m_e is the electron rest mass, and $f_i(E_i)$ is the occupation probability of species i at energy E_i. Eq. (G.2) contains two integrals over angles involving q_3: trivial integration over azimuthal angle ϕ_3; and non-trivial integration over elevation angle θ_3 in $P_1 \cdot Q_3$. Let us define θ_3 as the angle between $\vec{p}_1$ and $\vec{q}_3$ expounding Eq.(G.2) as:

$$\begin{aligned} R_2 = & \frac{1}{16(2\pi)^4} \int_0^{2\pi} d\phi_3 \int_0^{\infty} dq_3 \frac{q_3^2}{p_1 E_3} \int_0^{\pi} \sin\theta_3 d\theta_3 \frac{M_2(P_1 \cdot Q_3)}{|\vec{p}_1 - \vec{q}_3|} \\ & \times \int_0^{\infty} q_2 dq_2 \frac{1}{E_2} \int_a^b du\, \delta(p_1 + E_2 - E_3 - u) F(p_1, E_2, E_3, u) \end{aligned} \tag{G.7}$$

$$\equiv \frac{1}{16(2\pi)^3} \int_{m_e}^{\infty} dE_3 \frac{q_3}{p_1} \int_{-1}^{1} dx \frac{M_2(P_1 \cdot Q_3)}{|\vec{p}_1 - \vec{q}_3|} \int_{m_e}^{\infty} dE_2 \int_a^b du\, \delta(p_1 + E_2 - E_3 - u) F \tag{G.8}$$

where we made a change of variables using $x \equiv \cos\theta_3$, converted the integrals over momentum q_2, q_3 into integrals over energy E_2, E_3, and dropped the arguments of F for convenience. We make a change of variables to simplify the integrand in the integral over x:

$$y \equiv |\vec{p}_1 - \vec{q}_3| = \sqrt{p_1^2 + q_3^2 - 2p_1 q_3 x} \tag{G.9}$$

$$\Longrightarrow dx = -dy\frac{y}{p_1 q_3} \tag{G.10}$$

The argument in M_2 changes to:

$$p_1 E_3 - p_1 q_3 x = p_1 E_3 - \frac{1}{2}(p_1^2 + q_3^2 - y^2) \tag{G.11}$$

$$= \frac{1}{2}y^2 - \frac{1}{2}(p_1^2 - 2p_1 E_3 + q_3^2) \tag{G.12}$$

$$= \frac{1}{2}y^2 - \frac{1}{2}[(p_1 - E_3)^2 - m_e^2] \tag{G.13}$$

This leaves us with the following expression for Eq.(G.8):

$$R_2 = \frac{1}{16(2\pi)^3}\int_{m_e}^{\infty} dE_3 \frac{q_3}{p_1}\int_{p_1+q_3}^{|p_1-q_3|}\left(-\frac{ydy}{p_1 q_3}\right)\frac{M_2\left\{\frac{1}{2}y^2 - \frac{1}{2}[(p_1-E_3)^2 - m_e^2]\right\}}{y}$$

$$\times \int_{m_e}^{\infty} dE_2 \int_a^b du\,\delta(p_1 + E_2 - E_3 - u)F \tag{G.14}$$

$$= \frac{1}{16(2\pi)^3}\int_{m_e}^{\infty} dE_3 \frac{1}{p_1^2}\int_{|p_1-q_3|}^{p_1+q_3} dy\, M_2\left\{\frac{1}{2}y^2 - \frac{1}{2}[(p_1-E_3)^2 - m_e^2]\right\}$$

$$\times \int_{m_e}^{\infty} dE_2 \int_a^b du\,\delta(p_1 + E_2 - E_3 - u)F. \tag{G.15}$$

$$\tag{G.16}$$

The integral over u is non-zero when

$$|y-q_2| < p_1+E_2-E_3 < y+q_2, \tag{G.17}$$

for $y \equiv |\vec{p}_1 - \vec{q}_3|$.

First, consider the case that $y > q_2 \implies E_2 < \sqrt{y^2+m_e^2}$. We have:

$$y-q_2 < p_1+E_2-E_3 < y+q_2 \tag{G.18}$$

$$\implies -q_2 < E_2-(E_3-p_1+y) < q_2 \tag{G.19}$$

$$\implies E_2^2-2E_2(E_3-p_1+y)+(E_3-p_1+y)^2 < q_2^2 = E_2^2-m_e^2 \tag{G.20}$$

$$\implies (E_3-p_1+y)^2+m_e^2 < 2E_2(E_3-p_1+y) \tag{G.21}$$

$$\implies E_2 > \frac{1}{2}\left(E_3-p_1+y+\frac{m_e^2}{E_3-p_1+y}\right) \equiv E_{\min} \tag{G.22}$$

Observe that $E_3-p_1+y > E_3-p_1+(p_1-q_3) = E_3-q_3 > 0$. Therefore, $E_3-p_1+y > 0$. Note two important points. Firstly, in this case, $E_{\min} < E_2 < \sqrt{y^2+m_e^2}$. Secondly, $E_{\min} > m_e$. To see this, fix p_1 and E_3 and solve for y when $E_{\min} = m_e$:

$$E_{\min} = m_e \tag{G.23}$$

$$\implies \frac{1}{2}\left(E_3-p_1+y+\frac{m_e^2}{E_3-p_1+y}\right) = m_e \tag{G.24}$$

$$\implies (E_3-p_1+y)^2-2m_e(E_3-p_1+y)+m_e^2 = 0 \tag{G.25}$$

$$\implies (E_3-p_1+y-m_e)^2 = 0 \tag{G.26}$$

$$\implies y = p_1-E_3+m_e \tag{G.27}$$

The above value $y = p_1-E_3+m_3$ may or may not fall into the range of $\int dy$. Regardless,

taking the derivative of $E_{\min}$ with respect to y yields:

$$\frac{\partial E_{\min}}{\partial y} = \frac{1}{2}\left(1 - \frac{m_e^2}{(E_3 - p_1 + y)^2}\right) \tag{G.28}$$

The derivative is equal to zero when $y = p_1 - E_3 + m_e$, less than zero when $y < p_1 - E_3 + m_e$, and greater than zero when $y > p_1 - E_3 + m_e$. Therefore, m_e is a global minimum of $E_{\min}$.

Second, consider the case $y < q_2 \implies E_2 > \sqrt{y^2 + m_e^2}$. We have:

$$q_2 - y < p_1 + E_2 - E_3 < y + q_2 \tag{G.29}$$

$$\implies -q_2 < q_2 - 2y < E_2 - (E_3 - p_1 + y) < q_2 \tag{G.30}$$

$$\implies -q_2 < E_2 - (E_3 - p_1 + y) < q_2 \tag{G.31}$$

$$\implies E_2 > E_{\min} \tag{G.32}$$

Also, consider the first inequality by itself:

$$q_2 - y < p_1 + E_2 - E_3 \tag{G.33}$$

$$\implies q_2 < E_2 - (E_3 - p_1 - y) \tag{G.34}$$

$$\implies q_2^2 = E_2^2 - m_e^2 < E_2^2 - 2E_2(E_3 - p_1 - y) + (E_3 - p_1 - y)^2 \tag{G.35}$$

$$\implies 2E_2(E_3 - p_1 - y) < (E_3 - p_1 - y)^2 + m_e^2 \tag{G.36}$$

If $E_3 - p_1 - y < 0$, then there is no constraint on E_2. If $E_3 - p_1 - y > 0$:

$$E_2 < \frac{1}{2}\left(E_3 - p_1 - y + \frac{m_e^2}{E_3 - p_1 - y}\right) \equiv E_{\max}^{(\mathrm{B})}. \tag{G.37}$$

We will define $E_{\max}$ as the following:

$$E_{\max} \equiv \begin{cases} E_{\max}^{(\mathrm{B})} & \text{if } E_3 - p_1 - y > 0 \\ \infty & \text{if } E_3 - p_1 - y < 0 \end{cases} \tag{G.38}$$

The minimum limit on $\int dE_2$ was $E_{\min}$ when $E_2 < \sqrt{y^2 + m_e^2}$ or $E_2 > \sqrt{y^2 + m_e^2}$. Therefore, the minimum limit on $\int dE_2$ is always $E_{\min}$. This leaves us with the following expression for R_2:

$$R_2 = \frac{1}{16(2\pi)^3} \int_{m_e}^{\infty} dE_3 \frac{1}{p_1^2} \int_{|p_1 - q_3|}^{p_1 + q_3} dy M_2 \left\{ \frac{1}{2} y^2 - \frac{1}{2} [(p_1 - E_3)^2 - m_e^2] \right\} \int_{E_{\min}}^{E_{\max}} dE_2 F \tag{G.39}$$

There may be a case where $E_{\min} = E_{\max}^{(\mathrm{B})}$:

$$\frac{1}{2}\left(E_3 - p_1 + y + \frac{m_e^2}{E_3 - p_1 + y}\right) = \frac{1}{2}\left(E_3 - p_1 - y + \frac{m_e^2}{E_3 - p_1 - y}\right) \tag{G.40}$$

$$\implies 2y = m_e^2 \left(\frac{1}{E_3 - p_1 - y} - \frac{1}{E_3 - p_1 + y}\right) \tag{G.41}$$

$$\implies 2y = m_e^2 \frac{2y}{(E_3 - p_1)^2 - y^2} \tag{G.42}$$

Ignoring the $y = 0$ solution for the time being, we find:

$$y = \sqrt{(E_3 - p_1)^2 - m_e^2} \tag{G.43}$$

For $E_{\max} = E_{\max}^{(\mathrm{B})}$, $y < E_3 - p_1$ which $\sqrt{(E_3 - p_1)^2 - m_e^2}$ satsfies. $\sqrt{(E_3 - p_1)^2 - m_e^2}$ must

fall within the range in $\int dy$, i.e. $|p_1 - q_3| < \sqrt{(E_3 - p_1)^2 - m_e^2}$. However:

$$\sqrt{(E_3 - p_1)^2 - m_e^2} = \sqrt{p_1^2 - 2p_1E_3 + E_3^2 - m_e^2} \tag{G.44}$$

$$= \sqrt{p_1^2 - 2p_1E_3 + q_3^2} \tag{G.45}$$

$$< \sqrt{p_1^2 - 2p_1q_3 + q_3^2} \tag{G.46}$$

$$= |p_1 - q_3| \tag{G.47}$$

Therefore, y never assumes the value $\sqrt{(E_3 - p_1)^2 - m_e^2}$ and $E_{\max}^{(B)} > E_{\min}$ for all $y < E_3 - p_1$. If $y = 0$, then $E_{\max}^{(B)} = E_{\min}$. However, this can only happen when $q_3 = p_1$ so we neglect it. Eq.(G.39) is a three-dimensional integral for R_2. We will reduce R_2 to two dimensions by eliminating $\int dy$ since F has no angular dependence.

G.2 Writing $\int dE_2$ in terms of θ functions

We have two distinct $\int dE_2$, which we can write in terms of θ functions:

$$\int_{E_{\min}}^{E_{\max}^{(B)}} dE_2 = \int_{m_e}^{\infty} dE_2 \theta(E_2 - E_{\min})\theta(E_{\max}^{(B)} - E_2), \tag{G.48}$$

$$\int_{E_{\min}}^{\infty} dE_2 = \int_{m_e}^{\infty} dE_2 \theta(E_2 - E_{\min}). \tag{G.49}$$

We define the θ function as:

$$\theta(x) = \begin{cases} 1 & \text{if } x > 0 \\ 0 & \text{if } x < 0. \end{cases} \tag{G.50}$$

Let's first consider $\theta(E_2 - E_{\min})$:

$$E_2 - E_{\min} = E_2 - \frac{1}{2}\left(E_3 - p_1 + y + \frac{m_e^2}{E_3 - p_1 + y}\right) > 0 \tag{G.51}$$

$$\implies (2E_2 - E_3 + p_1 - y)(E_3 - p_1 + y) - m_e^2 > 0 \tag{G.52}$$

$$\implies -y^2 + 2y(E_2 + p_1 - E_3) - (E_3 - p_1)^2 + 2E_2(E_3 - p_1) - m_e^2 > 0 \tag{G.53}$$

$$\implies y^2 - 2y(E_2 + p_1 - E_3) + (E_3 - p_1)^2 - 2E_2(E_3 - p_1) + m_e^2 < 0 \tag{G.54}$$

We can solve for y if we set Eq.(G.54) to zero:

$$y = p_1 + E_2 - E_3 \pm \frac{1}{2}\sqrt{4[(E_2 - (E_3 - p_1)]^2 - 4[(E_3 - p_1)^2 - 2E_2(E_3 - p_1) + m_e^2]} \tag{G.55}$$

$$= p_1 + E_2 - E_3 \pm \sqrt{E_2^2 - m_e^2} \tag{G.56}$$

$$= p_1 + E_2 - E_3 \pm q_2 \tag{G.57}$$

For $E_2 - E_{\min} > 0$:

$$y < p_1 - E_3 + E_2 + q_2 \;\;\&\;\; y > p_1 - E_3 + E_2 - q_2. \tag{G.58}$$

The second θ function of Eq.(G.48) implies the following:

$$E_{\max}^{(B)} - E_2 = \frac{1}{2}\left(E_3 - p_1 - y + \frac{m_e^2}{E_3 - p_1 - y}\right) - E_2 > 0 \tag{G.59}$$

$$\implies (E_3 - p_1 - y - 2E_2)(E_3 - p_1 - y) + m_e^2 > 0 \tag{G.60}$$

$$\implies y^2 - 2y(E_3 - p_1 - E_2) + (E_3 - p_1)^2 - 2E_2(E_3 - p_1) + m_e^2 > 0 \tag{G.61}$$

Solving for y by setting Eq.(G.61) to zero:

$$y < E_3 - p_1 - E_2 - q_2 \;\; \& \;\; y > E_3 - p_1 - E_2 + q_2. \tag{G.62}$$

$y \geq 0$ so the first inequality of Eq.(G.62) is extraneous.

We cannot move forward with the step functions because we do not have a specific expression for $E_{\max}$ on $\int dE_2$. We have two cases, and the qualifier depends on the value y. We must determine the conditions when we assume a given value for $E_{\max}$. Clearly, there is a transition point when $y = E_3 - p_1$. We want to know at what values of E_3 does $E_3 - p_1$ equal the limits of $\int dy$. Consider the top limit:

$$E_3 - p_1 = p_1 + q_3 \tag{G.63}$$

$$\implies E_3 - 2p_1 = q_3 \tag{G.64}$$

For Eq.(G.64) to be meaningful, $2p_1 < m_e \implies p_1 < \frac{m_e}{2}$. Solving Eq.(G.64) for E_3 yields:

$$E_3^2 - 4p_1E_3 + 4p_1^2 = E_3^2 - m_e^2 \tag{G.65}$$

$$\implies E_{\text{cut}}^{(1)} \equiv p_1 + \frac{m_e^2}{4p_1} = E_3 \tag{G.66}$$

Similarily, for the bottom limit:

$$E_3 - p_1 = |p_1 - q_3| \tag{G.67}$$

$$\implies E_3 - p_1 = p_1 - q_3 \tag{G.68}$$

$$\implies q_3 = 2p_1 - E_3 \tag{G.69}$$

We do not consider the case $|p_1 - q_3| = q_3 - p_1$ as that never produces equality with

$E_3 - p_1$. For Eq.(G.69) to be meaningful, $2p_1 > m_e \implies p_1 > \frac{m_e}{2}$. Solving Eq.(G.69) for E_3 yields the same quantity in Eq.(H.37): $E_3 = E_{\text{cut}}^{(1)}$. It will prove useful to consider five different cases for p_1:

$$\frac{p_1}{m_e} < \frac{\sqrt{5}-1}{4} \tag{G.70}$$

$$\frac{\sqrt{5}-1}{4} < \frac{p_1}{m_e} < \frac{1}{2\sqrt{2}} \tag{G.71}$$

$$\frac{1}{2\sqrt{2}} < \frac{p_1}{m_e} < \frac{1}{2} \tag{G.72}$$

$$\frac{1}{2} < \frac{p_1}{m_e} < \frac{3}{4} \tag{G.73}$$

$$\frac{3}{4} < \frac{p_1}{m_e} \tag{G.74}$$

In addition, when writing R_2, we will drop the integrands and overall multiplicative factor for notational simplicity, yielding:

$$R_2 = \int_{m_e}^{\infty} dE_3 \int_{|p_1-q_3|}^{p_1+q_3} dy \int_{E_{\min}}^{E_{\max}} dE_2 \tag{G.75}$$

G.3 Finding limits of $\int dy$

G.3.1 Case 1: $\frac{p_1}{m_e} < \frac{\sqrt{5}-1}{4}$

We have a cut point at $E_3 = E_{\text{cut}}^{(1)}$:

$$R_2^{(1)} = \int_{m_e}^{E_{\text{cut}}^{(1)}} dE_3 \int_{|p_1-q_3|}^{p_1+q_3} dy \int_{E_{\min}}^{E_{\max}} dE_2 + \int_{E_{\text{cut}}^{(1)}}^{\infty} dE_3 \int_{|p_1-q_3|}^{p_1+q_3} dy \int_{E_{\min}}^{E_{\max}} dE_2 \tag{G.76}$$

$$= \int_{m_e}^{E_{\text{cut}}^{(1)}} dE_3 \int_{|p_1-q_3|}^{p_1+q_3} dy \int_{E_{\min}}^{E_{\max}^{(\text{B})}} dE_2 + \int_{E_{\text{cut}}^{(1)}}^{\infty} dE_3 \left(\int_{|p_1-q_3|}^{E_3-p_1} dy \int_{E_{\min}}^{E_{\max}^{(\text{B})}} dE_2 + \int_{E_3-p_1}^{p_1+q_3} dy \int_{E_{\min}}^{\infty} dE_2 \right) \tag{G.77}$$

(G.78)

Let us define $E_{\text{cut}}^{(3)}$ as the cut point where $p_1 = q_3$, i.e.

$$E_{\text{cut}}^{(3)} \equiv \sqrt{p_1^2 + m_e^2}. \tag{G.79}$$

Equality between $E_{\rm cut}^{(1)}$ and $E_{\rm cut}^{(3)}$ occurs when:

$$E_{\rm cut}^{(1)} = E_{\rm cut}^{(3)} \tag{G.80}$$

$$\Longrightarrow p_1 + \frac{m_e^2}{4p_1} = \sqrt{p_1^2 + m_e^2} \tag{G.81}$$

$$\Longrightarrow 4p_1^2 + m_e^2 = 4p_1\sqrt{p_1^2 + m_e^2} \tag{G.82}$$

$$\Longrightarrow 16p_1^4 + 8p_1^2 m_e^2 + m_e^4 = 16p_1^4 + 16p_1^2 m_e^2 \tag{G.83}$$

$$\Longrightarrow m_e^4 = 8p_1^2 m_e^2 \tag{G.84}$$

$$\Longrightarrow \frac{m_e}{2\sqrt{2}} = p_1 \tag{G.85}$$

$$\Longrightarrow \begin{cases} E_{\rm cut}^{(1)} > E_{\rm cut}^{(3)} & \text{if } p_1 < \frac{m_e}{2\sqrt{2}} \\ E_{\rm cut}^{(1)} < E_{\rm cut}^{(3)} & \text{if } p_1 > \frac{m_e}{2\sqrt{2}} \end{cases} \tag{G.86}$$

Eq.(G.77) becomes:

$$\begin{aligned} R_2^{(1)} = &\int_{m_e}^{E_{\rm cut}^{(3)}} dE_3 \int_{p_1-q_3}^{p_1+q_3} dy \int_{E_{\rm min}}^{E_{\rm max}^{\rm (B)}} dE_2 + \int_{E_{\rm cut}^{(3)}}^{E_{\rm cut}^{(1)}} dE_3 \int_{q_3-p_1}^{p_1+q_3} dy \int_{E_{\rm min}}^{E_{\rm max}^{\rm (B)}} dE_2 \\ &+ \int_{E_{\rm cut}^{(1)}}^{\infty} dE_3 \left(\int_{q_3-p_1}^{E_3-p_1} dy \int_{E_{\rm min}}^{E_{\rm max}^{\rm (B)}} dE_2 + \int_{E_3-p_1}^{p_1+q_3} dy \int_{E_{\rm min}}^{\infty} dE_2 \right) \end{aligned} \tag{G.87}$$

We will consider separately each of the four integrals of Eq.(G.120).

First Integral

We have the following expression for the first integral of Eq.(G.120):

$$I_1 \equiv \int_{m_e}^{E_{\rm cut}^{(3)}} dE_3 \int_{p_1-q_3}^{p_1+q_3} dy \int_{E_{\rm min}}^{E_{\rm max}^{\rm (B)}} dE_2 \tag{G.88}$$

$$= \int_{m_e}^{E_{\rm cut}^{(3)}} dE_3 \int_{p_1-q_3}^{p_1+q_3} dy \int_{m_e}^{\infty} dE_2 \theta(E_2 - E_{\rm min})\theta(E_{\rm max}^{\rm (B)} - E_2) \tag{G.89}$$

$$= \int_{m_e}^{E_{\rm cut}^{(3)}} dE_3 \int_{m_e}^{\infty} dE_2 \int_{b_1}^{t_1} dy \tag{G.90}$$

where:

$$\begin{cases} t_1 = \min(p_1 + q_3, p_1 - E_3 + E_2 + q_2) \\ b_1 = \max(p_1 - q_3, p_1 - E_3 + E_2 - q_2, E_3 - p_1 - E_2 + q_2) \end{cases} \tag{G.91}$$

Before we continue with finding the transition points for t_1 and b_1, we need to make a few observations. We will keep the integrals over energy, and not momentum. The equations tend to be simpler if solving for E as compared to q. Also, we will solve for E_2 instead of E_3, implying that $\int dE_2$ is within $\int dE_3$. There will be many cases when the top limit of $\int dE_2$ is unbounded.

The top limit goes through a transition point at $E_2 = E_3$,

$$t_1 = \begin{cases} p_1 - E_3 + E_2 + q_2 & \text{if } E_2 < E_3 \\ p_1 + q_3 & \text{if } E_2 > E_3 \end{cases} \tag{G.92}$$

The bottom limit goes through one transition point at $E_2 = E_3$,

$$b_1 = \begin{cases} p_1 - E_3 + E_2 - q_2 & \text{if } E_2 < E_3 \\ p_1 - q_3 & \text{if } E_2 > E_3 \end{cases}, \tag{G.93}$$

and another transition point when $p_1 - q_3 = E_3 - p_1 - E_2 + q_2$. This occurs when:

$$p_1 - q_3 = E_3 - p_1 - E_2 + q_2 \tag{G.94}$$

$$\implies 2p_1 - E_3 - q_3 + E_2 = q_2 \tag{G.95}$$

Eq.(H.112) is physically meaningful if $-m_e < 2p_1 - E_3 - q_3 < 0$. The first inequality is equivalent to:

$$q_3 < 2p_1 + m_e - E_3 \tag{G.96}$$

$$\implies E_3^2 - m_e^2 < 4p_1^2 + 4p_1 m_e + m_e^2 - 2E_3(2p_1 + m_e) + E_3^2 \tag{G.97}$$

$$\implies E_3 < \frac{4p_1^2 + 4p_1 m_e + 2m_e^2}{2(2p_1 + m_e)} \tag{G.98}$$

$$\implies E_3 < p_1 + m_e \frac{p_1 + m_e}{2p_1 + m_e} \equiv E_{\text{cut}}^{(2)} \tag{G.99}$$

Therefore, for Eq.(H.112) to be physically meaningful, $E_3 < E_{\text{cut}}^{(2)}$. $p_1 < \frac{m_e}{2}$ so the second inequality holds. We investigate the possibility when the second inequality does not hold, i.e. if $p_1 > \frac{m_e}{2}$:

$$2p_1 - E_3 - q_3 < 0 \tag{G.100}$$

$$\implies 2p_1 - E_3 < q_3 \tag{G.101}$$

$$\implies E_{\text{cut}}^{(1)} < E_3. \tag{G.102}$$

The expression for I_1 is an integral over $m_e < E_3 < E_{\text{cut}}^{(3)}$. We can compare $E_{\text{cut}}^{(2)}$ to $E_{\text{cut}}^{(3)}$ to see if Eq.(H.112) is physically meaningful:

$$E_{\text{cut}}^{(3)} \sim E_{\text{cut}}^{(2)} \tag{G.103}$$

$$\implies \sqrt{p_1^2+m_e^2} \sim p_1 + m_e \frac{p_1+m_e}{2p_1+m_e} \tag{G.104}$$

$$\implies p_1^2+m_e^2 \sim p_1^2 + 2p_1 m_e \frac{p_1+m_e}{2p_1+m_e} + m_e^2 \frac{(p_1+m_e)^2}{(2p_1+m_e)^2} \tag{G.105}$$

$$\implies m_e^2(2p_1+m_e)^2 \sim 2p_1 m_e (2p_1+m_e)(p_1+m_e) + m_e^2(p_1+m_e)^2 \tag{G.106}$$

$$\implies 4p_1^2 m_e + 4p_1 m_e^2 + m_e^3 \sim 4p_1^3 + 6p_1^2 m_e + 2p_1 m_e^2 + p_1^2 m_e + 2p_1 m_e^2 + m_e^3 \tag{G.107}$$

$$\implies 0 \sim 4p_1^3 + 3p_1^2 m_e \tag{G.108}$$

Thus, $E_{\text{cut}}^{(3)} < E_{\text{cut}}^{(2)}$ for all $p_1 > 0$. Eq.(H.112) is indeed physically meaningful:

$$-(E_3+q_3-2p_1)+E_2 = q_2 \tag{G.109}$$

$$\implies (E_3+q_3-2p_1)^2 - 2E_2(E_3+q_3-2p_1) + E_2^2 = E_2^2 - m_e^2 \tag{G.110}$$

$$\implies E_{\text{trans}}^{(2)} \equiv \frac{1}{2}\left(E_3+q_3-2p_1+\frac{m_e^2}{E_3+q_3-2p_1}\right) = E_2 \tag{G.111}$$

We need to investigate when $E_3 = E_{\text{trans}}^{(2)}$:

$$E_3 = \frac{1}{2}\left(E_3 + q_3 - 2p_1 + \frac{m_e^2}{E_3 + q_3 - 2p_1}\right) \tag{G.112}$$

$$\implies 2E_3(E_3 + q_3 - 2p_1) = (E_3 + q_3 - 2p_1)^2 + m_e^2 \tag{G.113}$$

$$\implies 2E_3^2 + 2E_3q_3 - 4p_1E_3 = E_3^2 + 2E_3q_3 - 4p_1E_3 + q_3^2 - 4p_1q_3 + 4p_1^2 + m_e^2 \tag{G.114}$$

$$\implies E_3^2 = E_3^2 - m_e^2 - 4p_1q_3 + 4p_1^2 + m_e^2 \tag{G.115}$$

$$\implies 4p_1q_3 = 4p_1^2 \tag{G.116}$$

$$\implies E_3 = E_{\text{cut}}^{(3)} \tag{G.117}$$

$$\implies \begin{cases} E_3 < E_{\text{trans}}^{(2)} & \text{if } E_3 < E_{\text{cut}}^{(3)} \\ E_3 > E_{\text{trans}}^{(2)} & \text{if } E_3 > E_{\text{cut}}^{(3)} \end{cases} \tag{G.118}$$

For the bottom limit:

$$b_1 = \begin{cases} p_1 - E_3 + E_2 - q_2 & \text{if } E_2 < E_3 \\ p_1 - q_3 & \text{if } E_3 < E_2 < E_{\text{trans}}^{(2)} \\ E_3 - p_1 - E_2 + q_2 & \text{if } E_2 > E_{\text{trans}}^{(2)} \end{cases}. \tag{G.119}$$

We have the following expression for I_1:

$$I_1 = \int_{m_e}^{E_{\text{cut}}^{(3)}} dE_3 \left(\int_{m_e}^{E_3} dE_3 \int_{p_1 - E_3 + E_2 - q_2}^{p_1 - E_3 + E_2 + q_2} dy + \int_{E_3}^{E_{\text{trans}}^{(2)}} dE_3 \int_{p_1 - q_3}^{p_1 + q_3} dy + \int_{E_{\text{trans}}^{(2)}}^{\infty} dE_3 \int_{E_3 - p_1 - E_2 + q_2}^{p_1 + q_3} dy \right). \tag{G.120}$$

However, Eq.(G.120) is incorrect as the limits on the last $\int dy$ may be equal, implying

that the last $\int dE_2$ must have a finite upper bound:

$$E_3 - p_1 - E_2 + q_2 = p_1 + q_3 \tag{G.121}$$

$$\Longrightarrow q_2 = E_2 + 2p_1 - E_3 + q_3 \tag{G.122}$$

For Eq.(H.78) to be physically meaningful, $-m_e < 2p_1 - E_3 + q_3 < 0$. The first inequality is always true. The second inequality implies $E_3 < E_{\text{cut}}^{(1)}$ and $p_1 < \frac{m_e}{2}$ which are also satisfied in this case. Solving Eq.(H.78) for E_2:

$$E_2^2 - m_e^2 = E_2^2 - 2E_2(E_3 - q_3 - 2p_1) + (E_3 - q_3 - 2p_1)^2 \tag{G.123}$$

$$\Longrightarrow E_2 = \frac{1}{2}\left(E_3 - q_3 - 2p_1 + \frac{m_e^2}{E_3 - q_3 - 2p_1}\right) \equiv E_{\text{lim}}^{(1)} \tag{G.124}$$

Finally, I_1 becomes:

$$I_1 = \int_{m_e}^{E_{\text{cut}}^{(3)}} dE_3 \left(\int_{m_e}^{E_3} dE_2 \int_{p_1 - E_3 + E_2 - q_2}^{p_1 - E_3 + E_2 + q_2} dy + \int_{E_3}^{E_{\text{trans}}^{(2)}} dE_2 \int_{p_1 - q_3}^{p_1 + q_3} dy + \int_{E_{\text{trans}}^{(2)}}^{E_{\text{lim}}^{(1)}} dE_2 \int_{E_3 - p_1 - E_2 + q_2}^{p_1 + q_3} dy \right). \tag{G.125}$$

Here is a summary of the validity of the expressions used in Eq.(G.125):

$$\begin{cases} E_3 < E_{\text{trans}}^{(2)} & \text{if } E_3 < E_{\text{cut}}^{(3)} \\ E_3 > E_{\text{trans}}^{(2)} & \text{if } E_3 > E_{\text{cut}}^{(3)} \end{cases}$$

$$\begin{cases} \text{if } \frac{p_1}{m_e} < \frac{1}{2} \text{ and } E_3 < E_{\text{cut}}^{(2)} \implies E_{\text{trans}}^{(2)} \text{ defined} \\ \text{if } \frac{p_1}{m_e} > \frac{1}{2} \text{ and } E_{\text{cut}}^{(1)} < E_3 < E_{\text{cut}}^{(2)} \implies E_{\text{trans}}^{(2)} \text{ defined} \\ \text{if } E_3 > E_{\text{cut}}^{(2)} \implies E_{\text{trans}}^{(2)} \text{ not defined} \end{cases}$$

$$\begin{cases} \text{if } E_3 < E_{\text{cut}}^{(1)} \text{ and } \frac{p_1}{m_e} < \frac{1}{2} \implies E_{\text{lim}}^{(1)} \text{ defined} \\ \text{else} \implies E_{\text{lim}}^{(1)} \text{ not defined} \end{cases}$$

$$E_{\text{cut}}^{(3)} < E_{\text{cut}}^{(2)} \text{ for all } p_1 > 0 \tag{G.126}$$

Second Integral

We have the following expression for the second integral of Eq.(G.120):

$$I_2 \equiv \int_{E_{\text{cut}}^{(3)}}^{E_{\text{cut}}^{(1)}} dE_3 \int_{q_3-p_1}^{p_1+q_3} dy \int_{E_{\min}}^{E_{\max}^{(\text{B})}} dE_2 \tag{G.127}$$

$$= \int_{E_{\text{cut}}^{(3)}}^{E_{\text{cut}}^{(1)}} dE_3 \int_{m_e}^{\infty} dE_2 \int_{b_2}^{t_2} dy \tag{G.128}$$

where:

$$\begin{cases} t_1 = \min(p_1+q_3, p_1-E_3+E_2+q_2) \\ b_1 = \max(q_3-p_1, p_1-E_3+E_2-q_2, E_3-p_1-E_2+q_2) \end{cases} . \tag{G.129}$$

Before we continue, we need to determine how $E_{\text{cut}}^{(1)}$ and $E_{\text{cut}}^{(2)}$ compare:

$$E_{\text{cut}}^{(1)} \sim E_{\text{cut}}^{(2)} \tag{G.130}$$

$$\implies p_1 + \frac{m_e^2}{4p_1} \sim p_1 + m_e \frac{p_1 + m_e}{2p_1 + m_e} \tag{G.131}$$

$$\implies m_e(2p_1 + m_e) \sim 4p_1(p_1 + m_e) \tag{G.132}$$

$$\implies 0 \sim 4p_1^2 + 2p_1 m_e - m_e^2 \tag{G.133}$$

$$\implies m_e \frac{\pm\sqrt{5} - 1}{4} \sim p_1. \tag{G.134}$$

The negative solution is extraneous, implying

$$\begin{cases} E_{\text{cut}}^{(2)} < E_{\text{cut}}^{(1)} \text{ if } \frac{p_1}{m_e} < \frac{\sqrt{5}-1}{4} \\ E_{\text{cut}}^{(2)} > E_{\text{cut}}^{(1)} \text{ if } \frac{p_1}{m_e} > \frac{\sqrt{5}-1}{4} \end{cases}. \tag{G.135}$$

Hence, we write I_2 as:

$$I_2 = \int_{E_{\text{cut}}^{(3)}}^{E_{\text{cut}}^{(2)}} dE_3 \int_{m_e}^{\infty} dE_2 \int_{b_2}^{t_2} dy + \int_{E_{\text{cut}}^{(2)}}^{E_{\text{cut}}^{(1)}} dE_3 \int_{m_e}^{\infty} dE_2 \int_{b_2}^{t_2} dy. \tag{G.136}$$

The top limit goes through a transition point at $E_2 = E_3$. The bottom limit goes through one transition point at $E_2 = E_3$. For the integral of $E_{\text{cut}}^{(3)} < E_3 < E_{\text{cut}}^{(2)}$, the bottom limit goes through a transition point at $E_2 = E_{\text{trans}}^{(2)} < E_3$. For the integral of $E_{\text{cut}}^{(2)} < E_3 < E_{\text{cut}}^{(1)}$, $E_{\text{trans}}^{(2)}$ is not defined. However, notice how the top limit $(p_1 - E_3 + E_2 + q_2)$ and bottom limit $(q_3 - p_1)$ compare:

$$p_1 - E_3 + E_2 + q_2 \sim q_3 - p_1 \tag{G.137}$$

$$\implies q_2 \sim -E_2 + E_3 + q_3 - 2p_1. \tag{G.138}$$

For Eq.(H.144) to be physically meaningful, $E_3+q_3-2p_1 > m_e \implies E_3 > E_{\text{cut}}^{(2)}$, which is the case for this integral. Solving for E_2 in Eq.(H.144):

$$q_2 \sim -E_2+E_3+q_3-2p_1 \tag{G.139}$$

$$\implies E_2 \sim \frac{1}{2}\left(E_3+q_3-2p_1+\frac{m_e^2}{E_3+q_3-2p_1}\right) \equiv E_{\text{lim}}^{(2)} \tag{G.140}$$

$$\implies \begin{cases} p_1-E_3+E_2+q_2 < q_3-p_1 & \text{if } E_2 < E_{\text{lim}}^{(2)} \\ p_1-E_3+E_2+q_2 > q_3-p_1 & \text{if } E_2 > E_{\text{lim}}^{(2)} \end{cases}. \tag{G.141}$$

Note that $E_{\text{lim}}^{(2)}$ has the same form as $E_{\text{trans}}^{(2)}$. However, the expressions are derived from <u>different</u> equations under <u>different</u> conditions. We are left with the following expression for I_2:

$$\begin{aligned} I_2 = &\int_{E_{\text{cut}}^{(3)}}^{E_{\text{cut}}^{(2)}} dE_3 \left(\int_{m_e}^{E_{\text{trans}}^{(2)}} dE_2 \int_{p_1-E_3+E_2-q_2}^{p_1-E_3+E_2+q_2} dy \right. \\ &\left. + \int_{E_{\text{trans}}^{(2)}}^{E_3} dE_2 \int_{q_3-p_1}^{p_1-E_3+E_2+q_2} dy + \int_{E_3}^{E_{\text{lim}}^{(1)}} dE_2 \int_{E_3-p_1-E_2+q_2}^{p_1+q_3} dy \right) \\ &+ \int_{E_{\text{cut}}^{(2)}}^{E_{\text{cut}}^{(1)}} dE_3 \left(\int_{E_{\text{lim}}^{(2)}}^{E_3} dE_2 \int_{q_3-p_1}^{p_1-E_3+E_2+q_2} dy + \int_{E_3}^{E_{\text{lim}}^{(1)}} dE_2 \int_{E_3-p_1-E_2+q_2}^{p_1+q_3} dy \right) \end{aligned} \tag{G.142}$$

Here is another summary of the validity of the expressions used in Eq.(G.125):

$$\begin{cases} \text{if } E_3 < E_{\text{cut}}^{(2)} \implies E_{\text{trans}}^{(2)} \text{ defined} \\ \text{if } E_3 > E_{\text{cut}}^{(2)} \implies E_{\text{lim}}^{(2)} \text{ defined} \end{cases} \tag{G.143}$$

Third Integral

We have the following expression for the third integral of Eq.(G.120):

$$I_3 \equiv \int_{E_{\text{cut}}^{(1)}}^{\infty} dE_3 \int_{q_3-p_1}^{E_3-p_1} dy \int_{E_{\text{min}}}^{E_{\text{max}}^{(\text{B})}} dE_2 \tag{G.144}$$

$$= \int_{E_{\text{cut}}^{(1)}}^{\infty} dE_3 \int_{m_e}^{\infty} dE_2 \int_{b_3}^{t_3} dy \tag{G.145}$$

where:

$$\begin{cases} t_3 = \min(E_3 - p_1, p_1 - E_3 + E_2 + q_2) \\ b_3 = \max(q_3 - p_1, p_1 - E_3 + E_2 - q_2, E_3 - p_1 - E_2 + q_2) \end{cases} \tag{G.146}$$

The bottom limit has a transition point at $E_2 = E_3$ and a limit point at $E_2 = E_{\text{lim}}^{(2)}$. For the top limit:

$$E_3 - p_1 = p_1 - E_3 + E_2 + q_2 \tag{G.147}$$

$$\Longrightarrow 2(E_3 - p_1) - E_2 = q_2 \tag{G.148}$$

For Eq.(G.148) to be physically meaningful:

$$2(E_3 - p_1) > m_e \tag{G.149}$$

$$\Longrightarrow E_3 > p_1 + \frac{m_e}{2} \equiv E_{\text{cut}}^{(4)} \tag{G.150}$$

Clearly, for $p_1 < \frac{m_e}{2}$ the above inequality is satisfied. Solving Eq.(G.148) for E_2:

$$2(E_3 - p_1) - E_2 = q_2 \tag{G.151}$$

$$\implies 4(E_3 - p_1)^2 - 4E_2(E_3 - p_1) + E_2^2 = E_2^2 - m_e^2 \tag{G.152}$$

$$\implies E_{\text{trans}}^{(3)} \equiv E_3 - p_1 + \frac{m_e^2}{4(E_3 - p_1)} = E_2 \tag{G.153}$$

We observe how E_3 and $E_{\text{trans}}^{(3)}$ compare to one another:

$$E_3 \sim E_{\text{trans}}^{(3)} \tag{G.154}$$

$$\implies E_3 \sim E_3 - p_1 + \frac{m_e^2}{4(E_3 - p_1)} \tag{G.155}$$

$$\implies 4(E_3 - p_1)p_1 \sim m_e^2 \tag{G.156}$$

$$\implies E_3 \sim p_1 + \frac{m_e^2}{4p_1} = E_{\text{cut}}^{(1)} \tag{G.157}$$

Thus, if $E_3 > E_{\text{cut}}^{(1)}$, then $E_3 > E_{\text{trans}}^{(3)}$. We now have an expression for I_3:

$$I_3 = \int_{E_{\text{cut}}^{(1)}}^{\infty} dE_3 \left(\int_{E_{\text{lim}}^{(2)}}^{E_{\text{trans}}^{(3)}} dE_2 \int_{q_3 - p_1}^{p_1 - E_3 + E_2 + q_2} dy + \int_{E_{\text{trans}}^{(3)}}^{E_3} dE_2 \int_{q_3 - p_1}^{E_3 - p_1} dy + \int_{E_3}^{\infty} dE_2 \int_{E_3 - p_1 - E_2 + q_2}^{E_3 - p_1} dy \right). \tag{G.158}$$

We need to determine how $E_{\text{cut}}^{(1)}$ and $E_{\text{cut}}^{(4)}$ compare for general p_1:

$$E_{\text{cut}}^{(1)} \sim E_{\text{cut}}^{(4)} \tag{G.159}$$

$$\implies p_1 + \frac{m_e^2}{4p_1} \sim p_1 + \frac{m_e}{2} \tag{G.160}$$

$$\implies \frac{m_e}{2} \sim p_1 \tag{G.161}$$

Also, we compare $E_{\text{cut}}^{(4)}$ with $E_{\text{cut}}^{(3)}$:

$$E_{\text{cut}}^{(4)} \sim E_{\text{cut}}^{(3)} \tag{G.162}$$

$$\implies p_1 + \frac{m_e}{2} \sim \sqrt{p_1^2 + m_e^2} \tag{G.163}$$

$$\implies p_1^2 + p_1 m_e + \frac{m_e^2}{4} \sim p_1^2 + m_e^2 \tag{G.164}$$

$$\implies p_1 \sim m_e \frac{3}{4}, \tag{G.165}$$

$$\tag{G.166}$$

and $E_{\text{cut}}^{(4)}$ with $E_{\text{cut}}^{(2)}$:

$$E_{\text{cut}}^{(4)} \sim E_{\text{cut}}^{(2)} \tag{G.167}$$

$$\implies p_1 + \frac{m_e}{2} \sim p_1 + m_e \frac{p_1 + m_e}{2p_1 + m_e} \tag{G.168}$$

$$\implies 2p_1 + m_e \sim 2(p_1 + m_e). \tag{G.169}$$

The cut hierarchy is:

$$E_{\text{cut}}^{(4)} < E_{\text{cut}}^{(3)} < E_{\text{cut}}^{(2)} < E_{\text{cut}}^{(1)} \text{ if } \quad \frac{p_1}{m_e} < \frac{\sqrt{5}-1}{4} \tag{G.170}$$

$$E_{\text{cut}}^{(4)} < E_{\text{cut}}^{(3)} < E_{\text{cut}}^{(1)} < E_{\text{cut}}^{(2)} \text{ if } \frac{\sqrt{5}-1}{4} < \frac{p_1}{m_e} < \frac{1}{2\sqrt{2}} \tag{G.171}$$

$$E_{\text{cut}}^{(4)} < E_{\text{cut}}^{(1)} < E_{\text{cut}}^{(3)} < E_{\text{cut}}^{(2)} \text{ if } \quad \frac{1}{2\sqrt{2}} < \frac{p_1}{m_e} < \frac{1}{2} \tag{G.172}$$

$$E_{\text{cut}}^{(1)} < E_{\text{cut}}^{(4)} < E_{\text{cut}}^{(3)} < E_{\text{cut}}^{(2)} \text{ if } \quad \frac{1}{2} < \frac{p_1}{m_e} < \frac{3}{4} \tag{G.173}$$

$$E_{\text{cut}}^{(1)} < E_{\text{cut}}^{(3)} < E_{\text{cut}}^{(4)} < E_{\text{cut}}^{(2)} \text{ if } \quad \frac{3}{4} < \frac{p_1}{m_e} \tag{G.174}$$

Fourth Integral

We have the following expression for the fourth integral of Eq.(G.120):

$$I_4 \equiv \int_{E_{\text{cut}}^{(1)}}^{\infty} dE_3 \int_{E_3-p_1}^{p_1+q_3} dy \int_{E_{\min}}^{\infty} dE_2 \tag{G.175}$$

$$= \int_{E_{\text{cut}}^{(1)}}^{\infty} dE_3 \int_{m_e}^{\infty} dE_2 \int_{b_4}^{t_4} dy \tag{G.176}$$

where:

$$\begin{cases} t_4 = \min(p_1+q_3, p_1-E_3+E_2+q_2) \\ b_4 = \max(E_3-p_1, p_1-E_3+E_2-q_2) \end{cases} \tag{G.177}$$

The transition point for the top limit is $E_2 = E_3$. For the bottom limit:

$$E_3 - p_1 \sim p_1 - E_3 + E_2 - q_2 \tag{G.178}$$

$$\implies q_2 \sim E_2 + 2(p_1 - E_3) \tag{G.179}$$

For Eq.(G.179) to be physically meaningful, $-m_e < 2(p_1-E_3) \implies E_3 < p_1 + \frac{m_e}{2} = E_{\text{cut}}^{(4)}$ which does not hold. There is no transition point for the bottom limit. Observe the comparison between the bottom and top limits:

$$E_3 - p_1 \sim p_1 - E_3 + E_2 + q_2 \tag{G.180}$$

$$\implies 2(E_3 - p_1) - E_2 \sim q_2 \tag{G.181}$$

$$\implies E_{\text{lim}}^{(3)} \equiv E_3 - p_1 + \frac{m_e^2}{4(E_3-p_1)} = E_2 \tag{G.182}$$

Note that $E_{\text{lim}}^{(3)}$ is derived from the same equation Eq.(G.151) as $E_{\text{trans}}^{(3)}$. However, we give it a different label as it is used in a limiting context instead of a transition context.

I_4 becomes:

$$I_4 = \int_{E_{\text{cut}}^{(1)}}^{\infty} dE_3 \left(\int_{E_{\text{lim}}^{(3)}}^{E_3} dE_2 \int_{E_3 - p_1}^{p_1 - E_3 + E_2 + q_2} dy + \int_{E_3}^{\infty} dE_2 \int_{E_3 - p_1}^{p_1 + q_3} dy \right) \tag{G.183}$$

Here is another summary of the validity of $E_{\text{trans}}^{(3)}$ and $E_{\text{lim}}^{(3)}$:

$$\begin{cases} \text{if } E_2 < E_{\text{trans}}^{(3)} \implies p_1 - E_3 + E_2 + q_2 < E_3 - p_1 \\ \text{if } E_2 > E_{\text{trans}}^{(3)} \implies p_1 - E_3 + E_2 + q_2 > E_3 - p_1 \\ \text{if } E_3 > E_{\text{cut}}^{(4)} \implies p_1 - E_3 + E_2 - q_2 < E_3 - p_1 \implies E_{\text{lim}}^{(3)} \text{ defined} \end{cases} .$$

Combined expression for R_2 in case 1

The combined expression for $R_2 = I_1 + I_2 + I_3 + I_4$ is:

$$
\begin{aligned}
R_2^{(1)} = &\int_{m_e}^{E_{\rm cut}^{(3)}} dE_3 \quad \left(\int_{m_e}^{E_3} dE_2 \int_{p_1-E_3+E_2-q_2}^{p_1-E_3+E_2+q_2} dy \right. \\
&\qquad \left. + \int_{E_3}^{E_{\rm trans}^{(2)}} dE_2 \int_{p_1-q_3}^{p_1+q_3} dy + \int_{E_{\rm trans}^{(2)}}^{E_{\rm lim}^{(1)}} dE_2 \int_{E_3-p_1-E_2+q_2}^{p_1+q_3} dy \right) \\
&+ \int_{E_{\rm cut}^{(3)}}^{E_{\rm cut}^{(2)}} dE_3 \quad \left(\int_{m_e}^{E_{\rm trans}^{(2)}} dE_2 \int_{p_1-E_3+E_2-q_2}^{p_1-E_3+E_2+q_2} dy \right. \\
&\qquad \left. + \int_{E_{\rm trans}^{(2)}}^{E_3} dE_2 \int_{q_3-p_1}^{p_1-E_3+E_2+q_2} dy + \int_{E_3}^{E_{\rm lim}^{(1)}} dE_2 \int_{E_3-p_1-E_2+q_2}^{p_1+q_3} dy \right) \\
&+ \int_{E_{\rm cut}^{(2)}}^{E_{\rm cut}^{(1)}} dE_3 \quad \left(\int_{E_{\rm lim}^{(2)}}^{E_3} dE_2 \int_{q_3-p_1}^{p_1-E_3+E_2+q_2} dy + \int_{E_3}^{E_{\rm lim}^{(1)}} dE_2 \int_{E_3-p_1-E_2+q_2}^{p_1+q_3} dy \right) \\
&+ \int_{E_{\rm cut}^{(1)}}^{\infty} dE_3 \quad \left(\int_{E_{\rm lim}^{(2)}}^{E_{\rm trans}^{(3)}} dE_2 \int_{q_3-p_1}^{p_1-E_3+E_2+q_2} dy + \int_{E_{\rm trans}^{(3)}}^{E_3} dE_2 \int_{q_3-p_1}^{E_3-p_1} dy + \int_{E_3}^{\infty} dE_2 \int_{E_3-p_1-E_2+q_2}^{E_3-p_1} dy \right. \\
&\qquad \left. + \int_{E_{\rm lim}^{(3)}}^{E_3} dE_2 \int_{E_3-p_1}^{p_1-E_3+E_2+q_2} dy + \int_{E_3}^{\infty} dE_2 \int_{E_3-p_1}^{p_1+q_3} dy \right) . \qquad \text{(G.184)}
\end{aligned}
$$

We can use the fact that $E^{(3)}_{\text{trans}} = E^{(3)}_{\text{lim}}$ to combine the expressions within $\int dE_3$ for $E_3 > E^{(1)}_{\text{cut}}$:

$$
\begin{aligned}
R^{(1)}_2 = \int_{m_e}^{E^{(3)}_{\text{cut}}} dE_3 \Bigg(& \int_{m_e}^{E_3} dE_3 \int_{p_1-E_3+E_2-q_2}^{p_1-E_3+E_2+q_2} dy + \int_{E_3}^{E^{(2)}_{\text{trans}}} dE_3 \int_{p_1-q_3}^{p_1+q_3} dy + \int_{E^{(2)}_{\text{trans}}}^{E^{(1)}_{\text{lim}}} dE_3 \int_{E_3-p_1-E_2+q_2}^{p_1+q_3} dy \Bigg) \\
& + \int_{E^{(3)}_{\text{cut}}}^{E^{(2)}_{\text{cut}}} dE_3 \Bigg(\int_{m_e}^{E^{(2)}_{\text{trans}}} dE_2 \int_{p_1-E_3+E_2-q_2}^{p_1-E_3+E_2+q_2} dy \\
& \qquad + \int_{E^{(2)}_{\text{trans}}}^{E_3} dE_2 \int_{q_3-p_1}^{p_1-E_3+E_2+q_2} dy + \int_{E_3}^{E^{(1)}_{\text{lim}}} dE_2 \int_{E_3-p_1-E_2+q_2}^{p_1+q_3} dy \Bigg) \\
& + \int_{E^{(2)}_{\text{cut}}}^{E^{(1)}_{\text{cut}}} dE_3 \Bigg(\int_{E^{(2)}_{\text{lim}}}^{E_3} dE_2 \int_{q_3-p_1}^{p_1-E_3+E_2+q_2} dy + \int_{E_3}^{E^{(1)}_{\text{lim}}} dE_2 \int_{E_3-p_1-E_2+q_2}^{p_1+q_3} dy \Bigg) \\
& + \int_{E^{(1)}_{\text{cut}}}^{\infty} dE_3 \Bigg(\int_{E^{(2)}_{\text{lim}}}^{E^{(3)}_{\text{trans}}} dE_2 \int_{q_3-p_1}^{p_1-E_3+E_2+q_2} dy \\
& \qquad + \int_{E^{(3)}_{\text{trans}}}^{E_3} dE_2 \int_{q_3-p_1}^{p_1-E_3+E_2+q_2} dy + \int_{E_3}^{\infty} dE_2 \int_{E_3-p_1-E_2+q_2}^{p_1+q_3} dy \Bigg),
\end{aligned}
\tag{G.185}
$$

yielding:

$$
\begin{aligned}
R_2^{(1)} = &\int_{m_e}^{E_{\text{cut}}^{(3)}} dE_3 \left(\int_{m_e}^{E_3} dE_3 \int_{p_1-E_3+E_2-q_2}^{p_1-E_3+E_2+q_2} dy + \int_{E_3}^{E_{\text{trans}}^{(2)}} dE_3 \int_{p_1-q_3}^{p_1+q_3} dy + \int_{E_{\text{trans}}^{(2)}}^{E_{\text{lim}}^{(1)}} dE_3 \int_{E_3-p_1-E_2+q_2}^{p_1+q_3} dy \right) \\
&+ \int_{E_{\text{cut}}^{(3)}}^{E_{\text{cut}}^{(2)}} dE_3 \left(\int_{m_e}^{E_{\text{trans}}^{(2)}} dE_2 \int_{p_1-E_3+E_2-q_2}^{p_1-E_3+E_2+q_2} dy \right. \\
&\left. + \int_{E_{\text{trans}}^{(2)}}^{E_3} dE_2 \int_{q_3-p_1}^{p_1-E_3+E_2+q_2} dy + \int_{E_3}^{E_{\text{lim}}^{(1)}} dE_2 \int_{E_3-p_1-E_2+q_2}^{p_1+q_3} dy \right) \\
&+ \int_{E_{\text{cut}}^{(2)}}^{E_{\text{cut}}^{(1)}} dE_3 \left(\int_{E_{\text{lim}}^{(2)}}^{E_3} dE_2 \int_{q_3-p_1}^{p_1-E_3+E_2+q_2} dy + \int_{E_3}^{E_{\text{lim}}^{(1)}} dE_2 \int_{E_3-p_1-E_2+q_2}^{p_1+q_3} dy \right) \\
&+ \int_{E_{\text{cut}}^{(1)}}^{\infty} dE_3 \left(\int_{E_{\text{lim}}^{(2)}}^{E_3} dE_2 \int_{q_3-p_1}^{p_1-E_3+E_2+q_2} dy + \int_{E_3}^{\infty} dE_2 \int_{E_3-p_1-E_2+q_2}^{p_1+q_3} dy \right).
\end{aligned}
\tag{G.186}
$$

Here is a summary of the validity of the quantities in Eq.(G.186):

$$
\begin{cases} E_3 < E_{\text{trans}}^{(2)} & \text{if } E_3 < E_{\text{cut}}^{(3)} \\ E_3 > E_{\text{trans}}^{(2)} & \text{if } E_3 > E_{\text{cut}}^{(3)} \end{cases}
$$

$$
\begin{cases} \text{if } \frac{p_1}{m_e} < \frac{1}{2} \text{ and } E_3 < E_{\text{cut}}^{(2)} \implies E_{\text{trans}}^{(2)} \text{ defined} \\ \text{if } \frac{p_1}{m_e} > \frac{1}{2} \text{ and } E_{\text{cut}}^{(1)} < E_3 < E_{\text{cut}}^{(2)} \implies E_{\text{trans}}^{(2)} \text{ defined} \\ \text{if } E_3 > E_{\text{cut}}^{(2)} \implies E_{\text{trans}}^{(2)} \text{ not defined} \end{cases}
$$

$$
\begin{cases} E_3 < E_{\text{cut}}^{(1)} \implies E_{\text{trans}}^{(3)} \text{ not applicable} \\ E_3 > E_{\text{cut}}^{(1)} \implies E_{\text{trans}}^{(3)} \text{ applicable} \\ E_3 < E_{\text{cut}}^{(4)} \implies E_{\text{trans}}^{(3)} \text{ not defined} \\ E_{\text{trans}}^{(3)} < E_3 \end{cases}
$$

$$
\begin{cases} \text{if } E_2 < E_{\text{trans}}^{(3)} \implies p_1 - E_3 + E_2 + q_2 < E_3 - p_1 \\ \text{if } E_2 > E_{\text{trans}}^{(3)} \implies p_1 - E_3 + E_2 + q_2 > E_3 - p_1 \\ \text{if } E_3 > E_{\text{cut}}^{(4)} \implies p_1 - E_3 + E_2 - q_2 < E_3 - p_1 \implies E_{\text{lim}}^{(3)} \text{ defined} \end{cases}
$$

$$
\begin{cases} \text{if } E_3 < E_{\text{cut}}^{(1)} \text{ and } \frac{p_1}{m_e} < \frac{1}{2} \implies E_{\text{lim}}^{(1)} \text{ defined} \\ \text{else} \implies E_{\text{lim}}^{(1)} \text{ not defined} \end{cases}
$$

$$
\begin{cases} E_{\text{cut}}^{(3)} < E_{\text{cut}}^{(2)} \\ E_{\text{cut}}^{(4)} < E_{\text{cut}}^{(2)} \end{cases}
\tag{G.187}
$$

G.3.2 Case 2: $\frac{\sqrt{5}-1}{4} < \frac{p_1}{m_e} < \frac{1}{2\sqrt{2}}$

The cut hierarchy is:

$$E_{\rm cut}^{(4)} < E_{\rm cut}^{(3)} < E_{\rm cut}^{(1)} < E_{\rm cut}^{(2)} \tag{G.188}$$

which gives us the following for R_2:

$$R_2^{(2)} = \int_{m_e}^{E_{\rm cut}^{(3)}} dE_3 \int_{p_1-q_3}^{p_1+q_3} dy \int_{E_{\rm min}}^{E_{\rm max}^{\rm (B)}} dE_2 + \int_{E_{\rm cut}^{(3)}}^{E_{\rm cut}^{(1)}} dE_3 \int_{q_3-p_1}^{p_1+q_3} dy \int_{E_{\rm min}}^{E_{\rm max}^{\rm (B)}} dE_2$$
$$+ \int_{E_{\rm cut}^{(1)}}^{E_{\rm cut}^{(2)}} dE_3 \left(\int_{q_3-p_1}^{E_3-p_1} dy \int_{E_{\rm min}}^{E_{\rm max}^{\rm (B)}} dE_2 + \int_{E_3-p_1}^{p_1+q_3} dy \int_{E_{\rm min}}^{\infty} dE_2 \right) \tag{G.189}$$
$$+ \int_{E_{\rm cut}^{(2)}}^{\infty} dE_3 \left(\int_{q_3-p_1}^{E_3-p_1} dy \int_{E_{\rm min}}^{E_{\rm max}^{\rm (B)}} dE_2 + \int_{E_3-p_1}^{p_1+q_3} dy \int_{E_{\rm min}}^{\infty} dE_2 \right) \tag{G.190}$$

We will consider separately each of the six integrals of Eq.(G.190).

First and Second Integrals

These integrals are similar to those of Case 1.

$$I_1 \equiv \int_{m_e}^{E_{\rm cut}^{(3)}} dE_3 \int_{p_1-q_3}^{p_1+q_3} dy \int_{E_{\rm min}}^{E_{\rm max}^{\rm (B)}} dE_2 \tag{G.191}$$
$$= \int_{m_e}^{E_{\rm cut}^{(3)}} dE_3 \left(\int_{m_e}^{E_3} dE_2 \int_{p_1-E_3+E_2-q_2}^{p_1-E_3+E_2+q_2} dy + \int_{E_3}^{E_{\rm trans}^{(2)}} dE_2 \int_{p_1-q_3}^{p_1+q_3} dy + \int_{E_{\rm trans}^{(2)}}^{E_{\rm lim}^{(1)}} dE_2 \int_{E_3-p_1-E_2+q_2}^{p_1+q_3} dy \right) \tag{G.192}$$

$$I_2 \equiv \int_{E_{\rm cut}^{(3)}}^{E_{\rm cut}^{(1)}} dE_3 \int_{q_3-p_1}^{p_1+q_3} dy \int_{E_{\rm min}}^{E_{\rm max}^{(\rm B)}} dE_2 \tag{G.193}$$

$$= \int_{E_{\rm cut}^{(3)}}^{E_{\rm cut}^{(1)}} dE_3 \left(\int_{m_e}^{E_{\rm trans}^{(2)}} dE_2 \int_{p_1-E_3+E_2-q_2}^{p_1-E_3+E_2+q_2} dy \right.$$

$$\left. + \int_{E_{\rm trans}^{(2)}}^{E_3} dE_2 \int_{q_3-p_1}^{p_1-E_3+E_2+q_2} dy + \int_{E_3}^{E_{\rm lim}^{(1)}} dE_2 \int_{E_3-p_1-E_2+q_2}^{p_1+q_3} dy \right). \tag{G.194}$$

Third Integral

The expression for I_3 is:

$$I_3 \equiv \int_{E_{\rm cut}^{(1)}}^{E_{\rm cut}^{(2)}} dE_3 \int_{q_3-p_1}^{E_3-p_1} dy \int_{E_{\rm min}}^{E_{\rm max}^{(\rm B)}} dE_2 \tag{G.195}$$

$$= \int_{E_{\rm cut}^{(1)}}^{E_{\rm cut}^{(2)}} dE_3 \int_{m_e}^{\infty} dE_2 \int_{b_3}^{t_3} dy \tag{G.196}$$

The transition points on $\int dE_2$ are $E_3, E_{\rm trans}^{(2)}$ and $E_{\rm trans}^{(3)}$. $E_{\rm trans}^{(3)} < E_3$, and in this integral, $E_{\rm trans}^{(2)} < E_3$. We need to compare $E_{\rm trans}^{(2)}$ and $E_{\rm trans}^{(3)}$:

$$E_{\rm trans}^{(3)} \sim E_{\rm trans}^{(2)} \tag{G.197}$$

$$\implies E_{\rm trans}^{(3)} - E_{\rm trans}^{(2)} \sim 0 \tag{G.198}$$

$$\implies 0 \sim m_e^4 + 4p_1 m_e^2 (E_3 - p_1) - 16 p_1 (E_3 - p_1)^3 \tag{G.199}$$

$$\implies E_3 \sim E_? \tag{G.200}$$

We will not use the quantity $E_?$ in our analysis. Instead, we use a Boole's rule integration and change the limits as a function of E_3:

$$I_3 = \int_{E_{\rm cut}^{(1)}}^{E_{\rm cut}^{(2)}} dE_3 \left(\int_{m_e}^{E_{\rm sort}^{(1)}} dE_2 \int_{p_1-E_3+E_2-q_2}^{p_1-E_3+E_2+q_2} dy + \int_{E_{\rm sort}^{(1)}}^{E_{\rm sort}^{(2)}} dE_2 \int_{b_{\rm sort}}^{t_{\rm sort}} dy \right.$$
$$\left. + \int_{E_{\rm sort}^{(2)}}^{E_3} dE_2 \int_{q_3-p_1}^{E_3-p_1} dy + \int_{E_3}^{\infty} dE_2 \int_{E_3-p_1-E_2+q_2}^{E_3-p_1} dy \right) \tag{G.201}$$

where:

$$E_{\rm sort}^{(1)} = \min(E_{\rm trans}^{(2)}, E_{\rm trans}^{(3)}) \tag{G.202}$$

$$E_{\rm sort}^{(2)} = \max(E_{\rm trans}^{(2)}, E_{\rm trans}^{(3)}) \tag{G.203}$$

$$b_{\rm sort} = \begin{cases} p_1 - E_3 + E_2 - q_2 & \text{if } E_{\rm sort}^{(1)} = E_{\rm trans}^{(3)} \\ q_3 - p_1 & \text{if } E_{\rm sort}^{(1)} = E_{\rm trans}^{(2)} \end{cases} \tag{G.204}$$

$$t_{\rm sort} = \begin{cases} E_3 - p_1 & \text{if } E_{\rm sort}^{(1)} = E_{\rm trans}^{(3)} \\ p_1 - E_3 + E_2 + q_2 & \text{if } E_{\rm sort}^{(1)} = E_{\rm trans}^{(2)} \end{cases} \tag{G.205}$$

Fourth Integral

The expression for I_4 is:

$$I_4 \equiv \int_{E_{\rm cut}^{(1)}}^{E_{\rm cut}^{(2)}} dE_3 \int_{E_3-p_1}^{p_1+q_3} dy \int_{E_{\rm min}}^{\infty} dE_2 \tag{G.206}$$

$$= \int_{E_{\rm cut}^{(1)}}^{E_{\rm cut}^{(2)}} dE_3 \int_{m_e}^{\infty} dE_2 \int_{b_4}^{t_4} dy \tag{G.207}$$

This integral is similar to the fourth integral of Case 1:

$$I_4 = \int_{E_{\rm cut}^{(1)}}^{E_{\rm cut}^{(2)}} dE_3 \left(\int_{E_{\rm lim}^{(3)}}^{E_3} dE_2 \int_{E_3-p_1}^{p_1-E_3+E_2+q_2} dy + \int_{E_3}^{\infty} dE_2 \int_{E_3-p_1}^{p_1+q_3} dy \right) \tag{G.208}$$

Fifth Integral

The expression for I_5 is:

$$I_5 \equiv \int_{E_{\rm cut}^{(2)}}^{\infty} dE_3 \int_{q_3-p_1}^{E_3-p_1} dy \int_{E_{\rm min}}^{E_{\rm max}^{(\rm B)}} dE_2 \tag{G.209}$$

$$= \int_{E_{\rm cut}^{(2)}}^{\infty} dE_3 \int_{m_e}^{\infty} dE_2 \int_{b_5}^{t_5} dy. \tag{G.210}$$

This integral is similar to the third integral of Case 1:

$$I_5 = \int_{E_{\rm cut}^{(2)}}^{\infty} dE_3 \left(\int_{E_{\rm lim}^{(2)}}^{E_{\rm trans}^{(3)}} dE_2 \int_{q_3-p_1}^{p_1-E_3+E_2+q_2} dy + \int_{E_{\rm trans}^{(3)}}^{E_3} dE_2 \int_{q_3-p_1}^{E_3-p_1} dy + \int_{E_3}^{\infty} dE_2 \int_{E_3-p_1-E_2+q_2}^{E_3-p_1} dy \right). \tag{G.211}$$

Sixth Integral

The expression for I_6 is:

$$I_6 \equiv \int_{E_{\rm cut}^{(2)}}^{\infty} dE_3 \int_{E_3-p_1}^{p_1+q_3} dy \int_{E_{\rm min}}^{\infty} dE_2 \tag{G.212}$$

$$= \int_{E_{\rm cut}^{(2)}}^{\infty} dE_3 \int_{m_e}^{\infty} dE_2 \int_{b_6}^{t_6} dy. \tag{G.213}$$

This integral is identical to the fourth integral except for a change in the limits of $\int dE_3$:

$$I_6 = \int_{E_{\text{cut}}^{(2)}}^{\infty} dE_3 \left(\int_{E_{\text{lim}}^{(3)}}^{E_3} dE_2 \int_{E_3-p_1}^{p_1-E_3+E_2+q_2} dy + \int_{E_3}^{\infty} dE_2 \int_{E_3-p_1}^{p_1+q_3} dy \right) \tag{G.214}$$

Combined expression for R_2 in case 2

The combined expression for $R_2 = I_1 + I_2 + (I_3 + I_4) + (I_5 + I_6)$ is:

$$\begin{aligned}
R_2^{(2)} = &\int_{m_e}^{E_{\text{cut}}^{(3)}} dE_3 \left(\int_{m_e}^{E_3} dE_2 \int_{p_1-E_3+E_2-q_2}^{p_1-E_3+E_2+q_2} dy + \int_{E_3}^{E_{\text{trans}}^{(2)}} dE_2 \int_{p_1-q_3}^{p_1+q_3} dy + \int_{E_{\text{trans}}^{(2)}}^{E_{\text{lim}}^{(1)}} dE_2 \int_{E_3-p_1-E_2+q_2}^{p_1+q_3} dy \right) \\
&+ \int_{E_{\text{cut}}^{(3)}}^{E_{\text{cut}}^{(1)}} dE_3 \left(\int_{m_e}^{E_{\text{trans}}^{(2)}} dE_2 \int_{p_1-E_3+E_2-q_2}^{p_1-E_3+E_2+q_2} dy \right. \\
&\qquad \left. + \int_{E_{\text{trans}}^{(2)}}^{E_3} dE_2 \int_{q_3-p_1}^{p_1-E_3+E_2+q_2} dy + \int_{E_3}^{E_{\text{lim}}^{(1)}} dE_2 \int_{E_3-p_1-E_2+q_2}^{p_1+q_3} dy \right) \\
&+ \int_{E_{\text{cut}}^{(1)}}^{E_{\text{cut}}^{(2)}} dE_3 \left(\int_{m_e}^{E_{\text{sort}}^{(1)}} dE_2 \int_{p_1-E_3+E_2-q_2}^{p_1-E_3+E_2+q_2} dy + \int_{E_{\text{sort}}^{(1)}}^{E_{\text{sort}}^{(2)}} dE_2 \int_{b_{\text{sort}}}^{t_{\text{sort}}} dy + \int_{E_{\text{sort}}^{(2)}}^{E_3} dE_2 \int_{q_3-p_1}^{E_3-p_1} dy \right. \\
&\qquad \left. + \int_{E_3}^{\infty} dE_2 \int_{E_3-p_1-E_2+q_2}^{E_3-p_1} dy + \int_{E_{\text{lim}}^{(3)}}^{E_3} dE_2 \int_{E_3-p_1}^{p_1-E_3+E_2+q_2} dy + \int_{E_3}^{\infty} dE_2 \int_{E_3-p_1}^{p_1+q_3} dy \right) \\
&+ \int_{E_{\text{cut}}^{(2)}}^{\infty} dE_3 \left(\int_{E_{\text{lim}}^{(2)}}^{E_{\text{trans}}^{(3)}} dE_2 \int_{q_3-p_1}^{p_1-E_3+E_2+q_2} dy + \int_{E_{\text{trans}}^{(3)}}^{E_3} dE_2 \int_{q_3-p_1}^{E_3-p_1} dy + \int_{E_3}^{\infty} dE_2 \int_{E_3-p_1-E_2+q_2}^{E_3-p_1} dy \right. \\
&\qquad \left. + \int_{E_{\text{lim}}^{(3)}}^{E_3} dE_2 \int_{E_3-p_1}^{p_1-E_3+E_2+q_2} dy + \int_{E_3}^{\infty} dE_2 \int_{E_3-p_1}^{p_1+q_3} dy \right)
\end{aligned}$$

Combining the integrals on $\int dE_3$ for $E_3 > E_{\text{cut}}^{(2)}$ is equivalent to case 1. For $E_{\text{cut}}^{(1)} < E_3 < E_{\text{cut}}^{(2)}$, we need to change the top limit of t_{sort} to $p_1 - E_3 + E_2 + q_2$:

$$
\begin{aligned}
R_2^{(2)} = &\int_{m_e}^{E_{\text{cut}}^{(3)}} dE_3 \left(\int_{m_e}^{E_3} dE_2 \int_{p_1-E_3+E_2-q_2}^{p_1-E_3+E_2+q_2} dy + \int_{E_3}^{E_{\text{trans}}^{(2)}} dE_2 \int_{p_1-q_3}^{p_1+q_3} dy + \int_{E_{\text{trans}}^{(2)}}^{E_{\text{lim}}^{(1)}} dE_2 \int_{E_3-p_1-E_2+q_2}^{p_1+q_3} dy \right) \\
&+ \int_{E_{\text{cut}}^{(3)}}^{E_{\text{cut}}^{(1)}} dE_3 \left(\int_{m_e}^{E_{\text{trans}}^{(2)}} dE_2 \int_{p_1-E_3+E_2-q_2}^{p_1-E_3+E_2+q_2} dy \right. \\
&\qquad \left. + \int_{E_{\text{trans}}^{(2)}}^{E_3} dE_2 \int_{q_3-p_1}^{p_1-E_3+E_2+q_2} dy + \int_{E_3}^{E_{\text{lim}}^{(1)}} dE_2 \int_{E_3-p_1-E_2+q_2}^{p_1+q_3} dy \right) \\
&+ \int_{E_{\text{cut}}^{(1)}}^{E_{\text{cut}}^{(2)}} dE_3 \left(\int_{m_e}^{E_{\text{sort}}^{(1)}} dE_2 \int_{p_1-E_3+E_2-q_2}^{p_1-E_3+E_2+q_2} dy + \int_{E_{\text{sort}}^{(1)}}^{E_{\text{sort}}^{(2)}} dE_2 \int_{b_{\text{sort}}}^{p_1-E_3+E_2+q_2} dy \right. \\
&\qquad \left. + \int_{E_{\text{sort}}^{(2)}}^{E_3} dE_2 \int_{q_3-p_1}^{p_1-E_3+E_2+q_2} dy + \int_{E_3}^{\infty} dE_2 \int_{E_3-p_1-E_2+q_2}^{p_1+q_3} dy \right) \\
&+ \int_{E_{\text{cut}}^{(2)}}^{\infty} dE_3 \left(\int_{E_{\text{lim}}^{(2)}}^{E_3} dE_2 \int_{q_3-p_1}^{p_1-E_3+E_2+q_2} dy + \int_{E_3}^{\infty} dE_2 \int_{E_3-p_1-E_2+q_2}^{p_1+q_3} dy \right) . \qquad \text{(G.215)}
\end{aligned}
$$

Furthermore, Eq.(G.215) eliminates the need for $E_{\text{trans}}^{(3)}$, thereby eliminating the $E_{\text{sort}}^{(1)}$, $E_{\text{sort}}^{(2)}$, and b_{sort} notation:

$$
\begin{aligned}
R_2^{(2)} = &\int_{m_e}^{E_{\text{cut}}^{(3)}} dE_3 \left(\int_{m_e}^{E_3} dE_2 \int_{p_1-E_3+E_2-q_2}^{p_1-E_3+E_2+q_2} dy + \int_{E_3}^{E_{\text{trans}}^{(2)}} dE_2 \int_{p_1-q_3}^{p_1+q_3} dy + \int_{E_{\text{trans}}^{(2)}}^{E_{\text{lim}}^{(1)}} dE_2 \int_{E_3-p_1-E_2+q_2}^{p_1+q_3} dy \right) \\
&+ \int_{E_{\text{cut}}^{(3)}}^{E_{\text{cut}}^{(1)}} dE_3 \left(\int_{m_e}^{E_{\text{trans}}^{(2)}} dE_2 \int_{p_1-E_3+E_2-q_2}^{p_1-E_3+E_2+q_2} dy \right. \\
&\left. + \int_{E_{\text{trans}}^{(2)}}^{E_3} dE_2 \int_{q_3-p_1}^{p_1-E_3+E_2+q_2} dy + \int_{E_3}^{E_{\text{lim}}^{(1)}} dE_2 \int_{E_3-p_1-E_2+q_2}^{p_1+q_3} dy \right) \\
&+ \int_{E_{\text{cut}}^{(1)}}^{E_{\text{cut}}^{(2)}} dE_3 \left(\int_{m_e}^{E_{\text{trans}}^{(2)}} dE_2 \int_{p_1-E_3+E_2-q_2}^{p_1-E_3+E_2+q_2} dy \right. \\
&\left. + \int_{E_{\text{trans}}^{(2)}}^{E_3} dE_2 \int_{q_3-p_1}^{p_1-E_3+E_2+q_2} dy + \int_{E_3}^{\infty} dE_2 \int_{E_3-p_1-E_2+q_2}^{p_1+q_3} dy \right) \\
&+ \int_{E_{\text{cut}}^{(2)}}^{\infty} dE_3 \left(\int_{E_{\text{lim}}^{(2)}}^{E_3} dE_2 \int_{q_3-p_1}^{p_1-E_3+E_2+q_2} dy + \int_{E_3}^{\infty} dE_2 \int_{E_3-p_1-E_2+q_2}^{p_1+q_3} dy \right)
\end{aligned}
\tag{G.216}
$$

Therefore, there is no need for Boole's rule on $\int dE_3$ for $E_{\text{cut}}^{(1)} < E_3 < E_{\text{cut}}^{(2)}$.

G.3.3 Case 3: $\frac{1}{2\sqrt{2}} < \frac{p_1}{m_e} < \frac{1}{2}$

The cut hierarchy is:

$$
E_{\text{cut}}^{(4)} < E_{\text{cut}}^{(1)} < E_{\text{cut}}^{(3)} < E_{\text{cut}}^{(2)} \tag{G.217}
$$

which gives us the following for R_2:

$$
\begin{aligned}
R_2^{(3)} = & \int_{m_e}^{E_{\text{cut}}^{(1)}} dE_3 \int_{p_1-q_3}^{p_1+q_3} dy \int_{E_{\min}}^{E_{\max}^{(\text{B})}} dE_2 \\
& + \int_{E_{\text{cut}}^{(1)}}^{E_{\text{cut}}^{(3)}} dE_3 \left(\int_{p_1-q_3}^{E_3-p_1} dy \int_{E_{\min}}^{E_{\max}^{(\text{B})}} dE_2 + \int_{E_3-p_1}^{p_1+q_3} dy \int_{E_{\min}}^{\infty} dE_2 \right) \\
& + \int_{E_{\text{cut}}^{(3)}}^{E_{\text{cut}}^{(2)}} dE_3 \left(\int_{q_3-p_1}^{E_3-p_1} dy \int_{E_{\min}}^{E_{\max}^{(\text{B})}} dE_2 + \int_{E_3-p_1}^{p_1+q_3} dy \int_{E_{\min}}^{\infty} dE_2 \right) \\
& + \int_{E_{\text{cut}}^{(2)}}^{\infty} dE_3 \left(\int_{q_3-p_1}^{E_3-p_1} dy \int_{E_{\min}}^{E_{\max}^{(\text{B})}} dE_2 + \int_{E_3-p_1}^{p_1+q_3} dy \int_{E_{\min}}^{\infty} dE_2 \right) .
\end{aligned}
\tag{G.218}
$$

The first, third, fourth, fifth, sixth, and seventh integrals are similar to what has been done in the previous two cases. The second integral is similar to the fourth and sixth integrals, except that the bottom limit on $\int dy$ is $p_1 - q_3$. In this case, $E_{\text{trans}}^{(2)}$ is defined and $E_{\text{trans}}^{(3)} < E_3 < E_{\text{trans}}^{(2)}$, so there is no need for $E_?$ on the second integral. After combining

integrals with $E_3 - p_1$ in the top and bottom limits, the expression for R_2 is:

$$
\begin{aligned}
R_2^{(3)} = &\int_{m_e}^{E_{\rm cut}^{(1)}} dE_3 \left(\int_{m_e}^{E_3} dE_2 \int_{p_1-E_3+E_2-q_2}^{p_1-E_3+E_2+q_2} dy + \int_{E_3}^{E_{\rm trans}^{(2)}} dE_2 \int_{p_1-q_3}^{p_1+q_3} dy + \int_{E_{\rm trans}^{(2)}}^{E_{\rm lim}^{(1)}} dE_2 \int_{E_3-p_1-E_2+q_2}^{p_1+q_3} dy \right) \\
&+ \int_{E_{\rm cut}^{(1)}}^{E_{\rm cut}^{(3)}} dE_3 \left(\int_{m_e}^{E_3} dE_2 \int_{p_1-E_3+E_2-q_2}^{p_1-E_3+E_2+q_2} dy + \int_{E_3}^{E_{\rm trans}^{(2)}} dE_2 \int_{p_1-q_3}^{p_1+q_3} dy + \int_{E_{\rm trans}^{(2)}}^{\infty} dE_2 \int_{E_3-p_1-E_2+q_2}^{p_1+q_3} dy \right) \\
&+ \int_{E_{\rm cut}^{(3)}}^{E_{\rm cut}^{(2)}} dE_3 \left(\int_{m_e}^{E_{\rm trans}^{(2)}} dE_2 \int_{p_1-E_3+E_2-q_2}^{p_1-E_3+E_2+q_2} dy \right. \\
&\left. + \int_{E_{\rm trans}^{(2)}}^{E_3} dE_2 \int_{q_3-p_1}^{p_1-E_3+E_2+q_2} dy + \int_{E_3}^{\infty} dE_2 \int_{E_3-p_1-E_2+q_2}^{p_1+q_3} dy \right) \\
&+ \int_{E_{\rm cut}^{(2)}}^{\infty} dE_3 \left(\int_{E_{\rm lim}^{(2)}}^{E_3} dE_2 \int_{q_3-p_1}^{p_1-E_3+E_2+q_2} dy + \int_{E_3}^{\infty} dE_2 \int_{E_3-p_1-E_2+q_2}^{p_1+q_3} dy \right)
\end{aligned}
\tag{G.219}
$$

G.3.4 Case 4: $\frac{1}{2} < \frac{p_1}{m_e} < \frac{3}{4}$

The cut hierarchy is:

$$
E_{\rm cut}^{(1)} < E_{\rm cut}^{(4)} < E_{\rm cut}^{(3)} < E_{\rm cut}^{(2)} \tag{G.220}
$$

which gives us the following for R_2:

$$
\begin{aligned}
R_2^{(4)} = & \int_{m_e}^{E_{\text{cut}}^{(1)}} dE_3 \int_{p_1-q_3}^{p_1+q_3} dy \int_{E_{\min}}^{E_{\max}^{(\text{B})}} dE_2 \\
& + \int_{E_{\text{cut}}^{(1)}}^{E_{\text{cut}}^{(4)}} dE_3 \left(\int_{p_1-q_3}^{E_3-p_1} dy \int_{E_{\min}}^{E_{\max}^{(\text{B})}} dE_2 + \int_{E_3-p_1}^{p_1+q_3} dy \int_{E_{\min}}^{\infty} dE_2 \right) \\
& + \int_{E_{\text{cut}}^{(4)}}^{E_{\text{cut}}^{(3)}} dE_3 \left(\int_{p_1-q_3}^{E_3-p_1} dy \int_{E_{\min}}^{E_{\max}^{(\text{B})}} dE_2 + \int_{E_3-p_1}^{p_1+q_3} dy \int_{E_{\min}}^{\infty} dE_2 \right) \\
& + \int_{E_{\text{cut}}^{(3)}}^{E_{\text{cut}}^{(2)}} dE_3 \left(\int_{q_3-p_1}^{E_3-p_1} dy \int_{E_{\min}}^{E_{\max}^{(\text{B})}} dE_2 + \int_{E_3-p_1}^{p_1+q_3} dy \int_{E_{\min}}^{\infty} dE_2 \right) \\
& + \int_{E_{\text{cut}}^{(2)}}^{\infty} dE_3 \left(\int_{q_3-p_1}^{E_3-p_1} dy \int_{E_{\min}}^{E_{\max}^{(\text{B})}} dE_2 + \int_{E_3-p_1}^{p_1+q_3} dy \int_{E_{\min}}^{\infty} dE_2 \right)
\end{aligned}
\tag{G.221}
$$

Eq.(G.221) is identical to case 3, except for two issues: (1)the integral for $m_e < E_3 < E_{\text{cut}}^{(1)}$ neither contains the expressions for $E_{\text{trans}}^{(2)}$ nor $E_{\text{lim}}^{(1)}$; (2)there is a subcase where $E_{\text{cut}}^{(4)} < E_3 < E_{\text{cut}}^{(3)}$. For the second issue, Eq.(G.148) is not physically meaningful (implying no transition point for the top limit of $\int dE_2$ involving $E_3 - p_1$), and Eq.(G.179) is physically meaningful (implying a limit point for the bottom limit, i.e. $E_{\text{lim}}^{(3)}$). The implications are:

$$
\begin{cases}
E_3 - p_1 < p_1 - E_3 + E_2 - q_2 \text{ for } E_2 < E_{\text{lim}}^{(3)} \\
E_3 - p_1 > p_1 - E_3 + E_2 - q_2 \text{ for } E_2 > E_{\text{lim}}^{(3)} \\
E_3 - p_1 < p_1 - E_3 + E_2 + q_2 \text{ for all } E_{\text{cut}}^{(4)} < E_3 < E_{\text{cut}}^{(3)}
\end{cases}
\quad . \tag{G.222}
$$

We have the following expression for Eq.(G.221):

$$
\begin{aligned}
R_2^{(4)} = &\int_{m_e}^{E_{\rm cut}^{(1)}} dE_3 \quad \left(\int_{m_e}^{E_3} dE_2 \int_{p_1-E_3+E_2-q_2}^{p_1-E_3+E_2+q_2} dy + \int_{E_3}^{\infty} dE_2 \int_{p_1-q_3}^{p_1+q_3} dy \right) \\
&+ \int_{E_{\rm cut}^{(1)}}^{E_{\rm cut}^{(4)}} dE_3 \quad \left(\int_{E_{\rm lim}^{(3)}}^{E_3} dE_2 \int_{p_1-E_3+E_2-q_2}^{E_3-p_1} dy + \int_{E_3}^{E_{\rm trans}^{(2)}} dE_2 \int_{p_1-q_3}^{E_3-p_1} dy \right. \\
&\qquad + \int_{E_{\rm trans}^{(2)}}^{\infty} dE_2 \int_{E_3-p_1-E_2+q_2}^{E_3-p_1} dy + \int_{m_e}^{E_{\rm trans}^{(3)}} dE_2 \int_{p_1-E_3+E_2-q_2}^{p_1-E_3+E_2+q_2} dy \\
&\qquad \left. + \int_{E_{\rm trans}^{(3)}}^{E_3} dE_2 \int_{E_3-p_1}^{p_1-E_3+E_2+q_2} dy + \int_{E_3}^{\infty} dE_2 \int_{E_3-p_1}^{p_1+q_3} dy \right) \\
&+ \int_{E_{\rm cut}^{(4)}}^{E_{\rm cut}^{(3)}} dE_3 \quad \left(\int_{m_e}^{E_3} dE_2 \int_{p_1-E_3+E_2-q_2}^{p_1-E_3+E_2+q_2} dy \right. \\
&\qquad \left. + \int_{E_3}^{E_{\rm trans}^{(2)}} dE_2 \int_{p_1-q_3}^{p_1+q_3} dy + \int_{E_{\rm trans}^{(2)}}^{\infty} dE_2 \int_{E_3-p_1-E_2+q_2}^{p_1+q_3} dy \right) \\
&+ \int_{E_{\rm cut}^{(3)}}^{E_{\rm cut}^{(2)}} dE_3 \quad \left(\int_{m_e}^{E_{\rm trans}^{(2)}} dE_2 \int_{p_1-E_3+E_2-q_2}^{p_1-E_3+E_2+q_2} dy \right. \\
&\qquad \left. + \int_{E_{\rm trans}^{(2)}}^{E_3} dE_2 \int_{q_3-p_1}^{p_1-E_3+E_2+q_2} dy + \int_{E_3}^{\infty} dE_2 \int_{E_3-p_1-E_2+q_2}^{p_1+q_3} dy \right) \\
&+ \int_{E_{\rm cut}^{(2)}}^{\infty} dE_3 \quad \left(\int_{E_{\rm lim}^{(2)}}^{E_3} dE_2 \int_{q_3-p_1}^{p_1-E_3+E_2+q_2} dy + \int_{E_3}^{\infty} dE_2 \int_{E_3-p_1-E_2+q_2}^{p_1+q_3} dy \right). \qquad \text{(G.223)}
\end{aligned}
$$

Eq.(G.223) simplifies to:

$$
\begin{aligned}
R_2^{(4)} = &\int_{m_e}^{E_{\rm cut}^{(1)}} dE_3 \quad \left(\int_{m_e}^{E_3} dE_2 \int_{p_1-E_3+E_2-q_2}^{p_1-E_3+E_2+q_2} dy + \int_{E_3}^{\infty} dE_2 \int_{p_1-q_3}^{p_1+q_3} dy \right) \\
&+ \int_{E_{\rm cut}^{(1)}}^{E_{\rm cut}^{(4)}} dE_3 \quad \left(\int_{m_e}^{E_3} dE_2 \int_{p_1-E_3+E_2-q_2}^{p_1-E_3+E_2+q_2} dy + \int_{E_3}^{E_{\rm trans}^{(2)}} dE_2 \int_{p_1-q_3}^{p_1+q_3} dy + \int_{E_{\rm trans}^{(2)}}^{\infty} dE_2 \int_{E_3-p_1-E_2+q_2}^{p_1+q_3} dy \right) \\
&+ \int_{E_{\rm cut}^{(4)}}^{E_{\rm cut}^{(3)}} dE_3 \quad \left(\int_{m_e}^{E_3} dE_2 \int_{p_1-E_3+E_2-q_2}^{p_1-E_3+E_2+q_2} dy + \int_{E_3}^{E_{\rm trans}^{(2)}} dE_2 \int_{p_1-q_3}^{p_1+q_3} dy + \int_{E_{\rm trans}^{(2)}}^{\infty} dE_2 \int_{E_3-p_1-E_2+q_2}^{p_1+q_3} dy \right) \\
&+ \int_{E_{\rm cut}^{(3)}}^{E_{\rm cut}^{(2)}} dE_3 \quad \left(\int_{m_e}^{E_{\rm trans}^{(2)}} dE_2 \int_{p_1-E_3+E_2-q_2}^{p_1-E_3+E_2+q_2} dy \right. \\
&\qquad \left. + \int_{E_{\rm trans}^{(2)}}^{E_3} dE_2 \int_{q_3-p_1}^{p_1-E_3+E_2+q_2} dy + \int_{E_3}^{\infty} dE_2 \int_{E_3-p_1-E_2+q_2}^{p_1+q_3} dy \right) \\
&+ \int_{E_{\rm cut}^{(2)}}^{\infty} dE_3 \quad \left(\int_{E_{\rm lim}^{(2)}}^{E_3} dE_2 \int_{q_3-p_1}^{p_1-E_3+E_2+q_2} dy + \int_{E_3}^{\infty} dE_2 \int_{E_3-p_1-E_2+q_2}^{p_1+q_3} dy \right)
\end{aligned}
\tag{G.224}
$$

The arguments are identical for $\int dE_3$ for $E_{\text{cut}}^{(1)} < E_3 < E_{\text{cut}}^{(4)}$ and $E_{\text{cut}}^{(4)} < E_3 < E_{\text{cut}}^{(3)}$ so we can combine them into the final expression for $R_2^{(4)}$:

$$
\begin{aligned}
&= \int_{m_e}^{E_{\text{cut}}^{(1)}} dE_3 \quad \left(\int_{m_e}^{E_3} dE_2 \int_{p_1-E_3+E_2-q_2}^{p_1-E_3+E_2+q_2} dy + \int_{E_3}^{\infty} dE_2 \int_{p_1-q_3}^{p_1+q_3} dy \right) \\
&+ \int_{E_{\text{cut}}^{(1)}}^{E_{\text{cut}}^{(3)}} dE_3 \quad \left(\int_{m_e}^{E_3} dE_2 \int_{p_1-E_3+E_2-q_2}^{p_1-E_3+E_2+q_2} dy + \int_{E_3}^{E_{\text{trans}}^{(2)}} dE_2 \int_{p_1-q_3}^{p_1+q_3} dy + \int_{E_{\text{trans}}^{(2)}}^{\infty} dE_2 \int_{E_3-p_1-E_2+q_2}^{p_1+q_3} dy \right) \\
&+ \int_{E_{\text{cut}}^{(3)}}^{E_{\text{cut}}^{(2)}} dE_3 \quad \left(\int_{m_e}^{E_{\text{trans}}^{(2)}} dE_2 \int_{p_1-E_3+E_2-q_2}^{p_1-E_3+E_2+q_2} dy \right. \\
&\qquad \left. + \int_{E_{\text{trans}}^{(2)}}^{E_3} dE_2 \int_{q_3-p_1}^{p_1-E_3+E_2+q_2} dy + \int_{E_3}^{\infty} dE_2 \int_{E_3-p_1-E_2+q_2}^{p_1+q_3} dy \right) \\
&+ \int_{E_{\text{cut}}^{(2)}}^{\infty} dE_3 \quad \left(\int_{E_{\text{lim}}^{(2)}}^{E_3} dE_2 \int_{q_3-p_1}^{p_1-E_3+E_2+q_2} dy + \int_{E_3}^{\infty} dE_2 \int_{E_3-p_1-E_2+q_2}^{p_1+q_3} dy \right)
\end{aligned}
\tag{G.225}
$$

G.3.5 Case 5: $\frac{3}{4} < \frac{p_1}{m_e}$

The cut hierarchy is:

$$E_{\text{cut}}^{(1)} < E_{\text{cut}}^{(3)} < E_{\text{cut}}^{(4)} < E_{\text{cut}}^{(2)} \tag{G.226}$$

which gives us the following for R_2:

$$R_2^{(5)} = \int_{m_e}^{E_{\rm cut}^{(1)}} dE_3 \int_{p_1-q_3}^{p_1+q_3} dy \int_{E_{\rm min}}^{E_{\rm max}^{\rm (B)}} dE_2 \tag{G.227}$$

$$\begin{aligned}
&+ \int_{E_{\rm cut}^{(1)}}^{E_{\rm cut}^{(3)}} dE_3 \left(\int_{p_1-q_3}^{E_3-p_1} dy \int_{E_{\rm min}}^{E_{\rm max}^{\rm (B)}} dE_2 + \int_{E_3-p_1}^{p_1+q_3} dy \int_{E_{\rm min}}^{\infty} dE_2 \right) \\
&+ \int_{E_{\rm cut}^{(3)}}^{E_{\rm cut}^{(4)}} dE_3 \left(\int_{q_3-p_1}^{E_3-p_1} dy \int_{E_{\rm min}}^{E_{\rm max}^{\rm (B)}} dE_2 + \int_{E_3-p_1}^{p_1+q_3} dy \int_{E_{\rm min}}^{\infty} dE_2 \right) \\
&+ \int_{E_{\rm cut}^{(4)}}^{E_{\rm cut}^{(2)}} dE_3 \left(\int_{q_3-p_1}^{E_3-p_1} dy \int_{E_{\rm min}}^{E_{\rm max}^{\rm (B)}} dE_2 + \int_{E_3-p_1}^{p_1+q_3} dy \int_{E_{\rm min}}^{\infty} dE_2 \right) \\
&+ \int_{E_{\rm cut}^{(2)}}^{\infty} dE_3 \left(\int_{q_3-p_1}^{E_3-p_1} dy \int_{E_{\rm min}}^{E_{\rm max}^{\rm (B)}} dE_2 + \int_{E_3-p_1}^{p_1+q_3} dy \int_{E_{\rm min}}^{\infty} dE_2 \right)
\end{aligned} \tag{G.228}$$

We have the following expression for Eq.(G.228):

$$
\begin{aligned}
R_2^{(5)} = & \int_{m_e}^{E_{\rm cut}^{(1)}} dE_3 \qquad \left(\int_{m_e}^{E_3} dE_2 \int_{p_1-E_3+E_2-q_2}^{p_1-E_3+E_2+q_2} dy + \int_{E_3}^{\infty} dE_2 \int_{p_1-q_3}^{p_1+q_3} dy \right) \\
& + \int_{E_{\rm cut}^{(1)}}^{E_{\rm cut}^{(3)}} dE_3 \qquad \left(\int_{m_e}^{E_3} dE_2 \int_{p_1-E_3+E_2-q_2}^{p_1-E_3+E_2+q_2} dy \right. \\
& \qquad \left. + \int_{E_3}^{E_{\rm trans}^{(2)}} dE_2 \int_{p_1-q_3}^{p_1+q_3} dy + \int_{E_{\rm trans}^{(2)}}^{\infty} dE_2 \int_{E_3-p_1-E_2+q_2}^{p_1+q_3} dy \right) \\
& + \int_{E_{\rm cut}^{(3)}}^{E_{\rm cut}^{(4)}} dE_3 \qquad \left(\int_{E_{\rm lim}^{(3)}}^{E_{\rm trans}^{(2)}} dE_2 \int_{p_1-E_3+E_2-q_2}^{E_3-p_1} dy + \int_{E_{\rm trans}^{(2)}}^{E_3} dE_2 \int_{q_3-p_1}^{E_3-p_1} dy \right. \\
& \qquad + \int_{E_3}^{\infty} dE_2 \int_{E_3-p_1-E_2+q_2}^{E_3-p_1} dy + \int_{m_e}^{E_{\rm trans}^{(3)}} dE_2 \int_{p_1-E_3+E_2-q_2}^{p_1-E_3+E_2+q_2} dy \\
& \qquad \left. + \int_{E_{\rm trans}^{(3)}}^{E_3} dE_2 \int_{E_3-p_1}^{p_1-E_3+E_2+q_2} dy + \int_{E_3}^{\infty} dE_2 \int_{E_3-p_1}^{p_1+q_3} dy \right) \\
& + \int_{E_{\rm cut}^{(4)}}^{E_{\rm cut}^{(2)}} dE_3 \qquad \left(\int_{m_e}^{E_{\rm trans}^{(2)}} dE_2 \int_{p_1-E_3+E_2-q_2}^{p_1-E_3+E_2+q_2} dy \right. \\
& \qquad \left. + \int_{E_{\rm trans}^{(2)}}^{E_3} dE_2 \int_{q_3-p_1}^{p_1-E_3+E_2+q_2} dy + \int_{E_3}^{\infty} dE_2 \int_{E_3-p_1-E_2+q_2}^{p_1+q_3} dy \right) \\
& + \int_{E_{\rm cut}^{(2)}}^{\infty} dE_3 \qquad \left(\int_{E_{\rm lim}^{(2)}}^{E_3} dE_2 \int_{q_3-p_1}^{p_1-E_3+E_2+q_2} dy + \int_{E_3}^{\infty} dE_2 \int_{E_3-p_1-E_2+q_2}^{p_1+q_3} dy \right)
\end{aligned}
\tag{G.229}
$$

There exists potential danger that $E_{\text{sort}}^{(1)}$ and $E_{\text{sort}}^{(2)}$ would need to be used in concert with $\int dE_3$ for $E_{\text{cut}}^{(3)} < E_3 < E_{\text{cut}}^{(4)}$. However, substituting $E_3 = E_{\text{cut}}^{(4)}$ into Eq.(G.199), we see that $E_? > E_{\text{cut}}^{(4)}$. Therefore, we can combine the integrals for $\int dE_3$ with $E_{\text{cut}}^{(3)} < E_3 < E_{\text{cut}}^{(4)}$ and we obtain $R_2^{(5)} = R_2^{(4)}$, eliminating the need for case 5.

G.4 Summary

Cases 4 and 5 are identical to case 3. There is no need for Boole's rule on any $\int dE_3$. The quantities $E_{\text{cut}}^{(4)}$, $E_{\text{trans}}^{(3)}$, and $E_{\text{lim}}^{(3)}$ are superfluous. Here is a new summary of the validity of the quantities in Eq.(G.219):

$$
\begin{cases}
E_3 < E_{\text{trans}}^{(2)} & \text{if } E_3 < E_{\text{cut}}^{(3)} \\
E_3 > E_{\text{trans}}^{(2)} & \text{if } E_3 > E_{\text{cut}}^{(3)}
\end{cases}
$$

$$
\begin{cases}
\text{if } \frac{p_1}{m_e} < \frac{1}{2} \text{ and } E_3 < E_{\text{cut}}^{(2)} \implies E_{\text{trans}}^{(2)} \text{ defined} \\
\text{if } \frac{p_1}{m_e} > \frac{1}{2} \text{ and } E_{\text{cut}}^{(1)} < E_3 < E_{\text{cut}}^{(2)} \implies E_{\text{trans}}^{(2)} \text{ defined} \\
\text{if } E_3 > E_{\text{cut}}^{(2)} \implies E_{\text{trans}}^{(2)} \text{ not defined}
\end{cases}
$$

$$
\begin{cases}
\text{if } E_3 < E_{\text{cut}}^{(1)} \text{ and } \frac{p_1}{m_e} < \frac{1}{2} \implies E_{\text{lim}}^{(1)} \text{ defined} \\
\text{else} \implies E_{\text{lim}}^{(1)} \text{ not defined}
\end{cases}
$$

$$E_{\text{cut}}^{(3)} < E_{\text{cut}}^{(2)} \tag{G.230}$$

(G.231)

Appendix H

Charged lepton annihilation into neutrinos

The reaction of interest is annihilation of a neutrino and anti-neutrino into an $e^{\pm}$ pair:

$$\nu(1) + \bar{\nu}(4) \rightarrow e^{-}(3) + e^{+}(2) \tag{H.1}$$

The numbering scheme ensures the fourth particle is massless. We will use q's to denote the magnitude of three-momenta for massive particles, E's to denote energies of massive particles, and p's to denote the energy/momentum magnitude for massless particles. Four vectors are denoted P and Q for massless and massive particles, respectively. Energy conservation states $p_1 + p_4 = E_2 + E_3$.

H.1 Electron neutrinos

We start with the summed-squared-matrix element for the reaction in Eq.(H.1) for the case of electron neutrinos:

$$\begin{aligned}\langle|\mathcal{M}|^2\rangle &= 32G_F^2(1+2\sin^2\theta_w)^2\left[(P_1\cdot Q_2)^2+\frac{2\sin^2\theta_w}{1+2\sin^2\theta_w}m_e^2(P_1\cdot Q_2)\right]\\ &\quad+128G_F^2\sin^4\theta_w\left[(P_1\cdot Q_3)^2+\frac{1+2\sin^2\theta_w}{2\sin^2\theta_w}m_e^2(P_1\cdot Q_3)\right] \qquad \text{(H.2)}\\ &\equiv L_1(P_1\cdot Q_2)+L_2(P_1\cdot Q_3), \qquad \text{(H.3)}\end{aligned}$$

where G_F is the Fermi coupling constant, θ_w is the Weinberg angle, and m_e is the electron mass. We begin by focusing on L_1.

H.2 $L_1(P_1\cdot Q_2)$

We define R_1 to be the collision term in the Boltzmann equation:

$$R_1=\frac{1}{16(2\pi)^5}\int\frac{d^3q_2\,d^3q_3\,d^3p_4}{p_1E_2E_3p_4}L_1(P_1\cdot Q_2)\delta^4(P_1+P_4-Q_2-Q_3)F(p_1,p_4,E_2,E_3), \qquad \text{(H.4)}$$

where:

$$\begin{aligned}F(p_1,p_4,E_2,E_3) &= f_2(E_2)f_3(E_3)(1-f_1(p_1))(1-f_4(p_4))\\ &\quad-f_1(p_1)f_4(p_4)(1-f_2(E_2))(1-f_3(E_3)), \qquad \text{(H.5)}\end{aligned}$$

and $f_i(E_i)$ is the occupation probability for species i at energy E_i. We use the three-dimensional delta function to eliminate the integral over p_4:

$$R_1 = \frac{1}{16(2\pi)^5}\int \frac{d^3q_2\,d^3q_3}{p_1E_2E_3p_4} \times L_1(P_1\cdot Q_2)\delta(p_1+p_4-E_2-E_3)F(p_1,p_4,E_2,E_3)\Big|_{p_4=|\vec{q}_2+\vec{q}_3-\vec{p}_1|}. \tag{H.6}$$

We will write $|\vec{q}_2+\vec{q}_3-\vec{p}_1| = |\vec{p}_1-\vec{q}_2-\vec{q}_3|$ so that the $+$ sign is on $\vec{p}_1$. To use the last delta function, we will use a u-substitution to eliminate the $\int d\theta_3$. We set:

$$u^2 = p_4^2 \tag{H.7}$$

$$= |\vec{p}_1-\vec{q}_2-\vec{q}_3|^2 \tag{H.8}$$

$$= |\vec{p}_1-\vec{q}_2|^2+q_3^2-2|\vec{p}_1-\vec{q}_2|q_3\cos\theta_3, \tag{H.9}$$

where θ_3 is defined to be the angle between $\vec{p}_1-\vec{q}_2$ and $\vec{q}_3$. We have:

$$2u\,du = 2p_4du = -2|\vec{p}_1-\vec{q}_2|q_3(-\sin\theta_3)d\theta_3 \tag{H.10}$$

$$\implies \sin\theta_3\,d\theta_3 = \frac{p_4du}{|\vec{p}_1-\vec{q}_2|q_3} \tag{H.11}$$

The expression for Eq.(H.6) becomes:

$$R_1 = \frac{1}{16(2\pi)^5}\int \frac{d^3q_2\,d^3q_3}{p_1E_2E_3p_4}L_1(P_1\cdot Q_2)\delta(p_1+p_4-E_2-E_3)F(p_1,p_4,E_2,E_3) \quad \text{(H.12)}$$

$$= \frac{1}{16(2\pi)^5}\int \frac{d^3q_2}{p_1E_2}L_1(P_1\cdot Q_2)$$

$$\times \int_0^{2\pi} d\phi_3 \int_0^{\infty} dq_3 \frac{q_3^2}{E_3}\int_0^{\pi}\sin\theta_3 d\theta_3 \frac{1}{p_4}\delta(p_1+p_4-E_2-E_3)F(p_1,p_4,E_2,E_3) \quad \text{(H.13)}$$

$$= \frac{1}{16(2\pi)^5}\int \frac{d^3q_2}{p_1E_2}L_1(P_1\cdot Q_2)$$

$$\times (2\pi)\int_{m_e}^{\infty} dE_3\, q_3 \int_{u(\theta_3=0)}^{u(\theta_3=\pi)} \frac{p_4 du}{|\vec{p}_1-\vec{q}_2|q_3}\frac{1}{p_4}\delta(p_1+p_4-E_2-E_3)F(p_1,p_4,E_2,E_3) \quad \text{(H.14)}$$

$$= \frac{1}{16(2\pi)^4}\int \frac{d^3q_2}{p_1E_2}\frac{L_1(P_1\cdot Q_2)}{|\vec{p}_1-\vec{q}_2|}\int_{m_e}^{\infty} dE_3\int_a^b du\,\delta(p_1+u-E_2-E_3)F(p_1,u,E_2,E_3), \quad \text{(H.15)}$$

where:

$$a = u(\theta_3=0) = ||\vec{p}_1-\vec{q}_2|-q_3| \quad \text{(H.16)}$$

$$b = u(\theta_3=\pi) = |\vec{p}_1-\vec{q}_2|+q_3. \quad \text{(H.17)}$$

We reduce $\int d^3q_2$ to simplify Eq.(H.15):

$$R_1 = \frac{1}{16(2\pi)^4}\int_0^{2\pi} d\phi_2 \int_0^{\infty} dq_2 \frac{q_2^2}{p_1E_2}\int_0^{\pi}\sin\theta_2\, d\theta_2 \frac{L_1(P_1\cdot Q_2)}{|\vec{p}_1-\vec{q}_2|}$$

$$\times \int_{m_e}^{\infty} dE_3 \int_a^b du\,\delta(p_1+u-E_2-E_3)F(p_1,u,E_2,E_3). \quad \text{(H.18)}$$

We define the angle θ_2 as the angle between $\vec{p}_1$ and $\vec{q}_2$. We make a change of variables to simplify the integrand in the integral over θ_2:

$$y \equiv |\vec{p}_1 - \vec{q}_2| = \sqrt{p_1^2 + q_2^2 - 2p_1 q_2 \cos\theta_2} \tag{H.19}$$

$$\Longrightarrow \sin\theta_2 \, d\theta_2 = dy \frac{y}{p_1 q_2} \tag{H.20}$$

The argument in L_1 changes to:

$$P_1 \cdot Q_2 = p_1 E_2 - p_1 q_2 \cos\theta_2 \tag{H.21}$$

$$= p_1 E_2 - \frac{1}{2}(p_1^2 + q_2^2 - y^2) \tag{H.22}$$

$$= \frac{1}{2}y^2 - \frac{1}{2}(p_1^2 - 2p_1 E_2 + q_2^2) \tag{H.23}$$

$$= \frac{1}{2}y^2 - \frac{1}{2}[(p_1 - E_2)^2 - m_e^2] \tag{H.24}$$

Eq.(H.18) becomes:

$$R_1 = \frac{1}{16(2\pi)^4} \int_0^{2\pi} d\phi_2 \int_0^{\infty} dq_2 \frac{q_2^2}{p_1 E_2} \int_{|p_1 - q_2|}^{p_1 + q_2} dy \frac{y}{p_1 q_2} \frac{L_1\{\frac{1}{2}y^2 - \frac{1}{2}[(p_1 - E_2)^2 - m_e^2]\}}{y}$$

$$\times \int_{m_e}^{\infty} dE_3 \int_a^b du \, \delta(p_1 + u - E_2 - E_3) F(p_1, u, E_2, E_3) \tag{H.25}$$

$$= \frac{1}{16(2\pi)^4}(2\pi) \int_{m_e}^{\infty} dE_2 \frac{1}{p_1^2} \int_{|p_1 - q_2|}^{p_1 + q_2} dy L_1 \int_{m_e}^{\infty} dE_3 \int_a^b du \, \delta(p_1 + u - E_2 - E_3) F \tag{H.26}$$

$$= \frac{1}{16(2\pi)^3} \int_{m_e}^{\infty} dE_2 \frac{1}{p_1^2} \int_{|p_1 - q_2|}^{p_1 + q_2} dy L_1 \int_{m_e}^{\infty} dE_3 \int_a^b du \, \delta(p_1 + u - E_2 - E_3) F \tag{H.27}$$

where we have dropped the arguments for L_1 and F for notational simplicity. It will prove useful to consider the different cases for p_1:

$$\frac{p_1}{m_e} < \frac{1}{2} \tag{H.28}$$

$$\frac{1}{2} < \frac{p_1}{m_e} < \frac{1+\sqrt{5}}{4} \tag{H.29}$$

$$\frac{1+\sqrt{5}}{4} < \frac{p_1}{m_e} < 1 \tag{H.30}$$

$$1 < \frac{p_1}{m_e} \tag{H.31}$$

In addition, when writing R_1, we will drop the integrands and overall multiplicative factor for notational simplicity, yielding:

$$R_2 = \int_{m_e}^{\infty} dE_2 \int_{|p_1-q_2|}^{p_1+q_2} dy \int_{m_e}^{\infty} dE_3 \int_{a}^{b} du \tag{H.32}$$

H.2.1 Case 1: $\frac{p_1}{m_e} < \frac{1}{2}$

Eliminating $\int du$

The goal is to determine what values of E_3 give non-zero $\int du$ for Eq.(H.27). We first consider when equality is assumed between the two y values p_1+q_2 and E_2-p_1:

$$p_1 + q_2 = E_2 - p_1 \tag{H.33}$$

$$\implies q_2 = E_2 - 2p_1 \tag{H.34}$$

For Eq.(H.34) to be physically meaningful, $p_1 < \frac{m_e}{2}$ which it is in this case. Therefore:

$$q_2^2 = (E_2 - 2p_1)^2 \tag{H.35}$$

$$\implies E_2^2 - m_e^2 = E_2^2 - 4p_1E_2 + 4p_1^2 \tag{H.36}$$

$$\implies E_2 = p_1 + \frac{m_e^2}{4p_1} \equiv E_{\text{cut}}^{(1)} \tag{H.37}$$

$$\implies \begin{cases} p_1 + q_2 < E_2 - p_1 \text{ if } E_2 < E_{\text{cut}}^{(1)} \\ p_1 + q_2 > E_2 - p_1 \text{ if } E_2 > E_{\text{cut}}^{(1)} \end{cases} . \tag{H.38}$$

Before we eliminate $\int du$, notice the following for general p_1:

$$q_2(E_2 = E_{\text{cut}}^{(1)}) = \sqrt{\left(p_1 + \frac{m_e^2}{4p_1}\right)^2 - m_e^2} \tag{H.39}$$

$$= \frac{1}{4p_1}\sqrt{(4p_1^2 + m_e^2)^2 - 16p_1^2m_e^2} \tag{H.40}$$

$$= \frac{1}{4p_1}\sqrt{16p_1^4 + 8p_1^2m_e^2 + m_e^4 - 16p_1^2m_e^2} \tag{H.41}$$

$$= \frac{1}{4p_1}\sqrt{16p_1^4 - 8p_1^2m_e^2 + m_e^4} \tag{H.42}$$

$$= \frac{|4p_1^2 - m_e^2|}{4p_1}. \tag{H.43}$$

If $\frac{p_1}{m_e} > \frac{1}{2}$, then $q_2(E_2 = E_{\text{cut}}^{(1)}) < p_1$. For $\frac{p_1}{m_e} < \frac{1}{2}$, $E_2 - p_1 > |p_1 - q_2|$ for all q_2.

For $\int du$ to be non-zero, the argument of the delta function must fall in between the limits of $\int du$, implying:

$$a < u < b \tag{H.44}$$

$$\implies |y - q_3| < E_3 + E_2 - p_1 < y + q_3 \tag{H.45}$$

We will simultaneously consider the two cases. First, when $y < q_3$:

$$q_3 - y < E_3 + E_2 - p_1 < y + q_3 \tag{H.46}$$

$$\implies -q_3 < q_3 - 2y < E_3 - (p_1 - E_2 + y) < q_3 \tag{H.47}$$

$$\implies -q_3 < E_3 - (p_1 - E_2 + y) < q_3. \tag{H.48}$$

Second, when $y > q_3$. Then:

$$y - q_3 < E_3 + E_2 - p_1 < y + q_3 \tag{H.49}$$

$$\implies -q_3 < E_3 - (p_1 - E_2 + y) < q_3. \tag{H.50}$$

For Eq.(H.48) or (H.50) to be physically meaningful:

$$p_1 - E_2 + y > 0 \tag{H.51}$$

$$\implies y > E_2 - p_1 \tag{H.52}$$

$$\implies E_2 > E_{\text{cut}}^{(1)} \tag{H.53}$$

If $E_2 < E_{\text{cut}}^{(1)}$, then there does not exist any $y < q_3$ or $y > q_3$ such that E_3 produces a u which falls within the range of $\int du$. Therefore, $E_{\text{cut}}^{(1)}$ is the lower limit of $\int dE_2$. To determine the limits of $\int dE_3$, we return to Eq.(H.48):

$$-q_3 < E_3 - (p_1 - E_2 + y) < q_3 \tag{H.54}$$

$$\implies E_3^2 - 2E_3(p_1 - E_2 + y) + (p_1 - E_2 + y)^2 < q_3^2 = E_3^2 - m_e^2 \tag{H.55}$$

$$\implies E_{\text{min}} \equiv \frac{1}{2}\left[p_1 - E_2 + y + \frac{m_e^2}{p_1 - E_2 + y}\right] < E_3 \tag{H.56}$$

$E_{\min}$ is always greater than m_e. We investigate further the case $y < q_3$:

$$q_3 - y < E_3 + E_2 - p_1 \tag{H.57}$$

$$\Longrightarrow q_3 < E_3 + E_2 - p_1 + y \tag{H.58}$$

Notice:

$$E_2 - p_1 + y > E_2 - p_1 + |p_1 - q_2| \tag{H.59}$$

$$> E_2 - p_1 + p_1 - q_2 \tag{H.60}$$

$$= E_2 - q_2 \tag{H.61}$$

$$> 0 \tag{H.62}$$

Eq.(H.58) is true for all E_3 and provides no useful information. The expression for $R_1^{(1)}$ becomes:

$$R_1^{(1)} = \int_{E_{\text{cut}}^{(1)}}^{\infty} dE_2 \int_{E_2 - p_1}^{p_1 + q_2} dy \int_{E_{\min}}^{\infty} dE_3. \tag{H.63}$$

The $\int dy$ is normally bounded below by $|p_1 - q_2|$, but $E_2 - p_1 > |p_1 - q_2|$ for all $\frac{p_1}{m_e} < \frac{1}{2}$ and all q_2.

Writing $\int dE_3$ in terms of θ functions

We will use a θ function to write $\int dE_3$ over the maximum range:

$$\int_{E_{\min}}^{\infty} dE_3 = \int_{m_e}^{\infty} dE_3 \, \theta(E_3 - E_{\min}) \tag{H.64}$$

For $\int dE_3$ to be non-zero, the argument of the θ function must be positive, implying:

$$E_3 - E_{\min} > 0 \tag{H.65}$$

$$\implies E_3 - \frac{1}{2}\left[p_1 - E_2 + y + \frac{m_e^2}{p_1 - E_2 + y}\right] > 0 \tag{H.66}$$

$$\implies (2E_3 - p_1 + E_2 - y)(p_1 - E_2 + y) - m_e^2 > 0 \tag{H.67}$$

$$\implies -y^2 + 2y(E_3 - p_1 + E_2) - (p_1 - E_2)^2 + 2E_3(p_1 - E_2) - m_e^2 > 0 \tag{H.68}$$

If we set Eq.(H.68) to zero, and solve for y, we obtain:

$$\begin{aligned} y &= \frac{2(E_3 - p_1 + E_2)}{2} \\ &\pm \frac{1}{2}\sqrt{4(E_3 - p_1 + E_2)^2 + 4[-(p_1 - E_2)^2 + 2E_3(p_1 - E_2) - m_e^2]} \end{aligned} \tag{H.69}$$

$$= E_3 - p_1 + E_2$$

$$\pm \sqrt{E_3^2 - 2E_3(p_1 - E_2) + (p_1 - E_2)^2 - (p_1 - E_2)^2 + 2E_3(p_1 - E_2) - m_e^2} \tag{H.70}$$

$$= E_3 - p_1 + E_2 \pm q_3. \tag{H.71}$$

For Eq.(H.68) to be satisfied:

$$y < E_2 - p_1 + E_3 + q_3 \;\; \& \;\; y > E_2 - p_1 + E_3 - q_3. \tag{H.72}$$

We can write Eq.(H.63) as:

$$R_1^{(1)} = \int_{E_{\text{cut}}^{(1)}}^{\infty} dE_2 \int_{m_e}^{\infty} dE_3 \int_{b_1}^{t_1} dy, \tag{H.73}$$

where:

$$\begin{cases} b_1 = \max(E_2 - p_1, E_2 - p_1 + E_3 - q_3) \\ t_1 = \min(p_1 + q_2, E_2 - p_1 + E_3 + q_3) \end{cases} \tag{H.74}$$

Finding limits of $\int dy$

There is no transition point for b_1 as $E_2 - p_1 + E_3 - q_3 > E_2 - p_1$. For t_1, there is a transition point when:

$$p_1 + q_2 = E_2 - p_1 + E_3 + q_3 \tag{H.75}$$

$$\implies 2p_1 - E_2 + q_2 - E_3 = q_3 \tag{H.76}$$

For Eq.(H.76) to be physically meaningful, $2p_1 - E_2 + q_2 > m_e \implies q_2 > E_2 + m_e - 2p_1$ which is impossible for this case. Therefore, there is no transition point as $p_1 + q_2 < E_2 - p_1 + E_3 + q_3$. There is a limit point when $p_1 + q_2 = E_2 - p_1 + E_3 - q_3$:

$$p_1 + q_2 = E_2 - p_1 + E_3 - q_3 \tag{H.77}$$

$$\implies q_3 = E_3 - (2p_1 - E_2 + q_2) \tag{H.78}$$

For Eq.(H.78) to be physically meaningful $0 < 2p_1 - E_2 + q_2 < m_e$. Both conditions hold as $E_2 > E_{\text{cut}}^{(1)}$ and $\frac{p_1}{m_e} < \frac{1}{2}$. Solving Eq.(H.78) for E_3 yields:

$$E_3^2 - m_e^2 = E_3^2 - 2E_3(2p_1 - E_2 + q_2) + (2p_1 - E_2 + q_2)^2 \tag{H.79}$$

$$\implies E_3 = \frac{1}{2}\left(2p_1 - E_2 + q_2 + \frac{m_e^2}{2p_1 - E_2 + q_2}\right) \equiv E_{\text{lim}}^{(1)}, \tag{H.80}$$

implying that $p_1 + q_2 > E_2 - p_1 + E_3 - q_3$ if $E_3 > E_{\text{lim}}^{(1)}$.

We write Eq.(H.73) as:

$$R_1^{(1)} = \int_{E_{\text{cut}}^{(1)}}^{\infty} dE_2 \int_{E_{\text{lim}}^{(1)}}^{\infty} dE_3 \int_{E_2-p_1+E_3-q_3}^{p_1+q_2} dy \tag{H.81}$$

H.2.2 Case 2: $\frac{1}{2} < \frac{p_1}{m_e} < \frac{1+\sqrt{5}}{4}$

Eliminating $\int du$

We begin by considering equality between the two y values $p_1 - q_2$ and $E_2 - p_1$:

$$p_1 - q_2 = E_2 - p_1 \tag{H.82}$$

$$\implies 2p_1 - E_2 = q_2 \tag{H.83}$$

For Eq.(H.83) to be physically meaningful, $\frac{p_1}{m_e} > \frac{1}{2}$, which it is in this case. Thus:

$$\begin{cases} p_1 - q_2 > E_2 - p_1 \text{ if } E_2 < E_{\text{cut}}^{(1)} \\ p_1 - q_2 < E_2 - p_1 \text{ if } E_2 > E_{\text{cut}}^{(1)} \end{cases} . \tag{H.84}$$

Therefore, the expression for $R_1^{(2)}$ becomes:

$$R_1^{(2)} = \int_{m_e}^{E_{\text{cut}}^{(1)}} dE_2 \int_{p_1-q_2}^{p_1+q_2} dy \int_{E_{\text{min}}}^{\infty} dE_3 + \int_{E_{\text{cut}}^{(1)}}^{\infty} dE_2 \int_{E_2-p_1}^{p_1+q_2} dy \int_{E_{\text{min}}}^{\infty} dE_3 \tag{H.85}$$

Finding limits of $\int dy$

For $\theta(E_3 - E_{\text{min}})$, we have the following condition:

$$y < E_2 - p_1 + E_3 + q_3 \;\; \& \;\; y > E_2 - p_1 + E_3 - q_3. \tag{H.86}$$

Eq.(H.85) becomes:

$$R_1^{(2)} = \int_{m_e}^{E_{\text{cut}}^{(1)}} dE_2 \int_{m_e}^{\infty} dE_3 \int_{b_2}^{t_2} dy + \int_{E_{\text{cut}}^{(1)}}^{\infty} dE_2 \int_{m_e}^{\infty} dE_3 \int_{b_3}^{t_3} dy \tag{H.87}$$

where:

$$\begin{cases} b_2 = \max(p_1 - q_2, E_2 - p_1 + E_3 - q_3) \\ t_2 = \min(p_1 + q_2, E_2 - p_1 + E_3 + q_3) \end{cases} \tag{H.88}$$

$$\begin{cases} b_3 = \max(E_2 - p_1, E_2 - p_1 + E_3 - q_3) \\ t_3 = \min(p_1 + q_2, E_2 - p_1 + E_3 + q_3) \end{cases} . \tag{H.89}$$

For b_2, we have:

$$p_1 - q_2 = E_2 - p_1 + E_3 - q_3 \tag{H.90}$$

$$\implies q_3 = E_3 - (2p_1 - E_2 - q_2) \tag{H.91}$$

For Eq.(H.91) to be meaningful, $0 < 2p_1 - E_2 - q_2 < m_e$. The first condition is satisfied since $E_2 < E_{\text{cut}}^{(1)}$. For the second condition:

$$2p_1 - E_2 - q_2 < m_e \tag{H.92}$$

$$\implies 2p_1 - m_e - E_2 < q_2 \tag{H.93}$$

If $p_1 < m_e$, then Eq.(H.93) always holds. Before determining the transition point for b_2, we want to investigate the conditions when Eq.(H.93) does not hold, when $p_1 > m_e$:

$$2p_1 - m_e - E_2 = q_2 \tag{H.94}$$

$$\implies (2p_1 - m_e)^2 - 2E_2(2p_1 - m_e) + E_2^2 = E_2^2 - m_e^2 \tag{H.95}$$

$$\implies E_{\text{cut}}^{(2)} \equiv \frac{1}{2}\left(2p_1 - m_e + \frac{m_e^2}{2p_1 - m_e}\right) = E_2 \tag{H.96}$$

$$\implies \begin{cases} 2p_1 - m_e - E_2 < q_2 \text{ if } E_2 > E_{\text{cut}}^{(2)} \\ 2p_1 - m_e - E_2 > q_2 \text{ if } E_2 < E_{\text{cut}}^{(2)} \end{cases} \tag{H.97}$$

We need to compare $E_{\text{cut}}^{(1)}$ to $E_{\text{cut}}^{(2)}$:

$$E_{\text{cut}}^{(1)} \sim E_{\text{cut}}^{(2)} \tag{H.98}$$

$$\implies p_1 + \frac{m_e^2}{4p_1} \sim \frac{1}{2}\left(2p_1 - m_e + \frac{m_e^2}{2p_1 - m_e}\right) \tag{H.99}$$

$$\implies 4p_1^2(2p_1 - m_e) + m_e^2(2p_1 - m_e) \sim 2p_1(2p_1 - m_e)^2 + 2p_1 m_e^2 \tag{H.100}$$

$$\implies 8p_1^3 - 4p_1^2 m_e + 2p_1 m_e^2 - m_e^3 \sim 8p_1^3 - 8p_1^2 m_e + 2p_1 m_e^2 + 2p_1 m_e^2 \tag{H.101}$$

$$\implies 4p_1^2 m_e - 2p_1 m_e^2 - m_e^3 \sim 0 \tag{H.102}$$

$$\implies 4p_1^2 - 2p_1 m_e - m_e^2 \sim 0 \tag{H.103}$$

$$\implies p_1 \sim -\frac{-2m_e}{8} \pm \frac{1}{8}\sqrt{4m_e^2 - 16(-m_e^2)} \tag{H.104}$$

$$\implies \frac{p_1}{m_e} \sim \frac{1}{4} \pm \frac{\sqrt{5}}{4} \tag{H.105}$$

The negative solution is extraneous. For the positive solution:

$$\begin{cases} E_{\text{cut}}^{(1)} < E_{\text{cut}}^{(2)} \text{ if } \frac{p_1}{m_e} < \frac{1+\sqrt{5}}{4} \\ E_{\text{cut}}^{(1)} > E_{\text{cut}}^{(2)} \text{ if } \frac{p_1}{m_e} > \frac{1+\sqrt{5}}{4} \end{cases} \tag{H.106}$$

However, this $E_{\text{cut}}^{(2)}$ (as opposed to the one below) is only applicable in the case $\frac{p_1}{m_e} > 1 > \frac{1+\sqrt{5}}{4}$. Hence, $E_{\text{cut}}^{(1)} > E_{\text{cut}}^{(2)}$ for all $p_1 > m_e$. We return to determining the transition point for b_2:

$$q_3 = E_3 - (2p_1 - E_2 - q_2) \tag{H.107}$$

$$\implies E_3^2 - m_e^2 = E_3^2 - 2E_3(2p_1 - E_2 - q_2) + (2p_1 - E_2 - q_2)^2 \tag{H.108}$$

$$\implies E_3 = \frac{1}{2}\left(2p_1 - E_2 - q_2 + \frac{m_e^2}{2p_1 - E_2 - q_2}\right) \equiv E_{\text{trans}}^{(1)} \tag{H.109}$$

$$\implies \begin{cases} E_2 - p_1 + E_3 - q_3 > p_1 - q_2 \text{ if } E_3 < E_{\text{trans}}^{(1)} \\ E_2 - p_1 + E_3 - q_3 < p_1 - q_2 \text{ if } E_3 > E_{\text{trans}}^{(1)} \end{cases} \tag{H.110}$$

For t_2, we have:

$$p_1 + q_2 = E_2 - p_1 + E_3 + q_3 \tag{H.111}$$

$$\implies 2p_1 - E_2 + q_2 - E_3 = q_3 \tag{H.112}$$

For Eq.(H.112) to be meaningful, $2p_1 - E_2 + q_2 > m_e \implies q_2 > E_2 - 2p_1 + m_e$, which implies $0 < 2p_1 - m_e < m_e \implies \frac{1}{2} < \frac{p_1}{m_e} < 1$. Thus:

$$\begin{cases} 2p_1 - E_2 + q_2 < m_e \text{ if } E_2 < E_{\text{cut}}^{(2)} \\ 2p_1 - E_2 + q_2 > m_e \text{ if } E_2 > E_{\text{cut}}^{(2)} \end{cases} \tag{H.113}$$

We exercise caution that $E_{\text{cut}}^{(2)}$ obtained above has the same form as the $E_{\text{cut}}^{(2)}$ obtained from Eq.(H.93), but that the conditions are different for the two expressions. Since $\frac{1}{2} < \frac{p_1}{m_e} < \frac{1+\sqrt{5}}{4}$, $E_{\text{cut}}^{(1)} < E_{\text{cut}}^{(2)}$ and thus for t_2, $E_2 < E_{\text{cut}}^{(2)}$ implying $2p_1 - E_2 + q_2 < m_e$. Hence $p_1 + q_2 < E_2 - p_1 + E_3 + q_3$.

For the $\int dy$ limit b_3, $E_2 - p_1 + E_3 - q_3 > E_2 - p_1$. For t_3, we refer back to

Eq.(H.76):

$$2p_1 - E_2 + q_2 - E_3 = q_3, \tag{H.114}$$

with condition $2p_1 - E_2 + q_2 > m_e \implies q_2 > E_2 + m_e - 2p_1 \implies E_2 > E_{\text{cut}}^{(2)}$. If that is the case, then:

$$2p_1 - E_2 + q_2 - E_3 = q_3 \tag{H.115}$$

$$\implies (2p_1 - E_2 + q_2)^2 - 2E_3(2p_1 - E_2 + q_2) + E_3^2 = E_3^2 - m_e^2 \tag{H.116}$$

$$\implies E_{\text{trans}}^{(2)} \equiv \frac{1}{2}\left(2p_1 - E_2 + q_2 + \frac{m_e^2}{2p_1 - E_2 + q_2}\right) = E_3 \tag{H.117}$$

Thus, there is a transtion point for t_3 when $E_2 > E_{\text{cut}}^{(2)}$:

$$t_3 = \begin{cases} p_1 + q_2 & \text{if } E_2 < E_{\text{cut}}^{(2)} \\ E_2 - p_1 + E_3 + q_3 & \text{if } E_2 > E_{\text{cut}}^{(2)} \text{ and } E_3 < E_{\text{trans}}^{(2)} \\ p_1 + q_2 & \text{if } E_2 > E_{\text{cut}}^{(2)} \text{ and } E_3 > E_{\text{trans}}^{(2)} \end{cases}. \tag{H.118}$$

Note that $E_{\text{trans}}^{(2)}$ has the same form as $E_{\text{lim}}^{(1)}$, however the expressions were derived from different equations under different conditions.

We need to check for limit points:

$$p_1 + q_2 = E_2 - p_1 + E_3 - q_3 \tag{H.119}$$

$$\implies q_3 = E_3 + E_2 - 2p_1 - q_2. \tag{H.120}$$

For Eq.(H.120) to be physically meaningful, $2p_1 - E_2 + q_2 < m_e \implies E_2 < E_{\text{cut}}^{(2)}$. If

$E_2 < E_{\rm cut}^{(2)}$, then there is a limit point at $E_3 = E_{\rm lim}^{(1)}$. Eq.(H.85) becomes:

$$
\begin{aligned}
R_1^{(2)} = & \int_{m_e}^{E_{\rm cut}^{(1)}} dE_2 \left(\int_{E_{\rm lim}^{(1)}}^{E_{\rm trans}^{(1)}} dE_3 \int_{E_2-p_1+E_3-q_3}^{p_1+q_2} dy + \int_{E_{\rm trans}^{(1)}}^{\infty} dE_3 \int_{p_1-q_2}^{p_1+q_2} dy \right) \\
& + \int_{E_{\rm cut}^{(1)}}^{E_{\rm cut}^{(2)}} dE_2 \left(\int_{E_{\rm lim}^{(1)}}^{\infty} dE_3 \int_{E_2-p_1+E_3-q_3}^{p_1+q_2} dy \right) \\
& + \int_{E_{\rm cut}^{(2)}}^{\infty} dE_2 \left(\int_{m_e}^{E_{\rm trans}^{(2)}} dE_3 \int_{E_2-p_1+E_3-q_3}^{E_2-p_1+E_3+q_3} dy + \int_{E_{\rm trans}^{(2)}}^{\infty} dE_3 \int_{E_2-p_1+E_3-q_3}^{p_1+q_2} dy \right)
\end{aligned}
\tag{H.121}
$$

H.2.3 Case 3: $\frac{1+\sqrt{5}}{4} < \frac{p_1}{m_e} < 1$

For this case, $E_{\rm cut}^{(2)} < E_{\rm cut}^{(1)}$. Eq.(H.85) becomes:

$$
R_1^{(3)} = \int_{m_e}^{E_{\rm cut}^{(2)}} dE_2 \int_{m_e}^{\infty} dE_3 \int_{b_2}^{t_2} dy + \int_{E_{\rm cut}^{(2)}}^{E_{\rm cut}^{(1)}} dE_2 \int_{m_e}^{\infty} dE_3 \int_{b_2}^{t_2} dy + \int_{E_{\rm cut}^{(1)}}^{\infty} dE_2 \int_{m_e}^{\infty} dE_3 \int_{b_3}^{t_3} dy. \tag{H.122}
$$

For there to be a transition point for b_2, the conditions must be that $E_2 < E_{\rm cut}^{(1)}$, and $p_1 < m_e$. For there to be a transition point for t_2, the conditions must be that $E_2 > E_{\rm cut}^{(2)}$ and $\frac{p_1}{m_e} > \frac{1}{2}$.

We need to compare $E^{(1)}_{\text{trans}}$ to $E^{(2)}_{\text{trans}}$:

$$E^{(1)}_{\text{trans}} \sim E^{(2)}_{\text{trans}} \tag{H.123}$$

$$\implies \frac{1}{2}\left(2p_1 - E_2 - q_2 + \frac{m_e^2}{2p_1 - E_2 - q_2}\right) \sim \frac{1}{2}\left(2p_1 - E_2 + q_2 + \frac{m_e^2}{2p_1 - E_2 + q_2}\right) \tag{H.124}$$

$$\implies \frac{m_e^2}{2p_1 - E_2 - q_2} \sim 2q_2 + \frac{m_e^2}{2p_1 - E_2 + q_2} \tag{H.125}$$

$$\implies m_e^2(2p_1 - E_2 + q_2) \sim 2q_2(2p_1 - E_2 - q_2)(2p_1 - E_2 + q_2) + m_e^2(2p_1 - E_2 - q_2) \tag{H.126}$$

$$\implies 2q_2 m_e^2 \sim 2q_2[(2p_1 - E_2)^2 - q_2^2] \tag{H.127}$$

$$\implies 2q_2 m_e^2 \sim 2q_2(4p_1^2 - 4p_1E_2 + m_e^2) \tag{H.128}$$

$$\implies 4p_1E_2 \sim 4p_1^2. \tag{H.129}$$

In this case, $p_1 < m_e \implies E^{(1)}_{\text{trans}} > E^{(2)}_{\text{trans}}$. For t_3, there is a transition point when $E_2 > E^{(2)}_{\text{cut}}$. There is a limit point for $E_3 = E^{(1)}_{\text{lim}}$ if $E_2 < E^{(2)}_{\text{cut}}$. Thus, Eq.(H.122) becomes:

$$\begin{aligned}
R_1^{(3)} = &\int_{m_e}^{E^{(2)}_{\text{cut}}} dE_2 \left(\int_{E^{(1)}_{\text{lim}}}^{E^{(1)}_{\text{trans}}} dE_3 \int_{E_2 - p_1 + E_3 - q_3}^{p_1+q_2} dy + \int_{E^{(1)}_{\text{trans}}}^{\infty} dE_3 \int_{p_1 - q_2}^{p_1+q_2} dy \right) \\
&+ \int_{E^{(2)}_{\text{cut}}}^{E^{(1)}_{\text{cut}}} dE_2 \left(\int_{m_e}^{E^{(2)}_{\text{trans}}} dE_3 \int_{E_2 - p_1 + E_3 - q_3}^{E_2 - p_1 + E_3 + q_3} dy \right. \\
&\qquad \left. + \int_{E^{(2)}_{\text{trans}}}^{E^{(1)}_{\text{trans}}} dE_3 \int_{E_2 - p_1 + E_3 - q_3}^{p_1+q_2} dy + \int_{E^{(1)}_{\text{trans}}}^{\infty} dE_3 \int_{p_1 - q_2}^{p_1+q_2} dy \right) \qquad \text{(H.130)} \\
&+ \int_{E^{(1)}_{\text{cut}}}^{\infty} dE_2 \left(\int_{m_e}^{E^{(2)}_{\text{trans}}} dE_3 \int_{E_2 - p_1 + E_3 - q_3}^{E_2 - p_1 + E_3 + q_3} dy + \int_{E^{(2)}_{\text{trans}}}^{\infty} dE_3 \int_{E_2 - p_1 + E_3 - q_3}^{p_1+q_2} dy \right). \qquad \text{(H.131)}
\end{aligned}$$

H.2.4 Case 4: $1 < \frac{p_1}{m_e}$

For this case, we have the same initial expression for $R_1^{(4)}$ as we do for $R_1^{(3)}$ in terms of $\int dE_2 \int dy \int dE_3$. However, some of our transitions no longer satisfy conditions because $p_1 > m_e$.

For b_2:

$$p_1 - q_2 = E_2 - p_1 + E_3 - q_3 \tag{H.132}$$

$$\implies q_3 = E_3 - (2p_1 - E_2 - q_2). \tag{H.133}$$

For Eq.(H.133) to be physically meaningful $0 < 2p_1 - E_2 - q_2 < m_e$. The first condition holds if $E_2 < E_{\text{cut}}^{(1)}$. The second condition only holds for $E_2 > E_{\text{cut}}^{(2)}$. Thus, b_2 has a transition point ($E_{\text{trans}}^{(1)}$) for $E_{\text{cut}}^{(2)} < E_2 < E_{\text{cut}}^{(1)}$.

For t_2:

$$p_1 + q_2 = E_2 - p_1 + E_3 + q_3 \tag{H.134}$$

$$\implies 2p_1 - E_2 + q_2 - E_3 = q_3. \tag{H.135}$$

For Eq.(H.135) to be physically meaningful, $2p_1 - E_2 + q_2 > m_e$ which is always true if $p_1 > m_e$. Thus, t_2 (and t_3) has a transition point for all E_2.

There is a possibility that $E_{\text{trans}}^{(2)}$ could be larger than $E_{\text{trans}}^{(1)}$ for $p_1 > m_e$. Eq.(H.129) shows that $E_{\text{trans}}^{(1)} = E_{\text{trans}}^{(2)}$ when $E_2 = p_1$. $E_{\text{cut}}^{(1)}$ is always larger than p_1. Comparing $E_{\text{cut}}^{(2)}$ to

p_1:

$$\frac{1}{2}\left(2p_1 - m_e + \frac{m_e^2}{2p_1 - m_e}\right) \sim p_1 \tag{H.136}$$

$$\implies \frac{m_e^2}{2p_1 - m_e} \sim m_e \tag{H.137}$$

$$\implies m_e \sim 2p_1 - m_e \tag{H.138}$$

$$\implies m_e \sim p_1. \tag{H.139}$$

Therefore, $E_{\text{cut}}^{(2)} < p_1 < E_{\text{cut}}^{(1)}$ and:

$$\begin{cases} E_{\text{trans}}^{(1)} < E_{\text{trans}}^{(2)} \text{ if } E_2 < p_1 \\ E_{\text{trans}}^{(1)} > E_{\text{trans}}^{(2)} \text{ if } E_2 > p_1 \end{cases}. \tag{H.140}$$

For the limit point:

$$p_1 + q_2 = E_2 - p_1 + E_3 - q_3 \tag{H.141}$$

$$\implies q_3 = E_3 + E_2 - 2p_1 - q_2. \tag{H.142}$$

For Eq.(H.142) to be physically meaningful, $2p_1 - E_2 + q_2 < m_e$ which is impossible for $p_1 > m_e$. A new possibility for a limit point arises if:

$$p_1 - q_2 = E_2 - p_1 + E_3 + q_3 \tag{H.143}$$

$$\implies 2p_1 - E_2 - q_2 - E_3 = q_3. \tag{H.144}$$

For Eq.(H.144) to be physically meaninfgul, $2p_1 - E_2 - q_2 > m_e \implies E_{\text{cut}}^{(2)} > E_2$. Solving

Eq.(H.144) for E_3:

$$(2p_1 - E_2 - q_2)^2 - 2E_3(2p_1 - E_2 - q_2) + E_3^2 = E_3^2 - m_e^2 \tag{H.145}$$

$$\implies E_{\text{lim}}^{(2)} = \frac{1}{2}\left(2p_1 - E_2 - q_2 + \frac{m_e^2}{2p_1 - E_2 - q_2}\right) = E_3. \tag{H.146}$$

Note that $E_{\text{lim}}^{(2)}$ has the same form as $E_{\text{trans}}^{(1)}$, but it is derived from a different equation under different conditions. The expression for $R_1^{(4)}$ becomes:

$$\begin{aligned}
R_1^{(4)} = &\int_{m_e}^{E_{\text{cut}}^{(2)}} dE_2 \quad \left(\int_{E_{\text{lim}}^{(2)}}^{E_{\text{trans}}^{(2)}} dE_3 \int_{p_1-q_2}^{E_2-p_1+E_3+q_3} dy + \int_{E_{\text{trans}}^{(2)}}^{\infty} dE_3 \int_{p_1-q_2}^{p_1+q_2} dy \right) \\
&+ \int_{E_{\text{cut}}^{(2)}}^{p_1} dE_2 \quad \left(\int_{m_e}^{E_{\text{trans}}^{(1)}} dE_3 \int_{E_2-p_1+E_3-q_3}^{E_2-p_1+E_3+q_3} dy \right. \\
&\qquad \left. + \int_{E_{\text{trans}}^{(1)}}^{E_{\text{trans}}^{(2)}} dE_3 \int_{p_1-q_2}^{E_2-p_1+E_3+q_3} dy + \int_{E_{\text{trans}}^{(2)}}^{\infty} dE_3 \int_{p_1-q_2}^{p_1+q_2} dy \right) \\
&+ \int_{p_1}^{E_{\text{cut}}^{(1)}} dE_2 \quad \left(\int_{m_e}^{E_{\text{trans}}^{(2)}} dE_3 \int_{E_2-p_1+E_3-q_3}^{E_2-p_1+E_3+q_3} dy \right. \\
&\qquad \left. + \int_{E_{\text{trans}}^{(2)}}^{E_{\text{trans}}^{(1)}} dE_3 \int_{E_2-p_1+E_3-q_3}^{p_1+q_2} dy + \int_{E_{\text{trans}}^{(1)}}^{\infty} dE_3 \int_{p_1-q_2}^{p_1+q_2} dy \right) \\
&+ \int_{E_{\text{cut}}^{(1)}}^{\infty} dE_2 \quad \left(\int_{m_e}^{E_{\text{trans}}^{(2)}} dE_3 \int_{E_2-p_1+E_3-q_3}^{E_2-p_1+E_3+q_3} dy + \int_{E_{\text{trans}}^{(2)}}^{\infty} dE_3 \int_{E_2-p_1+E_3-q_3}^{p_1+q_2} dy \right).
\end{aligned} \tag{H.147}$$

H.3 $L_2(P_1 \cdot Q_3)$

Our energy conservation equation is $p_1 + p_4 = E_2 + E_3$. The treatment for $L_2(P_1 \cdot Q_3)$ is identical to $L_1(P_1 \cdot Q_2)$ with the permutation $2 \leftrightarrow 3$. We write the expressions for R_2 with the permutation for the four different cases.

For $\frac{p_1}{m_e} < \frac{1}{2}$:

$$R_2^{(1)} = \int_{E_{\text{cut}}^{(1)}}^{\infty} dE_3 \int_{E_{\text{lim}}^{(1)}}^{\infty} dE_2 \int_{E_3 - p_1 + E_2 - q_2}^{p_1+q_3} dy \tag{H.148}$$

For $\frac{1}{2} < \frac{p_1}{m_e} < \frac{1+\sqrt{5}}{4}$:

$$\begin{aligned} R_2^{(2)} = & \int_{m_e}^{E_{\text{cut}}^{(1)}} dE_3 \left(\int_{E_{\text{lim}}^{(1)}}^{E_{\text{trans}}^{(1)}} dE_2 \int_{E_3 - p_1 + E_2 - q_2}^{p_1+q_3} dy + \int_{E_{\text{trans}}^{(1)}}^{\infty} dE_2 \int_{p_1 - q_3}^{p_1+q_3} dy \right) \\ & + \int_{E_{\text{cut}}^{(1)}}^{E_{\text{cut}}^{(2)}} dE_3 \left(\int_{E_{\text{lim}}^{(1)}}^{\infty} dE_2 \int_{E_3 - p_1 + E_2 - q_2}^{p_1+q_3} dy \right) \\ & + \int_{E_{\text{cut}}^{(2)}}^{\infty} dE_3 \left(\int_{m_e}^{E_{\text{trans}}^{(2)}} dE_2 \int_{E_3 - p_1 + E_2 - q_2}^{E_3 - p_1 + E_2 + q_2} dy + \int_{E_{\text{trans}}^{(2)}}^{\infty} dE_2 \int_{E_3 - p_1 + E_2 - q_2}^{p_1+q_3} dy \right) \end{aligned} \tag{H.149}$$

For $\frac{1+\sqrt{5}}{4} < \frac{p_1}{m_e} < 1$:

$$
\begin{aligned}
R_2^{(3)} = &\int_{m_e}^{E_{\text{cut}}^{(2)}} dE_3 \quad \left(\int_{E_{\text{lim}}^{(1)}}^{E_{\text{trans}}^{(1)}} dE_2 \int_{E_3-p_1+E_2-q_2}^{p_1+q_3} dy + \int_{E_{\text{trans}}^{(1)}}^{\infty} dE_2 \int_{p_1-q_3}^{p_1+q_3} dy \right) \\
&+ \int_{E_{\text{cut}}^{(2)}}^{E_{\text{cut}}^{(1)}} dE_3 \quad \left(\int_{m_e}^{E_{\text{trans}}^{(2)}} dE_2 \int_{E_3-p_1+E_2-q_2}^{E_3-p_1+E_2+q_2} dy \right. \\
&\qquad \left. + \int_{E_{\text{trans}}^{(2)}}^{E_{\text{trans}}^{(1)}} dE_2 \int_{E_3-p_1+E_2-q_2}^{p_1+q_3} dy + \int_{E_{\text{trans}}^{(1)}}^{\infty} dE_2 \int_{p_1-q_3}^{p_1+q_3} dy \right) \\
&+ \int_{E_{\text{cut}}^{(1)}}^{\infty} dE_3 \quad \left(\int_{m_e}^{E_{\text{trans}}^{(2)}} dE_2 \int_{E_3-p_1+E_2-q_2}^{E_3-p_1+E_2+q_2} dy + \int_{E_{\text{trans}}^{(2)}}^{\infty} dE_2 \int_{E_3-p_1+E_2-q_2}^{p_1+q_3} dy \right). \quad \text{(H.150)}
\end{aligned}
$$

For $1 < \frac{p_1}{m_e}$:

$$
\begin{aligned}
R_2^{(4)} = &\int_{m_e}^{E_{\text{cut}}^{(2)}} dE_3 \quad \left(\int_{E_{\text{lim}}^{(2)}}^{E_{\text{trans}}^{(2)}} dE_2 \int_{p_1-q_3}^{E_3-p_1+E_2+q_2} dy + \int_{E_{\text{trans}}^{(2)}}^{\infty} dE_2 \int_{p_1-q_3}^{p_1+q_3} dy \right) \\
&+ \int_{E_{\text{cut}}^{(2)}}^{p_1} dE_3 \quad \left(\int_{m_e}^{E_{\text{trans}}^{(1)}} dE_2 \int_{E_3-p_1+E_2-q_2}^{E_3-p_1+E_2+q_2} dy \right. \\
&\qquad \left. + \int_{E_{\text{trans}}^{(1)}}^{E_{\text{trans}}^{(2)}} dE_2 \int_{p_1-q_3}^{E_3-p_1+E_2+q_2} dy + \int_{E_{\text{trans}}^{(2)}}^{\infty} dE_2 \int_{p_1-q_3}^{p_1+q_3} dy \right) \\
&+ \int_{p_1}^{E_{\text{cut}}^{(1)}} dE_3 \quad \left(\int_{m_e}^{E_{\text{trans}}^{(2)}} dE_2 \int_{E_3-p_1+E_2-q_2}^{E_3-p_1+E_2+q_2} dy \right. \\
&\qquad \left. + \int_{E_{\text{trans}}^{(2)}}^{E_{\text{trans}}^{(1)}} dE_2 \int_{E_3-p_1+E_2-q_2}^{p_1+q_3} dy + \int_{E_{\text{trans}}^{(1)}}^{\infty} dE_2 \int_{p_1-q_3}^{p_1+q_3} dy \right) \\
&+ \int_{E_{\text{cut}}^{(1)}}^{\infty} dE_3 \quad \left(\int_{m_e}^{E_{\text{trans}}^{(2)}} dE_2 \int_{E_3-p_1+E_2-q_2}^{E_3-p_1+E_2+q_2} dy + \int_{E_{\text{trans}}^{(2)}}^{\infty} dE_2 \int_{E_3-p_1+E_2-q_2}^{p_1+q_3} dy \right). \quad \text{(H.151)}
\end{aligned}
$$

The above integrals use the following expressions:

$$E_{\text{cut}}^{(1)} = p_1 + \frac{m_e^2}{4p_1} \tag{H.152}$$

$$E_{\text{cut}}^{(2)} = \frac{1}{2}\left(2p_1 - m_e + \frac{m_e^2}{2p_1 - m_e}\right) \tag{H.153}$$

$$E_{\text{trans}}^{(1)} = \frac{1}{2}\left(2p_1 - E_3 - q_3 + \frac{m_e^2}{2p_1 - E_3 - q_3}\right) \tag{H.154}$$

$$E_{\text{trans}}^{(2)} = \frac{1}{2}\left(2p_1 - E_3 + q_3 + \frac{m_e^2}{2p_1 - E_3 + q_3}\right) \tag{H.155}$$

$$E_{\text{lim}}^{(1)} = E_{\text{trans}}^{(2)} \tag{H.156}$$

$$E_{\text{lim}}^{(2)} = E_{\text{trans}}^{(1)} \tag{H.157}$$

H.4 Combining L_1 and L_2 into a single integral

The kinematics are identical for R_1 and R_2 except for the permutation $2 \leftrightarrow 3$. For this section, we will focus only on case 1, since it involves the fewest cut, limit, and transition points. The other three cases will follow from analogy. The total expression

for the derivative is:

$$\frac{df_1}{dt} = R_1 + R_2 \tag{H.158}$$

$$\begin{aligned}
&= \frac{1}{16(2\pi)^3} \int_{E_{\text{cut}}^{(1)}}^{\infty} dE_2 \frac{1}{p_1^2} \int_{E_{\text{lim}}^{(1)2}}^{\infty} dE_3 F(p_1, E_2 + E_3 - p_1, E_2, E_3) \\
&\times \int_{E_2 - p_1 + E_3 - q_3}^{p_1+q_2} dy L_1 \{\frac{1}{2}y^2 - \frac{1}{2}[(p_1 - E_2)^2 - m_e^2]\} \\
&+ \frac{1}{16(2\pi)^3} \int_{E_{\text{cut}}^{(1)}}^{\infty} dE_3 \frac{1}{p_1^2} \int_{E_{\text{lim}}^{(1)3}}^{\infty} dE_2 F(p_1, E_2 + E_3 - p_1, E_2, E_3) \\
&\times \int_{E_3 - p_1 + E_2 - q_2}^{p_1+q_3} dy L_2 \{\frac{1}{2}y^2 - \frac{1}{2}[(p_1 - E_3)^2 - m_e^2]\},
\end{aligned} \tag{H.159}$$

where:

$$E_{\text{lim}}^{(1)2} = \frac{1}{2}\left(2p_1 - E_2 + q_2 + \frac{m_e^2}{2p_1 - E_2 + q_2}\right) \tag{H.160}$$

$$E_{\text{lim}}^{(1)3} = \frac{1}{2}\left(2p_1 - E_3 + q_3 + \frac{m_e^2}{2p_1 - E_3 + q_3}\right). \tag{H.161}$$

We can combine R_1 and R_2 if we use generic expressions for the dummy variables E_2 and E_3. For R_1, let $E_2 = E_{\text{out}}$ for the outer integral and $E_3 = E_{\text{in}}$ for the inner integral.

For R_2, permute the indicies 2 and 3 to yield $E_3 = E_{\rm out}$ and $E_2 = E_{\rm in}$. Eq.(H.159) becomes:

$$\begin{aligned}\frac{df_1}{dt} &= \frac{1}{16(2\pi)^3}\int\limits_{E_{\rm cut}^{(1)}}^{\infty} dE_{\rm out}\,\frac{1}{p_1^2}\int\limits_{E_{\rm lim}^{(1)\rm o}}^{\infty} dE_{\rm in}\,F(p_1, E_{\rm out}+E_{\rm in}-p_1, E_{\rm out}, E_{\rm in}) \\ &\times \int\limits_{E_{\rm out}-p_1+E_{\rm in}-q_{\rm in}}^{p_1+q_{\rm out}} dy\,L_1\{\frac{1}{2}y^2 - \frac{1}{2}[(p_1-E_{\rm out})^2 - m_e^2]\} \\ &+ \frac{1}{16(2\pi)^3}\int\limits_{E_{\rm cut}^{(1)}}^{\infty} dE_{\rm out}\,\frac{1}{p_1^2}\int\limits_{E_{\rm lim}^{(1)\rm o}}^{\infty} dE_{\rm in}\,F(p_1, E_{\rm in}+E_{\rm out}-p_1, E_{\rm in}, E_{\rm out}) \\ &\times \int\limits_{E_{\rm out}-p_1+E_{\rm in}-q_{\rm in}}^{p_1+q_{\rm out}} dy\,L_2\{\frac{1}{2}y^2 - \frac{1}{2}[(p_1-E_{\rm out})^2 - m_e^2]\},\end{aligned} \tag{H.162}$$

where:

$$E_{\rm lim}^{(1)\rm o} = \frac{1}{2}\left(2p_1 - E_{\rm out} + q_{\rm out} + \frac{m_e^2}{2p_1 - E_{\rm out} + q_{\rm out}}\right) \tag{H.163}$$

$$q_{\rm out} \equiv \sqrt{E_{\rm out}^2 - m_e^2} \tag{H.164}$$

$$q_{\rm in} \equiv \sqrt{E_{\rm in}^2 - m_e^2}. \tag{H.165}$$

We see that the limits for R_1 and R_2 on Eq.(H.162) are identical, although the arguments are not. It is tempting to combine the integrals and use the fact that E_2 and E_3 are on the same sides of the energy conservation equation to write $F(...,E_{\rm out},E_{\rm in}) = F(...,E_{\rm in},E_{\rm out})$. However, we cannot do this. The second particle refers to a e^+ and the third particle refers to a e^-. In general, each species has a different chemical potential and so the occupation probability at a given energy is different, and the F factor is different. Therefore, when

we combine the integrals over $E_{\rm out}$ and $E_{\rm in}$ in Eq.(H.162), we arrive at:

$$\frac{df_1}{dt} = \frac{1}{16(2\pi)^3} \int\limits_{E_{\rm cut}^{(1)}}^{\infty} dE_{\rm out} \frac{1}{p_1^2} \int\limits_{E_{\rm lim}^{(1)\rm o}}^{\infty} dE_{\rm in} \times \tag{H.166}$$

$$\left[F(p_1, E_{\rm out}+E_{\rm in}-p_1, E_{\rm out}, E_{\rm in}) \int\limits_{E_{\rm out}-p_1+E_{\rm in}-q_{\rm in}}^{p_1+q_{\rm out}} dy L_1 \{ \frac{1}{2}y^2 - \frac{1}{2}[(p_1-E_{\rm out})^2 - m_e^2] \} \right.$$
$$\left. + F(p_1, E_{\rm out}+E_{\rm in}-p_1, E_{\rm in}, E_{\rm out}) \int\limits_{E_{\rm out}-p_1+E_{\rm in}-q_{\rm in}}^{p_1+q_{\rm out}} dy L_2 \{ \frac{1}{2}y^2 - \frac{1}{2}[(p_1-E_{\rm out})^2 - m_e^2] \} \right] \tag{H.167}$$

H.5 μ and τ neutrinos

For non-electron neutrinos, the summed-squared-matrix element is slightly different due to the absence of a charged current diagram:

$$\begin{aligned} \langle |\mathcal{M}|^2 \rangle = {} & 32 G_F^2 (2\sin^2\theta_w - 1)^2 \left[(P_1 \cdot Q_2)^2 + \frac{2\sin^2\theta_w}{2\sin^2\theta_w - 1} m_e^2 (P_1 \cdot Q_2) \right] \\ & + 128 G_F^2 \sin^4\theta_w \left[(P_1 \cdot Q_3)^2 + \frac{2\sin^2\theta_w - 1}{2\sin^2\theta_w} m_e^2 (P_1 \cdot Q_3) \right]. \end{aligned} \tag{H.168}$$

In other words, Eq.(H.168) is identical to Eq.(H.2) except for the swap $2\sin^2\theta_2 + 1 \rightarrow 2\sin^2\theta_w - 1$. The kinematics for finding the derivative are identical.

H.6 Annihilation for an anti-neutrino

When calculating the derivatives for annihilation, we assumed that particle 1 was a neutrino. If there is an asymmetry in the neutrino sector, we have to separately consider annihilation when particle 1 is an anti-neutrino. For the time being, only consider the

electron flavor of neutrinos. The reaction of interest is:

$$\bar{\nu}_e(1) + \nu_e(4) \to e^-(3) + e^+(2). \tag{H.169}$$

To calculate the summed-squared-matrix element, we permute $1 \leftrightarrow 4$:

$$\begin{aligned}\langle|\mathcal{M}|^2\rangle = 32G_F^2(1+2\sin^2\theta_w)^2\left[(P_4\cdot Q_2)^2 + \frac{2\sin^2\theta_w}{1+2\sin^2\theta_w}m_e^2(P_4\cdot Q_2)\right] \\ + 128G_F^2\sin^4\theta_w\left[(P_4\cdot Q_3)^2 + \frac{1+2\sin^2\theta_w}{2\sin^2\theta_w}m_e^2(P_4\cdot Q_3)\right].\end{aligned} \tag{H.170}$$

By conservation of four-momentum:

$$P_1 + P_4 = Q_2 + Q_3 \tag{H.171}$$

$$\implies P_4 - Q_2 = Q_3 - P_1 \tag{H.172}$$

$$\implies (P_4 - Q_2)^2 = (Q_3 - P_1)^2 \tag{H.173}$$

$$\implies P_4^2 + Q_2^2 - 2P_4\cdot Q_2 = P_1^2 + Q_3^2 - 2P_1\cdot Q_3 \tag{H.174}$$

$$\implies 0 + m_e^2 - 2P_4\cdot Q_2 = 0 + m_e^2 - 2P_1\cdot Q_3 \tag{H.175}$$

$$\implies P_4\cdot Q_2 = P_1\cdot Q_3 \tag{H.176}$$

A symmetrical argument shows $P_4\cdot Q_3 = P_1\cdot Q_2$. The expression for Eq.(H.170) becomes:

$$\begin{aligned}\langle|\mathcal{M}|^2\rangle &= 32G_F^2(1+2\sin^2\theta_w)^2\left[(P_1\cdot Q_3)^2 + \frac{2\sin^2\theta_w}{1+2\sin^2\theta_w}m_e^2(P_1\cdot Q_3)\right] \\ &\quad + 128G_F^2\sin^4\theta_w\left[(P_1\cdot Q_2)^2 + \frac{1+2\sin^2\theta_w}{2\sin^2\theta_w}m_e^2(P_1\cdot Q_2)\right] \qquad \text{(H.177)} \\ &= L_2(P_1\cdot Q_2) + L_1(P_1\cdot Q_3). \qquad \text{(H.178)}\end{aligned}$$

Thus, when we consider the annihilaion into the anti-neutrino, we need to permute $L_1 \leftrightarrow L_2$. Both expressions have the same general form, i.e. $L_{(1,2)}(\xi) \sim C_1(\xi^2 + C_2\xi)$ so

the kinematics are identical to what has been done before.

Bibliography

[1] E. Aver, K. A. Olive, R. L. Porter, and E. D. Skillman, *The primordial helium abundance from updated emissivities*, J. Cosmology Astropart. Phys. **11** (Nov., 2013) 17.

[2] Planck Collaboration, *Planck 2013 results. XVI. Cosmological parameters*, *ArXiv e-prints* (Mar., 2013) [arXiv:1303.5076].

[3] R. J. Cooke, M. Pettini, R. A. Jorgenson, M. T. Murphy, and C. C. Steidel, *Precision measures of the primordial abundance of deuterium*, *The Astrophysical Journal* **781** (2014), no. 1 31.

[4] WMAP Collaboration, *Nine-year Wilkinson Microwave Anisotropy Probe (WMAP) Observations: Cosmological Parameter Results*, ApJS **208** (Oct., 2013) 19.

[5] ACT Collaboration, *The Atacama Cosmology Telescope: cosmological parameters from three seasons of data*, J. Cosmology Astropart. Phys. **10** (Oct., 2013) 60.

[6] SPT Collaboration, *A Measurement of the Damping Tail of the Cosmic Microwave Background Power Spectrum with the South Pole Telescope*, ApJ **743** (Dec., 2011) 28.

[7] Planck Collaboration, *Planck 2013 results. I. Overview of products and scientific results*, *ArXiv e-prints* (Mar., 2013) [arXiv:1303.5062].

[8] Y. I. Izotov and T. X. Thuan, *The Primordial Abundance of ^{4}He: Evidence for Non-Standard Big Bang Nucleosynthesis*, ApJ **710** (Feb., 2010) L67–L71.

[9] M. Pettini and R. Cooke, *A new, precise measurement of the primordial abundance of deuterium*, MNRAS **425** (Oct., 2012) 2477–2486.

[10] M. Shimon, N. J. Miller, C. T. Kishimoto, C. J. Smith, G. M. Fuller, and B. G. Keating, *Using Big Bang Nucleosynthesis to extend CMB probes of neutrino physics*, J. Cosmology Astropart. Phys. **5** (May, 2010) 37.

[11] J. Hamann, J. Lesgourgues, and G. Mangano, *Using big bang nucleosynthesis in cosmological parameter extraction from the cosmic microwave background: a forecast for PLANCK*, J. Cosmology Astropart. Phys. **3** (Mar., 2008) 4.

[12] A. Vlasenko, G. M. Fuller, and V. Cirigliano, *Neutrino quantum kinetics*, Phys. Rev. D **89** (May, 2014) 105004, [arXiv:1309.2628].

[13] C. Volpe, D. Väänänen, and C. Espinoza, *Extended evolution equations for neutrino propagation in astrophysical and cosmological environments*, Phys. Rev. D **87** (June, 2013) 113010, [arXiv:1302.2374].

[14] J. Serreau and C. Volpe, *Neutrino-antineutrino correlations in dense anisotropic media*, Phys. Rev. D **90** (Dec., 2014) 125040, [arXiv:1409.3591].

[15] A. Lewis, A. Challinor, and A. Lasenby, *Efficient computation of CMB anisotropies in closed FRW models*, *Astrophys. J.* **538** (2000) 473–476, [astro-ph/9911177].

[16] G. M. Fuller, C. T. Kishimoto, and A. Kusenko, *Heavy sterile neutrinos, entropy and relativistic energy production, and the relic neutrino background*, *ArXiv e-prints* (Oct., 2011) [arXiv:1110.6479].

[17] K. M. Nollett and G. P. Holder, *An analysis of constraints on relativistic species from primordial nucleosynthesis and the cosmic microwave background*, *ArXiv e-prints* (Dec., 2011) [arXiv:1112.2683].

[18] Z. Hou, R. Keisler, L. Knox, M. Millea, and C. Reichardt, *How massless neutrinos affect the cosmic microwave background damping tail*, Phys. Rev. D **87** (Apr., 2013) 083008.

[19] E. W. Kolb and M. S. Turner, *The early universe.* 1990.

[20] S. Weinberg, *Cosmology*. Oxford University Press, 2008.

[21] R. K. Press, *Statistical Mechanics*. Butterworth-Heinemann, Woburn, MA, USA, 2nd ed., 1996.

[22] L. Kawano, *Let's go: Early universe 2. Primordial nucleosynthesis the computer way*, *NASA STI/Recon Technical Report N* **92** (Jan., 1992) 25163.

[23] S. Dodelson, *Modern Cosmology*. Academic Press. Academic Press, 2003.

[24] J. Bernstein, *Kinetic theory in the expanding universe*. 1988.

[25] R. V. Wagoner, W. A. Fowler, and F. Hoyle, *On the Synthesis of elements at very high temperatures*, *Astrophys.J.* **148** (1967) 3–49.

[26] R. V. Wagoner, *Synthesis of the Elements Within Objects Exploding from Very High Temperatures*, ApJS **18** (June, 1969) 247.

[27] M. S. Smith, L. H. Kawano, and R. A. Malaney, *Experimental, computational, and observational analysis of primordial nucleosynthesis*, ApJS **85** (Apr., 1993) 219–247.

[28] A. D. Dolgov, S. H. Hansen, and D. V. Semikoz, *Non-equilibrium corrections to the spectra of massless neutrinos in the early universe*, *Nuclear Physics B* **503** (Feb., 1997) 426–444, [hep-ph/9703315].

[29] N. Y. Gnedin and O. Y. Gnedin, *Cosmological Neutrino Background Revisited*, ApJ **509** (Dec., 1998) 11–15, [astro-ph/9712199].

[30] G. Mangano, G. Miele, S. Pastor, and M. Peloso, *A precision calculation of the effective number of cosmological neutrinos*, *Physics Letters B* **534** (May, 2002) 8–16, [astro-ph/0111408].

[31] R. N. Boyd, C. R. Brune, G. M. Fuller, and C. J. Smith, *New nuclear physics for big bang nucleosynthesis*, Phys. Rev. D **82** (Nov., 2010) 105005.

[32] G. M. Fuller and C. J. Smith, *Nuclear weak interaction rates in primordial nucleosynthesis*, Phys. Rev. D **82** (Dec., 2010) 125017, [arXiv:1009.0277].

[33] M. Abramowitz and I. A. Stegun, *Handbook of Mathematical Functions with Formulas, Graphs, and Mathematical Tables (Partially Mathcad-enabled)*. U. S. Department of Commerce, NIST, New York, 1972. Online version available at: http://app.knovel.com/hotlink/toc/id:kpHMFFGMT1/handbook-mathematical/handbook-mathematical.

[34] M. E. Peskin and D. V. Schroeder, *An introduction to quantum field theory*. Advanced book program. Westview Press Reading (Mass.), Boulder (Colo.), 1995. Autre tirage : 1997.

[35] R. Trotta and S. H. Hansen, *Constraining the helium abundance with CMB data*, Phys. Rev. D **69** (Jan., 2004) 023509.

[36] K. Ichikawa, T. Sekiguchi, and T. Takahashi, *Primordial helium abundance from cmb: A constraint from recent observations and a forecast*, *Phys. Rev. D* **78** (Aug, 2008) 043509.

[37] F. Iocco, G. Mangano, G. Miele, O. Pisanti, and P. D. Serpico, *Primordial nucleosynthesis: From precision cosmology to fundamental physics*, Phys. Rep. **472** (Mar., 2009) 1–76, [arXiv:0809.0631].

[38] G. Miele and O. Pisanti, *Primordial Nucleosynthesis: an updated comparison of observational light nuclei abundances with theoretical predictions*, *Nuclear Physics B Proceedings Supplements* **188** (Mar., 2009) 15–19, [arXiv:0811.4479].

[39] G. Miele, O. Pisanti, and S. Sarikas, *Primordial Nucleosynthesis and Neutrino Physics Beyond the Standard Model*, *Journal of Physics Conference Series* **259** (Nov., 2010) 012007.

[40] O. Pisanti, A. Cirillo, S. Esposito, F. Iocco, G. Mangano, G. Miele, and P. D. Serpico, *PArthENoPE: Public algorithm evaluating the nucleosynthesis of primordial elements*, *Computer Physics Communications* **178** (June, 2008) 956–971, [arXiv:0705.0290].

[41] C. J. Smith, G. M. Fuller, C. T. Kishimoto, and K. N. Abazajian, *Light element signatures of sterile neutrinos and cosmological lepton numbers*, Phys. Rev. D **74** (Oct., 2006) 085008, [astro-ph/0608377].

[42] SPT Collaboration, *SPT-3G: a next-generation cosmic microwave background polarization experiment on the South Pole telescope*, in *Society of Photo-Optical Instrumentation Engineers (SPIE) Conference Series*, vol. 9153 of *Society of Photo-Optical Instrumentation Engineers (SPIE) Conference Series*, p. 1, July, 2014. arXiv:1407.2973.

[43] The Polarbear Collaboration, *A Measurement of the Cosmic Microwave Background B-mode Polarization Power Spectrum at Sub-degree Scales with POLARBEAR*, ApJ **794** (Oct., 2014) 171, [arXiv:1403.2369].

[44] D. Silva, P. Hickson, C. Steidel, and M. Bolte, *TMT Detailed Science Case: 2007*, tech. rep., 2007. http://www.tmt.org.

[45] P. McCarthy and R. A. Bernstein, *Giant Magellan Telescope: Status and Opportunities for Scientific Synergy*, in *Thirty Meter Telescope Science Forum*, p. 61, July, 2014.

[46] I. Hook, *The science case for the European Extremely Large Telescope : the next step in mankind's quest for the Universe*. 2005.

[47] J. Silk, *Cosmic Black-Body Radiation and Galaxy Formation*, ApJ **151** (Feb., 1968) 459.

[48] M. Zaldarriaga and D. D. Harari, *Analytic approach to the polarization of the cosmic microwave background in flat and open universes*, Phys. Rev. D **52** (Sept., 1995) 3276–3287.

[49] W. Hu and M. White, *CMB anisotropies: Total angular momentum method*, Phys. Rev. D **56** (July, 1997) 596–615.

[50] S. Weinberg, *Cosmology*. Oxford University Press, 2008.

[51] P. J. E. Peebles, *Recombination of the Primeval Plasma*, ApJ **153** (July, 1968) 1.

[52] S. Seager, D. D. Sasselov, and D. Scott, *A New Calculation of the Recombination Epoch*, ApJ **523** (Sept., 1999) L1–L5.

[53] S. Seager, D. D. Sasselov, and D. Scott, *How Exactly Did the Universe Become Neutral?*, ApJS **128** (June, 2000) 407–430.

[54] Y. B. Zeldovich, V. G. Kurt, and R. A. Syunyaev, *Recombination of Hydrogen in the Hot Model of the Universe*, *Zhurnal Eksperimentalnoi i Teoreticheskoi Fiziki* **55** (July, 1968) 278–286.

[55] D. Pequignot, P. Petitjean, and C. Boisson, *Total and effective radiative recombination coefficients*, A&A **251** (Nov., 1991) 680–688.

[56] D. G. Hummer and P. J. Storey, *Recombination of helium-like ions - I. Photoionization cross-sections and total recombination and cooling coefficients for atomic helium*, MNRAS **297** (July, 1998) 1073–1078.

[57] G. M. Fuller and C. T. Kishimoto, *Quantum Coherence of Relic Neutrinos*, *Physical Review Letters* **102** (May, 2009) 201303, [arXiv:0811.4370].

[58] E. Grohs, G. M. Fuller, C. T. Kishimoto, and M. W. Paris, *Effects of N_{eff} and neutrino rest mass on ionization equilibrium freeze-out*, *ArXiv e-prints* (Dec., 2014) [arXiv:1412.6875].

[59] A. D. Dolgov, S. H. Hansen, and D. V. Semikoz, *Non-equilibrium corrections to the spectra of massless neutrinos in the early universe*, *Nuclear Physics B* **543** (Mar., 1999) 269–274, [hep-ph/9805467].

[60] J.-L. Cambier, J. R. Primack, and M. Sher, *Finite temperature radiative corrections to neutron decay and related processes*, *Nucl. Phys. B* **209** (Dec., 1982) 372–388.

[61] R. E. Lopez and M. S. Turner, *Precision prediction for the big-bang abundance of primordial ^{4}He*, Phys. Rev. D **59** (May, 1999) 103502, [astro-ph/9807279].

[62] J. Birrell, C.-T. Yang, P. Chen, and J. Rafelski, *Relic neutrinos: Physically consistent treatment of effective number of neutrinos and neutrino mass*, *Phys. Rev. D* **89** (Jan, 2014) 023008.

[63] Z. Hou, C. L. Reichardt, K. T. Story, B. Follin, R. Keisler, K. A. Aird, B. A. Benson, L. E. Bleem, J. E. Carlstrom, C. L. Chang, H.-M. Cho, T. M. Crawford, A. T. Crites, T. de Haan, R. de Putter, M. A. Dobbs, S. Dodelson, J. Dudley, E. M. George, N. W. Halverson, G. P. Holder, W. L. Holzapfel, S. Hoover, J. D. Hrubes,

M. Joy, L. Knox, A. T. Lee, E. M. Leitch, M. Lueker, D. Luong-Van, J. J. McMahon, J. Mehl, S. S. Meyer, M. Millea, J. J. Mohr, T. E. Montroy, S. Padin, T. Plagge, C. Pryke, J. E. Ruhl, J. T. Sayre, K. K. Schaffer, L. Shaw, E. Shirokoff, H. G. Spieler, Z. Staniszewski, A. A. Stark, A. van Engelen, K. Vanderlinde, J. D. Vieira, R. Williamson, and O. Zahn, *Constraints on Cosmology from the Cosmic Microwave Background Power Spectrum of the 2500 deg^2 SPT-SZ Survey*, ApJ **782** (Feb., 2014) 74, [arXiv:1212.6267].

[64] C. Howlett, A. Lewis, A. Hall, and A. Challinor, *CMB power spectrum parameter degeneracies in the era of precision cosmology*, *JCAP* **1204** (2012) 027, [arXiv:1201.3654].

[65] W. Hu and N. Sugiyama, *Small-Scale Cosmological Perturbations: an Analytic Approach*, ApJ **471** (Nov., 1996) 542, [astro-ph/9510117].

[66] O. Zahn and M. Zaldarriaga, *Probing the friedmann equation during recombination with future cosmic microwave background experiments*, *Phys. Rev. D* **67** (Mar, 2003) 063002.

[67] E. Grohs, G. M. Fuller, C. T. Kishimoto, and M. W. Paris, *Probing neutrino physics with a self-consistent treatment of the weak decoupling, nucleosynthesis, and photon decoupling epochs*, J. Cosmology Astropart. Phys. **5** (May, 2015) 17, [arXiv:1502.0271].

[68] A. D. Dolgov, M. V. Sazhin, and Y. B. Zeldovich, *Basics of modern cosmology*. 1990.

[69] A. D. Dolgov, S. H. Hansen, S. Pastor, S. T. Petcov, G. G. Raffelt, and D. V. Semikoz, *Cosmological bounds on neutrino degeneracy improved by flavor oscillations*, *Nucl. Phys. B* **632** (June, 2002) 363–382, [hep-ph/0201287].

[70] K. Abazajian et al., *Neutrino physics from the cosmic microwave background and large scale structure*, *Astroparticle Physics* **63** (2015), no. 0 66 – 80. Dark Energy and {CMB}.

[71] J. E. Carlstrom and Spt Collaboration, *The 8m South Pole Telescope*, *IAU Special Session* **2** (2003) 34.

[72] K. Abazajian, N. F. Bell, G. M. Fuller, and Y. Y. Y. Wong, *Cosmological lepton asymmetry, primordial nucleosynthesis and sterile neutrinos*, Phys. Rev. D **72** (Sept., 2005) 063004, [astro-ph/0410175].

[73] C. T. Kishimoto, G. M. Fuller, and C. J. Smith, *Coherent Active-Sterile Neutrino Flavor Transformation in the Early Universe*, *Phys. Rev. Lett.* **97** (Oct., 2006) 141301, [astro-ph/0607403].

[74] J. Hamann, S. Hannestad, G. G. Raffelt, I. Tamborra, and Y. Y. Y. Wong, *Cosmology Favoring Extra Radiation and Sub-eV Mass Sterile Neutrinos as an Option*, *Phys. Rev. Lett.* **105** (Oct., 2010) 181301, [arXiv:1006.5276].

[75] J. Hamann, S. Hannestad, G. G. Raffelt, and Y. Y. Y. Wong, *Sterile neutrinos with eV masses in cosmology - How disfavoured exactly?*, J. Cosmology Astropart. Phys. **9** (Sept., 2011) 34, [arXiv:1108.4136].

[76] C. Dvorkin, M. Wyman, D. H. Rudd, and W. Hu, *Neutrinos help reconcile Planck measurements with both the early and local Universe*, Phys. Rev. D **90** (Oct., 2014) 083503, [arXiv:1403.8049].

[77] M. Cirelli, G. Marandella, A. Strumia, and F. Vissani, *Probing oscillations into sterile neutrinos with cosmology, astrophysics and experiments*, *Nuclear Physics B* **708** (Feb., 2005) 215–267, [hep-ph/0403158].

[78] C. Athanassopoulos et al., *The liquid scintillator neutrino detector and LAMPF neutrino source*, *Nuclear Instruments and Methods in Physics Research A* **388** (Feb., 1997) 149–172, [nucl-ex/9605002].

[79] A. A. Aguilar-Arevalo et al., *Measurement of the neutrino neutral-current elastic differential cross section*, Phys. Rev. D **82** (Nov., 2010) 092005, [arXiv:1007.4730].

[80] Y. Abe et al., *Reactor $\bar{\nu}_e$ disappearance in the Double Chooz experiment*, Phys. Rev. D **86** (Sept., 2012) 052008, [arXiv:1207.6632].

[81] C. T. Kishimoto and G. M. Fuller, *Lepton-number-driven sterile neutrino production in the early universe*, Phys. Rev. D **78** (July, 2008) 023524, [arXiv:0802.3377].

[82] L. A. Gilbert, G. M. Fuller, and E. Grohs in preparation, 2015.

[83] J. L. Menestrina and R. J. Scherrer, *Dark radiation from particle decays during big bang nucleosynthesis*, Phys. Rev. D **85** (Feb., 2012) 047301, [arXiv:1111.0605].

[84] E. W. Otten and C. Weinheimer, *Neutrino mass limit from tritium β decay*, *Reports on Progress in Physics* **71** (Aug., 2008) 086201, [arXiv:0909.2104].

[85] G. Drexlin, *Direct neutrino mass measurements*, *Journal of Physics Conference Series* **136** (Nov., 2008) 022031.

[86] A. Kusenko, S. Pascoli, and D. Semikoz, *Bounds on heavy sterile neutrinos revisited*, *Journal of High Energy Physics* **11** (Nov., 2005) 28, [hep-ph/0405198].

[87] F. Bergsma et al., *A search for decays of heavy neutrinos*, *Physics Letters B* **128** (Sept., 1983) 361–366.

[88] G. Bernardi, G. Carugno, J. Chauveau, F. Dicarlo, M. Dris, J. Dumarchez, M. Ferro-Luzzi, J.-M. Levy, D. Lukas, J.-M. Perreau, Y. Pons, A.-M. Touchard, and F. Vannucci, *Search for neutrino decay*, *Physics Letters B* **166** (Jan., 1986) 479–483.

[89] G. Bernardi, G. Carugno, J. Chauveau, F. Dicarlo, M. Dris, J. Dumarchez, M. Ferro-Luzzi, J.-M. Levy, D. Lukas, J.-M. Perreau, Y. Pons, A.-M. Touchard, and F. Vannucci, *Further limits on heavy neutrino couplings*, *Physics Letters B* **203** (Mar., 1988) 332–334.

[90] S. Baranov, Y. Batusov, S. Bunyatov, O. Klimov, V. Lyukov, Y. Nefedov, B. Popov, V. Valuev, A. Borisov, V. Goryachev, M. Kirsanov, A. Kozhin, V. Kravtsov, A. Spiridonov, V. Tumakov, A. Vovenko, and D. Kiss, *Search for heavy neutrinos at the IHEP-JINR Neutrino Detector*, *Physics Letters B* **302** (Mar., 1993) 336–340.

[91] P. Nédélec, *Tau-sterile neutrino mixing in NOMAD*, *Nuclear Physics B Proceedings Supplements* **98** (Apr., 2001) 37–42.

[92] S. Mertens, K. Dolde, M. Korzeczek, F. Glueck, S. Groh, R. D. Martin, A. W. P. Poon, and M. Steidl, *Wavelet Approach to Search for Sterile Neutrinos in Tritium β-Decay Spectra*, *ArXiv e-prints* (Oct., 2014) [arXiv:1410.7684].

[93] A. D. Dolgov, S. H. Hansen, G. Raffelt, and D. V. Semikoz, *Heavy sterile neutrinos: bounds from big-bang nucleosynthesis and SN 1987A*, *Nuclear Physics B* **590** (Dec., 2000) 562–574, [hep-ph/0008138].

[94] M. Kaplinghat, L. Knox, and Y.-S. Song, *Determining Neutrino Mass from the Cosmic Microwave Background Alone*, *Physical Review Letters* **91** (Dec., 2003) 241301, [astro-ph/0303344].

[95] S. H. Hansen and Z. Haiman, *Do We Need Stars to Reionize the Universe at High Redshifts? Early Reionization by Decaying Heavy Sterile Neutrinos*, ApJ **600** (Jan., 2004) 26–31, [astro-ph/0305126].

[96] S. Hannestad and G. Raffelt, *Cosmological mass limits on neutrinos, axions, and other light particles*, J. Cosmology Astropart. Phys. **4** (Apr., 2004) 8, [hep-ph/0312154].

[97] F. de Bernardis, T. D. Kitching, A. Heavens, and A. Melchiorri, *Determining the neutrino mass hierarchy with cosmology*, Phys. Rev. D **80** (Dec., 2009) 123509, [arXiv:0907.1917].

[98] S. Hannestad, A. Mirizzi, G. G. Raffelt, and Y. Y. Y. Wong, *Neutrino and axion hot dark matter bounds after WMAP-7*, J. Cosmology Astropart. Phys. **8** (Aug., 2010) 1, [arXiv:1004.0695].

[99] M. Archidiacono, A. Cooray, A. Melchiorri, and S. Pandolfi, *CMB neutrino mass bounds and reionization*, Phys. Rev. D **82** (Oct., 2010) 087302, [arXiv:1010.5757].

[100] E. Giusarma, M. Corsi, M. Archidiacono, R. de Putter, A. Melchiorri, O. Mena, and S. Pandolfi, *Constraints on massive sterile neutrino species from current and future cosmological data*, Phys. Rev. D **83** (June, 2011) 115023, [arXiv:1102.4774].

[101] G. M. Fuller, E. Grohs, C. T. Kishimoto, M. W. Paris, and A. Vlasenko in preparation, 2015.

[102] M. J. Savage, R. A. Malaney, and G. M. Fuller, *Neutrino oscillations and the leptonic charge of the universe*, ApJ **368** (Feb., 1991) 1–11.

[103] K. N. Abazajian, J. F. Beacom, and N. F. Bell, *Stringent constraints on cosmological neutrino-antineutrino asymmetries from synchronized flavor transformation*, Phys. Rev. D **66** (July, 2002) 013008, [astro-ph/0203442].

[104] Y. Y. Wong, *Analytical treatment of neutrino asymmetry equilibration from flavor oscillations in the early universe*, Phys. Rev. D **66** (July, 2002) 025015, [hep-ph/0203180].

[105] G. M. Fuller, W. A. Fowler, and M. J. Newman, *Stellar weak interaction rates for intermediate-mass nuclei. IV - Interpolation procedures for rapidly varying lepton capture rates using effective log (ft)-values*, ApJ **293** (June, 1985) 1–16.

[106] J. P. Kneller and G. Steigman, *BBN for pedestrians*, *New Journal of Physics* **6** (Sept., 2004) 117, [astro-ph/0406320].

[107] J. N. Ariche, G. M. Fuller, and E. Grohs in preparation, 2015.

[108] W. H. Press, S. A. Teukolsky, W. T. Vetterling, and B. P. Flannery, *Numerical Recipes in FORTRAN; The Art of Scientific Computing*. Cambridge University Press, New York, NY, USA, 2nd ed., 1993.

[109] J. Birrell, C. T. Yang, and J. Rafelski, *Relic neutrino freeze-out: Dependence on natural constants*, *Nuclear Physics B* **890** (Jan., 2015) 481–517, [arXiv:1406.1759].

[110] D. A. Dicus, E. W. Kolb, A. M. Gleeson, E. C. G. Sudarshan, V. L. Teplitz, and M. S. Turner, *Primordial nucleosynthesis including radiative, Coulomb, and finite-temperature corrections to weak rates*, Phys. Rev. D **26** (Nov., 1982) 2694–2706.

[111] M. A. Herrera and S. Hacyan, *Relaxation time of neutrinos in the early universe*, ApJ **336** (Jan., 1989) 539–543.

[112] N. C. Rana and B. Mitra, *Effect of neutrino heating in the early Universe on neutrino decoupling temperatures and nucleosynthesis*, Phys. Rev. D **44** (July, 1991) 393–397.

[113] S. Dodelson and M. S. Turner, *Nonequilibrium neutrino statistical mechanics in the expanding Universe*, Phys. Rev. D **46** (Oct., 1992) 3372–3387.

[114] A. D. Dolgov and M. Fukugita, *Nonequilibrium effect of the neutrino distribution on primordial helium synthesis*, Phys. Rev. D **46** (Dec., 1992) 5378–5382.

[115] S. Hannestad and J. Madsen, *Neutrino decoupling in the early Universe*, Phys. Rev. D **52** (Aug., 1995) 1764–1769, [astro-ph/9506015].

[116] S. Esposito, G. Miele, S. Pastor, M. Peloso, and O. Pisanti, *Non equilibrium spectra of degenerate relic neutrinos*, *Nuclear Physics B* **590** (Dec., 2000) 539–561, [astro-ph/0005573].

[117] G. Mangano, G. Miele, S. Pastor, T. Pinto, O. Pisanti, and P. D. Serpico, *Relic neutrino decoupling including flavour oscillations*, *Nuclear Physics B* **729** (Nov., 2005) 221–234, [hep-ph/0506164].

[118] S. Elhay and J. Kautsky, *Algorithm 655: Iqpack: Fortran subroutines for the weights of interpolatory quadratures*, *ACM Trans. Math. Softw.* **13** (Dec., 1987) 399–415.

[119] A. B. Balantekin and N. Vassh, *Magnetic moments of active and sterile neutrinos*, Phys. Rev. D **89** (Apr., 2014) 073013, [arXiv:1312.6858].

[120] K. J. Bae, H. Baer, and A. Lessa, *Dark radiation constraints on mixed Axion/Neutralino dark matter*, J. Cosmology Astropart. Phys. **4** (Apr., 2013) 41, [arXiv:1301.7428].

[121] F. C. Adams, *Stars in other universes: stellar structure with different fundamental constants*, J. Cosmology Astropart. Phys. **8** (Aug., 2008) 10, [arXiv:0807.3697].

[122] F. C. Adams, K. R. Coppess, and A. M. Bloch, *Planets in Other Universes: Habitability constraints on density fluctuations and galactic structure*, *ArXiv e-prints* (May, 2015) [arXiv:1505.0615].